Report ADA281370

PROPERTY CONTROL OF (PERFLUORINATED IONOMER)/(INORGANIC OXIDE) COMPOSITES BY TAILORING THE NANOSCALE MORPHOLOGY

Kenneth A. Mauritz and Robert B. Moore
Department of Polymer Science
University of Southern Mississippi
P.O. Box 10076
Hattiesburg, MS 39406-0076

10 June 1994

First Annual Technical Report for Period 01 April 1993 - 31 March 1994

Prepared for

AIR FORCE OFFICE OF SCIENTIFIC RESEARCH (AFOSR/PKA)
110 Duncan Avenue, Suite B115
Bolling Air Force Base, D.C. 20332-0001

AIR FORCE OFFICE OF SCIENTIFIC RESEARCH (AFOSR/NC)
110 Duncan Avenue, Suite B115
Bolling Air Force Base, D.C. 20332-0001

CLASSIFICATION OF THIS PAGE

REPORT DOCUMENTATION PAGE

1a. REPORT SECURITY CLASSIFICATION	1b. RESTRICTIVE MARKINGS
2a. SECURITY CLASSIFICATION AUTHORITY	3. DISTRIBUTION AVAILABILITY
2b. DECLASSIFICATION/DOWNGRADING SCHEDULE	5. MONITORING ORGANIZATION REPORT NUMBER (S)
4. PERFORMING ORGANIZATION REPORT NUMBER (S) F49620-93-1-0189DEF	7a. NAME OF MONITORING ORGANIZATION AFOSR/PKA
6a. NAME OF PERFORMING ORGANIZATION The Univ. of Southern Miss. / 6b. OFFICE SYMBOL (If applicable)	7b. ADDRESS (City, State and ZIP Code) 110 Duncan Avenue, Suite B115 Bolling AFB, DC 20332-0001
6c. ADDRESS (City, State and ZIP Code) P.O. Box 5116 Hattiesburg, MS 39406-5116	
8a. NAME OF FUNDING/SPONSORING ORGANIZATION AFOSR/NC / 8b. OFFICE SYMBOL (If applicable)	9. PROCUREMENT INSTRUMENT IDENTIFICATION NUMBER
8c. ADDRESS (City, State and ZIP Code) 110 Duncan Avenue Suite B115 Bolling AFT, DC 20332-0001	10. SOURCE OF FUNDING NOS. PROGRAM ELEMENT NO. / PROJECT NO. / TASK NO. / WORK UNIT NO.
11. TITLE (Include Security Classification)	
12. PERSONAL AUTHOR (S) Kenneth A. Mauritz and Robert B. Moore	
13a. TYPE OF REPORT *Technical*	13b. TIME COVERED FROM 01 Apr 93 TO 31 Mar 94
14. DATE OF REPORT (Yr., Mo., Day) 1994, June, 13	15. PAGE COUNT 166
16. SUPPLEMENTARY NOTATION	

17. COSATI CODES			18. SUBJECT TERMS (Continue on reverse if necessary and identify by block number)
FIELD	GROUP	SUB. GR.	

19. ABSTRACT (Continue on reverse if necessary and identify by block number)

Unique perfluoro-organic/inorganic oxide hybrid materials have been formulated by merging processes recently developed by us for (1) the solution and melt processing of perfluorosulfonate ionomers (PFSI's) and (2) the production of nanocomposites by the *in situ* sol-gel reaction for silicon and metal alkoxides within the polar clusters of PFSI's. Our working hypothesis is that the resultant morphology of the inorganic phase is *ordered* by the nanophase-separated morphology of the PFSI matrix. In this research, the 3-dimensional *morphological template* presented by the PFSI is tailored by manipulating the primary polymer structure, polymer solution conditions, film casting procedure, and post-processing (*e.g.* drying, annealing, melt-quenching, mechanical orientation). The nanocomposites are then characterized for microstructure broadly ranging from light microscopic resolution down to the level of Angstroms using various microscopic, scattering, diffraction and spectroscopic methods.

20. DISTRIBUTION/AVAILABILITY OF ABSTRACT UNCLASSIFIED/UNLIMITED ☐ SAME AS RPT. ■ DTIC USERS ☐	21. ABSTRACT SECURITY CLASSIFICATION
22a. NAME OF RESPONSIBLE INDIVIDUAL	22b. TELEPHONE NUMBER (Include Area Code) / 22c. OFFICE SYMBOL

DD FORM 1473, 83 APR EDITION OF 1 JAN 73 IS OBSOLETE

SECURITY CLASSIFICATION OF THIS PAGE

TABLE OF CONTENTS

Research Objectives

Statement of Work

Perfluoro-organic/inorganic oxide hybrid materials, in the form of either coatings, films or membranes, will be formulated by merging our proven methods for the solution and melt processing of long and short sidechain perfluorosulfonate ionomers (PFSI's) with our proven methods for the production of nanocomposites by the *in situ* sol-gel reaction for silicon and metal alkoxides within the polar clusters of PFSI's.

We will investigate the effects on microstructure, and important physical properties, of systematic variance of solution-casting and thermal processing parameters of H^+ -form (unfilled) PFSI films. Then, hypothesizing that the quasi-ordered two-phase PFSI microstructure presents an interactive morphological template for in *in situ* alkoxide polymerization, the results of these studies will establish a rational basis for the systematic tailoring of the geometric disposition of the incorporated inorganic domains.

Structure-property disposition relationships for sol/gel - derived *nanocomposites* using form the systematic variation of (1) PFSI template morphology, (2) alkoxide type, (3) alkoxide: water ratio, (4) alkoxide: SO_3H ratio, (5) solvent type, (6) mixed silicon-metal alkoxide compositions, (7) drying/annealing protocol, and (8) the use of mechanically-oriented PFSI templates, will be investigated and exploited.

Resultant microstructures and physical properties of nanocomposites prepared by (1) solution-casting liquid mixtures of both the perfluoro-organic and inorganic components with nanocomposites prepared by (2) the 3-dimensional *polymeric template* method (use of preexisting, free-standing films) will be compared.

We seek to identify advanced nanocomposites having useful isotropic or directional properties relating to electrical and thermal conductivity, unusual dielectric and optical behavior, thermal-switching and pressure-sensitivity, and gas-permselectivity. These materials will possess good thermodegradative and solvent resistance as well as be mechanically-robust.

To this end, the nanocomposites will be extensively characterized for microstructure over dimensional scales spanning light microscopic resolution down to the level of Ångstroms using (light, electron) microscopic, small angle radiation/particle scattering, wide angle x-ray diffraction, and vibrational and NMR spectroscopic methods. Important structure-property relationships will issue form our investigation of the mechanical tensile, dynamic mechanical, thermal transition and thermal degradative, dielectric/electrical conductance and gas permeation characteristics of these materials. Oriented nanocomposites will possess directional (anisotropic) mechanical, thermal, electrical, optical and gas transport properties which will be explored in detail.

Finally, the scope of our microstructural investigation will be greatly broadened through strong interactions with investigators at governmental (small angle x-ray/neutron scattering: Sandia, Oak Ridge) as well as at industrial (DOW Chemical Co.) laboratories.

Project Summary

During the first year of this project, unique perfluoro-organic/inorganic oxide hybrid materials have been formulated by merging processes recently developed by us for (1) the solution and melt processing of perfluorosulfonate ionomers (PFSI's) and (2) the production of nanocomposites by the *in situ* sol-gel reaction for silicon and metal alkoxides within the polar clusters of PFSI's. Our working hypothesis is that the resultant morphology of the inorganic phase is *ordered* by the nanophase-separated morphology of the PFSI matrix. In this research, the 3-dimensional *morphological template* presented by the PFSI is tailored by manipulating the primary polymer structure, polymer solution conditions, film casting procedure, and post-processing (*e.g.* drying, annealing, melt-quenching, mechanical orientation). The nanocomposites are then characterized for microstructure broadly ranging from light microscopic resolution down to the level of Ångstroms using various microscopic, scattering, diffraction and spectroscopic methods.

The studies discussed below are being conducted in our effort to generate morphological templates from PFSI membranes, which, in turn, are used in the formulation of unique [*perfluoro-organic*]/[*inorganic oxide*] nanocomposites. An important discovery concerning a link between processing conditions and the mechanical integrity of the solution-processed PFSI membranes has lead to recent modifications of the solution-casting procedure. Without this procedure modification, the resulting PFSI templates were too weak to withstand the fairly harsh conditions encountered during the nanocomposite fabrication. Now that suitable processing conditions have been identified, the next phase of this project will be to fabricate nanocomposites with these new tailored membranes.

Using the industrially supplied PFSI membranes, one current project involves an attempt to create a "shell," of different chemical composition, around silicon oxide nanoparticles that already exist within a membrane by reacting surplus hydroxyl endgroups (≡Si-OH) with a different silane having hydrophobic groups (*e.g.* $(CH_3)_2Si(OH)_2$). Another project is concerned with reacting *mixed* alkoxides (*e.g.* $Si(OR)_4 + Ti(OR')_4$) within tailored PFSI template membranes. The structures of the inorganic oxide phase in both of these studies is being intensively analyzed via infrared spectroscopy, which can provide a view of degree of crosslinking.

With recent developments in various aspects of the nanocomposite synthesis, we are beginning to aim experiments at understanding the complex structure-property relationships (e.g., mechanical, thermal, dielectric/electrical conductance and gas permeation characteristics) of these materials that are expected to be rather chemically and thermally - robust. The percolative nature of the inorganic phase is anticipated to generate "smart" materials in the sense of acting as temperature and pressure sensors. Oriented nanocomposites will possess directional mechanical, thermal and electrical properties. Studies below demonstrate for the first time that the morphological templates may be highly oriented on the nanometer scale, and that these oriented templates may be used to create nanocomposites with an anisotropic morphology.

RESEARCH REPORT TO AFOSR

June 7, 1994

PART I

TABLE OF CONTENTS

PART I

Research work of Dr. Robert B. Moore

I. Morphological Tailoring of PFSI Templates

A. Effect of Uniaxial Extension on the Morphology of PFSI's

Preliminary small angle X-ray scattering data were collected on oriented tetrabutyl ammonium-form 1100 EW Nafion® to determine the effect of orientation on cluster morphology. The films were stretched to different extensional ratios, at elevated temperatures. Anisotropy in the two-dimensional scattering patterns developed dramatically with increasing extension indicating that the bulky alkyl ammonium counterions weaken the ionic interactions in the cluster regions and permit the cluster to become oriented or deformed.

PROCEDURE: As received 1100 EW Nafion® was cleaned by refluxing in 8M HNO_3 overnight and subsequently rinsed with large amounts of deionized H_2O. The material was then dried in a vacuum oven at 70°C overnight and neutralized by soaking the PFSI in a tetrabutyl ammonium hydroxide (TBAOH) solution. The neutralized PFSI was then dissolved in a methanol/water/propanol solution at 250°C/800psi for 1hr in a Parr® pressure reactor. The polymer was recovered by pouring the solution into boiling water and skimming the precipitated polymer off the top. This TBA^+-form PFSI was then ground into a powder and pressed into films at 200°C on a Carver® lab press. These "melt processed" films were then uniaxially stretched in a specially prepared jig at approximately 200°C to a variety of extensional ratios.

Small angle X-ray scattering (SAXS) was performed using a Siemens XPD-700P polymer diffraction system equipped with a two-dimensional, position sensitive, area detector. To avoid excess air scatter, the scattering path from the sample to the detector was sealed and purged with Helium gas. All data were collected in the transmission mode with a sample-to-detector distance of 49cm. Samples were background subtracted, corrected for absorption and normalized for film thickness.

RESULTS: Figure 1 shows four, two-dimensional scattering patterns of TBA^+-Nafion samples that have been stretched to different extensional ratios λ_b, which is equal to the final length (after stretching) divided by the initial length. The samples were stretched in the azimuthal direction = 0 °. For λ_b= 1 (i.e. the unoriented sample) the distinctive, isotropic small-angle scattering profile resulting from the scattering of the ionic clusters is evident. As the PFSI's are oriented to greater extensional ratios an anisotropic scattering pattern develops, with the intensity increasing perpendicular (= 90 °C) to the direction of orientation. Integrating a slice of the 2-D patterns in the equatorial direction (= 90 °C) reveals in Figure 2, that the intensity of the scattering in the equatorial direction increases dramatically with greater orientation.

B. Effect of Uniaxial Extension on Alkyl Ammonium Counterions

Polarized FTIR spectroscopy was performed on oriented TBA^+-form Nafion.® Infrared dichroism in the C-H stretching bands of the TBA^+ counterion was observed. This observation suggests that the alkyl chains become ordered as the cluster becomes extended.

PROCEDURE: A melt-processable powder of TBA^+-form Nafion® was prepared as previously reported. This powder was pressed into a thin film on a Carver laboratory press. The film was then stretched at ca. 200°C, to an extensional ratio (λ_b) of about 5.4 (λ_b = final length / initial length).

Polarized Fourier transform infrared (FTIR) spectroscopy was carried out using a Perkin-Elmer 1600 series spectrometer. The spectrometer was equipped with a gold grid polarizer set a 0°, 45°, and 90° relative to the direction of sample orientation.

RESULTS: Figure 3 shows the effect of elongation on the orientation of the C-H stretching vibrations for the $-CH_2-$ and $-CH_3$ groups in the alkyl segments of the TBA^+ counterions. The vibrational band attributed to the $-CH_3$ asymmetric stretch (2970 cm^{-1}) exhibits distinct infrared dichroism. This behavior indicates preferential orientation of the alkyl chains within the clusters. Since the TBA^+ ions preferentially exist within the ionic clusters, this internal orientation effect suggests that the shape of the ionic aggregates is transformed from an isotropic shape to an elongated (elliptical) shape. This deformation phenomenon is shown schematically in Figure 4. The unoriented sample shows spherical clusters residing in the bulk matrix, while the clusters are elongated in the direction of the applied stress for the highly oriented sample.

C. Anisotropic Ionic Conductivity in Permanently Oriented PFSI Membranes

Preliminary ionic conductivity experiments performed on oriented Na^+-form Nafion® reveals a definite directional dependance on the ionic conductivity. The conductivity in the direction parallel to the direction of orientation is greater than that of the conductivity perpendicular to the direction of orientation.

PROCEDURE: A TBA^+-form Nafion® film that had been melt pressed at 200°C was stretched at a temperature of approximately 200°C to an extensional ratio (λ_b) of ca. 3. The oriented film was then converted to the Na^+-form by first refluxing the film in 8M HNO_3 and then neutralizing in aqueous NaOH. During the conversion process the film was maintained under tension by an in-house built jig.

Conductivity measurements were conducted in the hydrated Na^+-form films using a Hewlett-Packard AC impedance analyzer at 5 Hz. A special electrode, consisting of two copper blocks (separated by a distance of 0.25mm), imbedded in epoxy, was used to test the films. The electrode was pressed into the hydrated film in directions both parallel and perpendicular to the direction of orientation. The result represents and average of thirteen pairs of measurements.

RESULTS: The orientation of PFSI films has a dramatic affect on the ionic conductivity. Figure 5 shows the result of the conductivity measurements made perpendicular and parallel to the direction of orientation. The ratio of the conductivity in the parallel direction ($\sigma_\parallel$) to that in the perpendicular direction ($\sigma_\perp$) is 1.3 indicating that the conductivity in the parallel direction is distinctly greater than in the perpendicular direction.

D. Solution-Cast Blends of Long and Short Side Chain PFSI's

Blends containing different ratios of the short side chain 1000 EW Dow PFSI and the long side chain 1100 EW Nafion® PFSI were prepared using a solution casting procedure. The morphology of these blends were characterized by water uptake, infrared spectroscopy, differential scanning calorimetry, and small angle X-ray scattering. The pure Dow material showed higher water uptake than the pure Nafion®. Preliminary DSC and SAXS data indicate that the Dow material forms smaller clusters than Nafion® PFSI.

PROCEDURE: Solutions of 1000 EW Dow PFSI and 1100 EW Nafion®, both in the Na^+-form, were prepared by dissolving the Na^+-form as-received PFSI in a water/ethanol solution at 250°C/800psi for 1hr. Films were cast by first adding approximately 1ml of dimethyl sulfoxide to the PFSI solution in the bottom of a small beaker. The solution was heated in an oil bath to 80°C until the ethanol was driven off. The temperature was then increased to 180°C until the DMSO evaporated. The resultant film was removed from the bottom of the beaker by swelling the membrane with ethanol. A series of films were prepared containing different ratios of Dow/Nafion®.

Water uptake was carried out by drying the films to constant mass in a vacuum oven at about 70°C. The membranes were then hydrated by boiling in DI H_2O for 1hr and then massed. From the mass difference between the hydrated and dry films and from the equivalent weight of the membrane the moles of H_2O per mole of SO_3^- was calculated.

Infrared spectroscopy of thin, solution-cast films of the PFSI blends were carried out using a Perkin-Elmer 1600 Series FTIR spectrometer. DSC data were collected on a Perkin-Elmer DSC-7 at a heating rate of 50°C/min. Samples were dried at about 120°C for approximately 10hrs before being put into the sample pans and then for another 4hrs after they had been placed into sample pans. Only a single scan was performed per sample; however, four samples of each composition were run to ensure good reproduciblity. SAXS was carried out on the Siemens XPD-700P system and samples were background subtracted, corrected for absorption, and normalized for film thickness.

RESULTS: Figure 6 shows water uptake for a variety of PFSI compositions. Though there is scatter in the data, the general trend is to lower water contents with increasing Nafion® content (long side chain PFSI). This analysis is being repeated.

The portion of the infrared spectra containing the SO_3^- symmetrical stretch ($1060cm^{-1}$) and the C-O-C symmetrical stretch ($980cm^{-1}$ and $965cm^{-1}$) is shown in Figure 7. While the SO_3^- band is unaffected by the blend composition the C-O-C bands show a gradual change in peak shapes going from pure Dow which contains only one peak at about $965cm^{-1}$ to the two peaks at $965cm^{-1}$ and $980cm^{-1}$,as seen in the pure Nafion® system.

The DSC data in Figure 8 focuses on the endothermic transition in the blends that has been previously attributed to an ionic cluster-phase transition. Increasing the Nafion® composition increases the peak position of this endotherm from 235°C to 260°C. Future investigations are aimed at discovering the detailed origin of this endothermic event.

Figure 9 shows a plot of the average Bragg distance between ionic clusters, d_{BRAGG} taken from the SAXS data, versus the blend composition. Despite the data scatter the trend to larger Bragg spacing with increasing Nafion® content is apparent. These data suggest that the size of the ionic clusters may increase with increasing Nafion® content.

E. Effect of annealing on the thermal behavior of PFSI membranes

Thermal analysis was carried out on the as-received Na^+ form 1100 EW Nafion® and Dow (1000 EW) PFSI membranes to study the effect of annealing. Samples were annealed for different times at temperatures ca 20 °C lower than the endotherm peak temperature around 250 °C (attributed to cluster T_g). The heat capacity values increased gradually with respect to time reaching an asymptote. The endotherm peak temperature also showed a gradual shift to higher temperature with respect to time. These results indicate that the morphology corresponding to the endotherm can be erased and then systematically reintroduced at will.

PROCEDURE: As received membranes were cleaned by refluxing in 8M HNO_3 overnight and subsequently rinsed with large amounts of deionized H_2O. After drying, the samples were neutralized with aqueous NaOH solution and rinsed with deionized H_2O. DSC thermograms were obtained after drying the samples at 120 °C for 2h. For the annealing experiments, previous sample history was erased by heating the sample to 330 °C and 350 °C for Nafion and Dow PFSI, respectively, and cooled back to ambient temperature rapidly. The samples were then annealed at 200°C (Nafion) and 230 °C (Dow PFSI) for different time intervals and cooled back to ambient temperature. The subsequent scan on the samples were recorded for analysis.

DSC data were collected on Perkin-Elmer DSC-7 at 20 °C/min under N_2. Tensile measurements were carried out on an MTS with a 100 lb load cell at 0.1 mm/sec.

RESULTS: Figure 10 shows the DSC thermograms of as received and annealed Nafion samples. The as received sample has a broad endotherm between 200 and 250 °C (attributed to cluster T_g) which was not observed in sample quenched to room temperature rapidly. This endotherm that appears between 200 and 250 °C is introduced back into the annealed samples as a narrow peak. The ΔH value corresponding to this endotherm increased with respect to annealing time from 0.7 J/g (for annealing time 1/2 h) to 2.7 J/g (for annealing time 24 h). The endotherm peak temperature increased from 225 to 240 °C under same conditions. The ΔH value reached a plateau after 12 h. The maximum ΔH value obtained is only 50% of the as received samples (5 J/g). We were able to achieve 5-6 J/g (similar to as received sample) through the solution processing technique. These results indicate restricted mobility in the solid-state should cause the difficulties in development of this morphology by annealing the as received membranes.

Figure 11 shows the DSC thermograms of the as received and annealed Dow PFSI samples. The as received sample had two endotherms at 275 and 325 °C with ΔH values

3.6 and 0.35 J/g, respectively. Annealing at 200 and 220 °C did not cause significant increase in the peak intensity of the initial endotherm (attributed to cluster T_g). Increase in peak intensity and temperature were observed when the samples were annealed at 230 °C for different time intervals. The ΔH value increased from 0.9 J/g (for annealing time 1/2 h) to 1.9 J/g (for annealing time 24 h) and the endotherm peak temperature shifted from 255 to 265 °C. Even after annealing for 24 h the ΔH value reached only half the value of the as received sample and peak temperature about 10 °C lower than the as received membrane. The temperature necessary to influence the endotherm is higher in Dow PFSI membranes than Nafion and can be attributed to the short side chain between the sulfonate groups and the backbone in Dow PFSI membranes. In general, these results suggests that the morphology leading to this endotherm around 250 °C can be erased or introduced at will.

The effect of thermal history on stress-strain behavior was analyzed for Nafion in the as received form, sample quenched from 330 °C, and sample annealed at 200 °C for 24 h after quenching from 330 °C (Figure 12). The initial modulus is within experimental deviation for all the samples. However, after the initial 10% strain the load bearing nature of the melt quenched and annealed samples were better than the as received membrane. The stress at the yield (pseudo) point has also increased after thermal history. This may be due complete drying of the samples in the samples taken up to 330 °C as water is known to plasticize these membranes.

F. Influence of processing temperature on the properties of Nafion PFSI membranes

Solution processed membranes were made at different processing temperatures between 160 to 210 °C at intervals of 10 °C. Thermal behavior, tensile properties and water uptake were tested on all these samples. Membranes processed at temperatures below 200 °C exhibited mechanical properties inferior to the as received membranes. At and above 200 °C the mechanical properties are in the useable range. The mechanical properties showed some correlation with the thermal behavior observed by DSC. The water uptake did not show any specific trend with the processing temperature.

PROCEDURE: Solution of 1100 EW Nafion in the Na^+ form were prepared by dissolving the Na^+ form as received PFSI (cleaned as in the previous experiment) in a water/Ethanol solution at 250 °C/800psi for 1h. Solutions were cast by adding approximately 2 ml of DMSO into the beaker containing ca 10 ml of the PFSI solution in a beaker. Two oil baths were used, one for the evaporation of ethanol/ water mixture and the other for evaporating DMSO. The first bath was kept between 80 to 85 °C for all the samples and after the solution became concentrated, it was transferred to the second bath that was maintained at the required processing temperature. After complete evaporation of DMSO the samples were taken and removed from the beaker by swelling in ethanol.

DSC data were collected on Perkin-Elmer DSC-7 at 20 °C/min under N_2. Tensile measurements were carried out on an MTS with a 100 lb load cell at 0.1 mm/sec. Water uptake test was carried out by drying the films to a constant mass at 70 °C. The membranes were then hydrated by boiling in DI water and from the mass difference the moles of water per mole of sulfonate group was calculated.

RESULTS: The endotherm observed around 250 °C in the as received membranes was seen in the solution processed films also. The endotherm peak temperature increased with increasing processing temperature. The DSC thermograms for the samples processed at different temperatures were given in Figure 13. The peak temperature shifted from 233 °C (at processing temperature 160 °C) to 252 °C (at processing temperature 210 °C). However the ΔH values remained between 5 and 6 J/g for all the samples also comparable to the as received membranes. Thus morphology corresponding to the endotherm has become more perfect with increased processing temperature without increasing in intensity. Also noticeable is the jump from 237 to 244 °C in going from 180 to 190 °C (boiling range of DMSO).

Effect of processing temperature on the tensile behavior of the PFSI membranes is given in Figure 14. For comparisons the stress-strain curve of as received Nafion is also given. In all the samples, the initial modulus is comparable. Film processed at 160 °C had only about 40 % extension at break and low stress at break. Samples processed at 170 and 180 °C showed increased elongation at break and stress at break. All these three samples exhibited similar stress at yield (pseudo yield point characteristic of ionomers). The yield stress has increased about 20 % in going from 180 to 190 °C. This may be related to the jumpwise increase in the endotherm peak temperature between 180 and 190 °C in DSC. In all these four samples the stress crystallization at high strains seen in the as received films was not observed. Samples processed at 200 and 210 °C showed increased elongation and stress at break and also the yield stress. The yield point was even higher than the as received membrane for samples processed at 200 and 210 °C. Samples processed at 200 and 210 °C also showed stress crystallization phenomena at high strains similar to the as received membrane. The tensile properties of the samples processed at 200 and 210 °C were thus in useable range for nanocomposite fabrication.

The water uptake data are summarized in Table I below. For all samples, the water content was found to be in the range of 17 to 22 moles water per mole sulfonate sites. At low processing/annealing temperatures, the water content decreased slightly; however, at higher processing/annealing temperatures, the water content began to increase. The increasing water content with increasing annealing temperature (observed for the membranes processed at high temperatures) is consistent with that observed for as-received PFSI's.

Table I
Maximum Water Contents for Na+ Solution-Processed Nafion® Membranes

Processing Temperature (°C)	Water Content (mol H_2O / mol SO_3^-)
160	21.4
170	21.1
180	17.9
190	16.9
200	19.0
210	21.9

G. Conversion of TBA^+-form Nafion® to the H^+-form: Minimum Conditions

The standard procedure for converting PFSI membranes, neutralized with alkyl ammonium counterions, to the H^+-form usually consists of refluxing the material in 8M HNO_3 for ca. 24 hrs. Due to the very harsh nature of this conversion procedure, preliminary work is underway to determine the minimum conditions necessary to achieve total conversion.

PROCEDURE: TBA^+-form Nafion® films were melt pressed on a Carver laboratory press at 200°C. The films were characterized with FTIR, using a Perkin-Elmer 1600 series spectrometer. The films were then treated with differing concentrations of either HNO_3 (4M or 8M) or H_2SO_4 (1M, 4M, or 8M) under the following conditions: 1) ultrasonication (1hr); 2) stirring (RT, 24 hrs); 3) reflux (1 hr); 4) reflux (24 hrs). After rinsing in deionized water and drying, the films were again analyzed with FTIR.

Table 1

ION-EXCHANGE CONVERSION					
Treatment	1M H_2SO_4	4M H_2SO_4	8M H_2SO_4	4M HNO_3	8M HNO_3
Ultrasonic bath 1 hr.	----	----	0.5013	0.2290	----
Stir 24 hr.	0.1664	0.3713	0.6033	0.4959	----
Reflux 1 hr.	0.1724	0.6322	0.7379	0.6127	----
Reflux 24 hr.	0.2791	0.7273	0.7640	0.7545	0.9395

RESULTS: Table 1 shows the results of the various acid treatments. The conversions were calculated using the following formula:

$$Conversion = \frac{A_{orig} - A_{con}}{A_{orig}}$$

where A_{orig} is the area of the C-H peak (ca. 2970 cm^{-1}) as processed in the TBA^+-form and A_{con} is the area of the C-H peak after conversion treatment. The values for the 1M and 2M H_2SO_4 ultrasonication experiments were inconclusive. The first three treatments in the 8M HNO_3 series have not been performed at the time of this writing.

Table 1 reveals that achieving effective conversions requires strong acids under rigorous conditions. Future work will concentrate on completing the 8M HNO_3 series. In addition, attention will be focused on the use of mixed acids and/or mixed solvents in the conversion process.

H. Thermal behavior of Nafion Cs^+ PFSI membranes

These investigations are aimed at understanding the subtle morphological changes in PFSIs which result from varying the membrane processing conditions. This fundamental information is then used to control the structure-property relationships of the morphological templates for nanocomposite growth (see below). The as-received Cs^+ form 1100 EW Nafion® PFSI membranes and the precursor for Nafion (SO_2F form) were annealed under different conditions to study the high temperature transition seen in Nafion. Neutralized samples were annealed for different times at 200 °C (close to the endotherm peak temperature around 250 °C, previously attributed to an ionic cluster T_g) and for a constant time at varying temperatures between 120 and 240 °C. The ΔH values of the high temperature, endothermic transition increased gradually with time at 200 °C.

The peak temperature also showed a small but gradual shift to higher temperature with respect to time. Samples annealed at temperatures much lower than 250 °C showed additional endothermic transitions 20-30 °C above the annealing temperature. Similar experiments on the SO_2F form showed presence of this high temperature transition even though over a broader range. As clustering is absent in the SO_2F form, this endotherm is now attributed to small imperfect crystals formed from statistically short segments of the PTFE backbone. These results indicates that the crystallinity can be eliminated and reintroduced through different thermal treatments.

PROCEDURE: As received membranes were cleaned by refluxing in 8M HNO_3 overnight and subsequently rinsed with large amounts of deionized H_2O. After drying, the samples were neutralized with CsOH in methanol and rinsed with deionized H_2O. DSC thermograms were obtained after drying the samples at 120 °C for 2h. For annealing experiments, previous sample history was erased by heating the sample to 330 °C and rapidly cooling back to ambient temperature. The samples were then annealed at 200 °C for different time intervals and cooled back to ambient temperature. The precursor was annealed at 200 °C (for 1/2 and 6h) and at 150 °C (for 1/2 h). In another annealing experiment for Cs^+ Nafion, the time was kept constant (2h) and the annealing temperature was varied between 120 and 240 °C (at 30 °C intervals). The subsequent scan on the samples were recorded for analysis. All DSC data were collected on a Perkin-Elmer DSC-7 at 20 °C/min under N_2.

RESULTS: Figure 15 shows the DSC thermograms of as-received and annealed Nafion samples. The as-received sample shows a broad endotherm between 200 and 250 °C which was not observed in the sample which was rapidly quenched to room temperature. In both the samples, a matrix T_g was observed close to 150 °C (top two curves of Figure 15). This endothermic transition has been attributed to the T_g of the amorphous Teflon like backbone material. The endotherm that appears between 200 and 250 °C, we believe comes from the crystalline regions in the sample. In Na+ form Nafion, this endotherm can be eliminated and introduced back into the annealed samples. We have found no significant difference between the melt quenched and annealed samples in their stress-strain behavior. So the crystalline regions must be small and do not contribute significantly to the observed tensile properties.

The high temperature, endothermic transition was observed over a broad temperature range in the as-received Nafion (both Na+ and Cs+ form) due to wider distribution of crystal size with similar ΔH values. As expected for semicrystalline polymers, annealing causes the ΔC_p at the T_g to diminish as the crystalline content of the sample increases. In addition to the differences in ΔC_p, the temperature range for the endotherm at ca 240 °C was found to be narrower in the annealed samples due to a relatively narrow distribution of crystal sizes as compared to the as-received sample. In conjunction, the peak areas and maximum temperatures corresponding to this endotherm increased with annealing time. Moreover, the increase in ΔH was much more rapid in the Cs^+ form than the Na^+ form. The ΔH values were 3.0, 4.8, and 5.3 J/g for samples annealed for 2, 6, and 24 h, respectively, in the range of the as-received membranes (5-6 J/g). In contrast the maximum ΔH value obtained in the Na^+ form is only 50% of the as received samples even after annealing for 24h. The increase in the endotherm peak

temperature is within a small range (from 232 to 237 °C) for the Cs^+ form as compared to the wider range for Na^+ form (from 225 to 240 °C). These results suggest that the crystalline ordering occurs more easily with Cs^+ counterion. Furthermore, this suggests that electrostatic interactions between the ionic sites influences the ordering of crystalline regions in the sample. In the Cs^+ form, these interactions are relatively weak as compared to the Na^+ form. Due to weak ionic interactions, the mobility of the side chains is higher in the Cs^+ form. This side chain mobility in turn facilitates organization of the crystalline domains during annealing. However, in the Na^+ form, the side chain mobility is greatly restricted leading to slow and incomplete development of the crystalline regions.

Figure 16 shows DSC thermograms for the precursor form of Nafion. The as-received sample showed a broad endotherm between 100 and 250 °C. On melt quenching this is reduced in intensity, but still observed. The thermal behavior is complex on annealing at 150 °C, with an endotherm 20 °C above the annealing temperature, additional transitions below and above this. The sample when annealed at 200 °C for 1/2h and 6h and the ΔH value did not change (ca 1.0 J/g) but the temperature of the endothermic peak maximum increased from 216 to 223 °C. This analysis confirms that there is a small amount of crystallinity in the precursor which melts over a wide range of temperatures beginning as low as 100 °C. Due to the absence of ionic groups, the side chains in the precursor are not anchored and can provide the mobility needed to induce melting of the small crystals present. Also, annealing does not cause significant morphological changes because the side chains are extremely mobile. In the neutralized form (Cs^+ and Na^+), however, the side chains are restricted in mobility which "locks-in" the crystalline structure upon annealing.

To investigate the formation of a wide distribution of crystallite size in Cs^+ form Nafion, melt quenched samples were annealed at different temperatures for a constant time. Figure 17 shows the DSC thermograms of the as-received Nafion Cs^+ form melt quenched from 330 °C and annealed at temperatures between 120 and 240 °C. On annealing at 120 °C, an endotherm over the "matrix glass transition" (similar to enthalpy relaxation) is observed. This endotherm increased in intensity and moved to higher temperature as the annealing temperature was increased. The endotherm peak is 20-30 °C higher than the annealing temperature for all the samples. The ΔH value increased from 0.3 J/g (for an annealing temperature of 120 °C) to 3.0 J/g (for an annealing temperature of 210 °C). A further increase in annealing temperature to 240 °C caused an increase in the peak temperature; however, a reduction in the resulting ΔH value was observed. This behavior is attributed to a competitive melting and crystal formation at 240 °C. These results suggests that the morphology leading to this endotherm around 250 °C is due to crystalline regions in the sample as seen both in the precursor and neutralized samples.

I. Dynamic mechanical properties of Nafion PFSI membranes

As-received Nafion membranes were neutralized as in the DSC experiments and analyzed for their thermal behavior by DMA. In agreement with the DSC data, the amorphous content in the sample increases after melt quenching the sample (seen by increase in height of the tan δ peak at 150 °C). This effect is observed in both Na^+ and Cs^+ neutralized samples. On annealing the samples, the tan δ peak shifts to higher

temperatures and reduces in intensity due to increased crystallinity. Another well defined loss peak was observed in the annealed sample corresponding to the melting of the crystalline region in the DSC at 240 °C.

PROCEDURE: Melt quenched and annealed samples for DMA were prepared at temperatures which were identical to those used in the DSC experiment. The melt quenched sample was obtained by heating a Nafion film to 330 °C in an muffle oven and cooling back to room temperature rapidly. Part of this sample was then annealed at 200 °C for 24 h. DMA data were collected on a Seiko Instruments SSC/5200H DMA at 4 °C/min under N_2. Multi-frequency mode was used to calculate the E_A.

RESULTS: The DMA results are given in Figures 18 and 19. In the storage modulus plot, the melt quenched sample has a lower modulus than the annealed sample throughout due to a lower degree of crystallinity. This lack of crystallinity is also the cause of an increased drop in modulus at the T_g for the quenched sample. The melt quenched sample showed a gradual reduction in modulus after this due to gradual disruption of the ionic clusters. In the annealed samples there is a second well defined drop in the modulus at a temperature corresponding to the melting of the crystalline regions observed in the DSC data. The tan δ peak at ca 150 °C is more intense in the melt quenched sample than the annealed sample (Figure 8). This confirms that, on annealing, a significant fraction of the amorphous content is converted to crystalline domains thus causing the tan δ peak to shift to higher temperatures and reduce in intensity. This behavior is consistent with similar experiments on semi-crystalline poly(vinylidene flouride). The energy of activation for the matrix glass transition for Nafion was found to be ca 500 kJ/mol for both Na^+ and Cs^+ form. The tan δ curve showed a narrow loss peak as a shoulder at 240 °C in the annealed sample due to melting of the crystalline region. This is not observed in the melt quenched sample due to lack of crystallinity.

II. Figures

FIGURE 1: Two-dimensional small angle X-ray diffraction patterns of oriented TBA^+-form Nafion®.

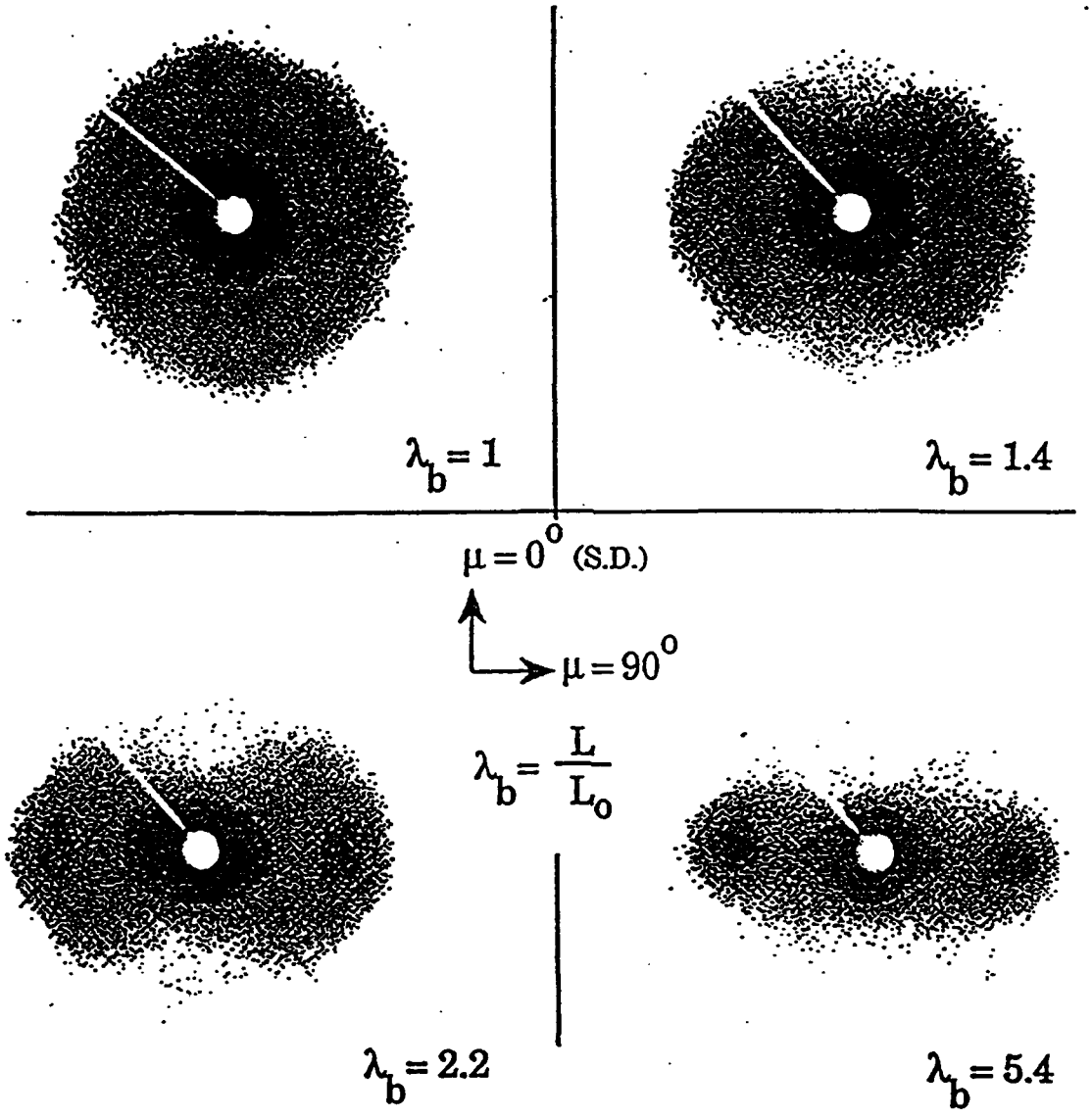

λ_b = extensional ratio

FIGURE 2: Intensity vs q (From integration of 2-D scattering patterns in the equatorial direction, μ= 90°.)

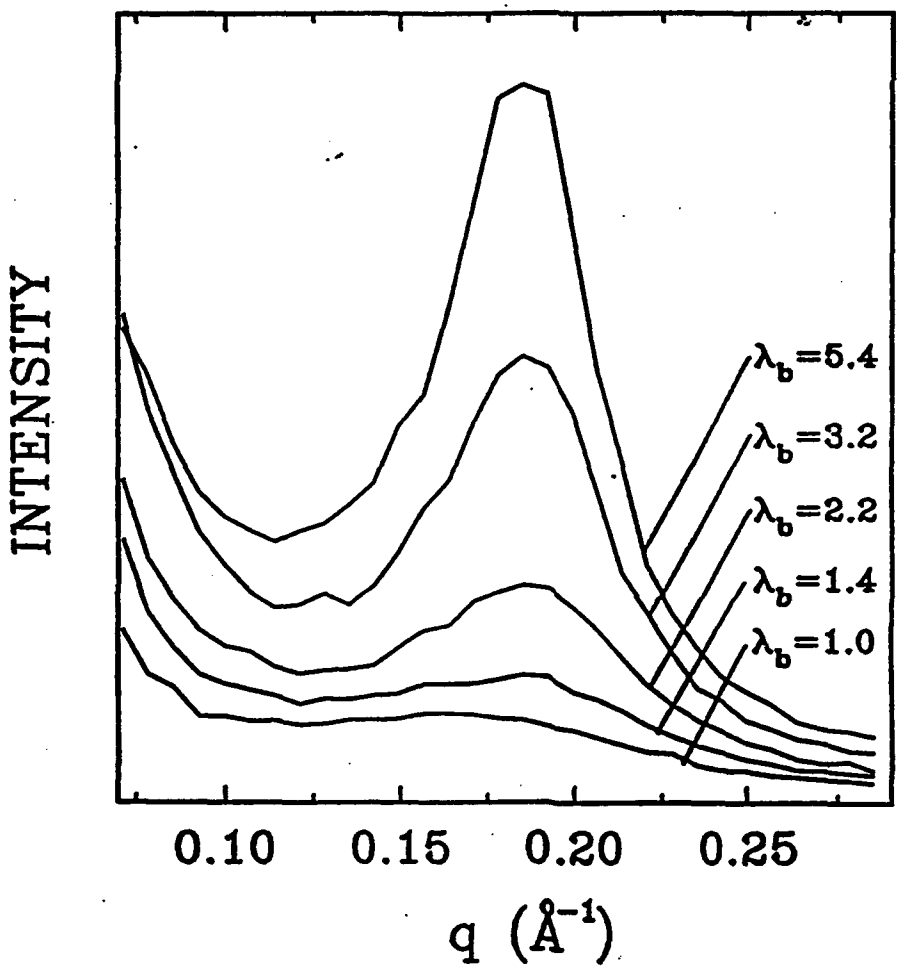

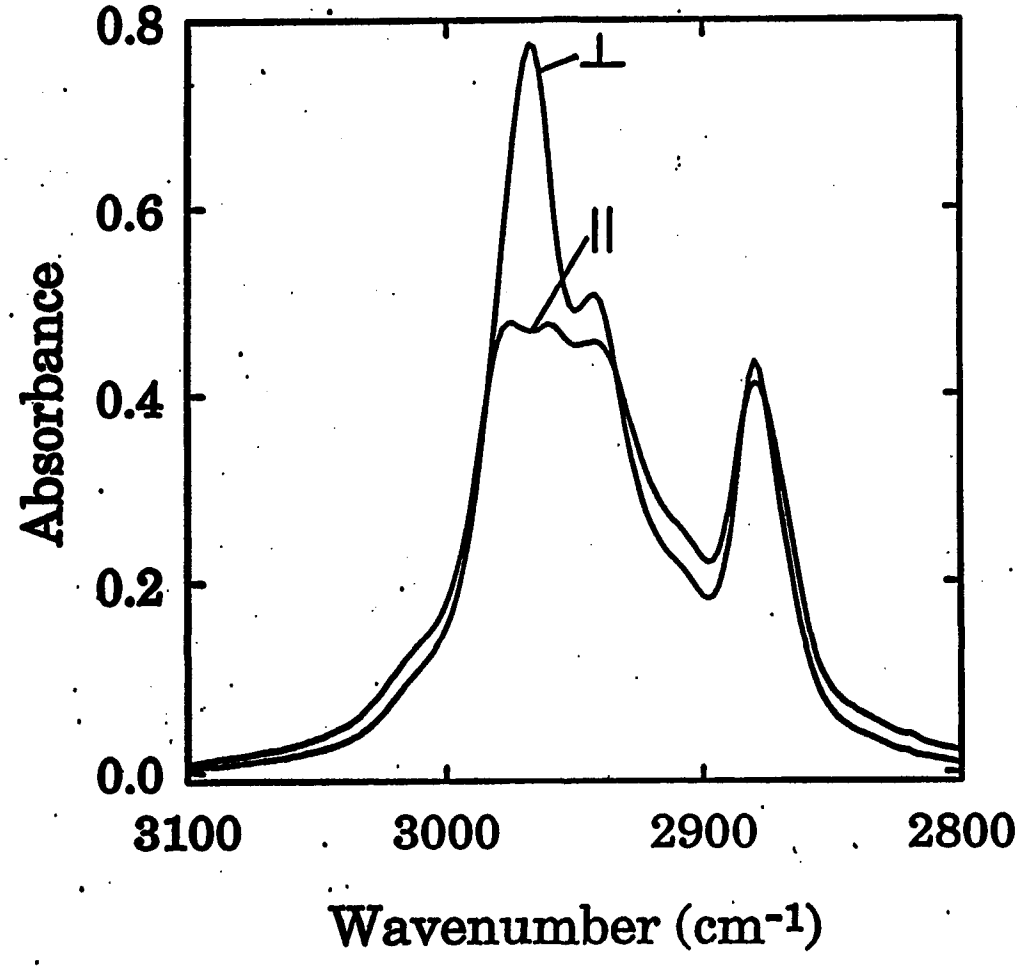

Figure 8. Portion of FTIR spectrum for the highly elongated sample with the polarizer set at an angle of 0°, 45°, and 90° to the stretch direction.

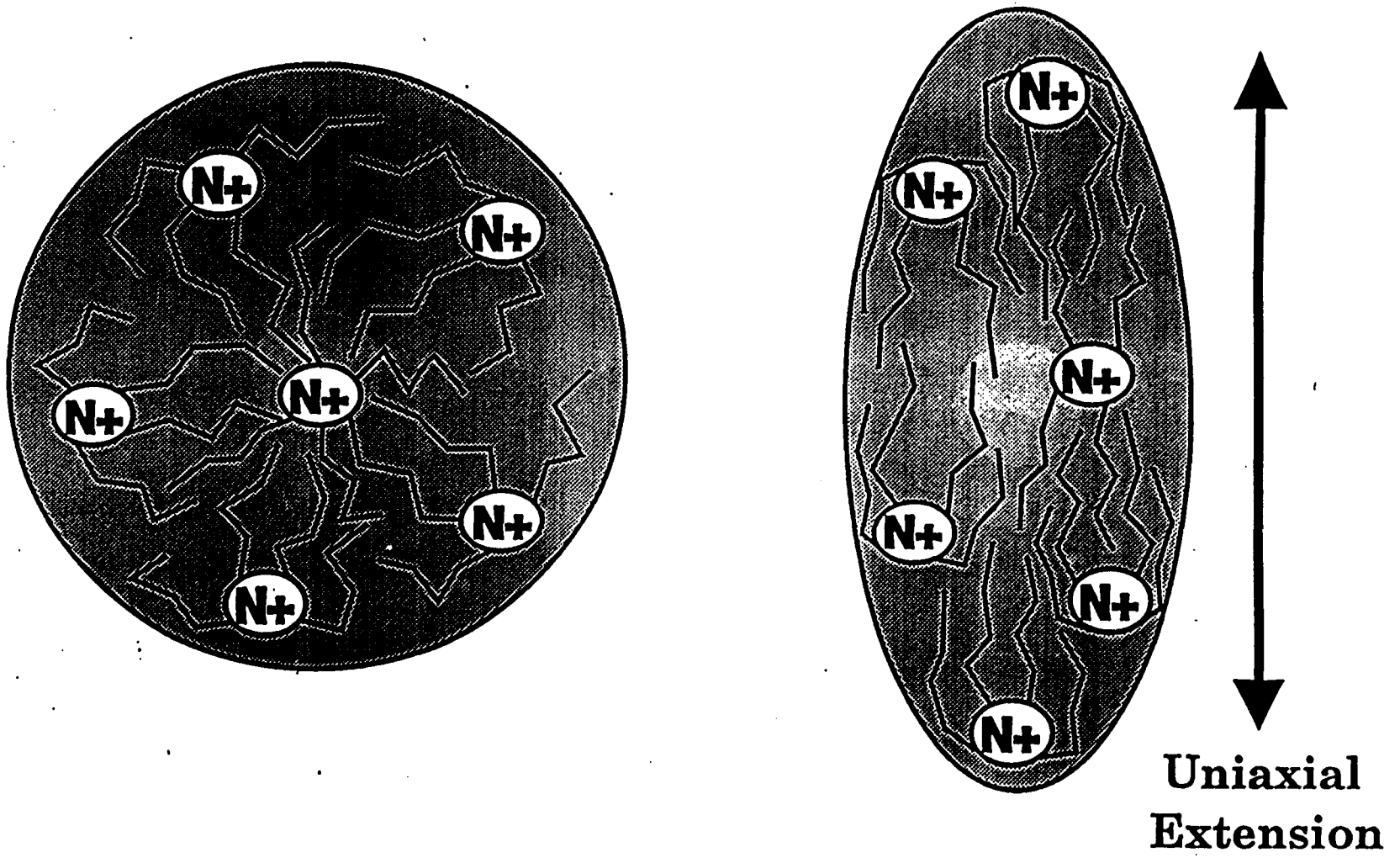

Figure 4. A schematic of cluster deformation with uniaxial extionsion.

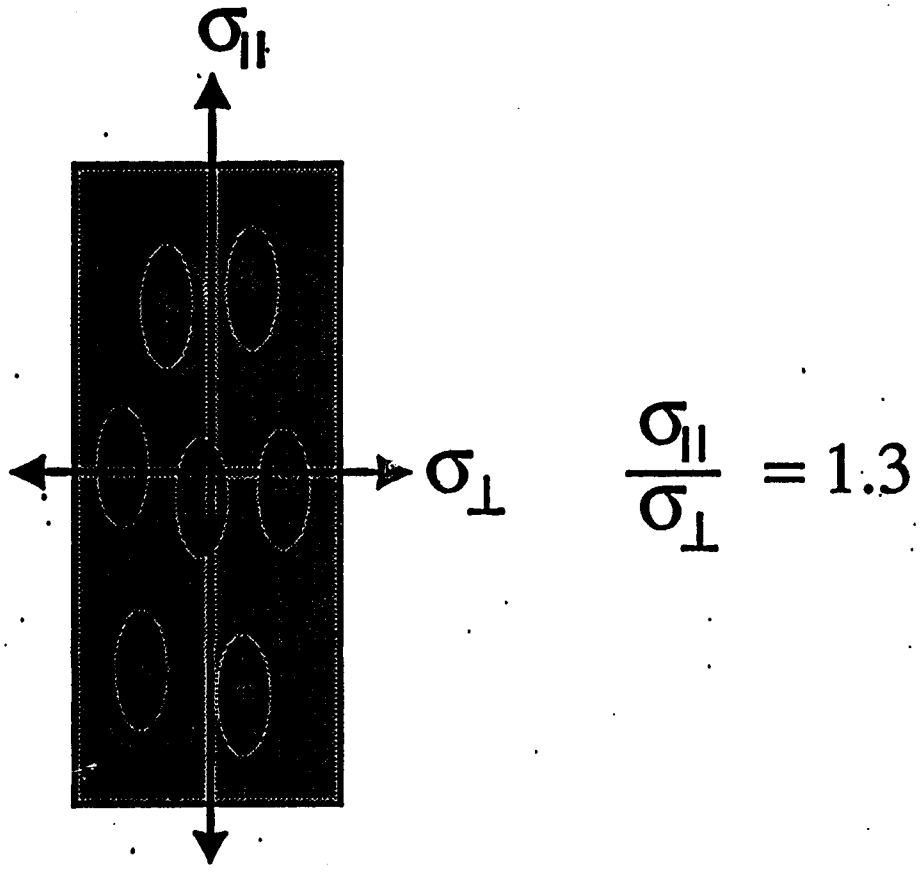

Figure 5. Anisortropic ionic conductivity in permanently oriented PFSI membranes. $\sigma_{\parallel}$ = conductivity parallel to the stretch direction; $\sigma_{\perp}$ = conductivity perpendicular to the stretch direction.

Figure 6. Water uptake for Nafion/Dow blends.

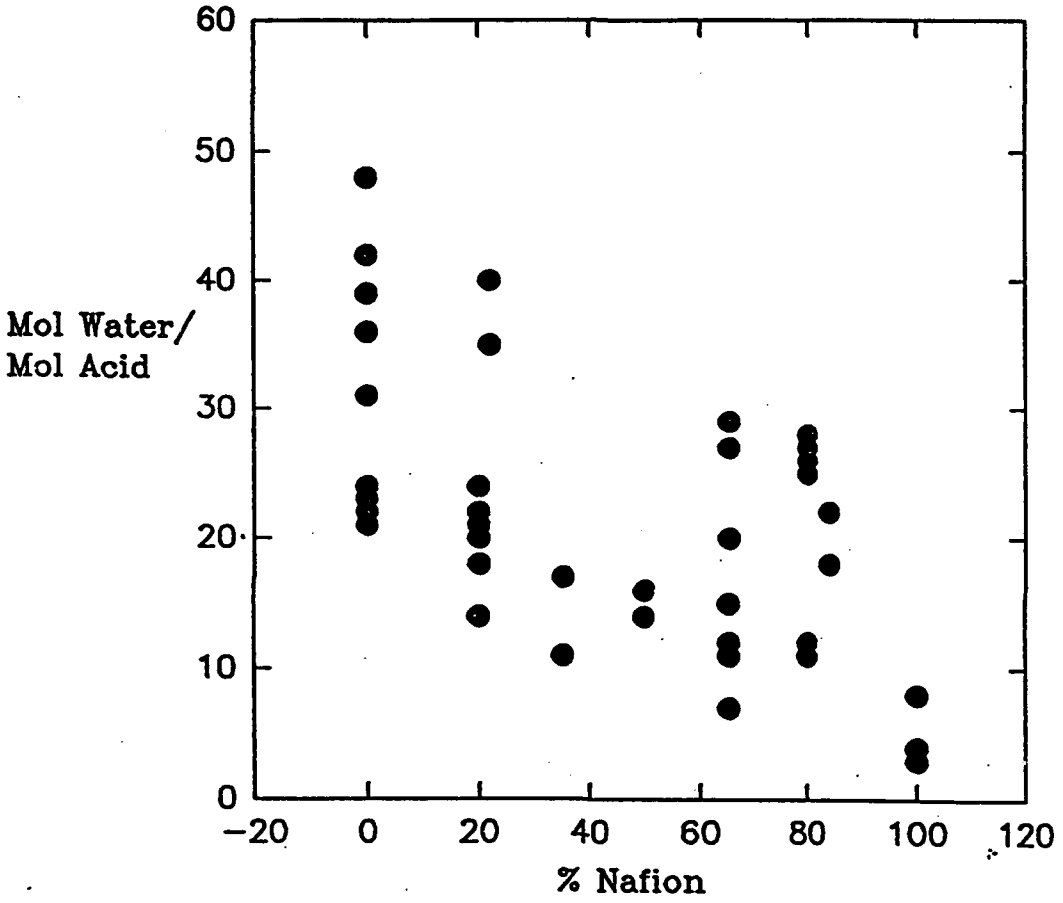

Figure 7. Portion of the IR spectrum showing the SO_3^- symmetrical stretch at ca. 1060 cm^{-1} and the C-O-C symmetrical stretch at ca. 980 cm^{-1} and 965 cm^{-1}.

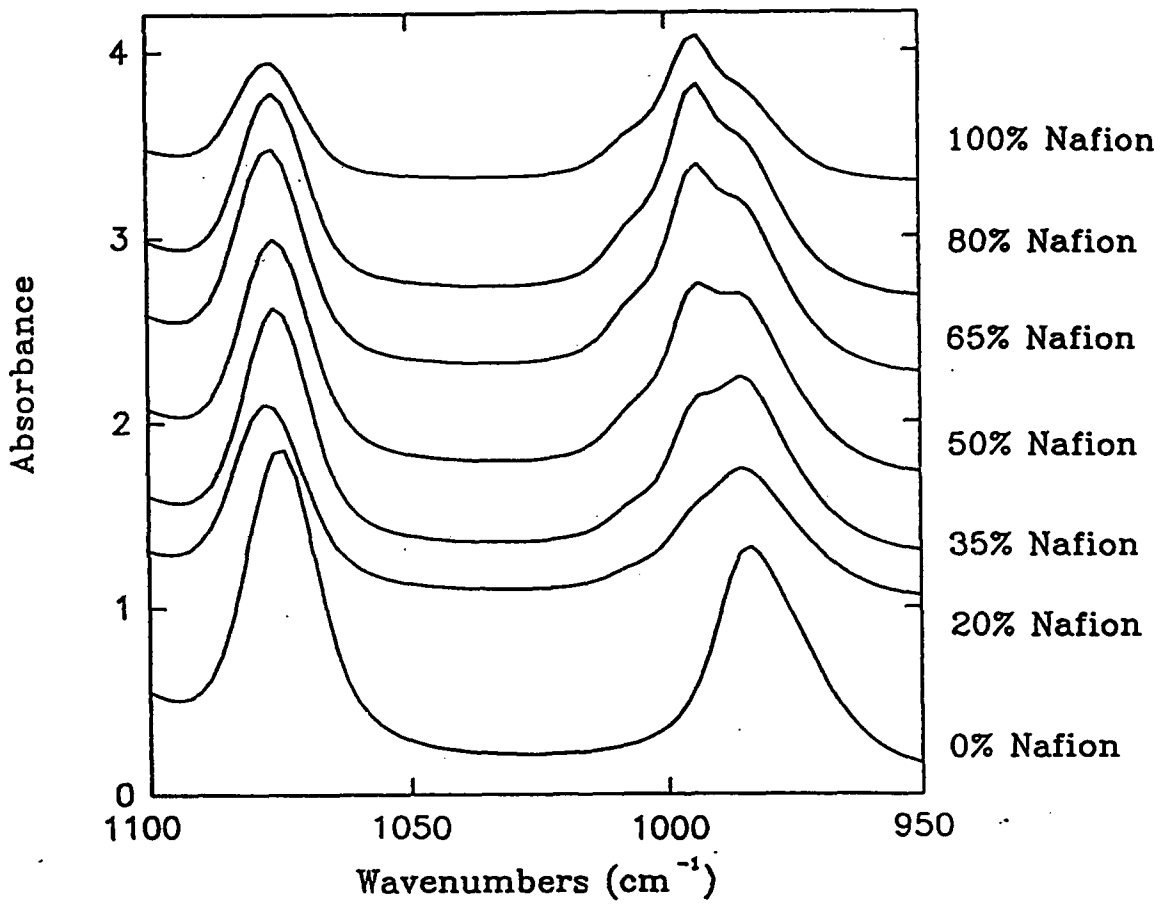

Figure 8. DSC endotherms showing cluster endotherm at ca. 240°C.

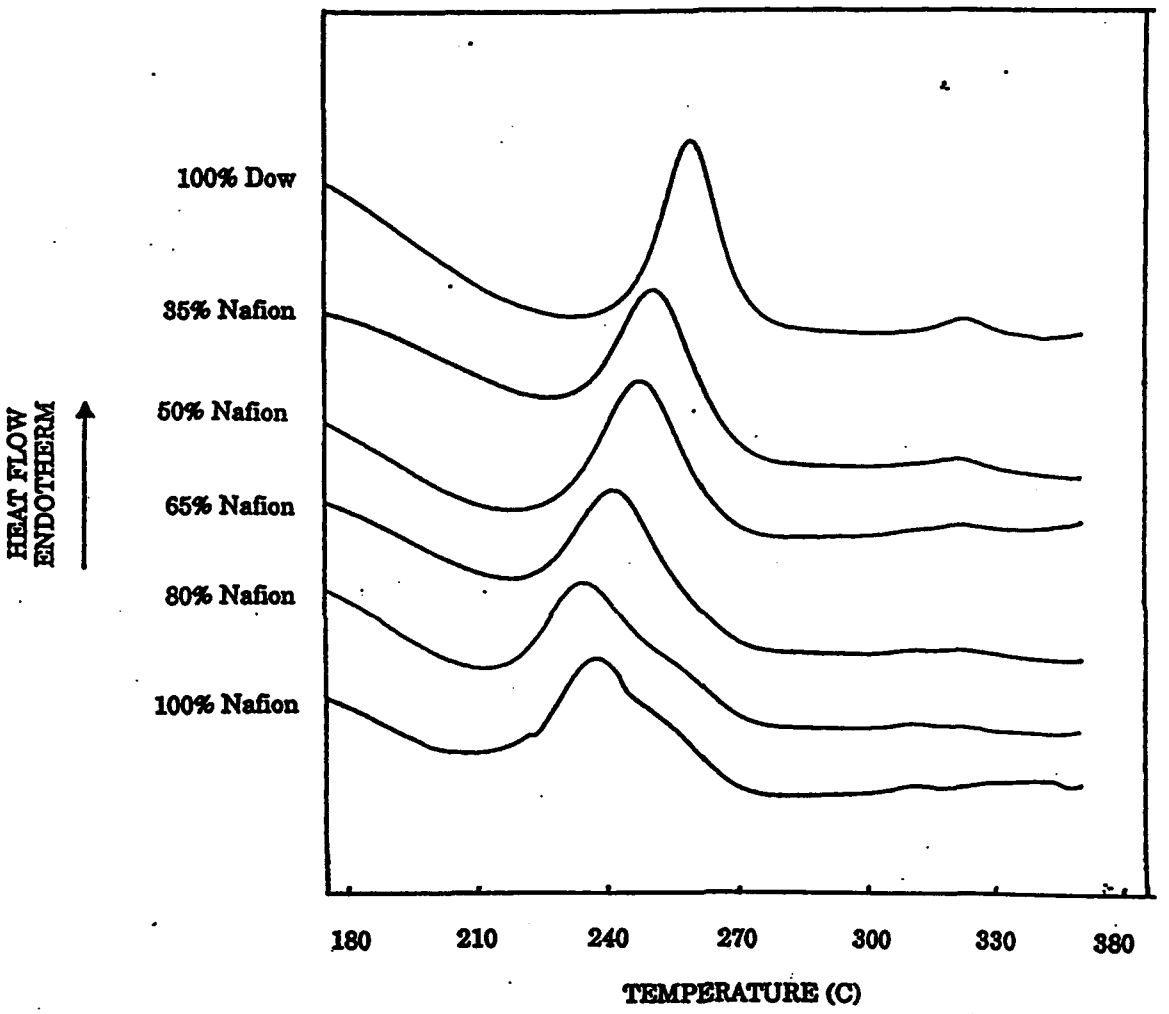

Figure 9. d_{BRAGG} vs % Nafion

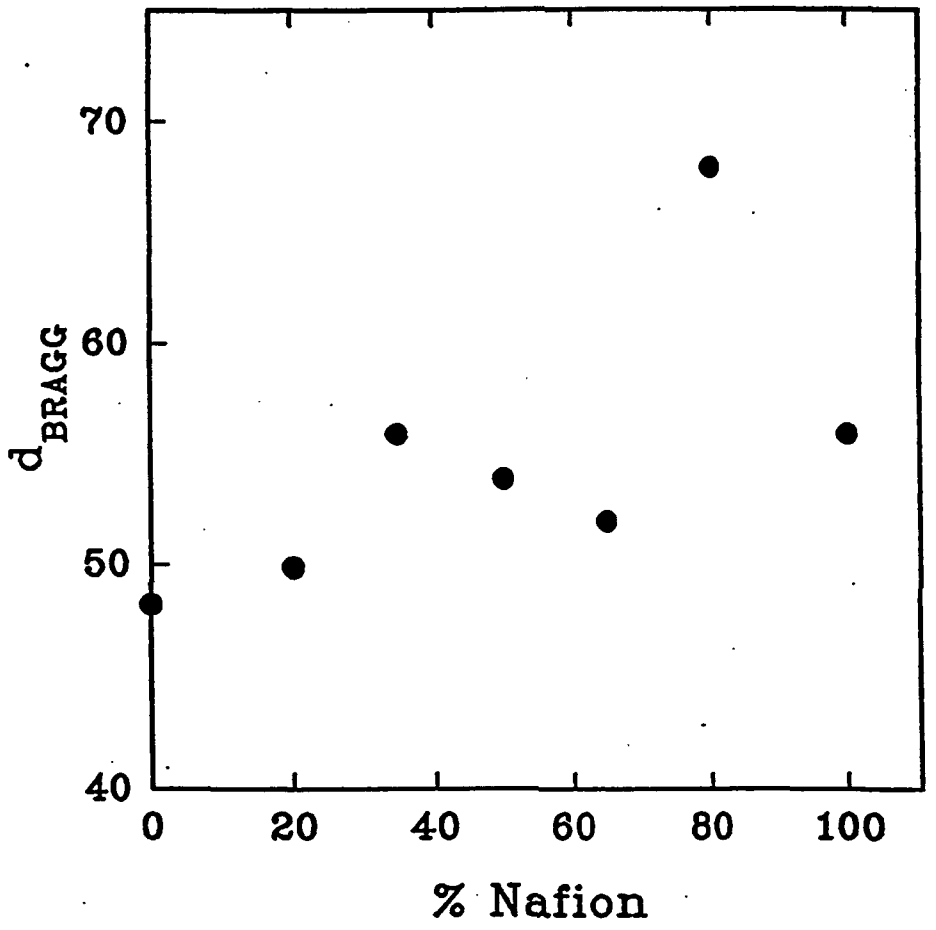

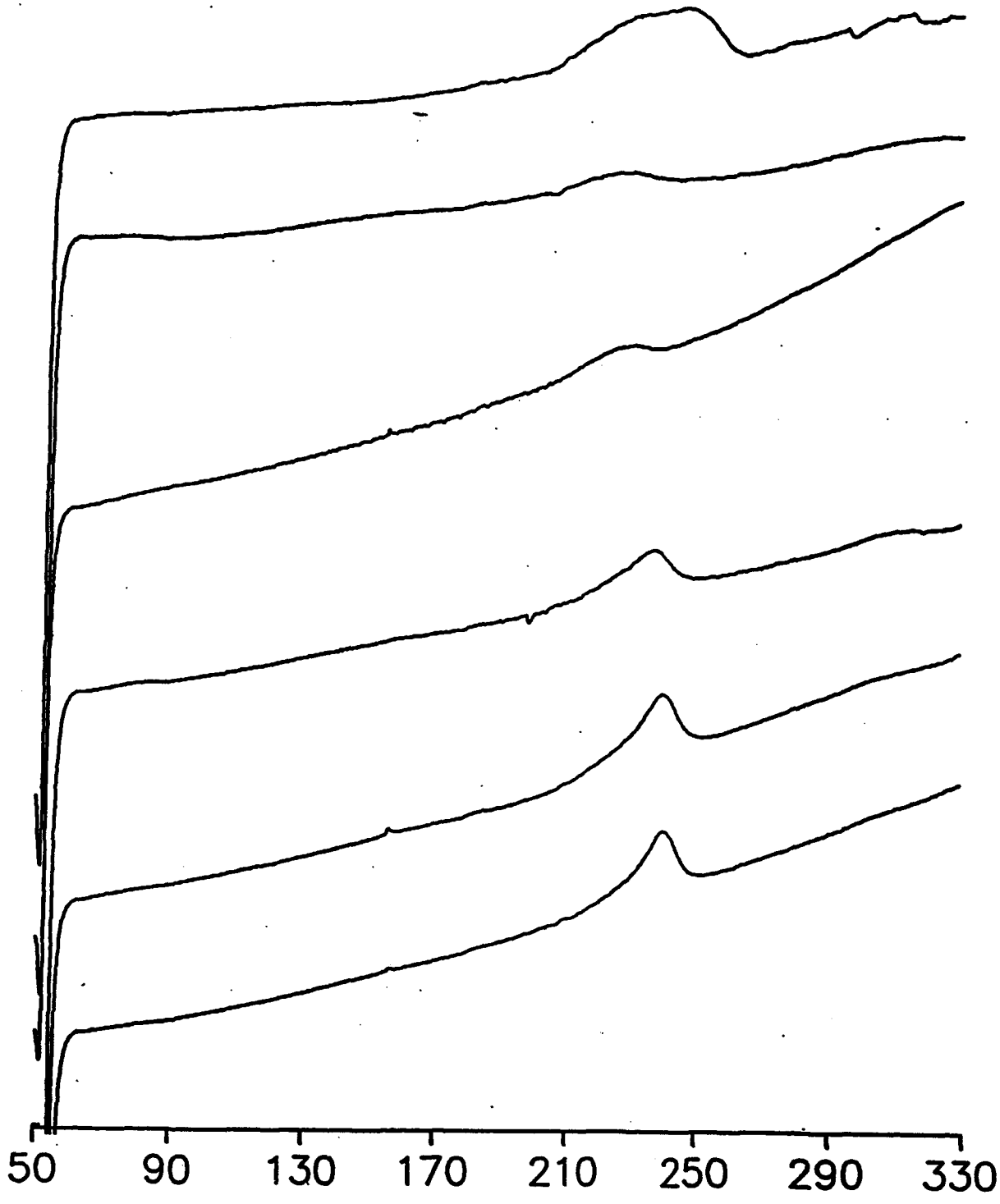

Figure 10. DSC thermograms of as received Nafion, Nafion annealed at 200 °C for 1/2, 2, 6, 12, and 24 h, top to bottom respectively, after taken up to 330 °C.

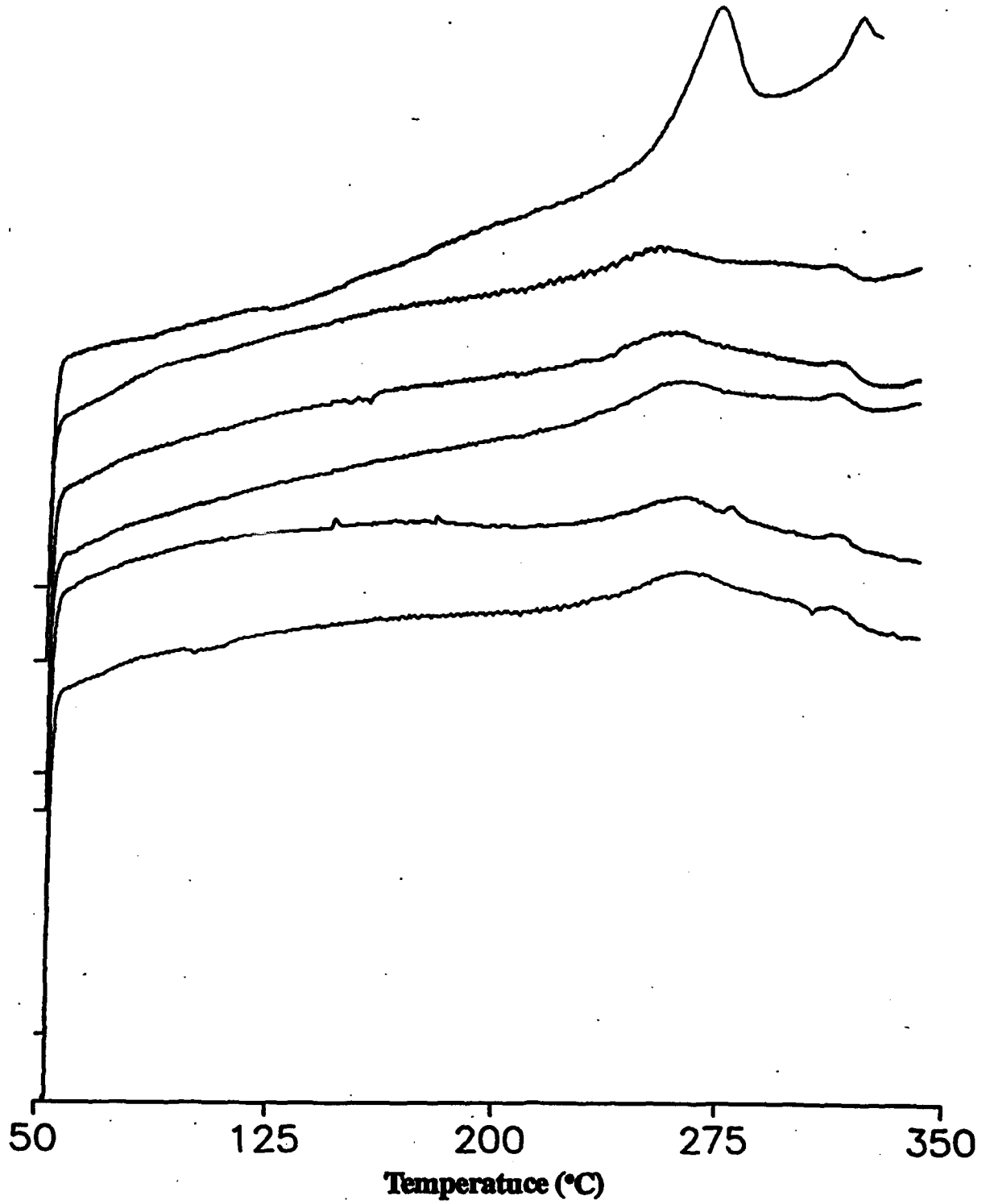

Figure 11.DSC thermograms of as received Dow PFSI membrane, annealed at 230 °C for 1/2, 2, 6, 12, and 24h, top to bottom respectively, after taken upto 350 °C.

Figure 12. Stress-Strain plots for Nafion as recieved membranes

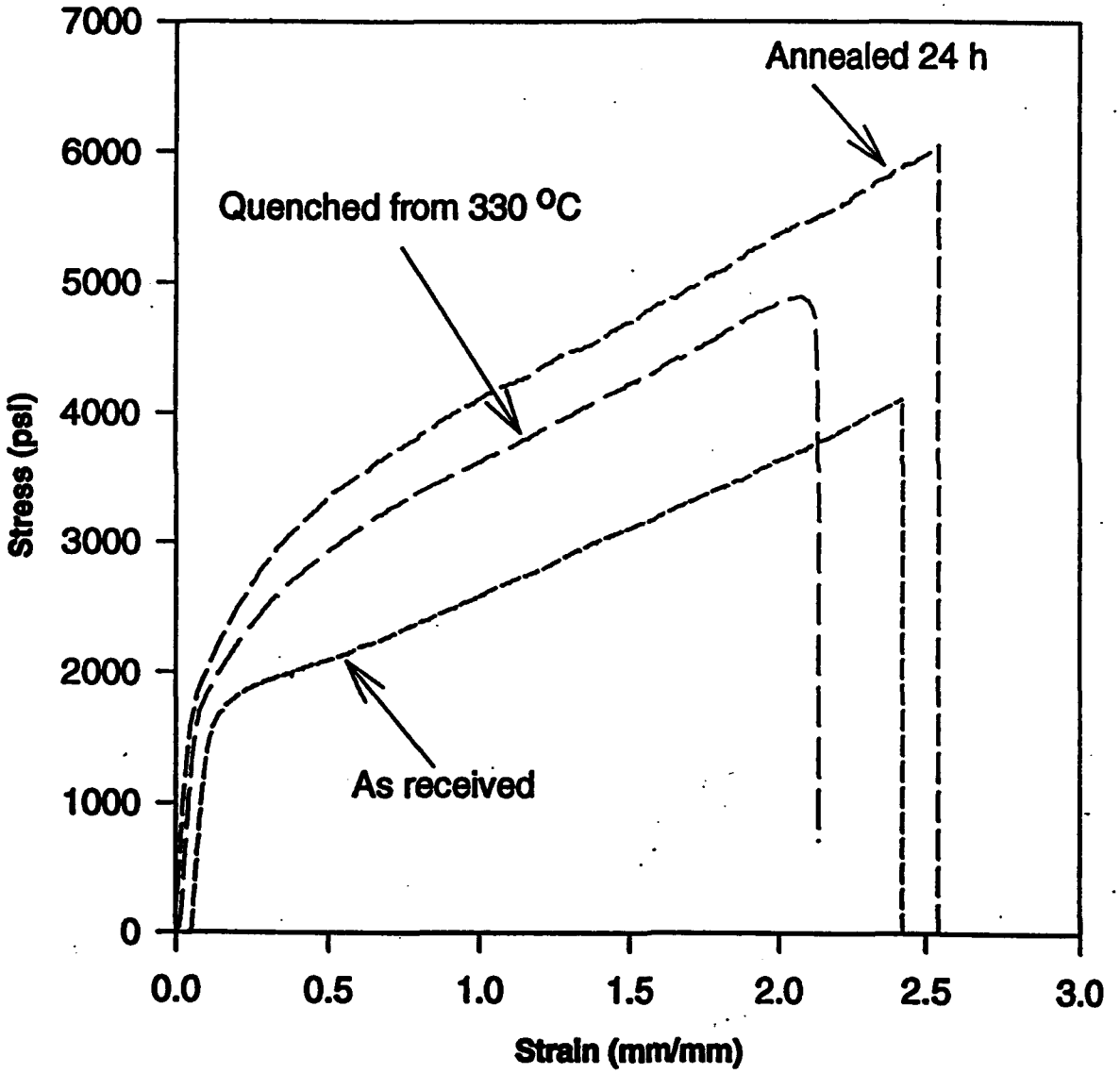

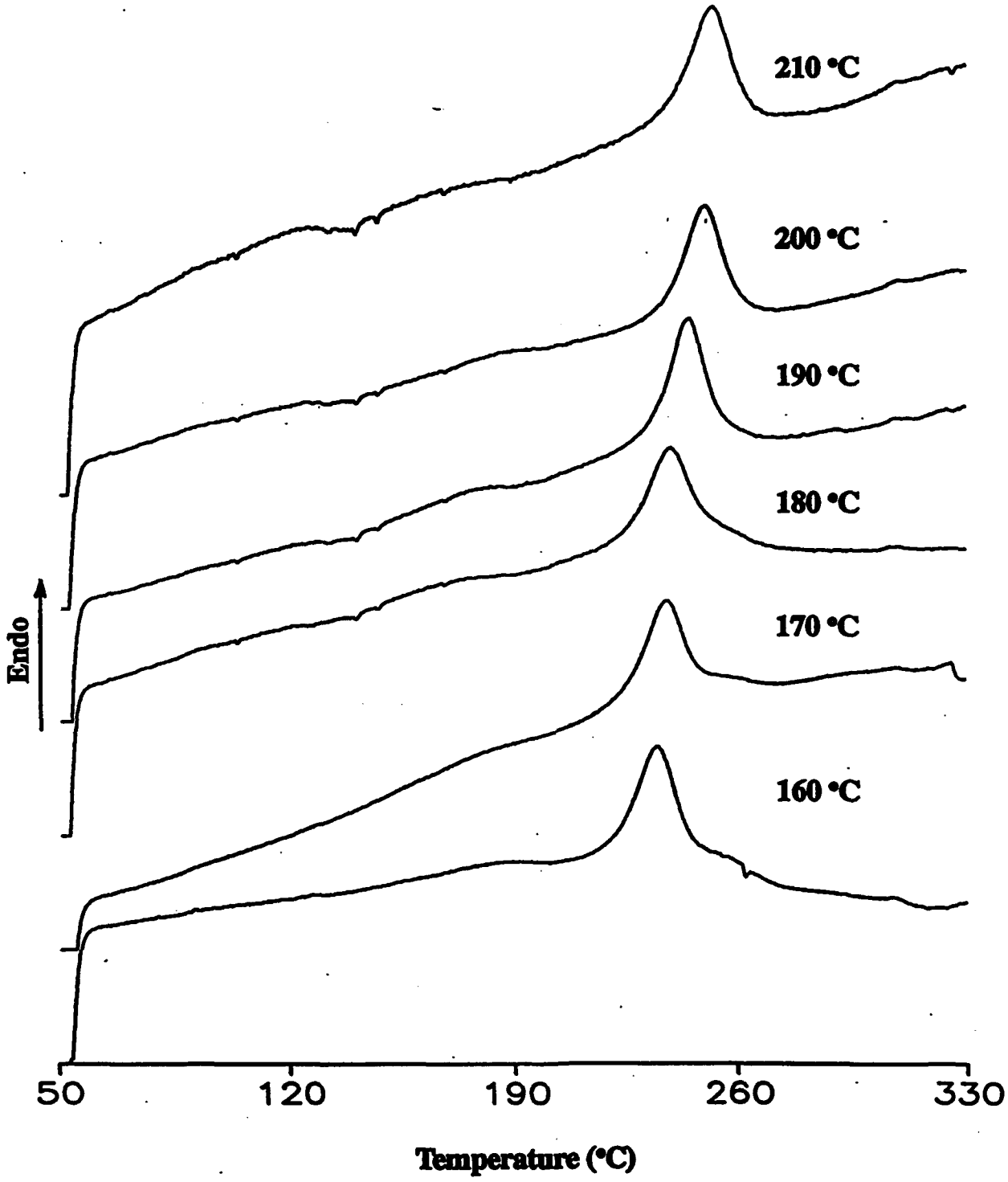

Figure 13.. DSC thermograms of solution processed Nafion (1100 EW) processed at temperatures as given

Figure 14. Stress-Strain Plots of Nafion Membranes Solution Processed at Different Temperatures and as Received Membrane

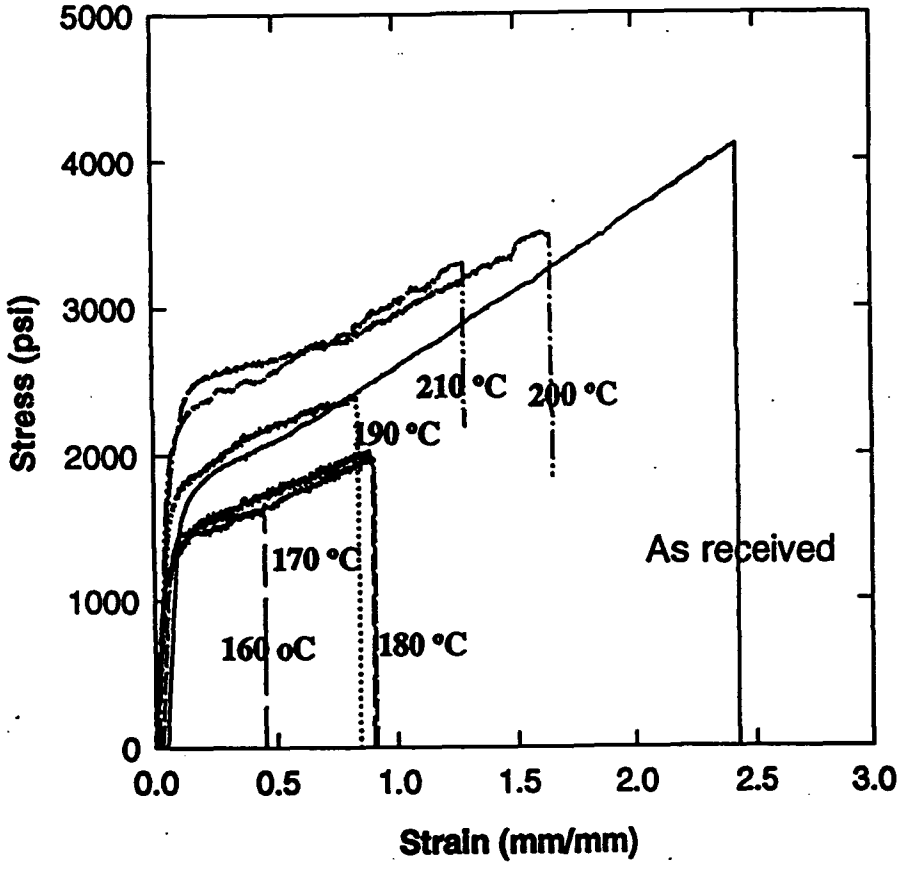

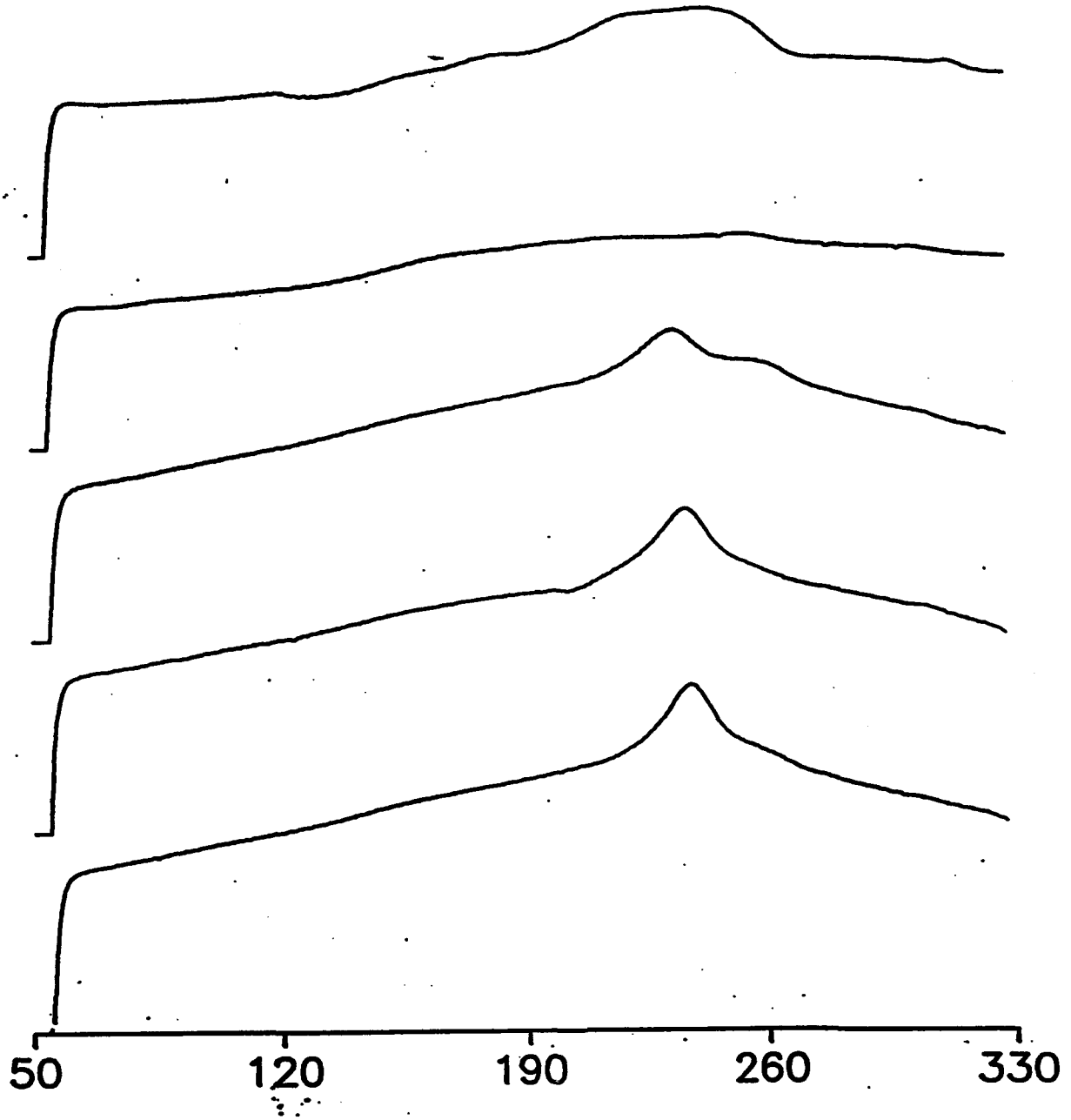

Figure 15. DSC thermograms of Nafion Cs+ form as received, melt quenched, and annealed at 200 °C for 2h, 6h, and 24h, respectively,(top to bottom).

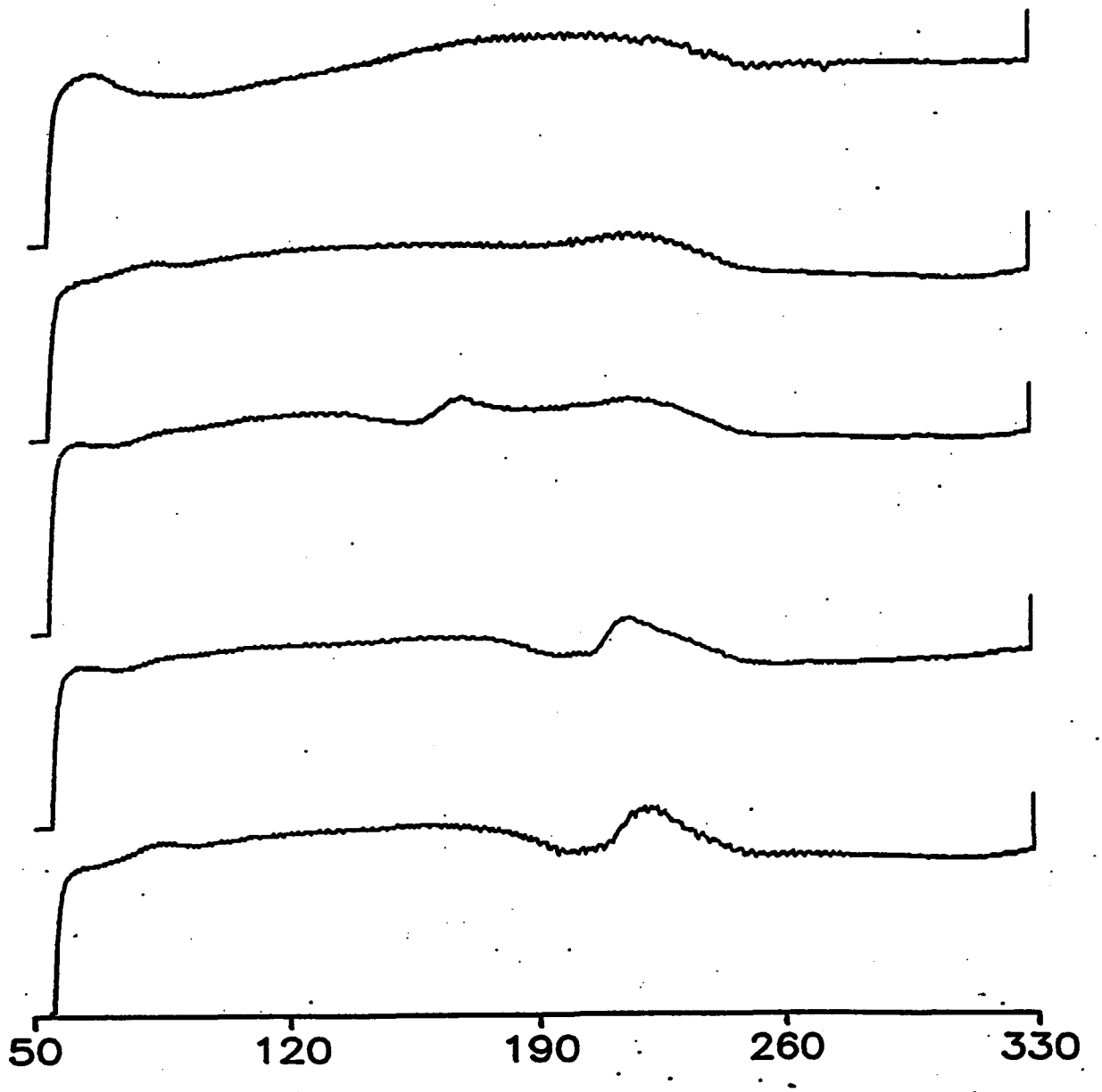

Figure 16. DSC thermograms of Nafion precursor (SO_2F form) as received, melt quenched, annealed at 150 °C (1/2h), annealed at 200 1/2h, and 6h, respectively (top to bottom).

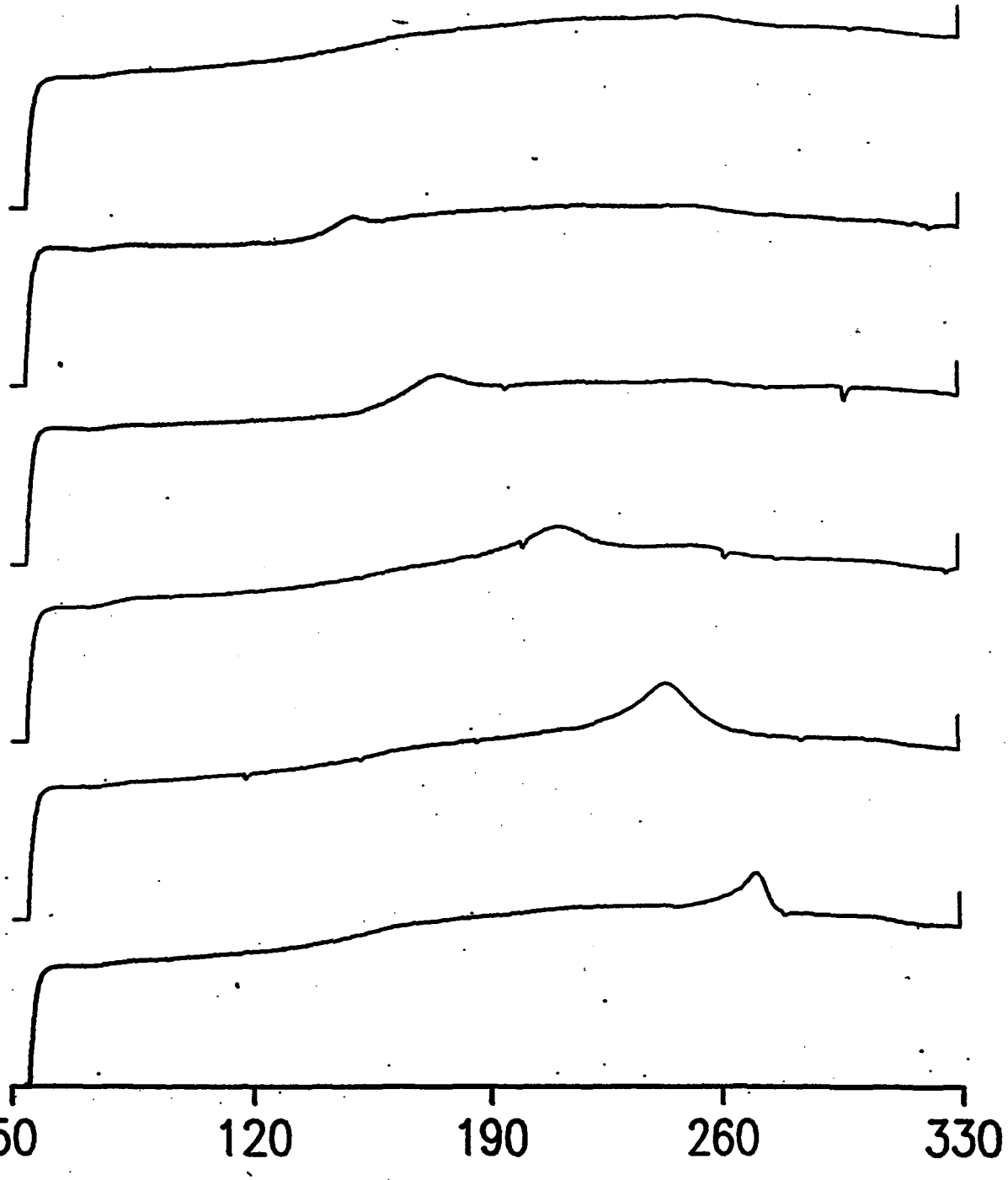

Figure 17. DSC thermograms of Nafion Cs+ form melt quenched, annealed for 2h at 120, 150, 180, 210, and 240 °C, respectively (top to bottom).

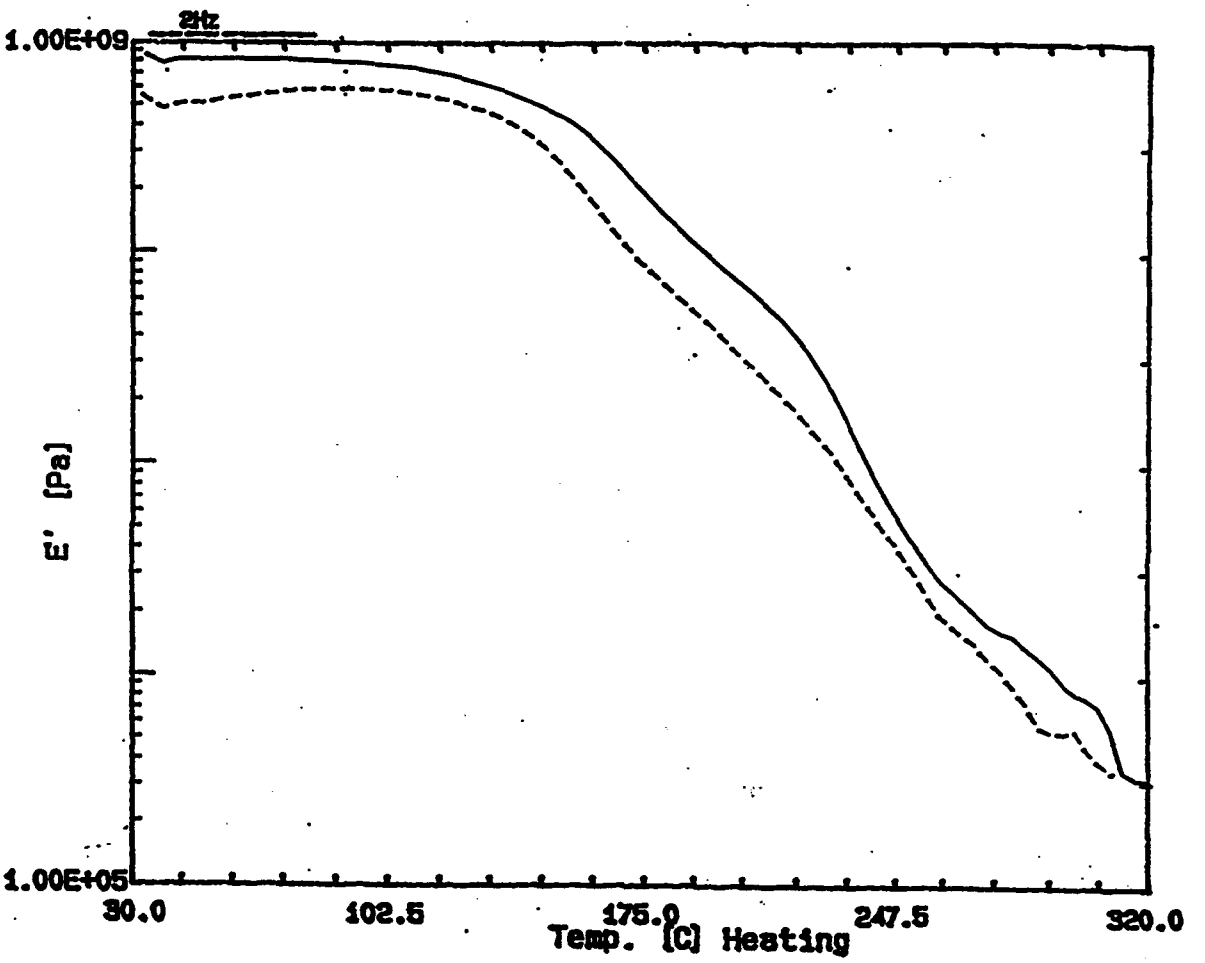

Figure 18. DMA analysis (storage modulus) of Nafion Cs^+ form melt quenched from 330 °C (- - -) and annealed at 200 °C for 24 h (- - -) after melt quenching from 330 °C.

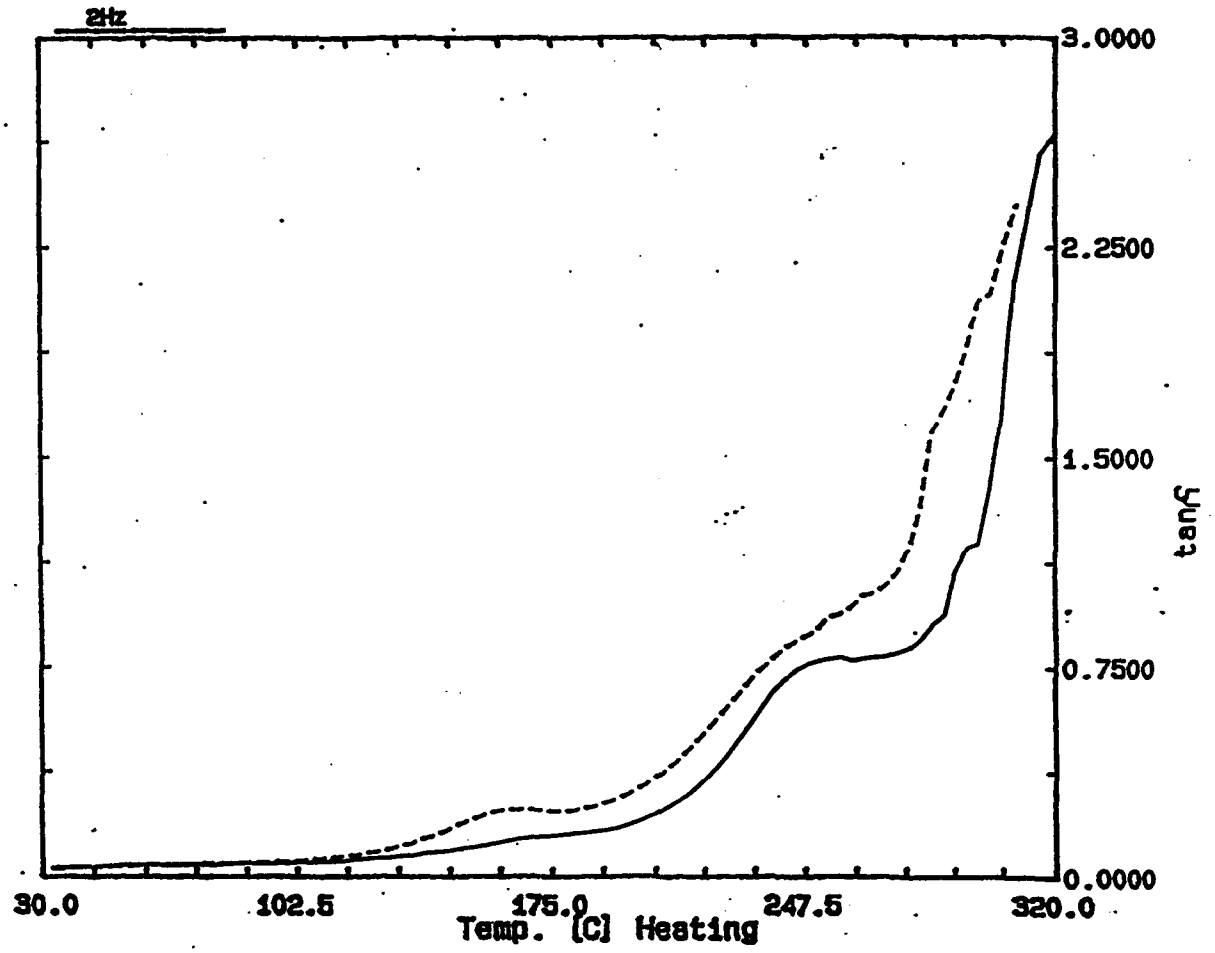

Figure 19. DMA analysis (tan δ) of Nafion Cs^+ form melt quenched from 330 °C (- - - -) and annealed at 200 °C for 24 h (- - - -) after melt quenching from 330 °C.

RESEARCH REPORT TO AFOSR

June 13, 1994

PART II

TABLE OF CONTENTS

PART II

The following is the work of S.V. Davis, Graduate Student, and K.A. Mauritz, Professor

I. Development of [Silicon Oxide]/PFSI Nanocomposites

A. PFSI Template Film Initialization Procedure

We reevaluated our past PFSI sample initialization procedure. The purpose of initialization is to render the PFSI to a *standard chemical state* prior to possible ion exchange to a cation-sulfonate form other than H^+, or if the film is simply used in the acid form. Ion exchange, if performed, occurs prior to the *in situ* sol-gel reaction for inorganic alkoxides. In one previous procedure, soaking in concentrated hydrochloric acid, followed by dialysis in DI water for two days to leach out excess acid, the films were able to sustain high temperatures (ca. 100°C) without discoloration. A second procedure consisted of using 50% nitric acid (refluxing) to initialize the films, followed by ultrasonication in water to aid in dialyzing excess acid from the film. This procedure resulted in a darkening of the film. We prefer that our samples have optical clarity.

In consideration of the industrial processing of these films, and taking into account advantages of both of the above methods, the following procedure was developed. First, the films are refluxed in 50% hydrochloric acid to reduce any residual DMSO (-introduced during conversion of films from the sulfonyl fluoride to the metal-sulfonate form). Second, the films are refluxed in distilled deionized water to prevent aqua regia formation in step three. Step three consists of refluxing the film in 50% nitric acid to perform the final exchange to the H^+ form and to remove salt forms (nitrates are more soluble than chlorides). Following initialization, the films are successively refluxed in methanol and three rounds of distilled deionized water until neutral pH of the solution (postrefluxing) is achieved.

It is expected that this careful procedure will lead to greater control over the *in situ* sol-gel reaction as excess, undesired acid catalyst is removed. Acid catalyzes the hydrolysis of the inorganic alkoxides. In order to impart all samples with a common swelling, chemical and thermal history, the ion exchange procedure has been modified to mimic the initialization procedure. Here, we reflux the initialized PFSI in a salt solution (nitrate or chloride, if the sulfate is not highly soluble). Next, we reflux the film in the sulfate form as the materials are in the sulfonate form to "hide" the effect of any anion that may resist removal by dialysis. Last, the films are refluxed according to the same procedure as the dialysis of the initialization step.

In addition to avoiding discolored films that do not contain unwanted free acid, this careful, uniformly-applied procedure promotes sample reproducibility.

B. Oriented PFSI/Silicon Oxide Nanocomposites

1. Concept

We utilized the nanometers-in-size polar clusters within PFSI films as reaction vessels in which $SiO_{2[1-x/4]}(OH)_x$ nanoparticles nucleate and grow via *in situ*, acid catalyzed sol-gel reactions for tetraethoxysilane (TEOS). It is our working hypothesis that the resultant morphology of the inorganic phase is directed by the clustered + semicrystalline morphology of the ionomer. This concept is illustrated in Figure 1. Given this hypothesis, and based on our earlier work,[1-5] we proceeded to formulate oriented nanocomposites via sol-gel reactions for TEOS within clusters possessing significant aspect ratios affected by uniaxial mechanical film orientation as illustrated in Figure 2. Clusters, assumed to possess rough spherical symmetry in the unstressed state, will elongate in the draw direction, as we have established and discussed earlier in this report. Whether or not this is an affine deformation is an interesting question that needs to be explored in future investigations. Additionally, PTFE-like crystallites between clusters may become realigned upon deformation so that polymer chains, on the average, lie more so in the draw direction.

Structural proof and extent of orientation is being determined via SAXS investigations of oriented, filled films as well as of unoriented, filled films that serve as a control. SAXS is sensitive to difference between the electron densities of the cluster and matrix phases. Therefore, a 2-D SAXS pattern reflects intercluster periodicities in different directions.

Anisotropic nanocomposites will possess different properties along different directions. Tensile modulus, strength, and toughness as well as elongation-to-break will be different for transverse and longitudinal film directions. Gas permeability and dielectric permittivity will be be sensitive to microstructural anisotropy. For optically transparent nanocomposites (heterogeneities with dimensions $\ll \lambda_{light}$), index of refraction should different for transverse and longitudinal directions.

2. Experimental Procedure

5 mil thick Nafion 1100 EW, K^+-form membranes were supplied by E.I. DuPont Co. TEOS, $CoSO_4$ metal salt, and methanol were all used as-received. In order to ensure that the as-received samples were in a known chemical state, they were initialized to the H^+-form by first refluxing them in a 50:50 v/v ratio of concentrated HCl and deionized H_2O for 24 hours to oxidize possible residual DMSO that may be present from industrial processing. The membranes were then dialyzed in deionized H_2O to leach out excess acid and refluxed again in a 50:50 v/v ratio of concentrated HNO_3 and deionized H_2O for 24 hours. After refluxing, the membranes were dialyzed in a series of deionized H_2O - then methanol - to leach out excess acid. The final reflux used both deionized H_2O and methanol.

We have discovered that, beyond a certain silicon oxide uptake threshold, Nafion H^+-form films form a layer of silica on the surface during the sol-gel reaction and subsequent drying. To inhibit this surface-attached glassy layer, the membranes were ion exchanged prior to the sol-gel reaction by refluxing the initialized membranes in a saturated solution of $CoSO_4$ for 24 hours. We determined that the cobalt form inhibits the

surface SiO_2 layer. The membranes were again refluxed in a series of deionized H_2O - then methanol - to leach out excess metal salt with the final reflux in deionized H_2O and methanol. After ion exchange, the membranes were vacuum-dried at 100°C for 2 days.

For comparison, several of these membranes were reacted with TEOS under no mechanical stress after vacuum-drying. The membranes were first allowed to swell in methanol and deionized H_2O for 5 hours. A mixture of TEOS and methanol was then added and allowed to permeate the membrane for different times. The films were then rinsed with methanol and annealed at 230°C for 2 days to remove volatiles and promote the condensation reaction for SiOH groups.

An Instron 1130, in conjunction with an in-house designed liquid reaction cell that fits around the clamped, strained film, was used to generate oriented nanocomposites. We modified the drive mechanism of the Instron (via a designed-fabricated gearbox) to stretch specimens at low rates. This system is pictured in Fig. 3. The samples were prepared as follows: A 2.54 cm x 4.00 cm Co^{++}-exchanged membrane was placed in modified Instron grips. To begin the sol-gel reaction, the liquid cell was first filled with a solution of methanol and deionized H_2O, allowing the membrane to swell for 20 minutes. During swelling, the solution was purged with argon gas, and the strain increased until a strain of either 50%, 100%, or 150% was attained and held constant. The solution was then drained and a mixture of TEOS and methanol added and allowed to permeate the film and react for a given amount of time while under the constant strain. The TEOS/MeOH solution was then drained and the film rinsed with methanol and purged with argon gas. While still under constant strain, the sample was annealed-dried at 220°C for 20 minutes to drive the condensation *reaction* (≡Si-OH + HO-Si≡ → ≡Si-O-Si≡ + H_2O) to completion and promote solidification of SiO_2 within the clusters. A special oven was designed and fabricated to wrap around the sample while still under tension.

3. Small Angle X-Ray Investigations

The hybrids were then investigated for existence of structural orientation using SAXS.

As shown in 2-dimensional SAXS patterns of the nanocomposite films reacted under uniaxial deformation (Figure 4) permanent orientation has indeed been imparted. Films reacted under so-called "medium" stress possess the greatest orientation as evidenced by azimuthal intensity periodicity of 180^0 that is seen in Fig. 5. Presently, we cannot account for the lesser orientation exhibited by the "high stress" sample. It appears, at least qualitatively, that intercluster spacings are different in the transverse and longitudinal film directions.

4. Mechanical Tensile Analysis

Tensile stress *vs* strain curves generated for both the longitudinal (draw) and transverse directions of these oriented nanocomposites were compared to those of unoriented hybrids of similar silicon oxide content (3.1%) and are shown in Fig. 6. The PFSI template was Nafion-Co^{+2}. The transverse direction of the oriented sample exhibited comparatively greater ductility and toughness than the longitudinal direction, although the latter displayed greater strength. Thus, these oriented nanocomposites display mechanical

as well as structural anisotropy, as expected. The unoriented sample showed greater strength than either longitudinal or transverse directions of the oriented sample.

Further SAXS and mechanical tensile studies will be conducted on oriented nanocomposites processed under different conditions. Wide angle x-ray diffraction will probe TFE crystallite orientation, and infrared (including polarized IR) as well as solid state ^{29}Si NMR spectroscopy will provide information on molecular structure within silicon oxide nanoparticles. DSC will be used to investigate crystalline and amorphous transitions as modified by orientation.

The following is the work of Dr. Qin Deng, Postdoctoral Associate, and K.A. Mauritz, Professor

C. In situ-Grown "Shelled" Silicon Oxide Nanoparticles

1. Concept

First, $SiO_{2[1-x/4]}(OH)_x$ particles were grown within initially hydrated, alcohol-swollen Nafion (1100 EW, 5 mil-thick) membranes via *in situ* sol-gel reactions for TEOS as in our earlier work. SO_3H groups in clusters catalyze alkoxide hydrolysis within these "nano-reactors." The array of clusters, with center-to-center spacings of 30-50Å, offers an interactive polymerization template that directs the morphology of the resultant dry, solid silicon oxide phase.

Our IR and ^{29}Si solid state NMR spectroscopic investigations of such dried-annealed systems indicate large relative populations of uncondensed Si-OH groups mainly near nanoparticle surfaces, as illustrated in Fig. 7 (top), although the concept of "surface" is somewhat vague here as it seems more appropriate to view these structures as fractal-like.

These SiOH groups are available for post-reaction with species as $R'_{4-x}Si(OR)_x$ (*e.g.* $R = -[CH_2]_nCH_3$), thereby producing organically, or hydrophobically "shelled" nanoparticles, as illustrated in Fig. 7 (bottom). Si-C bonds are stable against hydrolysis and condensation and this "shell" is expected to protect the silicon oxide phase from other forms of degradation. It was anticipated that the energetics of the hydrophilic/hydrophobic interface will be modified so that mechanical, thermal, diffusion, electrical, optical, etc. properties can be controlled by tailoring the "shell."

2. Experimental Procedure

Experimentally, vacuum dried (373K, 48h) SiO_2/Nafion hybrid films were swollen in MeOH for 24h to enhance permeation, then post-reacted with methyl ethoxysilanes for various times and finally vacuum dried (at 373K, 24h).

3. *Post-Reaction with Diethoxydimethylsilane*

a. FT-IR and ^{29}Si Solid State NMR Spectroscopic Studies

Fig. 8 shows FT-IR (ATR) difference spectra (i.e. {*silicon oxide containing + post-reacted*} - {*dry, unfilled H^+ form*) for a time series of post-reaction with $(CH_3)_2Si(OC_2H_5)_2$ (DEDMS = diethoxydimethylsilane). The appearance of the CH_3 deformation, Si-C stretching, and progressive suppression of the Si-OH stretching vibration with increasing reaction time indicates increasing degree of reaction of DEDMS with the silicon oxide "core." The Si-O-Si asymmetric stretching vibration is split into two components arising from groups in linear and cyclic configurations.[2] The relative intensities of these components provides a measure of molecular connectivity within the inorganic phase. Post-reaction renders the structure more linear, which is reasonable since DEDMS only has two alkoxy groups.

Fig. 9 is a ^{29}Si solid state NMR (CP-MAS) spectra for a composition having 13.4% wt $SiO_{2[1-x/4]}(OH)_x$ (henceforth abbreviated as "SiO_2") and the same composite, but post-reacted with DEDMS for 18h. While spectrum noise/signal is high, the chemical shift distribution in the Q-region obviously shifts to a greater degree of Si substitution about SiO_4 tetrahedra upon post-reaction. This fact, coupled with the presence of the $(CH_3)_2Si$ resonance, reinforces the IR result that dimethylsilane molecules are bonded onto SiO_2 cores.

b. Mechanical Tensile Studies

Tensile stress *vs* strain profiles for these samples (Fig. 10) show transition from ductility for pure SiO_2 filler to near-brittleness with increased tensile strength, and decreased elongation-to-break, upon post-reaction. Interestingly, elongation-to-break is the same for all post-reaction times. 13.4% is known to be below the threshold for percolation of the SiO_2 phase so that the intrinsically-ductile PFSI matrix-template is the load-bearing phase before post-reaction. However, since inter-cluster spacings are only ~10 Å, it is reasonable to consider that reactions of DEDMS form $-O(CH_3)_2Si-O-$ bridges between adjacent SiO_2 cores so that the now-interpenetrating glassy, inorganic component becomes the load-bearing phase as illustrated in Fig.11.

c. Differential Scanning Calorimetry, Dynamic Mechanical and Thermogravimetric Analyses

A major transition, with onset ~155 C and peak ~230 C, on the DSC thermogram for 13.4% SiO_2/Nafion (Fig. 12) might be the PFSI matrix glass transition. Post-reaction generates two transitions peaking ~185 and ~250 C. While it is reasonable that at least one peak is related to the glass transition, we hesitate to make definite mechanistic assignments at this time. A weaker transition, with peak ~100 C, that slightly shifts to lower temperatures with increasing reaction time, is also observed.

DMA *vs* temperature studies of these samples at various fixed frequencies (Fig. 13, top) indicate a transition ~ 150 C (temperature at tanδ maximum @ 0.01 Hz) which increases with increasing frequency for the pure SiO_2 -filled system; the transition onset

is around 100 C. Recall that the onset of the corresponding DSC endotherm occurs around this temperature. Actually, we hesitate to call this a glass transition because E' does not suffer a profound decrease, that is, less than an order of magnitude. A second peak ~ 219 C (@ 0.01 Hz), interestingly shifts oppositely to lower temperature with increasing frequency.

A similar major tanδ peak for DEDMS post-reacted samples (Fig. 13, bottom) is at approximately the same temperature and a second higher temperature peak only appears at 10 Hz. The E' curves for post-reacted samples begin to drop at an earlier temperature than corresponding curves for pure SiO_2. On comparing corresponding E' curves in the top with those in the bottom figure, we notice that those of the top undergo a considerable initial rise before the decrease occurs. We attribute this temporary enhanced rigidity to polycondensation involving residual SiOH groups that is driven by heating in the DMA sample chamber. This cannot occur to such a large extent with the post-reacted sample because a large fraction of SiOH groups have already been involved in the formation of Si-C bonds.

We are currently attempting to reconcile the DMA and DSC results as a number of questions relating to transition mechanisms remain unanswered.

TGA evaluation of these samples reveals that the multistage thermal decomposition profile characteristic of (pure SiO_2)/Nafion shifts to higher temperatures and narrows (more abrupt drop) after DEDMS post-reaction (Fig. 14). These and subsequent thermograms were obtained with samples in N_2 so that oxidative effects are not present. Inspection of these thermograms shows that the major DSC and DMA transitions seen above are not related to significant volatile release or chemical reactions, but to physical relaxations.

4. *Post-Reaction with Trimethylethoxysilane*

Post-reaction of a 14.3% SiO_2/Nafion hybrid with $(CH_3)_3Si(OC_2H_5)$ (TMES = trimethylethoxysilane) was accomplished using the procedure described above for DEDMS.

a. FT-IR Spectroscopic Studies

FT-IR (ATR) difference spectra, obtained as before (not shown), show that reaction of TMES is less complete than that for DEDMS (experimental post reaction time = 35 min), revealed by considerably lesser suppression of the Si-OH stretch absorbance peak. The same general conclusions are reached in a comparison of 35 min-reacted 6.5% SiO_2/Nafion hybrids (Fig. 15). Also note in Fig. 15 that the DEDMS, compared with the TMES, spectrum, depicts more Si-O-Si bonds in linear fragments as opposed to loops. In short, the IR evidence suggests that molecular connectivity of the filler in DEDMS-treated systems is more highly developed. Steric effects, less polar nature, and one less reactive group for the TMES molecule are all factors that might be implicated in explaining these spectroscopic results.

b. Mechanical Tensile, Differential Scanning Calorimetry and Dynamic Mechanical Analyses

Stress *vs* strain profiles for 14.3% SiO_2/Nafion (Fig. 16) reveal that while both DEDMS and TMES reactions (35 min.) increase strength, elongation-to-break for the TMES curve is only slightly less than that for pure SiO_2 filler. On the other hand, elongation-to-break for DEDMS-treatment is reduced to about one-half the unreacted value. This latter fact reinforces our concept of the linking of adjacent SiO_2 clusters by reactions of DEDMS as depicted in Fig. 11.

A single, high temperature DSC peak seen for pure 14.3% SiO_2 /Nafion around 230°C (Fig. 17) shifts to the same lower temperature (~205°C) for both DEDMS and TMES-treated samples (35 min post-reaction time). A vestige of a high temperature peak appears for both DEDMS and TMES post-treatments, although this thermal event might also be present for the pure SiO_2-filled sample, but off-scale. While we are unsure as to whether the major peak is a glass transition or crystallinity-related, it is true in either case that the underlying order ⇌ disorder molecular motions in the PFSI matrix have been rendered more facile by post-reaction. We also note a weaker transition ~100 C .

Stress *vs* strain profiles for 6.5% SiO_2 (not shown) indicate that both DEDMS and TMES post-treatment (35 min) enhances strength to about the same extent. However, contrasted with the 14.3% SiO_2/Nafion systems, both post treatments retain ductility almost as great as that for pure 6.5% SiO_2 filler. Perhaps the low SiO_2 level gives particle spacings too large for cluster linkage by the DEDMS reaction so that the PFSI remains the load-bearing phase. 5.0% SiO_2 samples also remain ductile when reacted with TMES at least up to 17h. Here, low SiO_2 content plus having only one reactive site on the $(CH_3)_3Si(OC_2H_5)$ molecule conspire to prevent inter-knitting of clusters, although similar ductility is also noted for the same conditions for TMES treatment, but for the higher SiO_2 content of 10.8%.

DMA spectra have been obtained for TMES-reacted materials and are currently being evaluated.

D. Silicon Oxide Network Modification

1. Concept

These experiments utilized the same inorganic phase precursor monomers, but rather than conducting a 2-step *in situ* reaction, TEOS, a network former, and DEDMS, a network modifier, were premixed in solution; then, this solution permeated a Nafion film. Thus, both monomers entered the film at the same time, although each species would not be expected to have the same solubility, diffusion coefficient, and relative reactivity in the PFSI environment. Nonetheless, the internal reaction can be considered to be a copolymerization leading to a structure that is more mixed than those resulting from the 2-step procedure described previously.

2. *Experimental Procedure*

First, PFSI films from the same lot, as those used to formulate the *in situ* "shelled" silicon oxide nanoparticles, were swollen in MeOH:H_2O = 5:1 (v/v) solutions for 24 hr at room temperature. The swollen films were then immersed in TEOS:DEDMS mixtures (in MeOH), with mole ratios 1:0, 2:1, 1:1, 1:2, 0:1 for 8 min with stirring. Overall, H_2O:TEOS = 4:1, H_2O:DEDMS = 2:1. To be sure, owing to different permeabilities, these molecular species are not expected to mix in these externally-measured proportions within the films. Finally, all samples were dried under vacuum at 373K for 48 hr. Weight uptakes, determined by balance, are 10.1, 11.3, 10.9, 12.5 and 6.7%, respectively, for the above series.

3. *FT-IR and ^{29}Si Solid State NMR Spectroscopic Studies*

FT-IR (ATR) spectra (Fig. 18) of these hybrids show that as TEOS:DEDMS decreases, the number of Si-OH relative to Si-O-Si groups drastically diminishes, indicating successful reaction between the two monomers. The observed symmetric CH_3 deformation as well as Si-C stretching vibration also provide evidence of $(CH_3)_2Si$ unit incorporation. The modified silicon oxide network becomes increasingly more linear in the compositional progression: 1:0 → 1:2, as seen in Fig 18, reflecting the increasing fraction of bifunctional monomer. The asymmetric Si-O-Si stretching vibration gradually shifts to lower wavenumbers, perhaps due to increase in the population of Si atoms that contain pendant -CH_3 and -OSi- groups relative to those having pendant -OH groups.

Corresponding ^{29}Si solid state NMR spectra (not displayed) show that the Q^3 [$(SiO)_3Si(OH)$] peak intensity decreases relative to that of the Q^4 [$(SiO)_4Si$] peak with decreasing TEOS:DEDMS, reflective of greater degree of Si atom substitution about SiO_4 tetrahedra. The Q^4 peak practically disappears into considerable background noise at the ratio 1:2, and for 0:1 there is a rather sharp peak corresponding to $(CH_3)_2Si$ units that could be in either chains or rings.

4. *Differential Scanning Calorimetry Studies*

DSC thermograms (Fig. 19) also show the major transition seen in Figs. 12 and 17 as the major event. This transition, which for the unfilled dry H^+ form has onset ~135 C and endothermic peak ~215 C, shifts upward for pure SiO_2 -filled to ~235 C. Regardless of mechanism, it is reasonable to think that a decrease in $(CF_2)_x$ chain mobility is caused by the rigid SiO_2 nanoparticle obstacles in the same way as for conventional composites. Thereafter, with decreasing TEOS:DEDMS, the transition monotonically shifts downward so that the peak is ~180 C for pure DEDMS-treatment. Reasonably, as TEOS:DEDMS decreases, the filler increasingly assumes the character of *linear* dimethylsiloxane (DMS) oligomers and/or polymers which are intrinsically quite flexible and act to *plasticize* the PFSI matrix.

This plasticization, or softening, is manifest on stress *vs* strain curves (Fig. 20) which show that the 0:1 (pure DEDMS-reacted) material not only retains a ductility approaching that of unfilled dry Nafion-H^+, but exhibits lower strength. For the compositional progression 0:1 → 1:2 → 1:1 → 2:1, the curves monotonically shift upward with

decreasing elongation-to-break, but, interestingly, the 1:0 (pure TEOS-reacted) curve is in the midst, rather than at the top of this series.

A TGA comparison of unfilled, dry H^+ - and pure DEDMS-reacted forms (scans not shown) reveals that the thermal stability of the latter is greatest.

The following is the work of Dr. Phoebe Shao, Postdoctoral Associate, and K.A. Mauritz, Professor

II. *In situ* -Grown "Mixed" Inorganic Oxide Nanoclusters

A. Concept

The inorganic alkoxides utilized in these experiments were TEOS in conjunction with the more rapidly-reacting metal (M) alkoxides $Al(OR)_3$ and $Ti(OR)_4$. Although these species can be mixed on a molecular level in macroscopic alcohol solutions, the possibility exists for ultimate *compositional segregation* within nanoparticles grown within the ionic clusters of dried-annealed films exists owing to considerable differences between hydrolysis-condensation rates for Si and metal alkoxides. Moreover, two inorganic alkoxides of different size, shape and outer groups are expected to have different permeation rates within the PFSI film. Different degrees of Si-M oxide molecular interconnectivity were anticipated and we are investigating this aspect using IR and ^{29}Si solid state NMR spectroscopies (not discussed in this report). Different Si/M ratios will generate varying degrees of intraparticle molecular connectivity, which will influence the convoluted intraparticle free volume. Perhaps [perfluoro-organic]/[inorganic oxide] interfaces having different fractal dimensions or "roughness" can be tailored. Finally, we are examining thermal transitions of the PFSI matrix as well as thermal degradation as modified by incorporation of inorganic oxide phases via DSC and TGA, respectively (not discussed in this report).

These structural concepts are roughly illustrated in Fig. 21. Variation of compositional contrast on the level of nanometers are expected to have important implications regarding the mechanical, optical, dielectric, diffusion and electrical transport properties of these hybrids.

B. [SiO_2 -TiO_2 (mixed)]/Nafion Nanocomposites: Sorption of Pre-Mixed Alkoxides

1. Experimental Procedure

All 1100EW, H^+ -form Nafion, 5 mil-thick membranes were placed in boiling water 30-60 min and then mildly dried at 50 C for 4 hr to remove loosely-bound, but not all, water; the remaining, more strongly bound water was intended for alkoxide hydrolysis. Then, the sparsely-hydrated membranes were swollen in 2-propanol for 1hr to promote subsequent permeation of inorganic alkoxides.

TEOS and tetrabutyltitanate (TB) were pre-mixed with various compositions in 2-propanol. Then, the alcohol-swollen membranes were immersed in the mixed alkoxide solutions for 30 min, then removed, and the surfaces rinsed with fresh 2-PrOH to minimize

precipitation of a surface-attached silica-titania layer. Samples were then placed in a 100% humidity environment for about 10 hr to further encourage hydrolysis. Large quantities of water were not introduced at a single time for the purpose of slowing the sol-gel reaction, given that TBT reacts rapidly. Finally, all samples were vacuum dried at 100 C for 24 hr.

The mixed alkoxide compositions and resultant dried mass uptakes in these experiments are listed in the following table. All uptakes do not differ by much from 7%.

ml TEOS/ml TBT/ml 2-propanol	% mass uptake	Ti/Si
15/5/40	7.60	9.61
10/10/40	7.06	13.45
5/15/40	6.56	23.31
0/20/40	6.42	-

2. Inorganic Oxide Concentration Profiles across Film Thickness Directions

a. Electron Microscopy-EDS

An environmental scanning electron microscope (Electroscan ESEM) was used to study large-scale morphologies of these nanocomposites. We present examples of our use of the x-ray energy dispersive elemental microprobe attachment of the ESEM (EDS) to determine Si, Ti, and Al profiles across sample thicknesses.

The ESEM, as well as optical microscope, was used to determine if an undesirable glassy inorganic oxide layer precipitated on the surfaces of films during nanocomposite formation. This layer, described in earlier studies,[6,7] would present not only an undesirable complication from the standpoint of materials applications, but structure-properties data (particularly FT-IR/ATR spectra) intended to be representative of the bulk, will thereby be distorted. We simply mention that microscopic inspection of the surfaces of samples in this study did reveal such a layer. The integrated intensity of the sulfur peak in the x-ray spectrum quantifies SO_3^- group population within a selected area and is adopted as a reference for the polymer matrix. Therefore, for example, Si/S intensity ratio is a relative measure of local silicon oxide content.

The inorganic oxide composition profile along the film thickness direction is a significant variable to be manipulated in tailoring these films as functional coatings or membranes, as will be discussed later.

Inorganic oxide compositional gradients might be rationalized in at least the following two ways: (1) Progressive difficulty of alkoxide molecules to diffuse to the center of the films due to the obstacles posed by already-precipitated inorganic structures in near-surface regions; (2) liquid surface tension operative during the sol period of the *in situ* reaction which might cause the alkoxide to be more concentrated near the surface.

b. Results-ESEM/EDS

Fig. 22 shows three typical composition profiles, each for the average Ti/Si ratio listed on the right. The curves are rather symmetrical about the film center plane. The

Ti/Si ratio is the greatest and increases with increasing average Ti/Si ratio in the near-surface regions. We attribute the large relative concentration of TiO_2 in the immediate sub-surface regions, as well as the sharp negative gradient toward the center, to the high TBT sol-gel reaction rate compared to the rate of inward TBT diffusion, as well as to the slow TEOS sol-gel reaction rate.

Fig. 23, which depicts the Ti/S ratio for the same system, shows that, in absolute terms, there is more TiO_2 near the surface than at any other location, especially the middle.

3. Mechanical Tensile Studies

Corresponding stress *vs* strain curves (Fig. 24) show that the pure SiO_2 -containing Nafion is ductile, reflecting that filler content is beneath the percolation threshold and therefore that the PFSI is the load-bearing phase. In sharp contrast, mixed incorporation of TiO_2 renders the material comparatively brittle, suggesting that the inorganic nanoparticles have a significant degree of interconnection. The higher the Ti/Si ratio, the higher the tensile strength. Elongation-to-break is about the same for all mixed compositions and tensile strength monotonically increases with increasing Ti/Si ratio. Given the fact that most of the TiO_2 in these brittle samples resides near the surface, it would seem that this glassy zone controls the mechanical properties of these nanocomposites.

III. [SiO_2-TiO_2 (mixed)]/Nafion Nanocomposites: Sequential Alkoxide Addition Procedure

A. Concept

The underlying concept in these experiments is identical to that expressed in the section *'In situ*-Grown "Shelled" Silicon Oxide Nanoparticles.' First, pre-formed $SiO_{[2-x/4]}(OH)_x$ nanoparticle "cores" are created within a PFSI via an *in situ* sol-gel reaction. Then, a "shell" is created about this core by post-reacting exterior residual SiOH groups with in-diffusing alkoxides of Ti or Al. This simple idea is illustrated in Fig 25.

B. Experimental Procedure

First, Nafion-H^+ films were immersed in (2 ml H_2O)/(40 ml 2-PrOH) solutions for 5 hr to promote subsequent TEOS hydrolysis. Then, a (28 ml TEOS)/(2-PrOH) mixture (3:1 v/v) was added to the previous solution (H_2O:TEOS [mole/mole] = 1:1). TEOS permeated the film and reacted therein (mainly hydrolysis) for various times. Then, films pre-reacted in this way were rinsed with fresh 2-PrOH to remove sorbed/generated water. TBT was diluted separately in 2-PrOH to various degrees and the pre-reacted films added to these solutions for 4 to 30 min. The reason for utilizing low H_2O:TEOS, and permitting TBT to be sorbed in dilute concentration only after the sorbed TEOS had sufficient opportunity to react, is that we sought to minimize rapid TiO_2 precipitation at the surface and within the near-surface zone. The surfaces of the films were rinsed again in 2-PrOH to remove excess (potentially surface layer-forming) TBT and the films were placed in air

overnight to promote complete hydrolysis and allow condensation to proceed. Finally, the samples were vacuum-dried at 100 C for 48 hr to drive the sol-gel reaction to high completion. Preparative data for these samples are in the following table.

Time of Immersion in TEOS Soln. (min.)	TBT/2-PrOH Solution Concentration (ml/ml)	Total Dry Uptake (% weight)	Ti/Si (overall)
20	2/40	16.3	0.202
20	4/40	14.1	0.546
15	10/40	16.5	1.658
10	20/40	15.7	1.509

Although the total weight uptake does not vary greatly for the different preparative conditions, it is seen in this table that the Ti/Si ratio does.

C. Inorganic Oxide Concentration Profiles

Fig. 26, displaying Ti/Si profiles for the entries in the above table, reveals a symmetric composition distribution with most of the inorganic phase residing near the surface, save for the curve for the lowest ratio, which is rather flat. Again, it is true that as the average Ti/Si ratio increases, this ratio increases in the near-surface regions.

Regardless of Ti/Si ratio, there is always less absolute SiO_2 in the middle than toward the surfaces, as seen in Fig. 27. Understandably, the symmetrical curves rise with decreasing Ti/Si ratio.

D. Mechanical Tensile Studies

The stress *vs* strain curve for pure SiO_2 -filled Nafion (Fig. 28) indicates ductility, implying that the silicon oxide phase at this uptake (16%) is isolated in domains rather than being percolative. There is also yield. In sharp contrast, the materials modified with TBT are brittle in a way that elongation-to-break decreases, and tensile strength increases with increasing Ti/Si ratio. Note that the overall inorganic oxide uptakes are very close (see previous table) so that the curves can be meaningfully compared. It is suggested that post-reaction with TBT links silicon oxide nanoparticles together. As suggested by the above SEM-EDS studies, this percolative intergrowth occurs in the near-surface regions.

Fig. 29 consists of stress *vs* strain curves for lower total SiO_2-TiO_2uptakes (~7%). The curve for pure SiO_2 -filled Nafion again exhibits yield and more ductility than its counterpart in Fig. 28, which is reasonable. The general comments made in the above discussion for Ti-containing samples can be made for this lesser-filled series, except that the latter exhibit more ductility, and elongation-to-break appears to be independent of Ti/Si ratio. Perhaps an understanding of this constancy of elongation-to-break with variable Ti/Si ratio for the ~7%-filled samples might begin with an inspection of Fig. 30. For *all* three cases there is a considerably greater concentration of Ti in the near-surface regions than toward the middle. In other words, all three compositions are exhibit essentially the same degree of ductility because the silicon oxide structure in the near-surface regions has been modified to practically the same extent by post-treatment with TBT.

IV. [SiO_2- Al_2O_3 (mixed)]/Nafion Nanocomposites: Sorption of Pre-Mixed Alkoxides

A. Experimental Procedure

All Nafion-H^+ films were placed in boiling water for 30-60 min, then mildly dried at 50 C for 4 hr to remove loosely-bound, but not all, water; the remaining bound water was retained for alkoxide hydrolysis. Then, the sparsely-hydrated membranes were swollen in 2-PrOH for 1 hr to promote subsequent permeation of the inorganic alkoxides.

TEOS and aluminum tri-*sec*-butoxide (ATB) were pre-mixed with various compositions in 2-PrOH solutions. Then, the alcohol-swollen films were immersed in the mixed alkoxide solutions for 1 hr, then removed, and their surfaces rinsed with fresh 2-PrOH to minimize precipitation of surface-attached silica-alumina layers. Experimental steps involving alkoxides were performed in a dry box to minimize the effect of atmospheric humidity. Samples were then placed in air for about 10 hr to further encourage hydrolysis. Finally, all samples were vacuum-dried at 100 C for 24 hr.

Precursor alkoxide solution compositions, final dried inorganic oxide weight uptakes, and average internal Al/Si ratios obtained by SEM-EDS analysis, are listed in the following table. Note that percent uptake for all formulations is somewhat low, particularly in the sense of being below the percolation threshold for this phase. Percent uptake does not in fact deviate greatly and there is no significant trend in uptake with increasing TEOS/ATB ratio. Average internal Al/Si ratio increases with decreasing solution TEOS/ATB ratio, as is reasonable.

ml TEOS/ml ATB/ml 2-propanol	% mass uptake	Al/Si
40/2/10	6.50	0.189
80/5/20	4.66	0.328
80/10/20	5.73	0.678
80/20/40	4.68	1.103

B. Inorganic Oxide Concentration Profiles

As seen in Fig. 31, the Al/Si ratio is relatively uniform across the film thickness for all average internal Al/Si ratios. This result stands in sharp contrast with the observed situation for the [TiO_2-SiO_2]/Nafion hybrids. In fact, there is actually less Al relative to Si in the near-surface regions. Fig. 32 shows that Al, in an absolute sense, can be rather homogeneously distributed across the thickness direction. It is quite interesting that for Al/Si = 0.328, the greatest concentration of Al is in the middle. Apparently, ATB has the ability to penetrate deep into the film before it is polymerizes to being immobile. In Fig. 33 it is seen that there can actually be more Si in the middle than near the film surfaces for the hybrid having the highest Al/Si ratio.

C. Mechanical Tensile Analysis

Stress *vs* strain curves for all [SiO_2- Al_2O_3]/Nafion hybrids portray ductility, but less elongation-to-break than pure SiO_2-filled Nafion. We suggest that the relatively

homogeneous distribution of the inorganic oxide phase, which exists at rather low levels to begin with, is a condition under which the percolation of this phase is impossible. Thus, the intrinsically-ductile PFSI matrix is always the load-bearing phase.

Tensile strength decreases while elongation-to-break remains approximately the same with increasing Al/Si ratio, excepting the case having the lowest ratio.

V. Conclusions

We formulated anisotropic nanocomposites via sol-gel reactions for TEOS occuring within oriented ionic clusters of a perfluorosulfonate ionomer. Ionic clusters were elongated by uniaxial mechanical film orientation using a modified Instron fitted with a fabricated liquid reaction cell fitted around the strained film. While strained, the sample was heated to drive condensation using a fabricated oven surrounding the sample. Evidence of orientation was provided by SAXS experiments. Stress *vs* strain profiles for these nanocomposites indicated mechanical anisotropy.

Residual SiOH groups on silicon oxide nanoparticles that were pre-formed within Nafion-H^+ were post-reacted with diethoxydimethylsilane and trimethylethoxysilane. This two step reaction resulted in interknitted and organically "shelled" nanoparticles, respectively. FT-IR and ^{29}Si solid state NMR spectroscopies probed structural incorporation of these silanes onto silicon oxide "cores" and degree of molecular connectivity within the inorganic phase. The reaction of TMES is less complete than that for DEDMS. Post-reaction with DEDMS renders the structure more linear. Mechanical tensile experiments indicated a ductile → brittle transformation upon DEDMS post-reaction, suggesting linking of previously-isolated silicon oxide nanoclusters. On the other hand, a measure of ductility persists after TMES post-reaction. Tensile strength was increased after both post-reactions. We are attempting to reconcile the results of DMA and DSC investigations as a number of questions relating to transition mechanisms are presently unanswered. There is a major transition in the PFSI phase that is profoundly affected by the *in situ* growths. TGA reveals that the multistage thermal decomposition profile characteristic of SiO_2/Nafion shifts to higher temperatures and the major degradation event becomes more abrupt after DEDMS post-reaction.

In another scheme, an alcohol solution of TEOS (network former) and DEDMS (network modifier) permeated hydrated Nafion-H^+ followed by their *in situ* copolymerization. FT-IR spectra reflected successful reaction between the monomers and a silicon oxide network that becomes increasingly more linear with decreasing TEOS:DEDMS. ^{29}Si solid state NMR spectra for these mixed hybrids were collected and are being analyzed to add to our knowledge of inorganic oxide phase topology. DSC shows the major transition shifting upward from the unfilled to pure SiO_2 -filled state, although, with decreasing TEOS:DEDMS, the transition shifts downward. As TEOS:DEDMS decreases, the filler increasingly assumes the character of polydimethylsiloxane which acts to *plasticize* the PFSI matrix, a concept reinforced by stress *vs* strain analysis. TGA studies of Nafion-H^+ and pure DEDMS-reacted Nafion reveals superior thermal stability of the latter.

[SiO_2 -TiO_2]/Nafion nanocomposites were formulated by sorption of pre-mixed alkoxides. The distribution of Ti/Si across the film thickness is symmetrical about the

center plane and this ratio is greatest in the near-surface regions, attributed to high TBT reaction rate compared to the rate of TBT diffusion and slow TEOS reaction rate. There is more TiO_2 near the surface than at any other location. In sharp contrast with a pure SiO_2-containing, ductile Nafion, mixed incorporation of TiO_2 renders the material comparatively brittle, suggesting the inorganic nanoparticles have a significant interconnection. Higher Ti/Si ratio produces higher tensile strength. Elongation-to-break is about the same for all mixed compositions and tensile strength monotonically increases with increasing Ti/Si. Since most of the TiO_2 is near the surface, it seems that this glassy zone controls the mechanical properties of these nanocomposites.

[SiO_2-TiO_2]/Nafion nanocomposites were also formulated via sequential alkoxide addition. Pre-formed $SiO_{2[1-x/4]}(OH)_x$ "cores" were "shelled" by post-reacting SiOH groups with alkoxides of Ti. Ti:Si composition profiles across the thickness dimension are symmetric with most of the inorganic phase near the surface. There is always less SiO_2 in the middle than toward the surfaces. Contrasted with the ductile SiO_2 -filled precursor, the TBT-post-reacted materials are brittle in a way that elongation-to-break decreases and tensile strength increases with increasing Ti/Si ratio. Post-reaction with TBT apparently links silicon oxide nanoparticles together and SEM-EDS studies show that this percolative intergrowth occurs in near-surface regions. For low total SiO_2-TiO_2uptakes the hybrids are more ductile and elongation-to-break is independent of Ti/Si ratio.

[SiO_2- Al_2O_3]/Nafion nanocomposites were produced via sorption of pre-mixed alkoxides. Percent uptake for all formulations was low, being below the percolation threshold. Al/Si ratios were relatively uniform across film thicknesses, contrasted with the situation for [TiO_2-SiO_2]/Nafion hybrids. There is less Al relative to Si in the near-surface regions. Al can be homogeneously distributed across the thickness direction or in some cases more concentrated in the middle. It is also possible for Si to be most concentrated in the middle. These hybrids are more ductile but display smaller elongation-to-break than pure SiO_2-filled Nafion. The relatively homogeneous distribution of the inorganic oxide phase at low uptake may be a condition under which percolation is impossible. Generally, tensile strength decreases while elongation-to-break is constant with increasing Al/Si ratio.

VI. References

1. Mauritz, K.A.; Storey, R.F.; Jones, C.K. in *Multiphase Polymer Materials: Blends,Ionomers and Interpenetrating Networks*, ACS Symp. Ser. No. 395, Ch. 16, L. A. Utracki and R. A. Weiss, Eds., 1989.
2. Mauritz, K.A.; Warren, R.M. *Macromolecules*, **1989**, 22, 4483.
3. Mauritz, K.A.; Stefanithis, I.D. *Macromolecules*, **1990**, 23, 1380.
4. Stefanithis, I.D.; Mauritz, K.A. *Macromolecules* **1990**, 23, 2397.
5. Mauritz, K.A.; Stefanithis, I.D.; Wilkes, G.L; Huang, Hao-Hsin, *ACS Div. Polym. Chem., Polym. Preprs.* **1991**, 32(1), 236.
6. Mauritz, K.A; Scheetz, R.W.; Pope, R.K.; Stefanithis, I.D. *ACS Div. Polym. Chem., Polym. Prepr.* **1991** 32(3), 528.
7. Davis, S.V.; Mauritz, K.A.; Moore, R.B. *Am. Chem. Soc. Polymer Prepr.* **1994**, 35(1), 419.

VII. Figures

☐ **Growth of Inorganic Nanophase within Ionomers via <u>in situ</u> Sol-Gel Reaction for Silicon/Metal Alkoxides:**

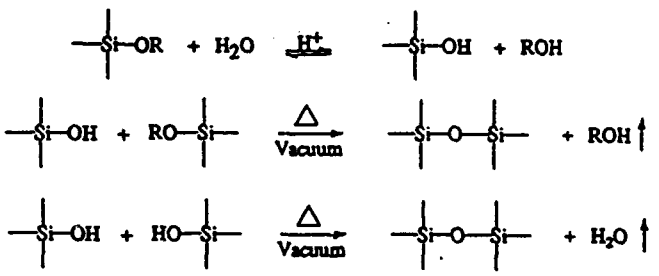

☐ <u>Hypothesis</u>: Morphology of Inorganic Phase is Ordered by Polar/Nonpolar Phase Separated Morphology: "Nanoparticles" in Ionic Clusters

☐ Morphological Templates:

<u>Perfluorosulfonate Ionomers</u>

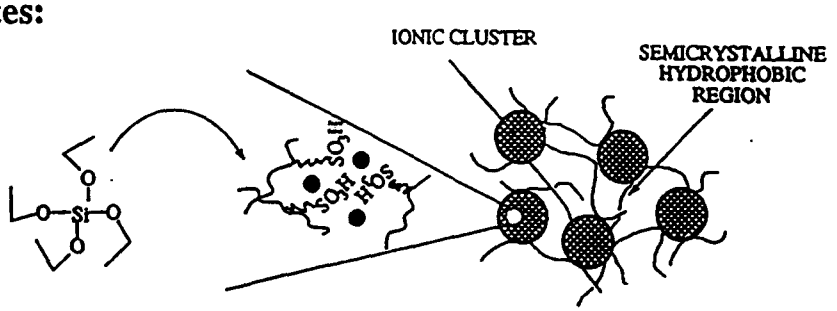

Figure 1

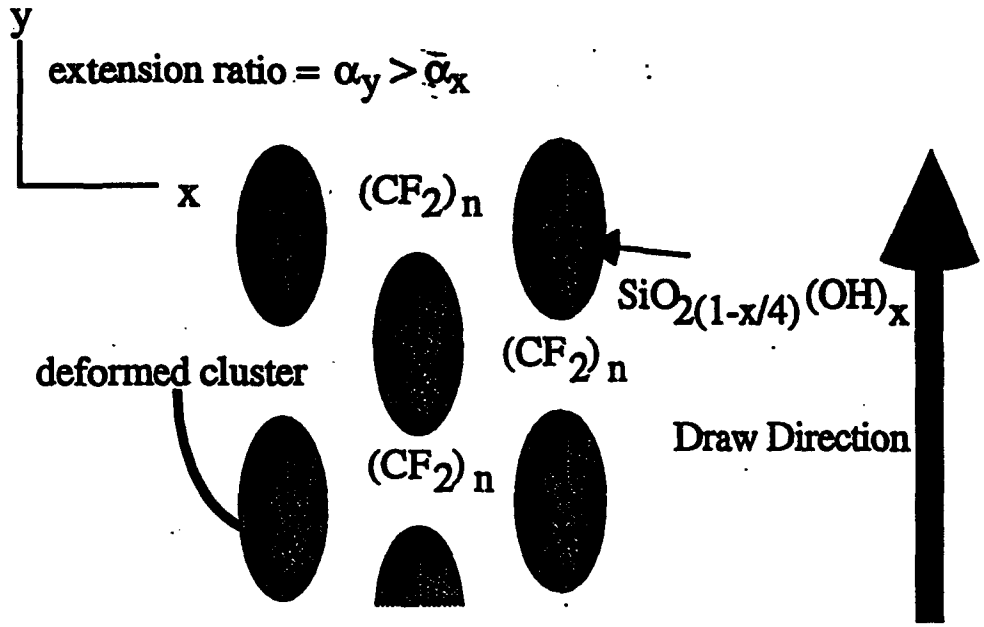

Silicon oxide-filled clusters oriented in direction of applied mechanical deformation.

Figure 2

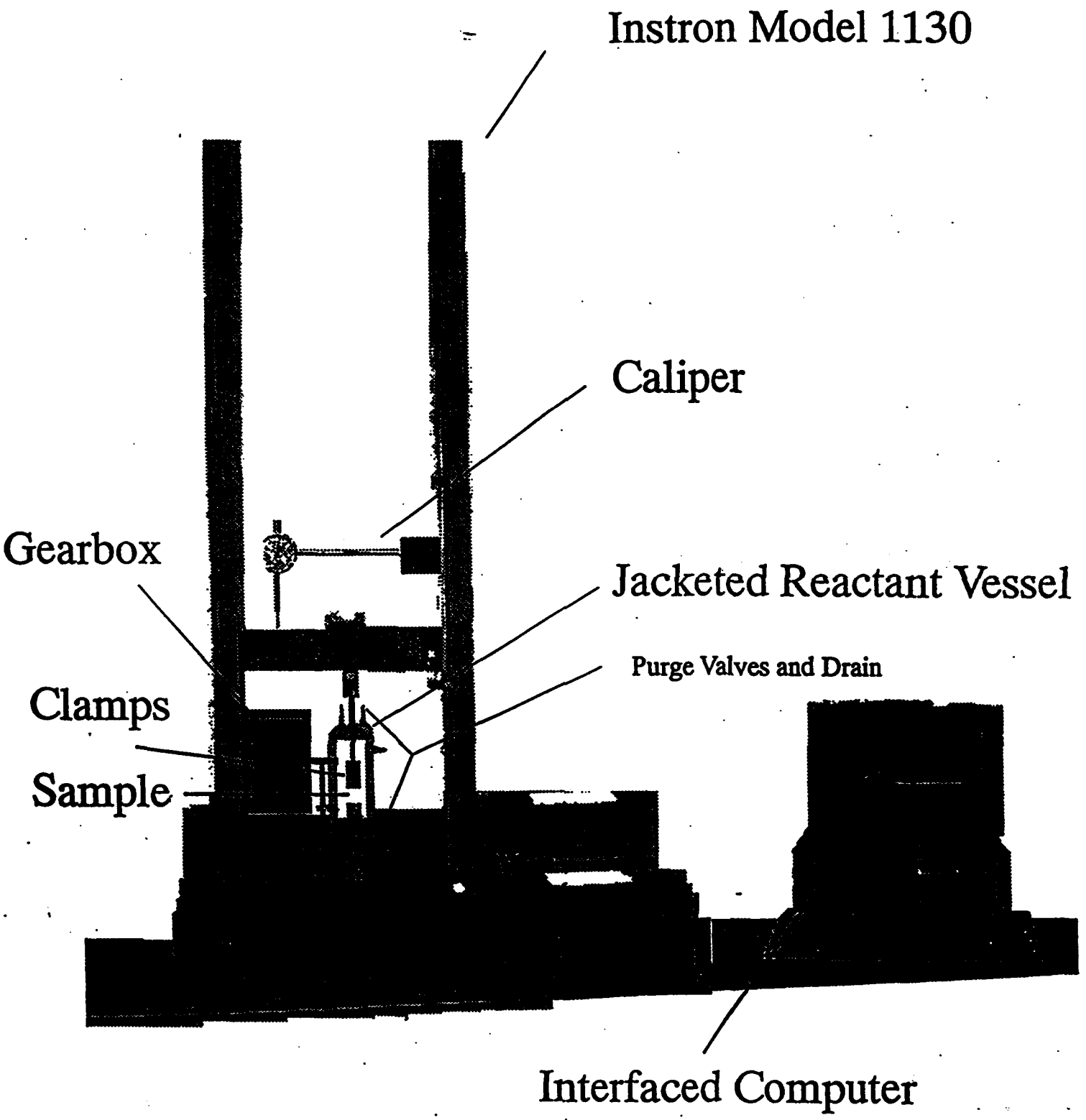
Instron Model 1130
Caliper
Gearbox
Jacketed Reactant Vessel
Purge Valves and Drain
Clamps
Sample
Interfaced Computer

Figure 3

Oriented PFSI-SiO_2 membranes

H_2O/MeOH - TEOS/MeOH (14min)
annealed at 220°C 20min

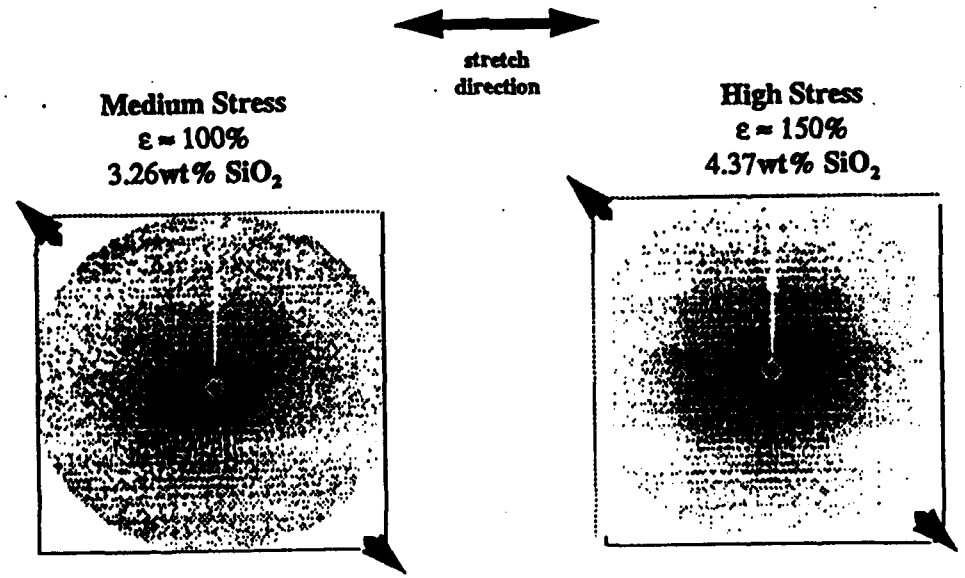

Figure 4

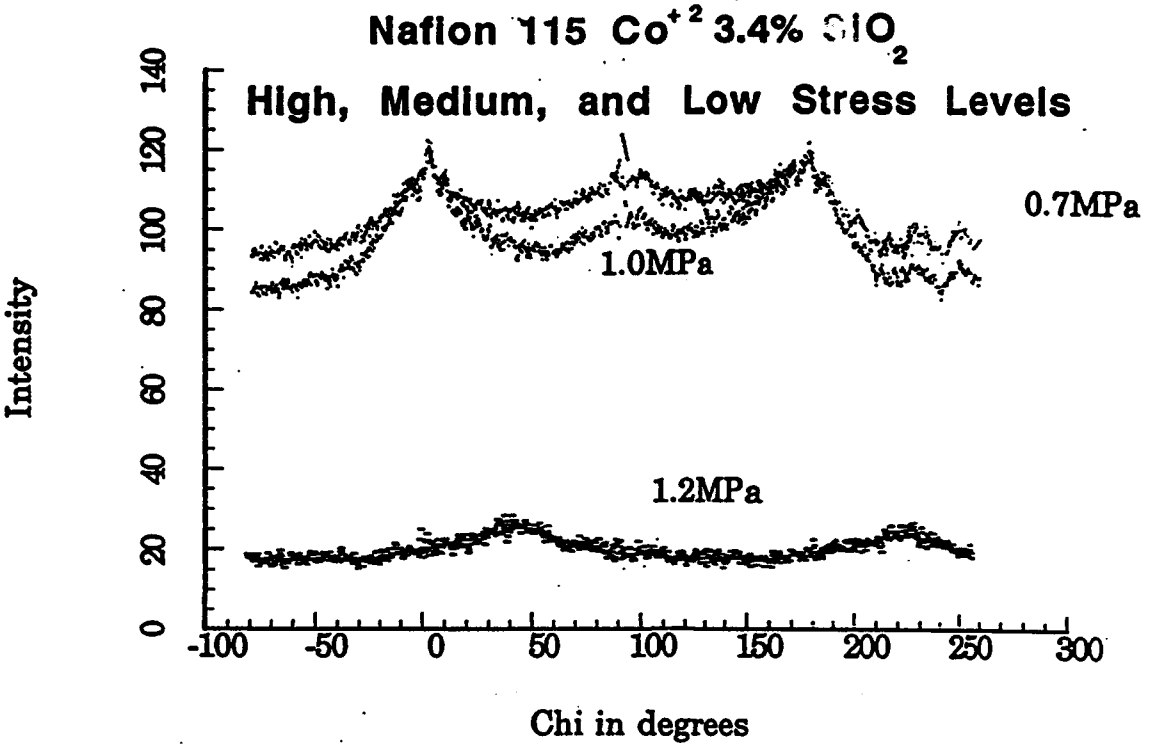
Nafion 115 Co+2 3.4% SiO2
High, Medium, and Low Stress Levels
0.7MPa
1.0MPa
1.2MPa
Intensity
0
20
40
60
80
100
120
140
-100
-50
0
50
100
150
200
250
300
Chi in degrees

Figure 5

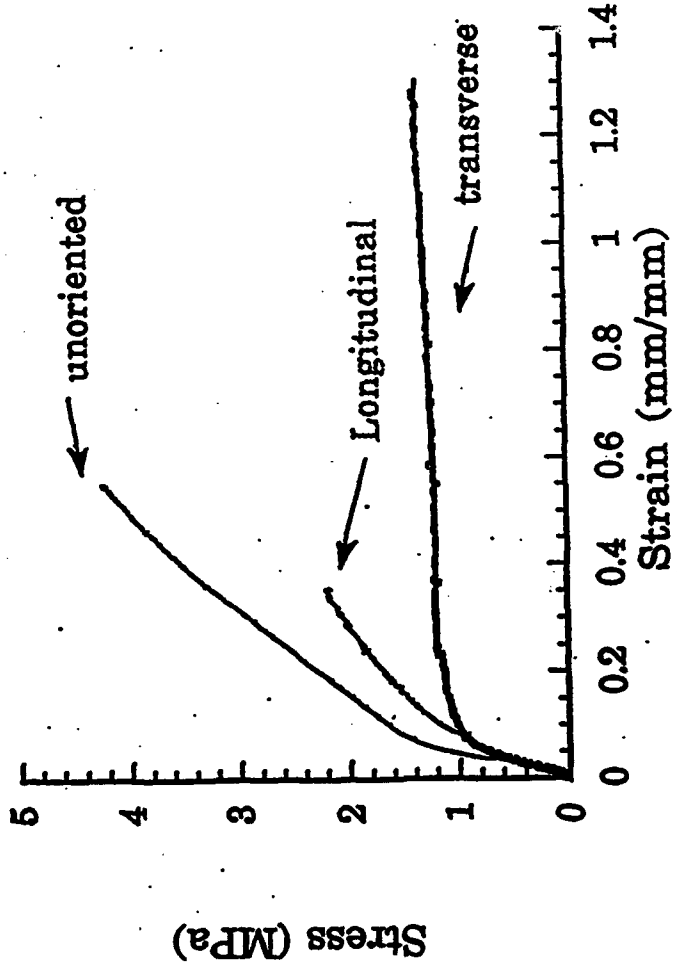
unoriented
Longitudinal
transverse
Stress (MPa)
0
1
2
3
4
5
0
0.2
0.4
0.6
0.8
1
1.2
1.4
Strain (mm/mm)

Figure 6

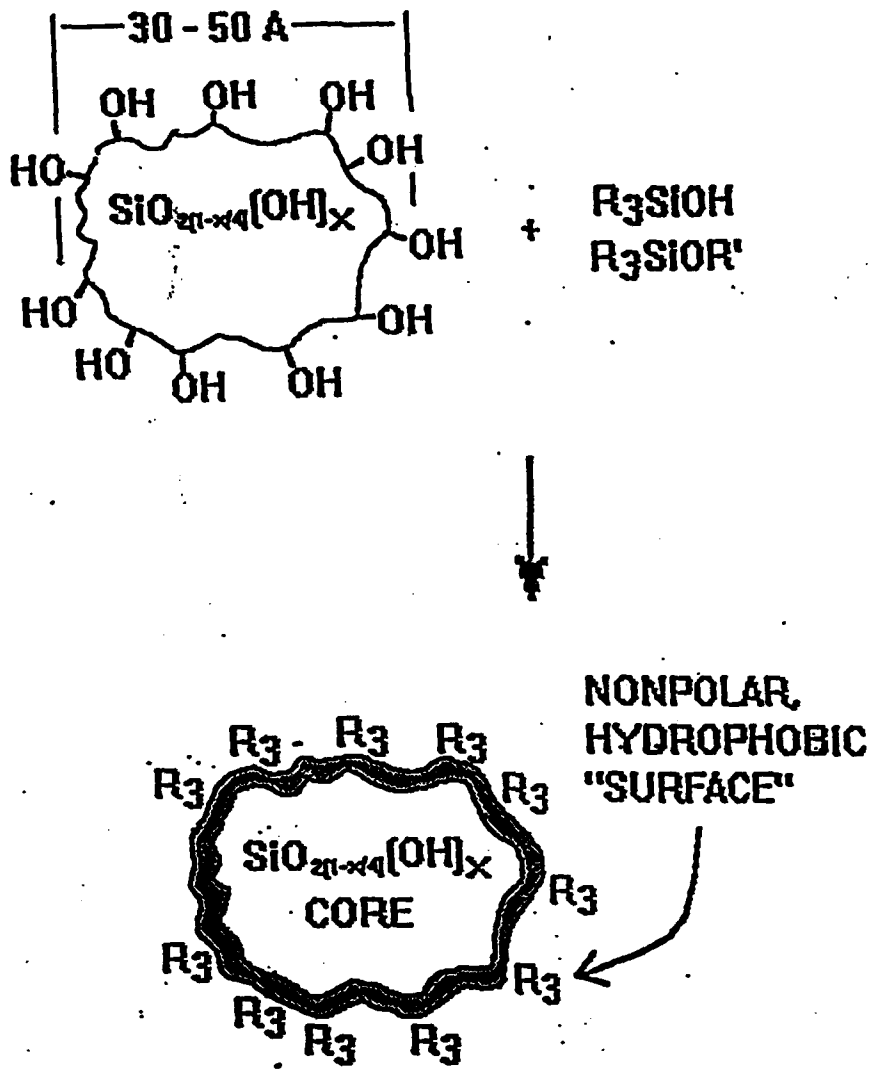

Hydrophobically "Shelled" Silicon Oxide Nanoparticles

Figure 7

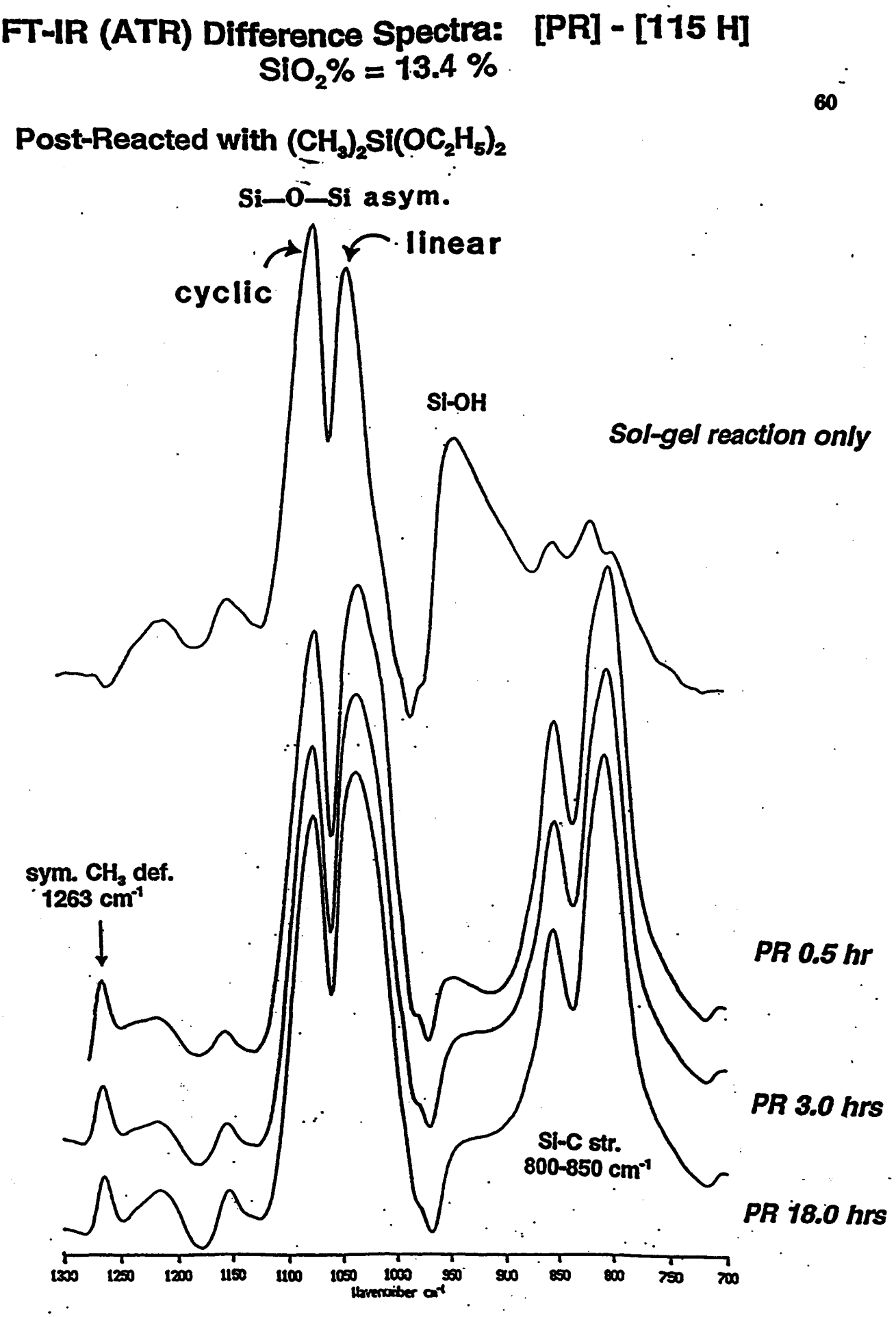
FT-IR (ATR) Difference Spectra: [PR] - [115 H]
SiO2% = 13.4 %
Post-Reacted with (CH3)2Si(OC2H5)2
Si—O—Si asym.
linear
cyclic
Si-OH
Sol-gel reaction only
sym. CH3 def.
1263 cm-1
PR 0.5 hr
PR 3.0 hrs
Si-C str.
800-850 cm-1
PR 18.0 hrs
1300 1250 1200 1150 1100 1050 1000 950 900 850 800 750 700
Wavenumber cm-1

Figure 8

^{29}Si Solid State NMR

$SiO_2\% = 13.4\ \%$

Sol-gel reaction only

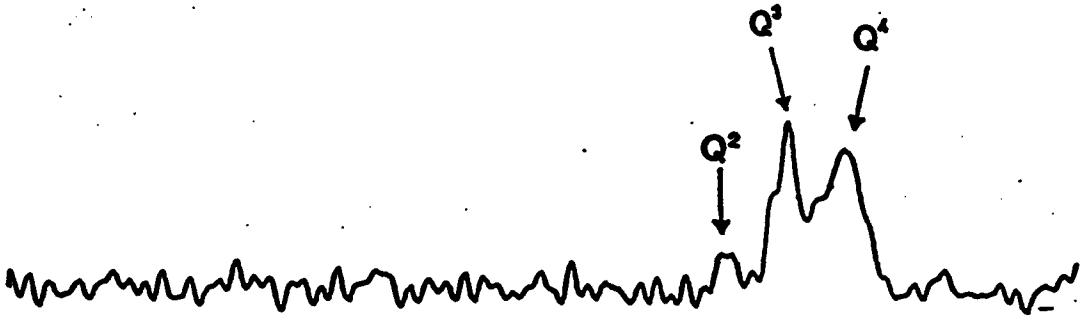

Post-reacted with $(CH_3)_2Si(OC_2H_5)_2$ for 18.0 hr

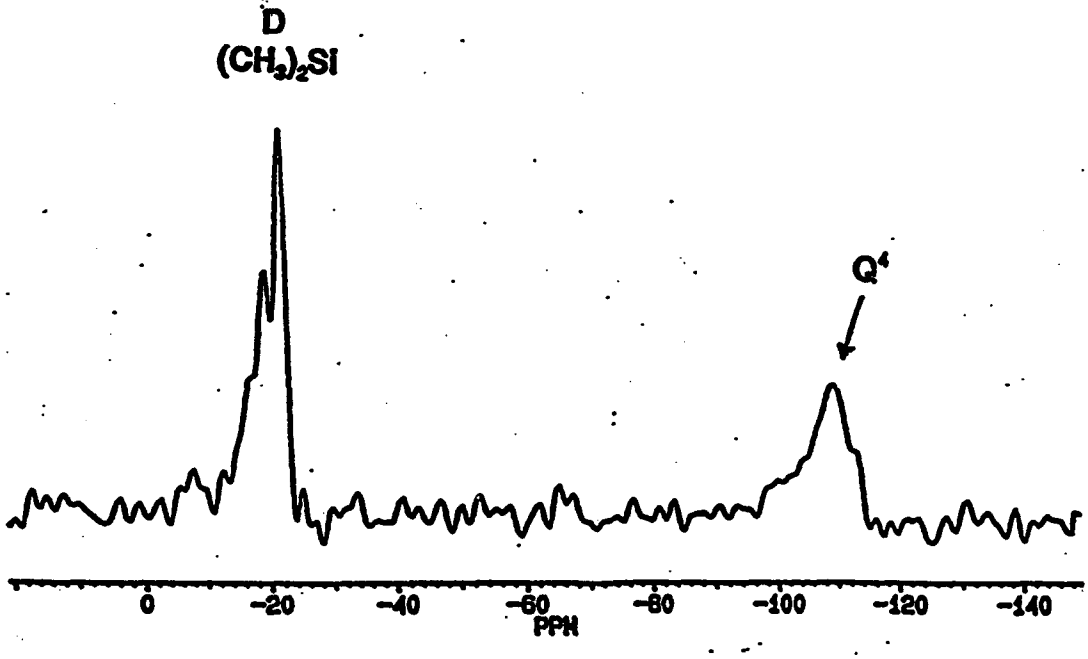

Figure 9

SiO_2% = 13.4 %

Post-Reacted with $(CH_3)_2Si(OC_2H_5)_2$

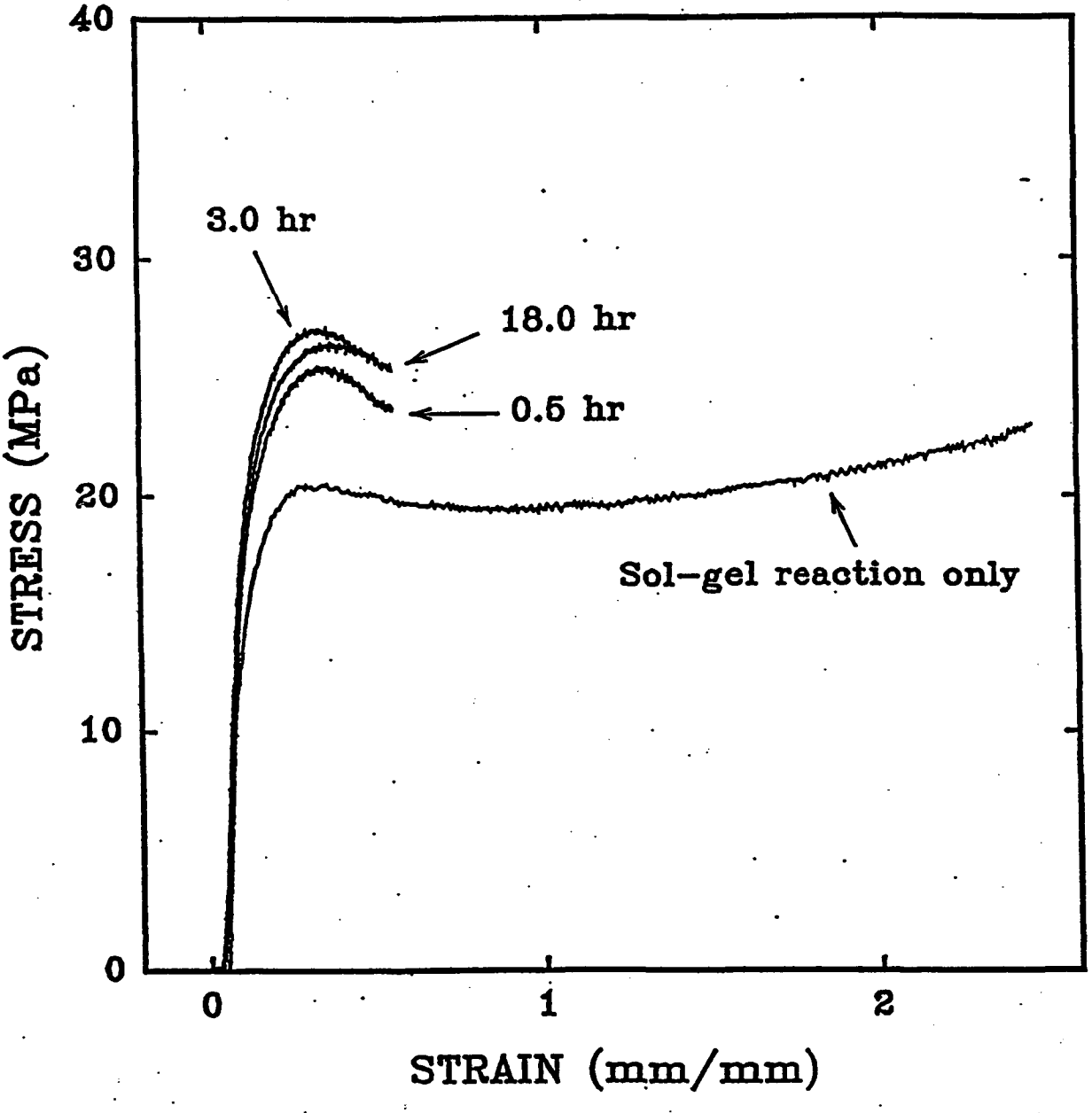

Figure 10

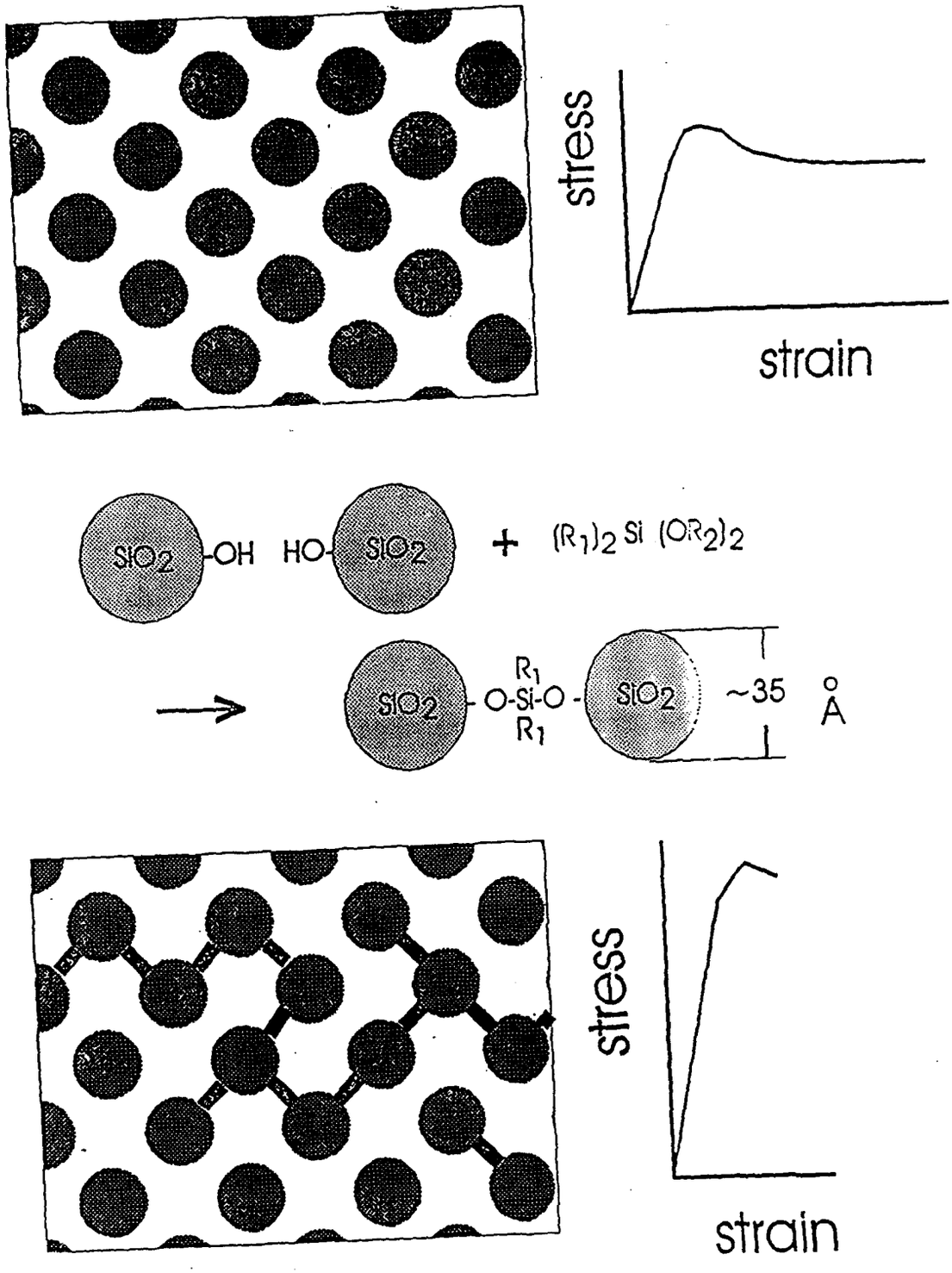
stress
strain
SiO2 -OH HO- SiO2
+ (R1)2 Si (OR2)2
SiO2 - O-Si-O - SiO2
R1
R1
~35 Å
stress
strain

Figure 11

$SiO_2\% = 13.4\ \%$

Post-Reacted with $(CH_3)_2Si(OC_2H_5)_2$

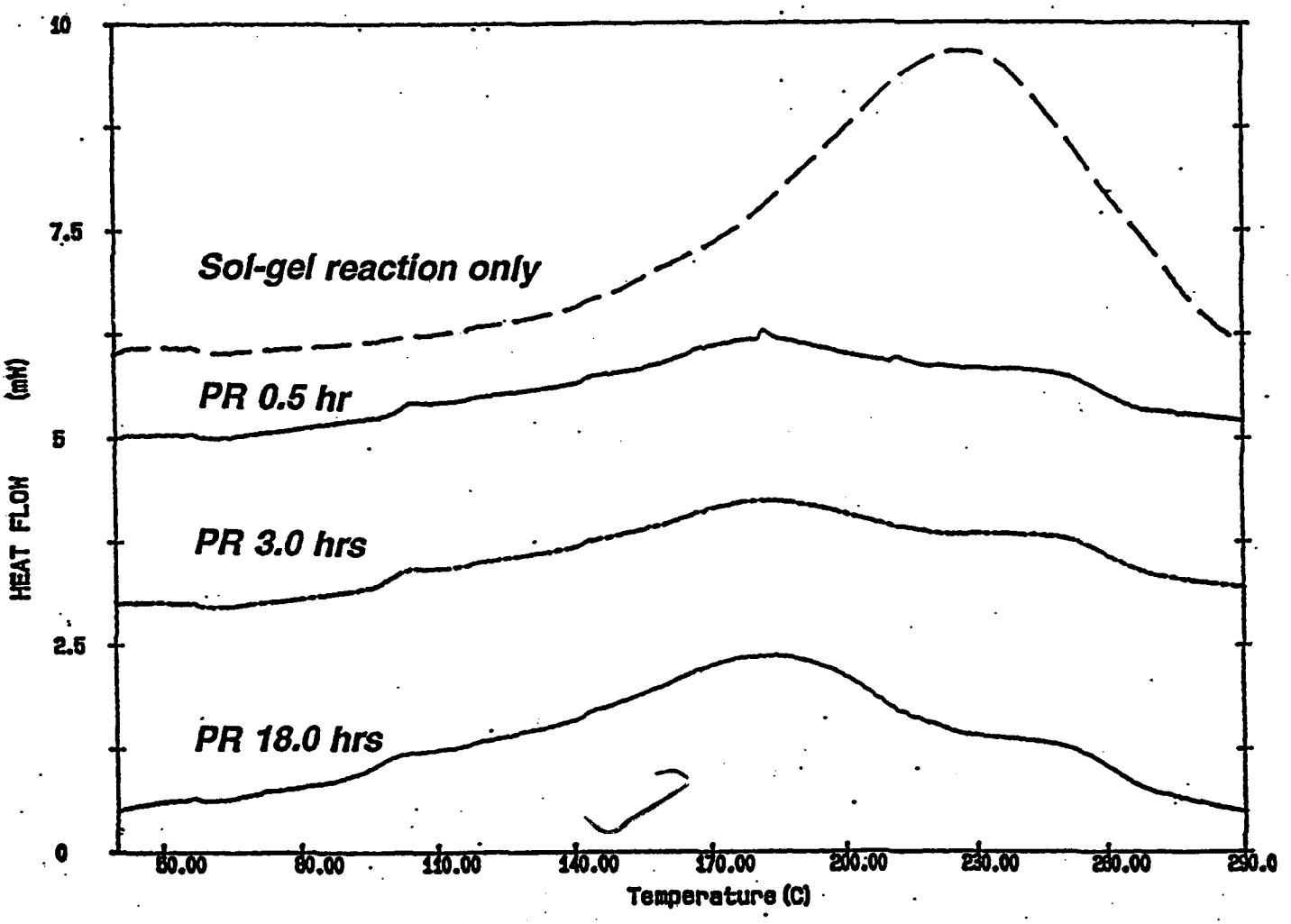

Figure 12

$SiO_2\%$ = 13.4 %

Sol-gel reaction only

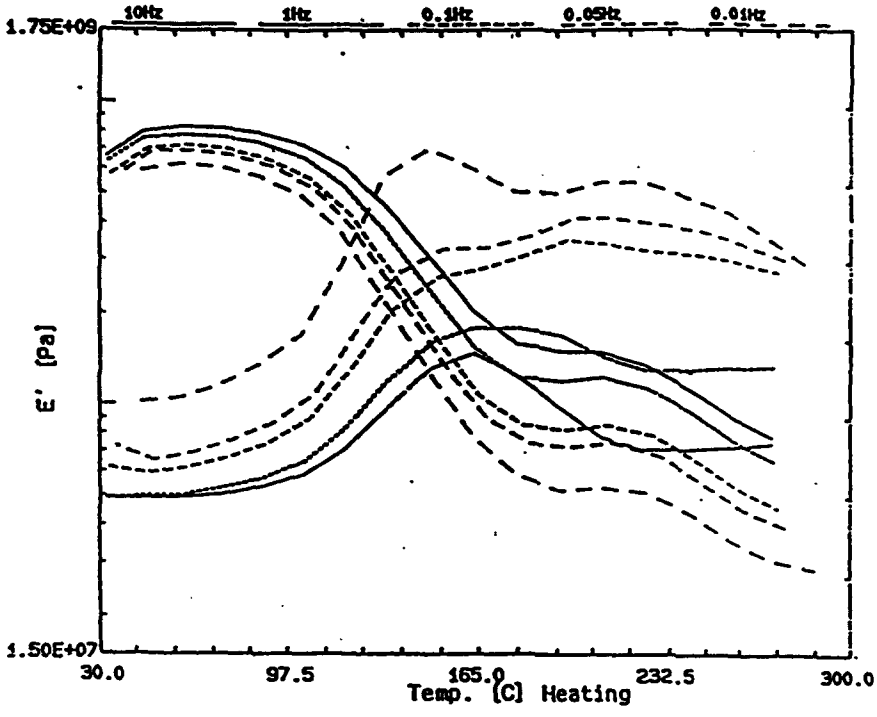

tan δ

Post-reacted with $(CH_3)_2Si(OC_2H_5)_2$ for 18 hr

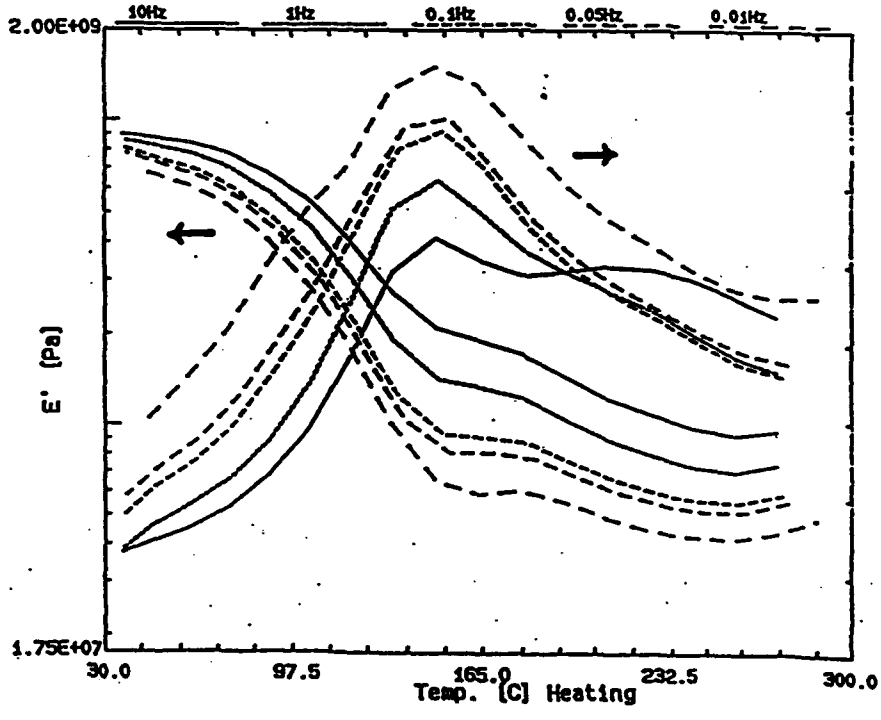

tan δ

Figure 13

$SiO_2\% = 13 - 14\ \%$

Sol-gel reaction only

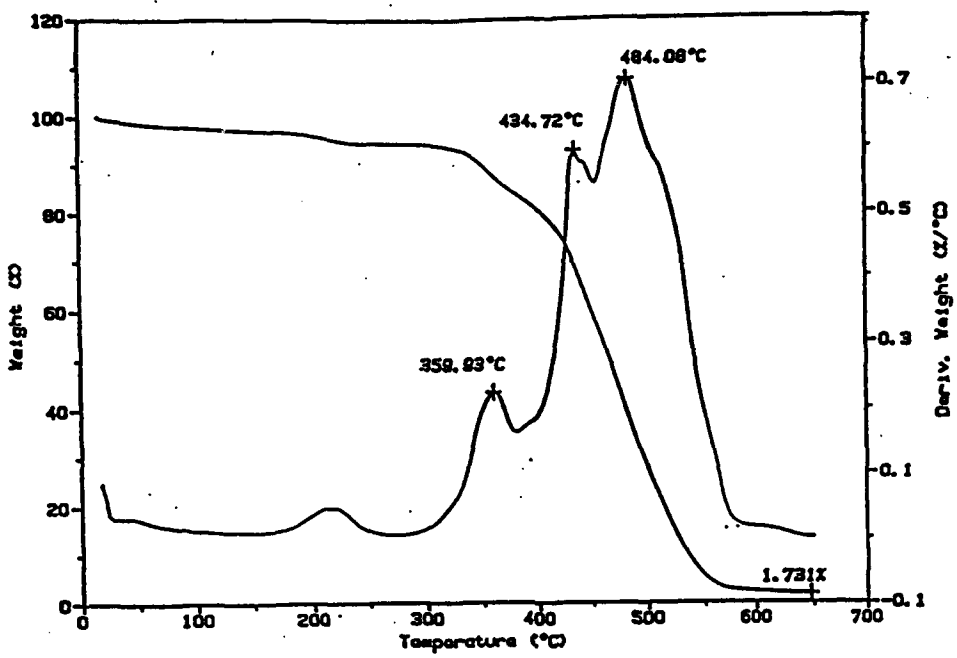

Post-reacted with $(CH_3)_2Si(OC_2H_5)_2$ for 0.5 hr

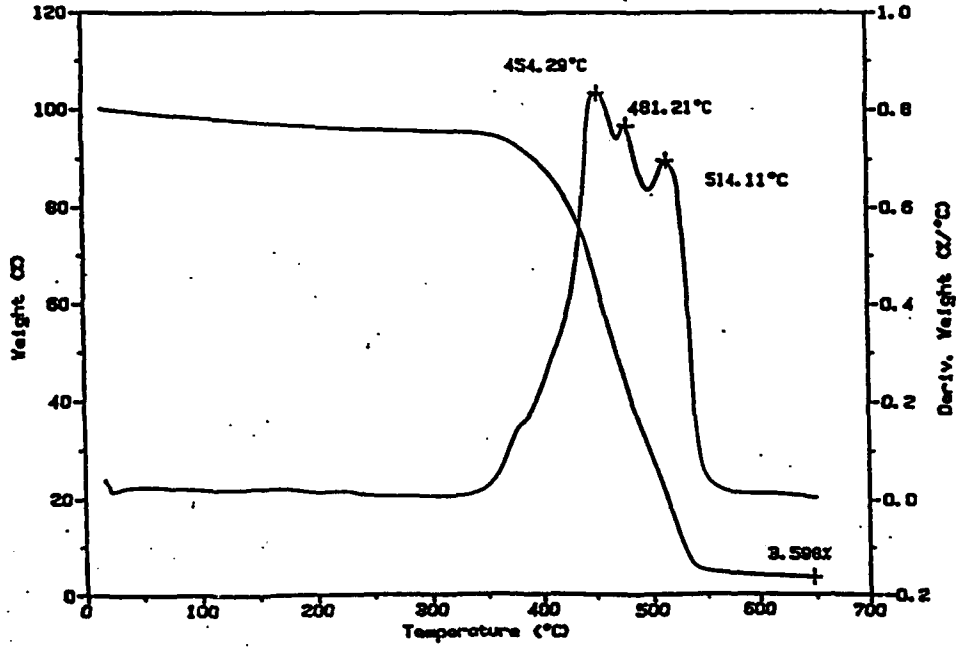

Figure 14

FT-IR (ATR) Difference Spectra: [PR] - [115 H]
SiO_2% = 6.5 %

Post-Reacted with $(CH_3)_2Si(OC_2H_5)_2$ or $(CH_3)_3Si(OC_2H_5)$ for 35 min

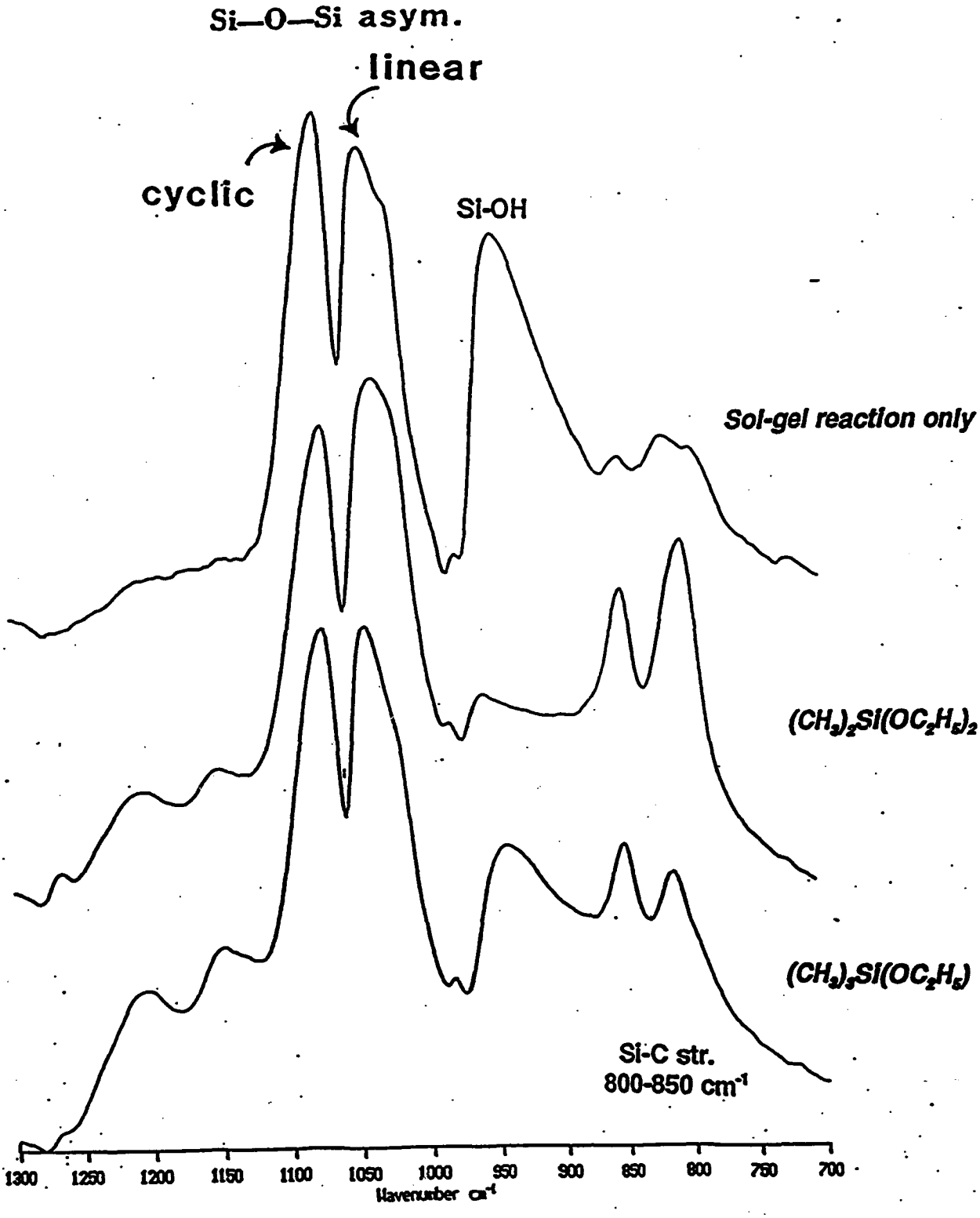

Figure 15

SiO_2% = 14.3 %

Post-Reacted with $(CH_3)_2Si(OC_2H_5)_2$ or $(CH_3)_3Si(OC_2H_5)$ for 35 min

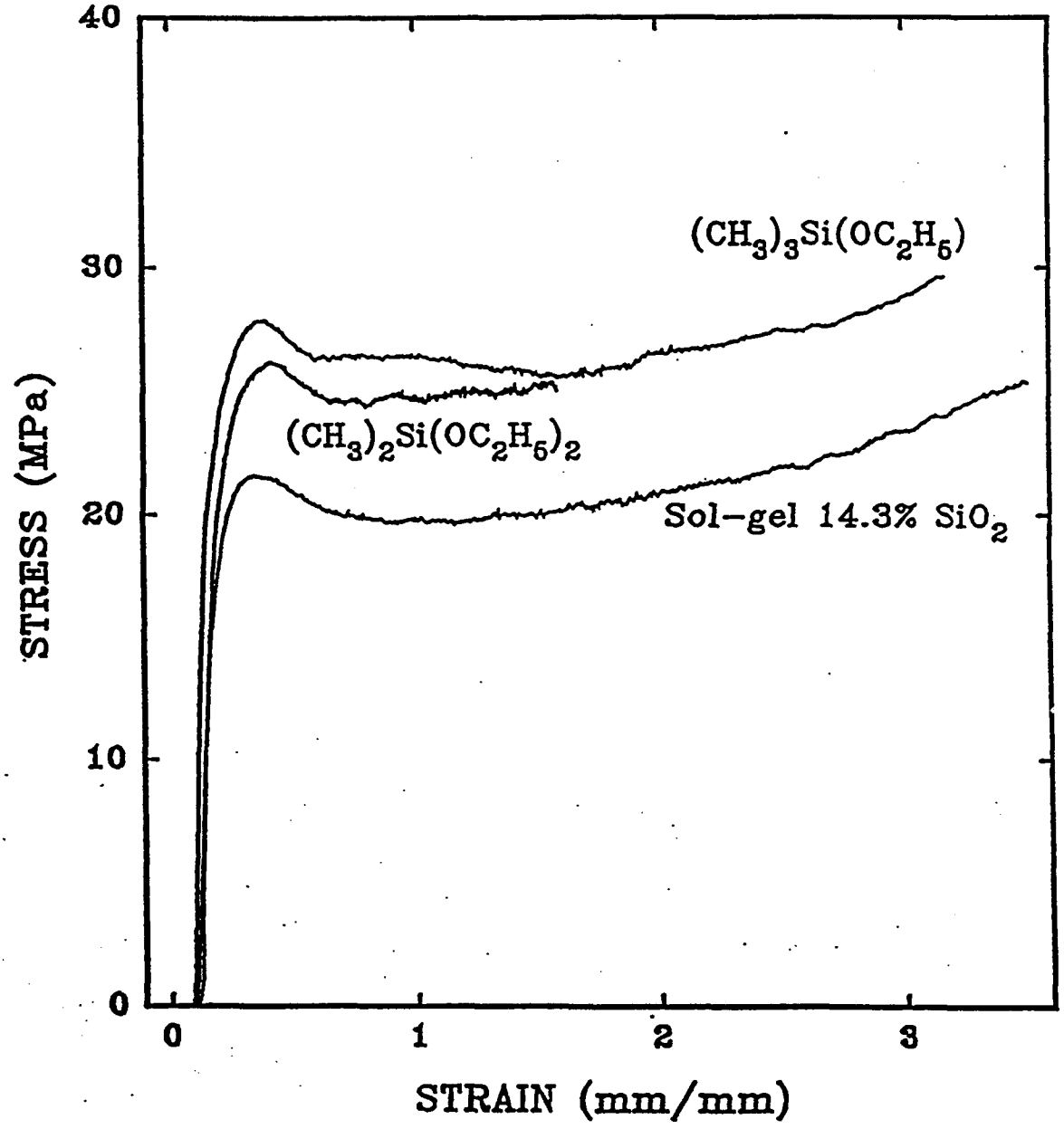

Figure 16

SiO_2% = 14.3 %

Post-Reacted with $(CH_3)_2Si(OC_2H_5)_2$ or $(CH_3)_3Si(OC_2H_5)$ for 35 min

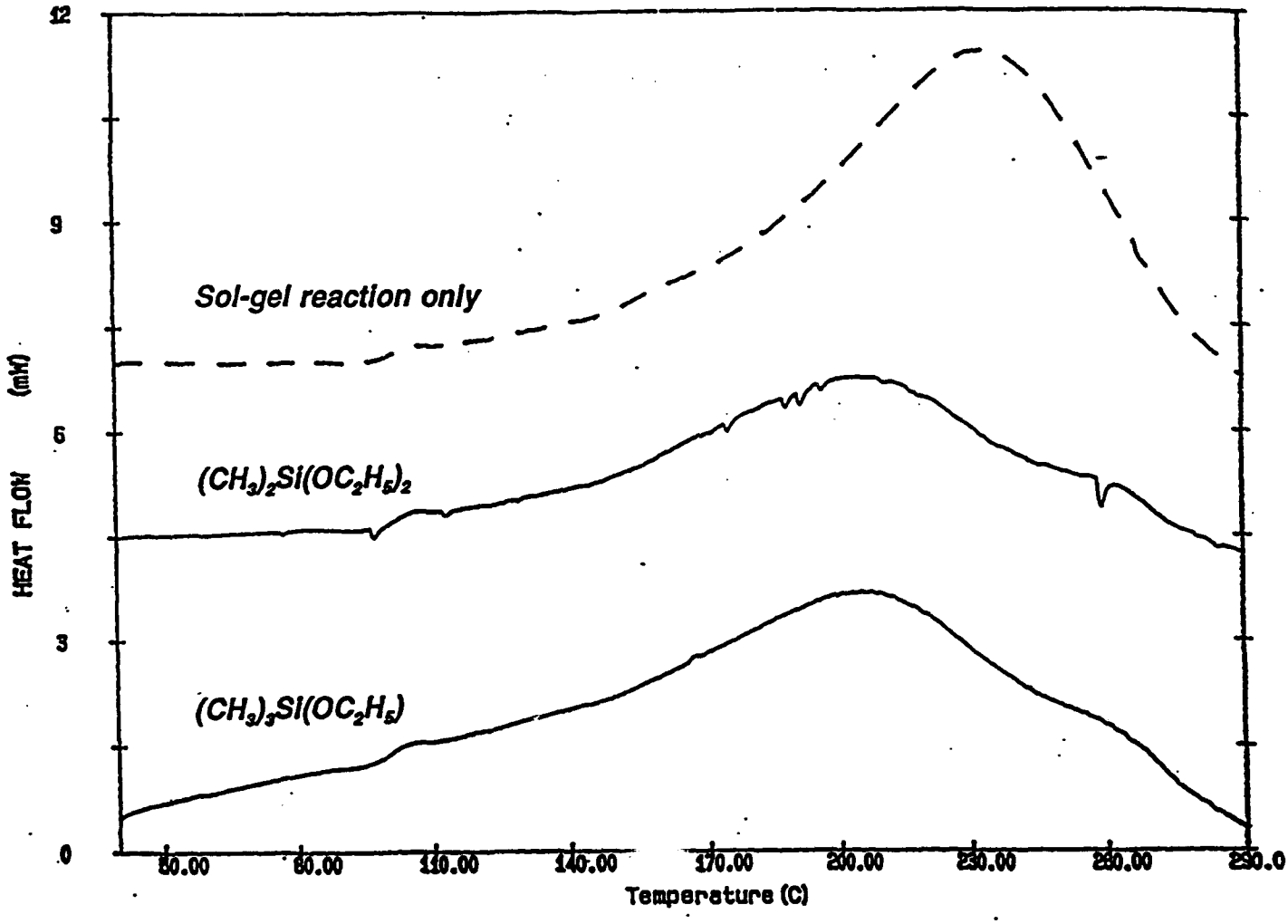

Figure 17

FT-IR (ATR) Difference Spectra: [PR] - [115 H]

Mixed Reaction of TEOS/DEDMS in Nafion Membrane
weight uptake around 10 %

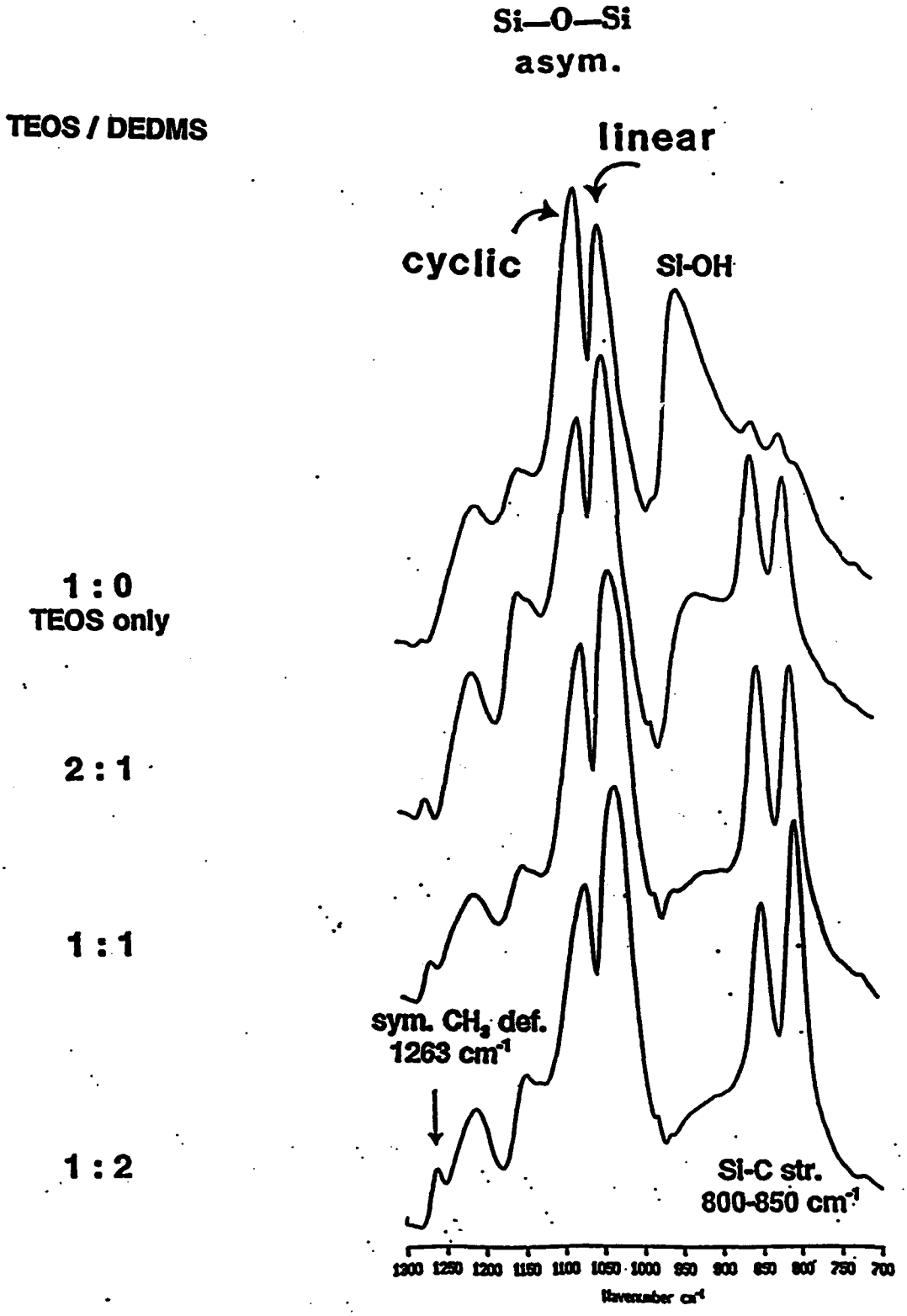

Figure 18

Mixed Reaction of TEOS/DEDMS in Nafion

weight uptake around 10 %

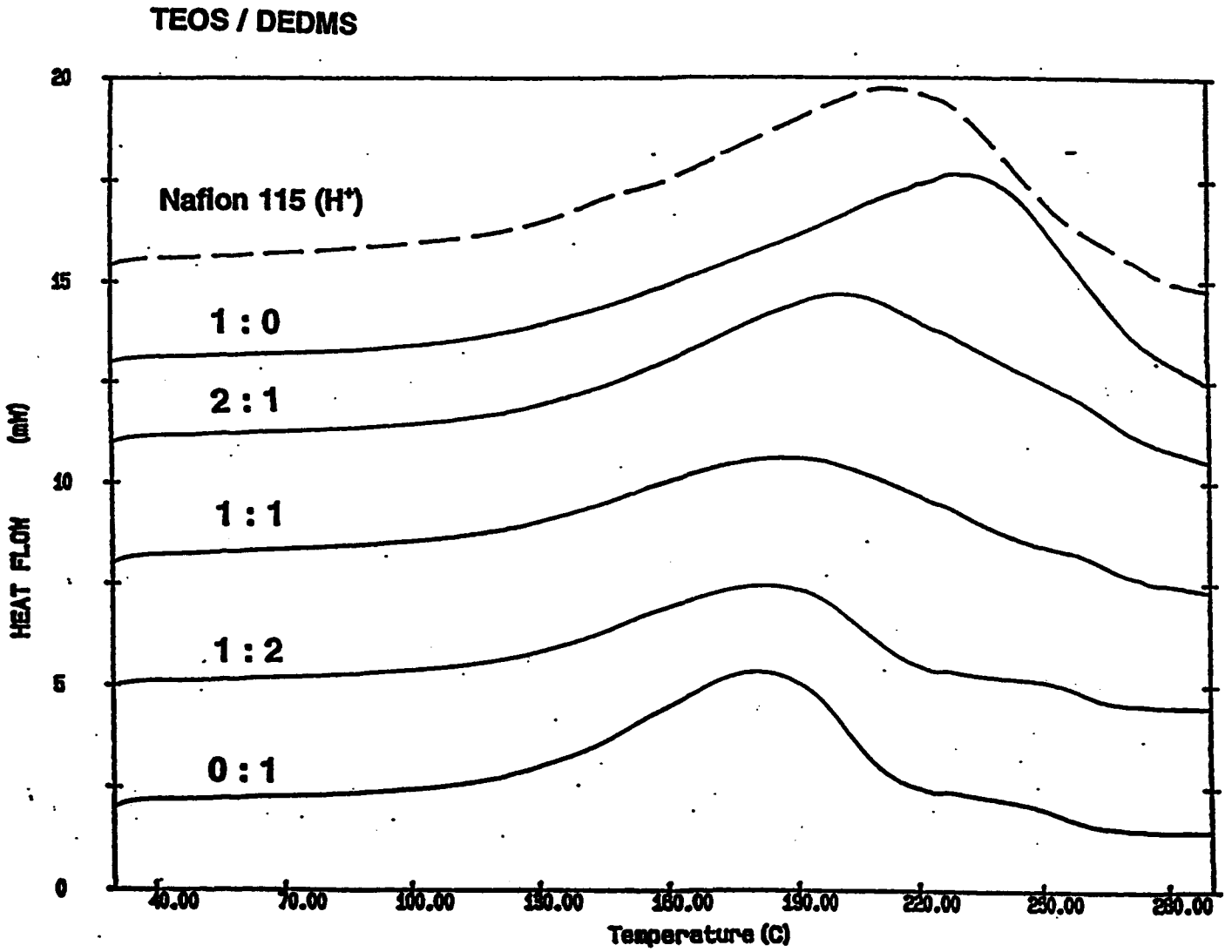

Figure 19

Mixed Reaction of TEOS/DEDMS in Nafion Membrane

weight uptake around 10 %

TEOS / DEDMS molar ratio as indicated

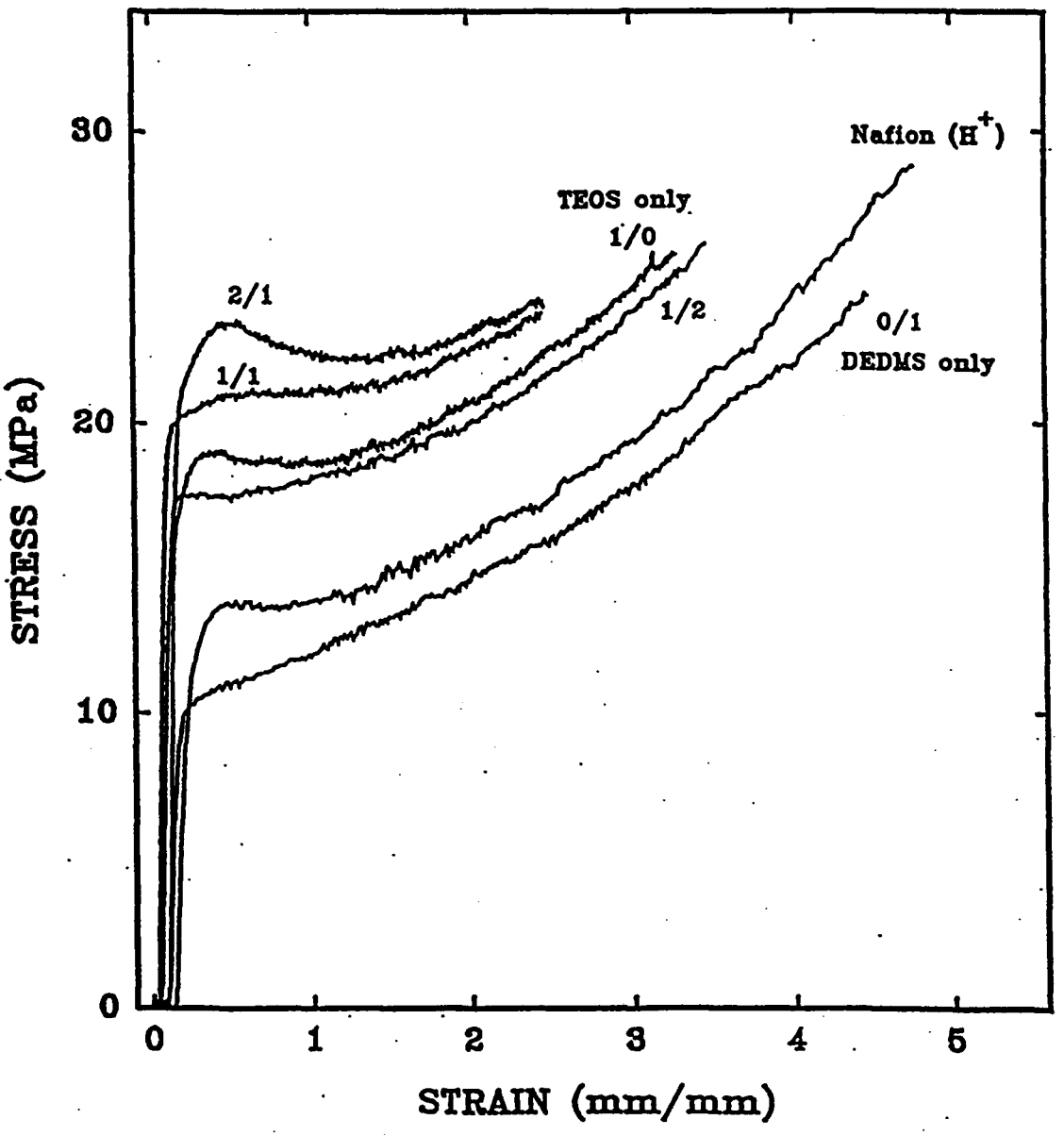

Figure 20

MIXED INORGANIC OXIDE NANOCLUSTERS

$$Si(OR)_4 + Ti(OR')_4 \text{ or } Al(OR'')_3$$

COMPOSITIONAL SEGREGATION:

Different reaction rates:

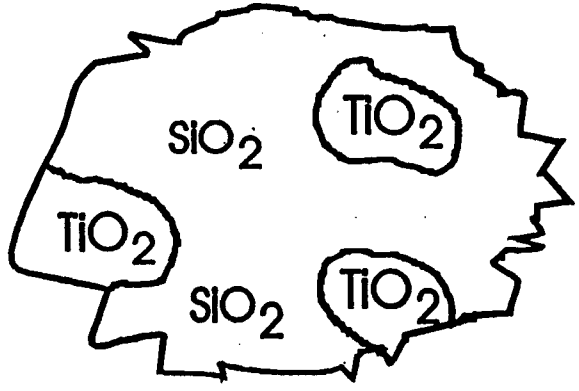

Different diffusion rates and solubilities for different alkoxides

INTRAPARTICLE MOLECULAR CONNECTIVITY:

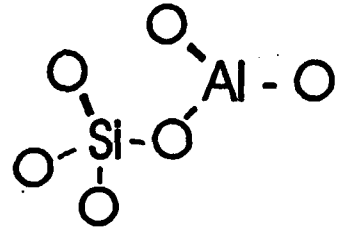

Hydrated -> Immersed in Premixed Si/Ti Alkoxide Solution

Total Uptake ~7 wt%

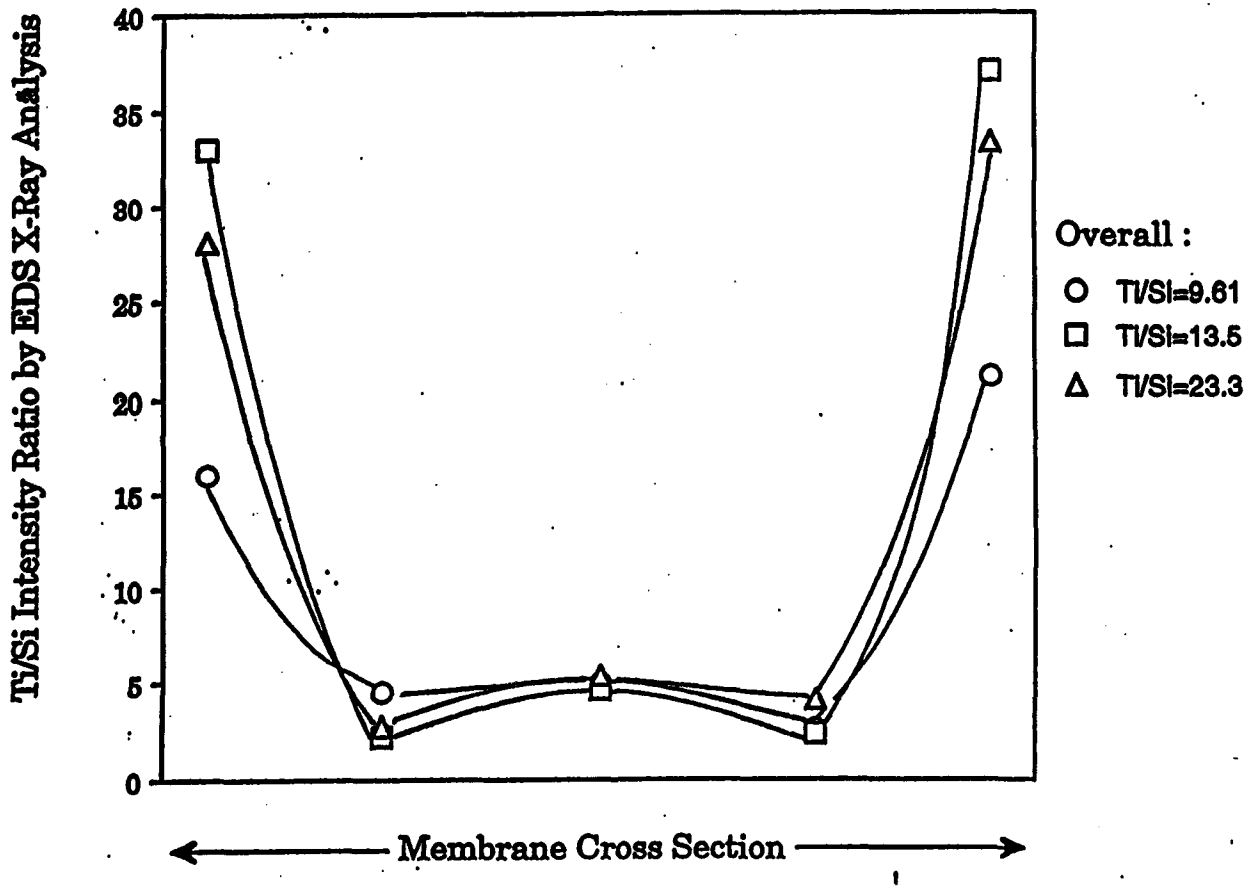

Figure 22

Hydrated -> Immersed in Premixed Si/Ti Alkoxide Solution

Total Uptake ~7 wt%

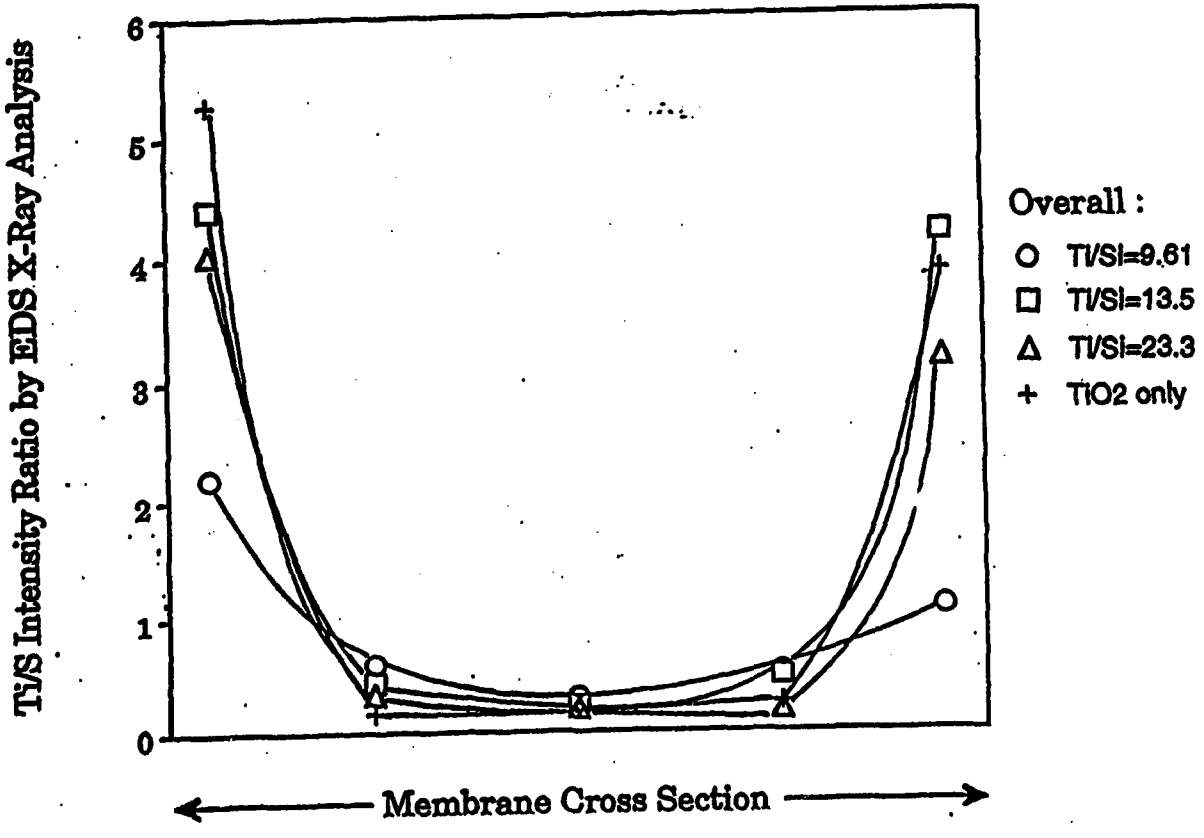

Figure 23

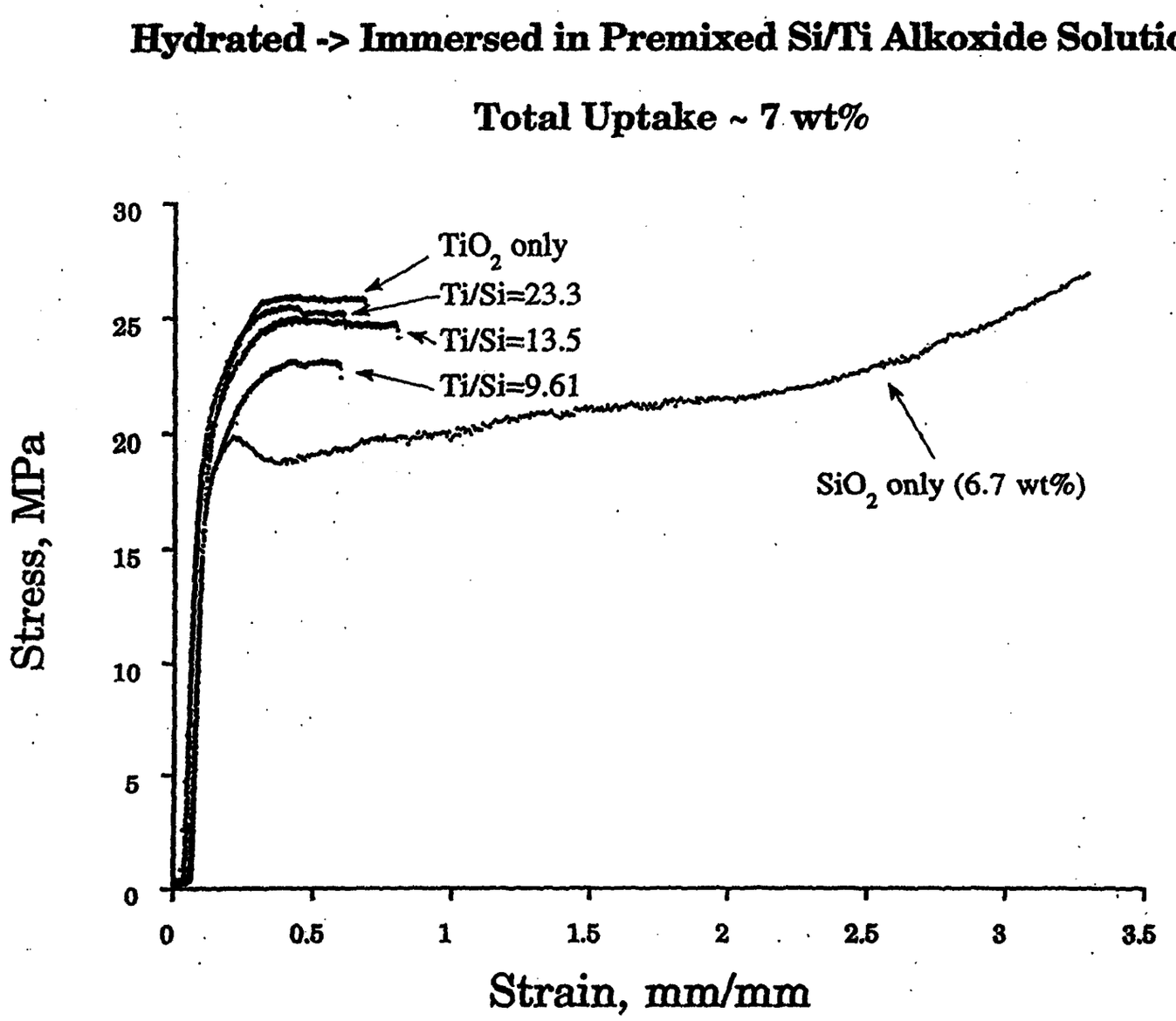
Hydrated -> Immersed in Premixed Si/Ti Alkoxide Solution
Total Uptake ~ 7 wt%
TiO2 only
Ti/Si=23.3
Ti/Si=13.5
Ti/Si=9.61
SiO2 only (6.7 wt%)
Stress, MPa
Strain, mm/mm
0
5
10
15
20
25
30
0
0.5
1
1.5
2
2.5
3
3.5

Figure 24

MIXED INORGANIC OXIDE NANOCLUSTERS

$Si(OR)_4 + Ti(OR')_4$ or $Al(OR'')_3$

SEQUENTIAL ALKOXIDE ADDITION

CORE-SHELL NANOPARTICLES:

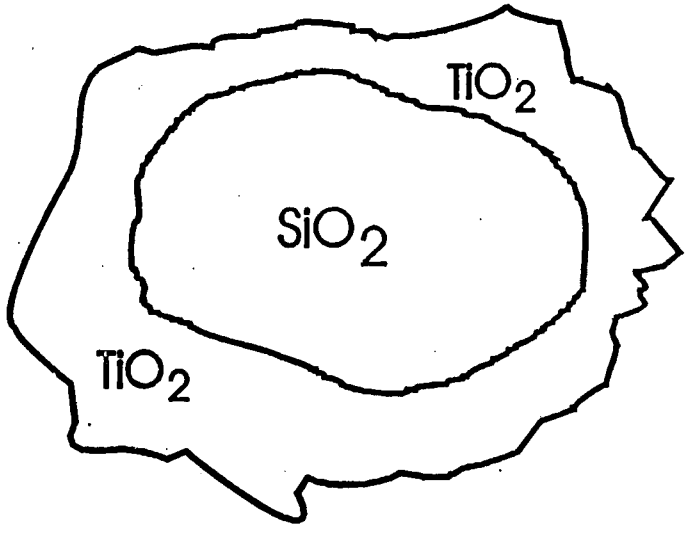

Figure 25

Swelled in H_2O/2-PrOH (1/20 v/v)
-> Added TEOS/2-PrOH (H_2O/TEOS=1/1 mol/mol)
-> Placed to TBT/2-PrOH

Total Uptake ~14-16 wt%

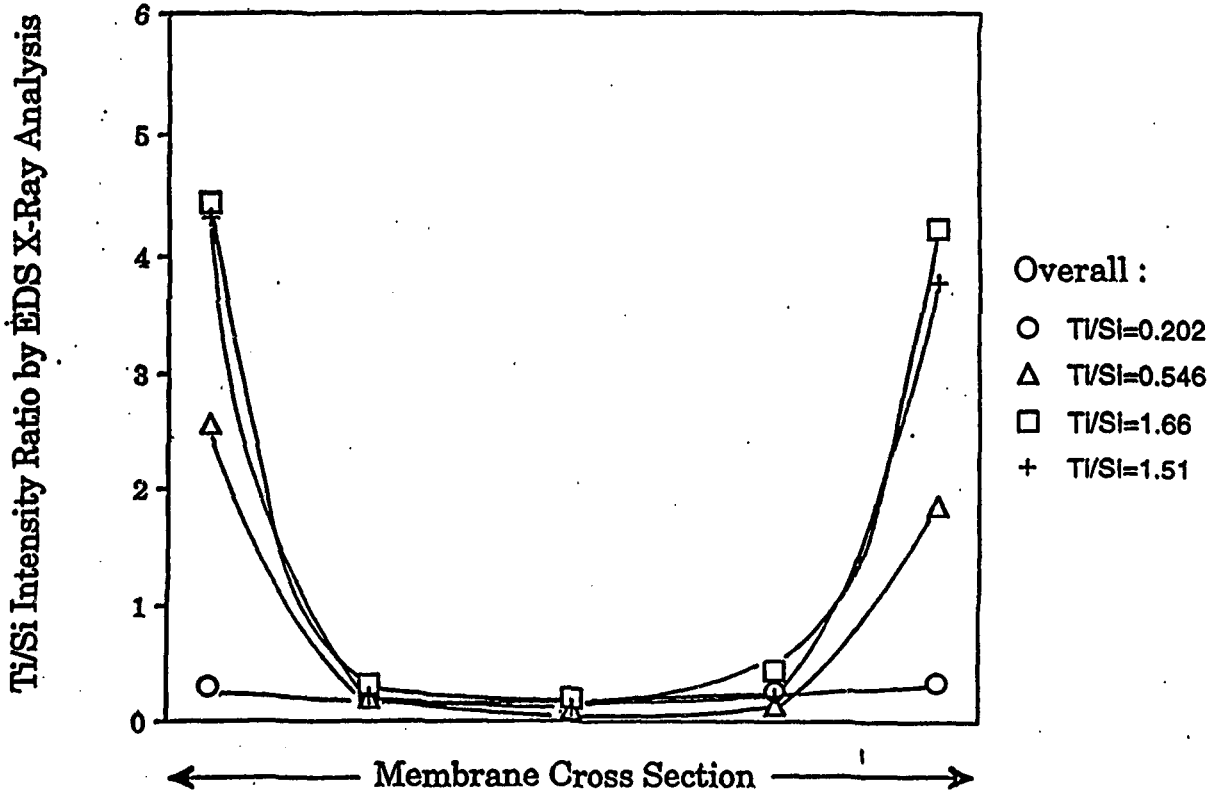

Figure 26

Swelled in H_2O/2-PrOH (1/20 v/v)
-> Added TEOS/2-PrOH (H_2O/TEOS=1/1 mol/mol)
-> Placed to TBT/2-PrOH

Total Uptake ~14-16 wt%

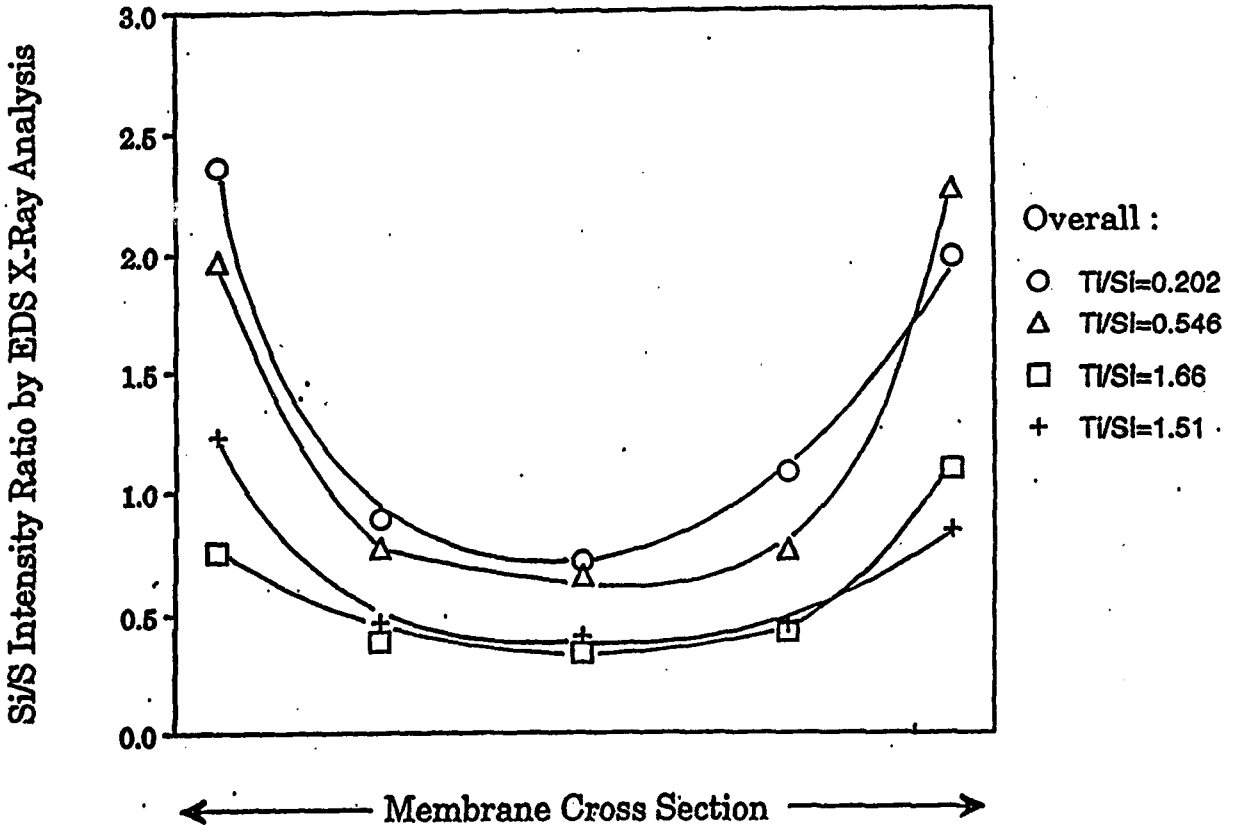

Figure 27

Swelled in H_2O/2-PrOH (1/20 v/v) -> Added TEOS/2-PrOH (H_2O/TEOS= 1/1 mol/mol)
-> Placed to TBT/2-PrOH
Total Uptake ~14-16 wt%
Ti/Si=1.66
Ti/Si=1.51
Ti/Si=0.202
Ti/Si=0.546
SiO_2 only (15.9 wt%)
Stress, MPa
Strain, mm/mm
0
5
10
15
20
25
30
35
40
0
0.2
0.4
0.6
0.8
1

Figure 28

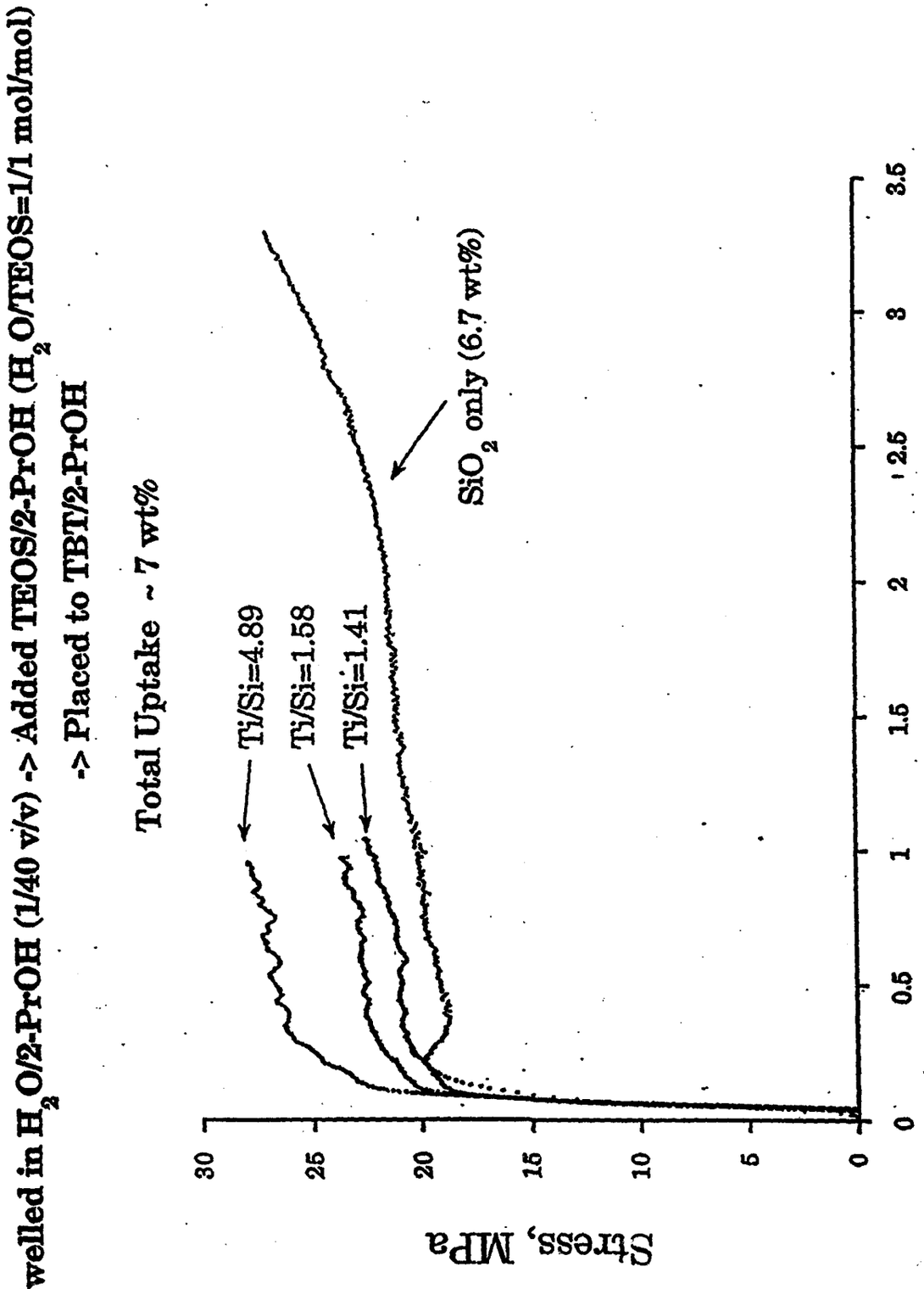
Swelled in H_2O/2-PrOH (1/40 v/v) -> Added TEOS/2-PrOH (H_2O/TEOS=1/1 mol/mol)
-> Placed to TBT/2-PrOH
Total Uptake ~ 7 wt%
Ti/Si=4.89
Ti/Si=1.58
Ti/Si=1.41
SiO_2 only (6.7 wt%)
Stress, MPa
Strain, mm/mm
0
5
10
15
20
25
30
0
0.5
1
1.5
2
2.5
3
3.5

Figure 29

Figure 30

Swelled in H_2O/2-PrOH (1/40 v/v)
-> Added TEOS/2-PrOH (H_2O/TEOS=1/1 mol/mol)
-> Placed to TBT/2-PrOH

Total Uptake ~7 wt%

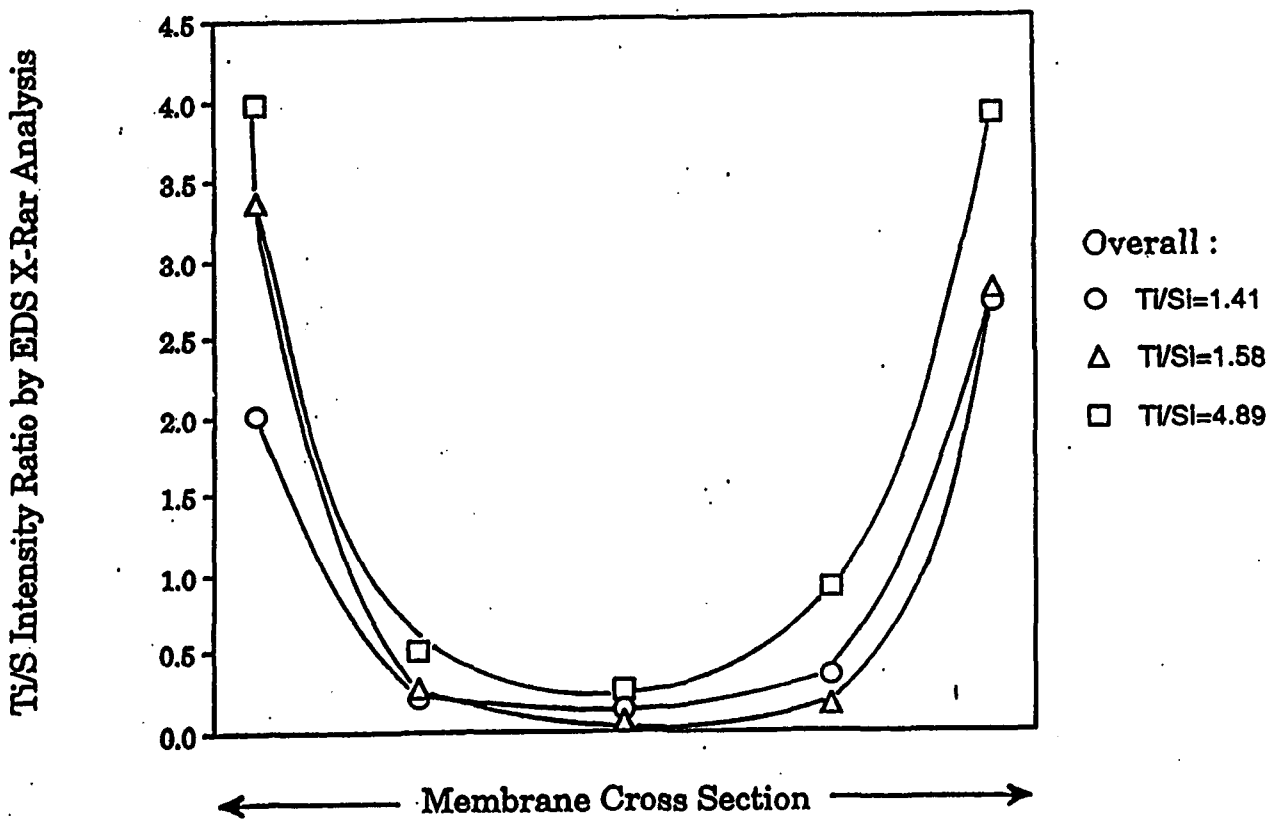

Figure 31

Hydrated -> Immersed in Premixed Si/Al Alkoxid Solution

Total uptake ~4-6 wt%

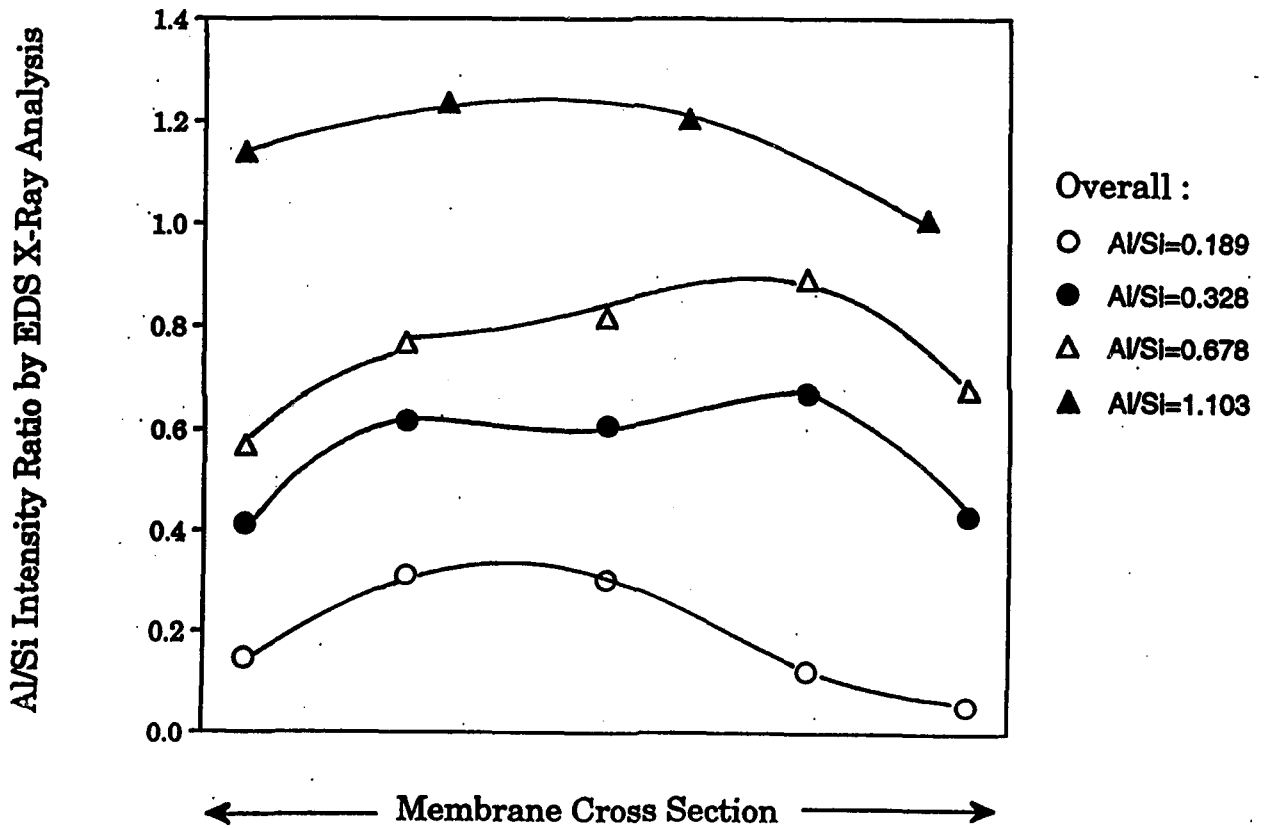

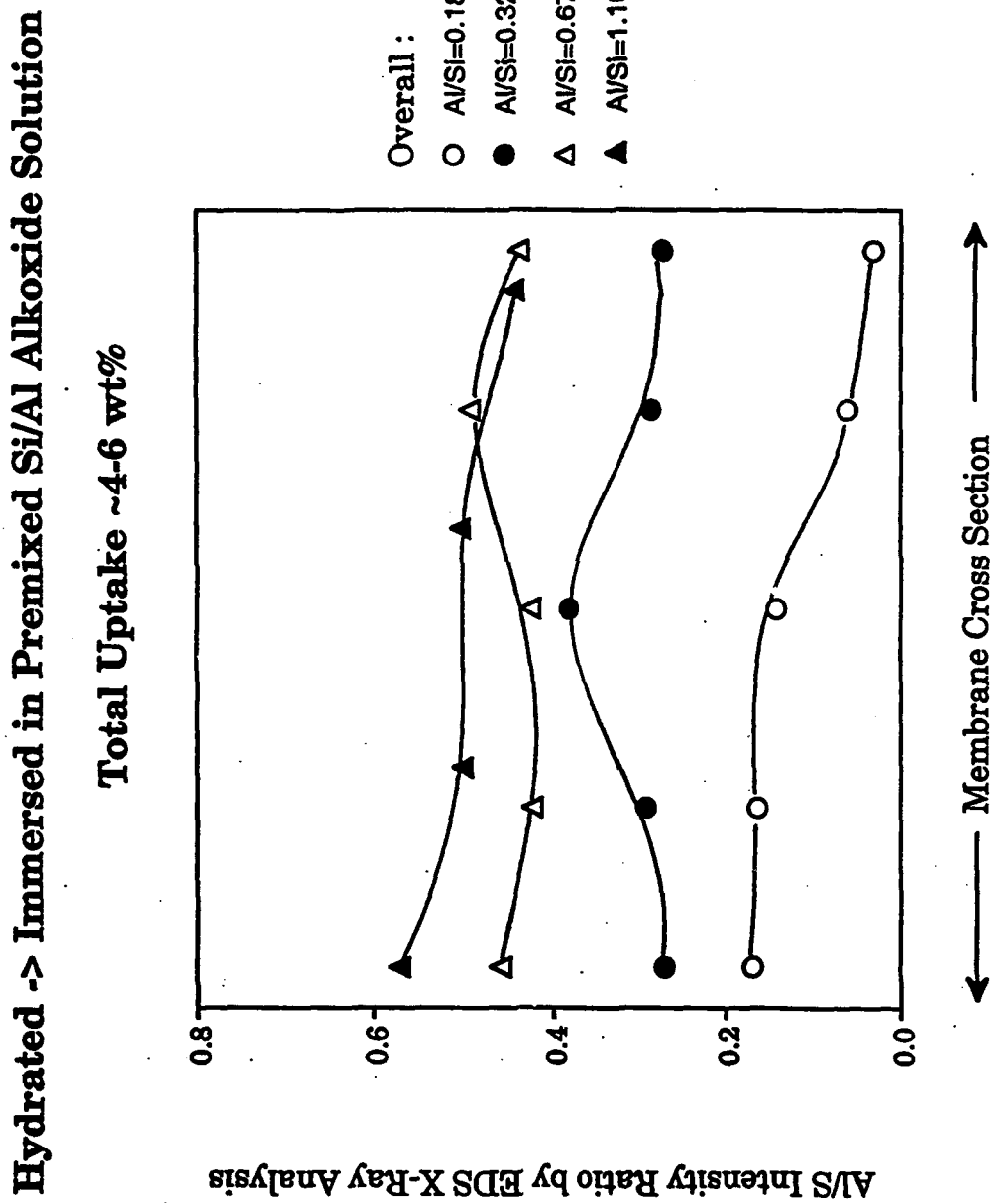
Hydrated -> Immersed in Premixed Si/Al Alkoxide Solution
Total Uptake ~4-6 wt%
Overall :
Al/Si=0.189
Al/Si=0.328
Al/Si=0.678
Al/Si=1.103
Al/S Intensity Ratio by EDS X-Ray Analysis
0.0
0.2
0.4
0.6
0.8
Membrane Cross Section

Figure 32

Hydrated -> Immersed in Premixed Si/Al Alkoxide Solution
Total Uptake ~4-6 wt%
Overall :
Al/Si=0.189
Al/Si=0.328
Al/Si=0.678
Al/Si=1.103
Si/S Intensity Ratio by EDS X-Ray Analysis
2.0
1.6
1.2
0.8
0.4
0.0
Membrane Cross Section

Figure 33

Hydrated -> Immersed in Premixed Si/Al Alkoxide Solution

Total Uptake ~4-6 wt%

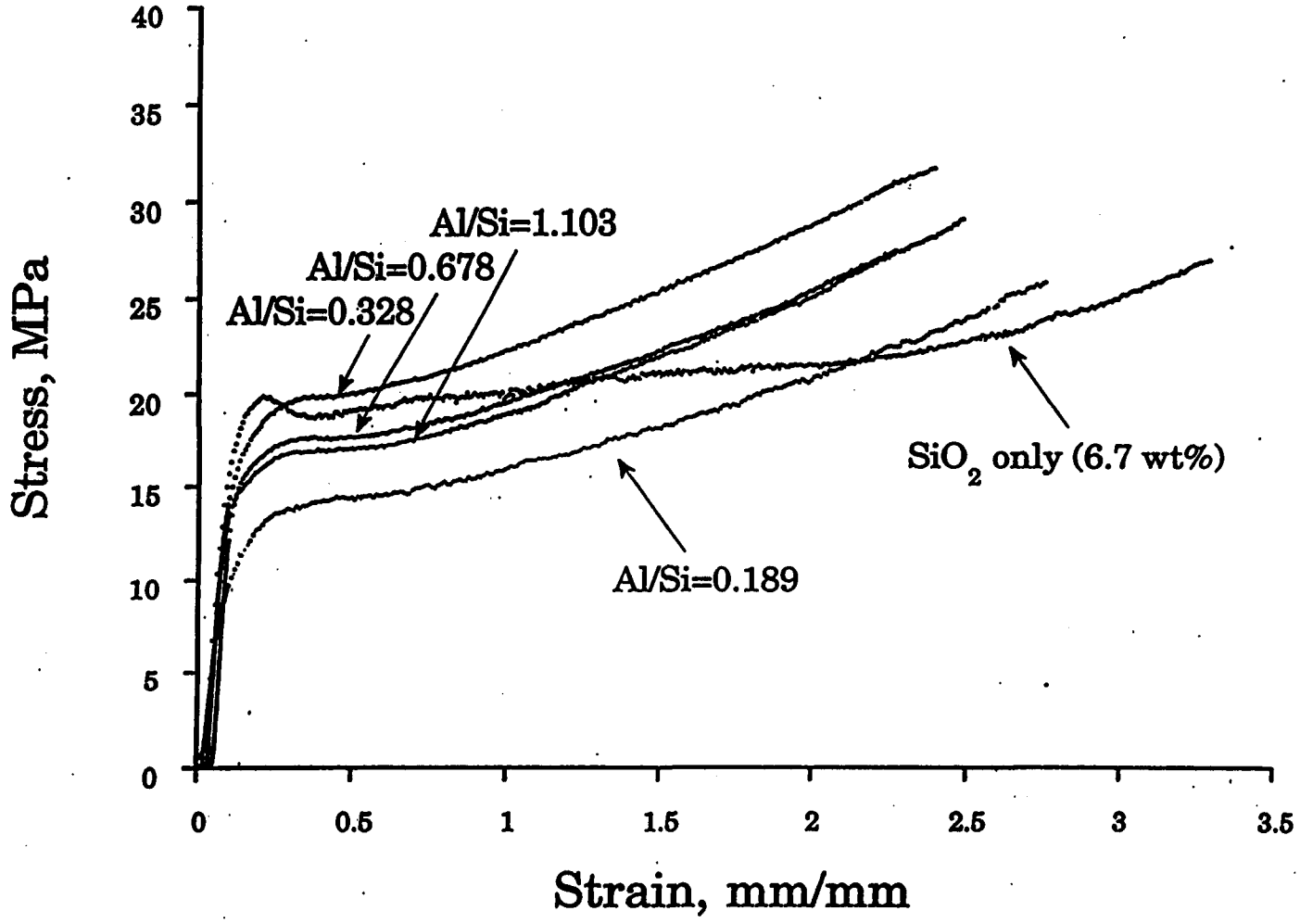

Figure 34

RESEARCH REPORT TO AFOSR

June 13, 1994

PART III

TABLE OF CONTENTS

PART III

Following is mainly the work of Dr. Qin Deng, Postdoctoral Associate, and K. A. Mauritz, Professor

I. TGA-FTIR Investigation of the Thermal Degradation of Nafion and Nafion/Silicon Oxide Nanocomposites

A. Unfilled Nafion-H⁺

Coupled TGA-FTIR is a powerful tool for analyzing thermal degradation in high performance polymers in its ability to identify molecular fragments evolved during specific weight loss events. The degradation of H^+-form Nafion using TGA-FTIR was earlier reported by Wilkie *et al.*[1]

We initiated TGA-FTIR investigations of [*Nafion*] (5 mil-thick, 1100 EW films)/[*Inorganic Oxide*] nanocomposites through collaboration with C.A. Wilkie (Marquette U.). Ultimately, we will have in-house capability for these experiments. TGA was carried out under N_2 with 20 °C/min heating. At this stage, our ongoing analysis of the data is rather incomplete and we offer preliminary observations with tentative interpretations.

These experiments are relevant in that Nafion, unfilled, is a thermally-robust material and stability enhancement will extend its range of application.

B. TGA/FT-IR Investigations of Unfilled Nafion-H⁺

The "dry," unfilled Nafion-H^+ in this study initiated decomposition around 300°C (TGA thermograms not shown): Around 6%, weight was lost in the interval 300-340°C, 18% loss accumulated up to 420°C, 35% to 480°C and 100% to 560°C. Nafion mainly degrades after final melting of TFE crystallites.

Numerous FT-IR spectra were recorded over the temperature interval seen on the horizontal axes of Figs. 1 and 2. IR signature bands of the evolved gases included SO_2 (1323-25 cm^{-1}), CO_2 (2345-50 cm^{-1}) and SiF_4 (1024-26 cm^{-1}). SO_2 evolution reflects rem of the important sulfonate ion exchange functionality. SiF_4 is presumed to issue from the known reaction for vitreous silica:

$$4HF + SiO_2 \rightarrow SiF_4 + 2H_2O(1)$$

While there is no Si in the unfilled Nafion, it is unintentionally generated by the reaction of HF with SiO_2 from the quartz tube sample container.

IR gas phase absorbances for different increasing temperatures are shown in Figs. 1 and 2. Absorbance is reduced to a *per gram of Nafion* basis, the inorganic fraction having been computationally split off. The initial weights of all samples are essentially the same. This computational adjustment is logical for composites in which the filler does not degrade. However, the rationale for this adjustment is somewhat "softer" for these nanocomposites because the inorganic phase can also suffer reactions, namely condensation involving SiOH groups and the above-discussed SiF_4-generating reactions.

We mention that, during the course of these experiments, the CO_2 IR band was complicated by the presence of atmospheric CO_2 in the chamber. Therefore, we cannot comment on the important CO_2 evolution until this confusion is resolved. Spectra was obtained for silicon oxide-containing Nafion, as well for these same samples that were post-reacted with DEDMS.

Up to ~400°C, little SO_2 and little SiF_4 was observed for unfilled Nafion and from 400 to ~480°C these products evolved slowly. For both gases, an increase in rate occurred after ~ 480°C with the absorbance increasing sharply to maxima ~615°C. Over the investigated temperature range, neither CO (2100 cm^{-1}) nor substituted carbonyl fluorides (1957, 1928 cm^{-1}) were seen.

These results differ somewhat from those of Wilkie *et al.*[1] who noted a 7% loss from 280 to 355°C. SO_2 and CO_2 increased throughout this region while water release decreased. They noted SiF_4, CO, HF, substituted carbonyl fluorides and the C-F stretching signature all appeared in this region. SO_2 and CO amounts decreased dramatically at 365°C to be of no consequence. Major decomposition products in the range 355-560°C were SiF_4, carbonyl fluorides, and species exhibiting C-F stretching vibration.

A proposed thermal degradation mechanism involves initial cleavage of the C-S bond leading to SO_2, OH radical, and a carbon-based radical which further degrades. Their materials were Nafion-H^+ beads and films provided by DuPont without further modification. Observed differences might arise from Nafion sample pre-history and equivalent weight variance. The significant difference between the two results is that the present studies show large increase of SO_2 with a maximum at 615°C, whereas the earlier studies do not. In the present experiment, not all C-S bonds appear to broken before 365°C; rather, this process maximizes ~615°C.

C. Nafion / SiO_2 Nanocomposites and Silane Post-reacted Nanocomposites

1. Nafion/SiO_2 Nanocomposites

Unfilled Nafion-H^+ decomposes slower, overall, than Nafion/SiO_2, although both initiate degradation at approximately the same temperature. Both Nafion and Nafion/SiO_2 appear to have at least two distinct thermodegradative steps, while Nafion/SiO_2 post-reacted (PR) with DEDMS = $(CH_3)_2Si(OC_2H_5)_2$ (referred to here as Nafion/SiO_2-PR) is unique in having but one abrupt degradation step. On the other hand, it has the highest thermal stability (60-70°C upward shift), under both N_2 and air.

A Nafion/SiO_2(14%) hybrid was produced via an *in-situ* sol-gel reaction for TEOS using the earlier-discussed procedure. Compared with Nafion-H^+, the hybrid initiated decomposition 5-10°C higher (~305-310 °C), but then proceeded to degrade faster. At 454°C, there is a cumulative weight loss of 40%; 6.6% of the original sample weight remained at 539 °C and 1.2% at 605°C.

FT-IR spectra (Figs. 1, 2) show that up to around 454°C, only small quantities of SO_2 and SiF_4 have been generated. Beyond this temperature, SO_2 uniformily increases to a maximum which is considerably lower than that for unfilled Nafion. A great increase in SiF_4 evolution ensues from 454 to a maximum ~575°C. In light of prior comments regarding SiF_4 evolution during the experiment with unfilled Nafion, the results for Nafion-incorporated SiO_2 are neccessarily confusing. Nonetheless, the fact that this

sample generates more SiF_4 than unfilled Nafion is not surprising since it contains internal SiO_2 that is immediately accessible for by generated HF. Compared with unfilled Nafion-H^+, SO_2 evolution is significantly reduced at higher temperatures although at lower temperatures, Nafion/SiO_2 actually generates discernably more SO_2. Over the temperature range CO(2100 cm^{-1}) and substituted carbonyl fluorides (1957 and 1928 cm^{-1}) were not observed.

Rationalization of the profound SO_2 inhibition is considered within the context of intimate silicon oxide incorporation within clusters of SO_3-terminated sidechains. Silicon oxide invasion of Nafion of this degree is thought to disrupt neither clusters nor TFE crystallinity significantly. Sidechains are envisioned as immobilized within silicon oxide "cages" that inhibit reactions involving -SO_3 groups. This cage, however, can be degraded by generated HF, unprotecting the sidechains. As backbone crystallinity is not greatly affected by the filler, the *onset* of degradation is not profoundly affected, as observed. On the other hand, crosslinking provided by ionic aggregation has already been disrupted by invasion of the 30-50 Å cluster spaces by $SiO_{2[1-1/4x]}(OH)_x$ structures. In this way, thermal decomposition for Nafion/SiO_2 occurs more abruptly. It would seem natural that, for silicon oxide-filled Nafion, HF produced from decomposition reacts with *in situ* SiO_2 first, the surplus HF attacking the TGA glass sample tube. The detection of SiF_4 resolves an earlier inexplicable observation that weight remaining after a high temperature TGA run is always less than the original SiO_2 weight uptake as measured by balance.

2. Post-treatment of Nafion/SiO_2 with Diethoxydimethylsilane.

For this system, only one sharp decomposition step, initiating ~370°C, was observed. Although decomposition proceeded even faster here than that for Nafion/SiO_2, this sample showed the highest temperature of degradation onset of the three cases. At 450°C there was 40% weight loss, 6.8% was left at 543°C and 6.0% at 653°C.

Up to 544°C, neither SiF_4 nor SO_2 were detected. From 544 to 652°C, SiF_4 was detected, although the curve that rises to a peak is below that of unfilled Nafion, but the curves are somewhat close to each other at the highest temperatures. The DEDMS post-treated absorbance curve is profoundly below that of Nafion/SiO_2. Apparently, the reaction of DEDMS with unreacted Si-OH groups on the pre-existing silicon oxide phase protects this phase from HF attack. SO_2 was detected in small quantities and the curve, exhibiting a maximum around 580°C, lay below the other two. Several methyl group peaks were always present. CH_3 groups are known to detach from Si-C around 500°C.

We conclude that the thermal degradation mechanism for Nafion-H^+ has been altered by incorporating either SiO_2 or SiO_2 that has been post-reacted with DEDMS, the latter system being superior.

II. Nafion-*In Situ* TEOS-DEDMS Co-Condensation-Dynamic Mechanical Analysis (DMA)

DMA spectra were obtained for a series of hybrids having various TEOS:DEDMS mole ratios; formulation of these samples was described in the previous report. TEOS and DEDMS were in premixed MeOH solutions so that both species began film permeation at

the same time. In these experiments, E' and tan δ spectra, all at 1 Hz, were obtained for heating at 2°C/min from 30 to 300°C.

For dried, unfilled Nafion-H^+, two tan δ peaks, around 136 and 240°C were observed (graphs not shown). These peaks correspond to previously-observed DSC transitions. Given the large corresponding drop in E', T_g (*i.e.* at tan δ maximum) is apparently 130°C. The nature of the high temperature peak has recently been in question; possibilities include: (1) a transition within, or influenced by clusters; (2) the melting of TFE crystallites that are packed less perfectly than those in PTFE; (3) a water-related transition.

For pure TEOS, two broad overlapping peaks appeared around 160 and 250°C (Fig. 3a); assumedly, these peaks reflect the same, but modified mechanisms present in unfilled Nafion. On comparing these curves with those for pure Nafion, it is obvious that T_g = 160° C, an increase from the unfilled state which suggests restricted chain segmental mobility. E' *increases* somewhat from ~35 to 100°C. We offer the suggestion that increasing temperature in the DMA drives further condensation of residual Si-OH groups, thereby enhancing material cohesion. The high temperature transition appears rather broad.

For TEOS/DEDMS = 2:1 (11.3 wt%), one strong tan δ peak ~145°C (*i.e.* T_g, given the corresponding E' drop) was detected (Fig. 3b). Here, E' does not undergo the initial increase with increasing temperature occurring for the pure TEOS case. Presumably, this is due to a lower relative population of residual Si-OH groups.

For TEOS:DEDMS = 1:1 (10.9 wt%), T_g~145°C and the initial rise in E' is absent (graphs not shown). For TEOS:DEDMS = 1:2, two peaks, one ~135 °C another ~250 °C are seen (Fig. 3c).

Finally, for pure DEDMS reacted in Nafion, three peaks were present around 105, 165, and 270°C (Fig. 3d). On inspection of the E' curve, 105°C appears to be a downwardly-displaced T_g.

These DMA trends with mixed TEOS:DEDMS content are harmonious with our earlier DSC results suggesting that these hybrids become more flexible as the "linear" inorganic comonomer (DEDMS) composition increases.

Pure poly(dimethylsiloxane) (PDMS) has a very low T_g (-125 °C) and incorporating it within another polymer of higher T_g, say as a component of an *interpenetrating network*, is expected to lower overall T_g. At this point, we cannot say that PDMS exists within Nafion for the TEOS:DEDMS = 0:1 case, although reasonably long and flexible oligomers must be present.

In order to further understand the interaction between Nafion and incorporated $[-(CH_3)_2Si\text{-}O]_x$ chains, we examined transitions in the lower temperature range: -160 to +30°C. A control sample of unfilled Nafion and Nafion/(TEOS:DEDMS = 0:1) were studied by DMA. For unfilled Nafion, a transition ~-69°C was detected (Fig. 4a). For Nafion/DEDMS, this transition shifts downward to ~-80 °C (Fig. 4b). While the origin of this glassy-state transition is presently unknown, it appears that a short-ranged molecular motion in Nafion has been imparted more mobility by interactions with interpenetrating PDMS chains.

III. Reaction of Pure DEDMS in Nafion-H^+ *vs* Time

Studies of the reaction of pure DEDMS in Nafion were conducted *vs* time to explore the possibility of generating Nafion/PDMS *interpenetrating networks*.

As before, Nafion 115 H^+ films were swollen in 50ml MeOH/15ml D.I. H_2O solutions for 24 hr. With H_2O:DEDMS = 2:1, 45ml DEDMS in 10ml MeOH was added to these solutions and sorbed by the membranes for immersion times of 6, 20, 45, 90 and 180 min. Thereafter, samples were transferred to an oven pre-set at 50°C, after which they were heated to 100°C within 1/2 hr. and held at 100°C for 48 hr. under vacuum. For comparison, samples of TEOS/DEDMS=1:1 were also prepared for reaction at immersion times of 6, 20 and 45 min.

Dried weight uptake *vs* immersion time were plotted for DEDMS (Fig. 5b) and TEOS/DEDMS = 1:1 (Fig. 5a). Surprisingly, uptake for DEDMS-reacted Nafion did not increase but decreased slightly, with fluctuation, from about 16% to 10% from 6 to 180 min, the lowest value being 8.8%. On the other hand, for TEOS/DEDMS = 1:1, weight uptake increased somewhat from about 9.9% to 12.6% from 6 to 45 min. Possible rationalizations might include the following. Pure DEDMS does not crosslink or form interconnected structures as does TEOS. Therefore, DMS monomers, oligomers or even polymers formed within Nafion can counter-diffuse back to the external solution driven by concentration gradients that increase with time, since the formation of PDMS inside clusters is favored over in external solution owing to the acidity in clusters. Thus, longer immersion time might lead to more DMS oligomer out-leaching. DMS is more hydrophobic than hydrolyzed TEOS or hydrolyzed TEOS/DEDMS mixtures which renders the former less energetically-compatible within polar cluster domains.

However, for TEOS:DEDMS = 1:1, interconnected rather than linear structures are formed in highly acidic clusters at longer times, as indicated by our IR and ^{29}Si solid state NMR studies. The bulkier, more energetically-compatible structures would have more difficulty in vacating the Nafion matrix once they have grown in place.

TGA analysis under N_2 was performed for both hybrids. The onset of thermal degradation always occurs ~400°C for films treated with pure DEDMS for 6 (Fig. 6a), 20 and 45 min - a significant improvement over unfilled Nafion-H^+, whereas this onset shifts downward to ~350° for 90 (Fig. 6b) and 180 min treatments. The latter two times generate profiles with two distinct weight loss regimes, whereas the prior times generated simple curves.

For the TEOS:DEDMS = 1:1 samples, the onset of degradation is constant at approximately 325°C for all immersion times and two major degradative events are apparent.

IV. FT-IR Study of Non-Nafion-Containing Films Cast from Pure TEOS/DEDMS Solutions

Films of various TEOS:DEDMS mole ratios were cast on the surfaces of NaCl IR sample plates. The TEOS/DEDMS solution compositions were the same as those contacting Nafion in the earlier-described process of nanocomposite formulation (H_2O:TEOS = 4:1, MeOH solvent, 0.1 ml of 0.5M HCl added for acid catalysis). In each experiment, one small drop of the solution was thinly spread between the two plates so

that a very small amount of NaCl could dissolve at any given place from the surfaces. On visual inspection, we did not observe dissolution-degradation of the plates due to this procedure, although a more vigorous elemental analysis of Na and Cl within the resultant films should be conducted in the future and these studies should be viewed as being preliminary.

These materials were intended to represent model, or reference structures for the corresponding inorganic phases in Nafion. In our effort to probe molecular structures of *in situ* inorganic phases by IR spectroscopy, we subtract the spectrum of unfilled Nafion-H^+ from that of the filled form; the assumption is that the difference spectrum corresponds to that of the inorganic phase, having subtracted obscuring Nafion vibrational modes. Of course, an *in situ*-grown structure is expected to possess a structure that is modified by interactions with the Nafion template. Nonetheless, inorganic phase band assignments are made with more confidence if the bands of the the particular pure phase are known beforehand. Also, given this the signature of this reference state, organic-inorganic phase interactions are inferred if the "free" or bulk state inorganic spectrum differs from that of the matrix-incorporated state.

The first experiment involves the series TEOS:DEDMS = 1:0 to 0:1. All solutions were mixed-reacted for 3 hr. One drop of each solution was placed between the IR plates for 2 min, including the data acquisition time of 0.5 min, during which 32 IR scans were collected at room temperature.

The following important bands are seen in the region 1500-700 cm^{-1}: a. Twin Si-O-Si asymmetric stretching peaks (1080-1040 cm^{-1}) indicative of bridging oxygens and network formation; b. Si-CH_3 (methyl group) symmetric deformation (1263 cm^{-1}) and two Si-C stretching peaks (~850-800 cm^{-1}) reflecting the presence of dimethylsiloxane; c. Si-OH stretching (~950 cm^{-1}) reflective of degree of incompletion of the inorganic network or degree of reaction with DEDMS; d. TEOS monomer peak at 880 cm^{-1}. The progression of these reference spectra is shown in Fig. 7.

Then, the same samples were mildly heated at 50°C under vacuum in an oven for 15 hr. This heating-drying was intended to promote polycondensation beyond the degree resulting from the first treatment. The resultant spectra varied from corresponding spectra for the first series.

As shown in Fig. 8, the Si-O-Si asymmetric peaks merge into a broad band for the 1:0 through 1:2 compositions. This suggests that the distinctions between Si-O-Si groups in linear runs *vs* those in loops has been blurred. The Si-OH/Si-O-Si(asym) peak area ratio diminishes for the same TEOS:DEDMS ratio upon drying-heating, reflecting condensation of unreacted SiOH groups.

As opposed to the preceding 1:0 to 1:2 peaks in this series, there are two reasonably-resolved peaks for the 0:1 case. The high frequency peak (~1090 cm^{-1}) is present in spectra for the entire preceding (nondried) 1:0 to 0:1 series. However, the low frequency peak (~1026 cm^{-1}) for 0:1 corresponds rather will to the low frequency shoulder on the peak at ~1048 cm^{-1} for all compositions of the first series of experiments. The monomer peak ~880 cm^{-1} is not visible in spectra for any composition, indicating a promotion of reactions by drying-heating. While the band ~847 cm^{-1} is related to network modification by DMS, it seems to shift to a considerably higher frequency for the 0:1 case both here as well as for the previous (non-dried-heated) series. The 940 cm^{-1} peak, a signature of incomplete SiOH

condensation reaction, is very weak for the 0:1 case, indicating rather complete polymerization of DEDMS into poly(dimethylsiloxane).

Finally, the same samples between the NaCl plates were treated in like fashion at 100°C, although the spectra changed but slightly.

The spectra for these simple model inorganic systems are essentially similar to corresponding difference spectra of corresponding nanocomposites. A more detailed analysis of these bands is in progress.

V. Water, Methanol and Iso-Butanol Sorption by TEOS-DEDMS-Treated Nafion

As the TEOS:DEDMS ratio for silanes sorbed by Nafion decreases, there will be more hydrophobic methyl groups and fewer hydrophilic SiOH groups, the composition of which can be monitored by FT-IR. Also, the internal inorganic network will be increasingly more linear with blocks of dimethylsiloxane. The sorption affinity of these nanocomposites for polar solvents will be reduced with decreasing TEOS:DEDMS ratio.

The three solvents utilized in the liquid sorption measurements were water, methanol and iso-butanol which gradually decrease in polarity.

Samples were dried at 100°C under vacuum for 24 hr, after which they were weighed to determine an initial weight. Then, samples were immersed in the above solvents for 40 hr at 22°C. After this time, they were surface-blotted dry and rapidly transferred to a balance to determine final weight. Weight uptake showed very good reproducibility.

The 3 nanocomposites have almost the same inorganic uptake (12-14%) so that sample intercomparison is meaningful.

A. Water Uptake

Nafion-H^+ exhibits 14.9% water uptake (Fig. 9, upper left).

For TEOS:DEDMS = 1:0 (12.4% silicon oxide content), the water uptake is 19.7%, about 5% higher than that of Nafion-H^+. We attribute this hydration increase to the addition of numerous hydrophilic, hydrogen bonding SiOH groups that accompanies silicon oxide incorporation within clusters.

For TEOS:DEDMS = 1:1 (11.8% mixed content) water uptake decreased to 11%, which is 9% lower than for the 1:0 and 4% lower than that of unfilled Nafion-H^+. While TEOS:DEDMS = 1:1 in the external solution, the actual internal ratio is unknown at this time. The internal ratio would depend, in part, on the relative solubilities of TEOS and DEDMS in Nafion as well as their reactivities, each with themselves as well as between each other within this confined acidic medium. Nonetheless, our IR and ^{29}Si NMR spectroscopic inquiries show that DMS is present in considerable quantity and its presence obviously renders the interior more hydrophobic.

The 0:1 case (pure PDMS) shows the lowest water uptake (8.7%). Very few SiOH groups, and those at chain ends, exist. This is about 11% lower than that for pure TEOS-reacted films.

A general conclusion is that the hydrophilicity of Nafion-H^+ can be tailored to be more or less than that of the unfilled form by adjusting the TEOS:DEDMS ratio.

B. Methanol Uptake

Methanol, being less polar than water, is energetically more compatible with the fluorocarbon matrix.

Mass uptake for the four samples is graphed in Fig.9 (upper right). Pure Nafion has the highest uptake ,~95%. For the 1:0 case, the uptake was rather low at 51%. Evidently, addition of SiOH groups does not promote MeOH sorption. Perhaps simple filling of free volume within clusters by silicon oxide nanoparticles inhibits further invasion of these spaces by solvent molecules (*i.e.* steric blocking). This hybrid nonetheless prefers methanol over water sorption. For TEOS/DEDMS = 1:1, the MeOH uptake increases to 63%. Here, the membrane interior is more hydrophobic than that for the 1:0 case, which accounts for this result. This material also prefers methanol over water because of the partial hydrophobic composition of the filler. Perhaps the circumstance of having a more open and flexible inorganic structure, suggested by our DSC and mechanical tensile studies, conspires to cause to increased MeOH uptake. For the 0:1 case, a slightly lower uptake of 61% was exhibited, despite the fact that the inorganic phase has a different structure than that of the 1:1 case. This film also prefers methanol to water.

C. Iso-Butanol Uptake

On comparing the histograms in Fig. 9 (bottom), i-BuOH is a considerably better agent for swelling Nafion, as well as the three hybrids, than water. The i-BuOH molecule has a substantially more hydrophobic character than MeOH that would suggest preferential incorporation away from the polar clusters in Nafion.

For pure Nafion, i-BuOH uptake ~ 85%, almost 10% lower than that for MeOH in Nafion. Interestingly, for the 1:0 case, the same uptake as that for MeOH (51%) is observed. This result, suggesting uptake is interaction-independent for the 1:0 case, reinforces the idea that a pure silicon oxide phase simply serves to provide an effective steric block of further molecular invasion of polar clusters.

For 1:1, there is a slight uptake decrease (to 48%) from that of the 1:0 hybrid. Consider the view that the inorganic phase is molecularly-convoluted (*i.e.* "porous"), the fact that cluster regions for 1:1 will be less polar than those for the 1:0, and the fact that the i-BuOH molecule is considerably larger than the MeOH molecule. We believe that the lower uptake of i-BuOH can be rationalized in terms of the above above facts.

For 0:1, the uptake greatly increased to 70%. Here, uptake seems to be governed by hydrophobic interactions, although there remains the question of how this molecule is distributed between the cluster and perfluorocarbon phases. H_2O, MeOH and i-BuOH uptake for 0:1 increased from 8.7%, 61% to 70%, reflecting a correlation of hydrophobic interactions.

VI. Dielectric Relaxation Experiments

Preliminary experiments were conducted wherein the real (storage) and imaginary (loss) components of the dielectric permittivity (ε', ε'', respectively) were determined at room temperature as a function of frequency (f) over the range 10Hz - 13MHz using an ac

impedance analyzer. Dry film samples from the nanocomposite series {Nafion-H^+, 1:0, 1:1, 0:1} were placed between gold parallel plate electrodes.

All samples showed high ε' values in the low frequency regime. This is attributed, as in earlier studies of Nafion-based nanocomposites, [2] to interfacial polarization, *i.e.* accumulation of charge at the perfluoro-organic/inorganic phase boundaries. This concept is roughly illustrated in Fig. 10. Trans-cluster polarization would, of course, have a longer lifetime with decreasing frequency.

The ε' and ε'' *vs* frequency curves for the 0:1 sample is positioned above those for the other inorganic compositions over most of the f-range while the curves for 1:0 lie beneath all other samples.

Perhaps the 0:1 (pure DEDMS-reacted) case behavior results from interpenetration of PDMS chains throughout the cluster network. These flexible hydrophobic chains, presumably compatible with the Nafion hydrophobic matrix might, in some sense, act as a plasticizer to increase molecular mobility throughout the template. Increased molecular mobility, in turn, would enhance overall polarizability and dielectric loss.

On the other hand, the lowest polarizability exhibited by the 1:0 (pure TEOS-reacted) case might be due to the crosslinked silicon oxide phase which is not only rigid in itself, but might also act to suppress molecular mobility within the Nafion template.

These preliminary studies will be extended and the results interpreted in terms of structure, polarity, and molecular mobility within the inorganic phase, nature of the perfluoro-organic/inorganic interface and nanophase-separated morphology. Dielectric relaxation/electrical impedance spectroscopy can diagnose long and short range charge motions within the heterophase morphologies of these nanocomposites.[3]

VII. Gas Permeation Studies

In-house fabrication of a system of temperature-controlled gas permeation cells, with data acquisition and data analysis by PC, is being completed by S.V. Davis, graduate student. The cells are operated in transient mode wherein downstream pressure rises to a maximum in a constant volume chamber. The solution of the differential equation for these diffusion conditions allows for determination of gas permeability (P), diffusion coefficient (D), and solubility (S). In addition to probing free volume and gas molecule permselectivity, the dual mode sorption phenomenon exhibited by these materials[4-5] will be utilized to investigate aspects of their two-phase morphology.

VIII. Asymmetric Nanocomposites

Work of R.V. Gummaraju, Graduate Student, and K.A Mauritz, Professor

Nafion membranes have been permeated-reacted with TEOS from only one surface to affect an *asymmetric silicon oxide composition profile* across the film thickness. These profiles were investigated using the EDS (X-Ray Energy Dispersive Spectroscopy) attachment of our ESEM. In particular, the silicon:sulfur ratio of peak intensities plotted along the film thickness provides a semiquantative measure of relative Si distribution. Fig. 11 shows a profile across the ~ 5 mil thickness of a pre-hydrated Nafion-H^+ film into

which TEOS permeated from the right relative to the graph. The total silicon oxide uptake after sample drying is 6.64% and the concentration increases in proceeding toward the right.

Molecular features of silicon oxide structure in the near-surface regions of both film surfaces were explored using FT-IR/ATR spectroscopy. At least two significant structural aspects can be deduced from the spectra: (1) The linear/cyclic peak absorbance ratio for the asymmetric Si-O-Si stretching region is greatest on the side exposed to TEOS; (2) the $Si\text{-}OH/(Si\text{-}O\text{-}Si)_{asym(total)}$ absorbance ratio is greatest on the TEOS-exposed side. Fig. 12 which shows spectra for both surfaces of a one-side TEOS-permeated (1100 EW Nafion-H^+) film (uptake = 15%). In topological terms, the silicon oxide phase is more linear, *i.e.* less interconnected, toward the side contacting the TEOS despite the fact that the silicon oxide phase is more concentrated there. These results are in harmony with our earlier FT-IR analysis of SiO_2/Nafion nanocomposites (*i.e.* "normal" two-side-permeated) that indicated decreasing silicon oxide phase interconnectedness with increasing uptake, or permeation time.[6] As a consequence of the diffusional time delay for TEOS molecules reaching the opposite near-surface, and applying the knowledge gained from our earlier studies,[6] the IR results for this asymmetric hybrid appear to be quite logical

Complementing these studies are gas permeation experiments that probe the convoluted interface between the silicon oxide and perfluoro-organic phase. The details of these experiments will issue in a future report.

These are the results of our initial investigations of asymmetric hybrids, performed by R. Gummaraju. Subsequent, more extensive studies by P. Shao are reported in another section of this report.

We are also considering the implications of inorganic oxide compositional variation with respect to *optical properties*, expecially since the nano-scale inorganic inclusions in these hybrids are too small to scatter radiation in the optical region of the electromagnetic spectrum.

A compositional gradient will generate a gradient of index of refraction. In theory, these gradients should give rise to the phenomenon of *optical rectification*, *i.e.* conversion of a single frequency light wave into one which is a superposition of a fundamental plus harmonics. This phenonomenon deserves to be explored from the standpoint of nonlinear optical response. Light rays would also be nonlinearly refracted (curved) in traversing this nonhomogeneous medium.

Rectification of periodic electrical signals impressed across these materials perpendicular to the film plane should also occur, in theory. This aspect will be explored, in part, using instrumentation used to monitor dielectric relaxation.

Fig. 13 is a list that includes other important material properties that are expected to display gradients resulting from inorganic oxide component gradients that can be tailored between the polymer film surfaces.

IX. Conclusions

We initiated TGA-FTIR investigation of the thermal degradation of [Inorganic Oxide]/[Nafion] nanocomposites. The thermal degradation mechanism for Nafion-H^+ has been altered by incorporating either SiO_2 via *in situ* sol-gel reactions, or by *in situ* SiO_2 that was post-reacted with DEDMS, the latter system being the most robust.

Dynamic mechanical spectra over the range 30 to 300°C were obtained for a series of [(silicon oxide)-*co* -(dioxydimethylsilane)]/[Nafion] hybrids. These samples were formulated by contacting Nafion-H^+ with premixed methanol solutions of various TEOS:DEDMS mole ratios and allowing *in situ* sol-gel reactions to occur. DMA spectral trends with mixed TEOS:DEDMS content are harmonious with our earlier DSC results that suggested these hybrids become more flexible as the "linear" inorganic comonomer composition increases. After T_g increases in passing from pure Nafion-H^+ to the pure silicon oxide-filled state, it then monotonically decreases with increasing dioxydimethylsilane content. The origin of an above-T_g (*ca.* 240 - 270°C) relaxation peak is currently unresolved, although we presently feel that it is related to crystallinity. We also studied the interaction between Nafion and incorporated $[-(CH_3)_2Si-O]_x$ (from DEDMS) chains at lower temperatures -160 to +30°C using DMA. A transition ~69°C for unfilled Nafion shifts downward to ~80 °C for Nafion/DEDMS. Perhaps short ranged motions in Nafion are restricted by interpenetrating PDMS chains. These results suggest that DMA is a powerful tool for probing molecular motions within the nanophase-separated morphologies of these hybrids.

We studied incorporation of pure DEDMS in Nafion *vs* time in consideration of Nafion/PDMS *interpenetrating networks*. Inorganic uptake actually decreased in time. Oppositely, for TEOS/DEDMS = 1:1, uptake increased . As DEDMS-formed structures do not interconnect, monomers or oligomers can back-diffuse to the external solution under increasing concentration gradients. For TEOS:DEDMS = 1:1, interconnected structures form. These bulkier, polar structures have more difficulty vacating Nafion clusters once they have incorporated. TGA analysis in N_2 indicated that degradation always occurs ~400°C for films treated with pure DEDMS - a significant improvement over unfilled Nafion-H^+. For TEOS:DEDMS = 1:1, the degradation onset is significantly lower at ~325°C.

FT-IR spectroscopy probed films cast from pure alkoxide solutions (TEOS:DEDMS = 1:0 → 0:1), the films being reference structures for corresponding inorganic phases in Nafion. Having collected reference state spectral signatures, [perfluoro-organic]-[inorganic oxide] phase interactions will be inferred from comparisons between bulk state and matrix-incorporated state spectra. As part of this model study, the effect of heating-vacuum drying, on the IR spectrum, was established.

As TEOS:DEDMS (pre-mixed) decreases, there are more hydrophobic CH_3 groups and fewer hydrophilic SiOH groups within the hybrid. Sorption affinity for the decreasing-in-polarity series: water → methanol → iso-butanol was determined. Although the pure TEOS hybrid was more hydrophilic than unfilled Nafion-H^+, water capacity decreases with decreasing TEOS:DEDMS. Methanol is favored over water for all TEOS:DEDMS ratios although relative uptake for the pure TEOS case is somewhat low. For isobutanol, the pure DEDMS hybrid displayed greatest uptake, reflecting dominance of hydrophobic interactions.

Dielectric permittivity experiments were conducted over the frequency range 10Hz - 13MHz. While analysis of these hybrids is incomplete, high ε' values in the low frequency regime suggest the presence of organic/inorganic interfacial polarization.

Fabrication of a gas diffusion diagnostic system is being completed. Free volume, gas molecule permselectivity and aspects of multiphase phase morphology in these hybrids will be investigated.

Nafion films were permeated-reacted with TEOS from only one surface, generating *asymmetric* silicon oxide composition profiles which were characterized via ESEM/EDS. Molecular structure in near-surface regions of both surfaces was explored using FT-IR/ATR spectroscopy. Topologically, the silicon oxide phase is more linear, *i.e.* less interconnected toward the TEOS-contacting side.

X. Literature References

1. Wilkie, C.A.; Thomsen, J.R.; Mittleman, M.L. *J. Appl. Polym. Sci.* **1991**, 42, 901.
2. Mauritz, K.A.; Stefanithis, I.D. *Macromolecules*, **1990**, 23, 1380.
3. Mauritz, K.A. *Macromolecules*, **1989**, 22, 4483.
4. Davis, S.V; Mauritz, K.A. *Am. Chem. Soc. Polymer Preprints*, 33(2), 363 (**1992**).
5. Davis, S.V.; Mauritz, K.A. *Am. Chem. Soc. Polymer Preprints*, 34 (1), 608 (**1993**).
6. Mauritz, K.A.; Warren, R.M. *Macromolecules* **1989**, 22, 1730.

XI. Figures

TGA/FTIR

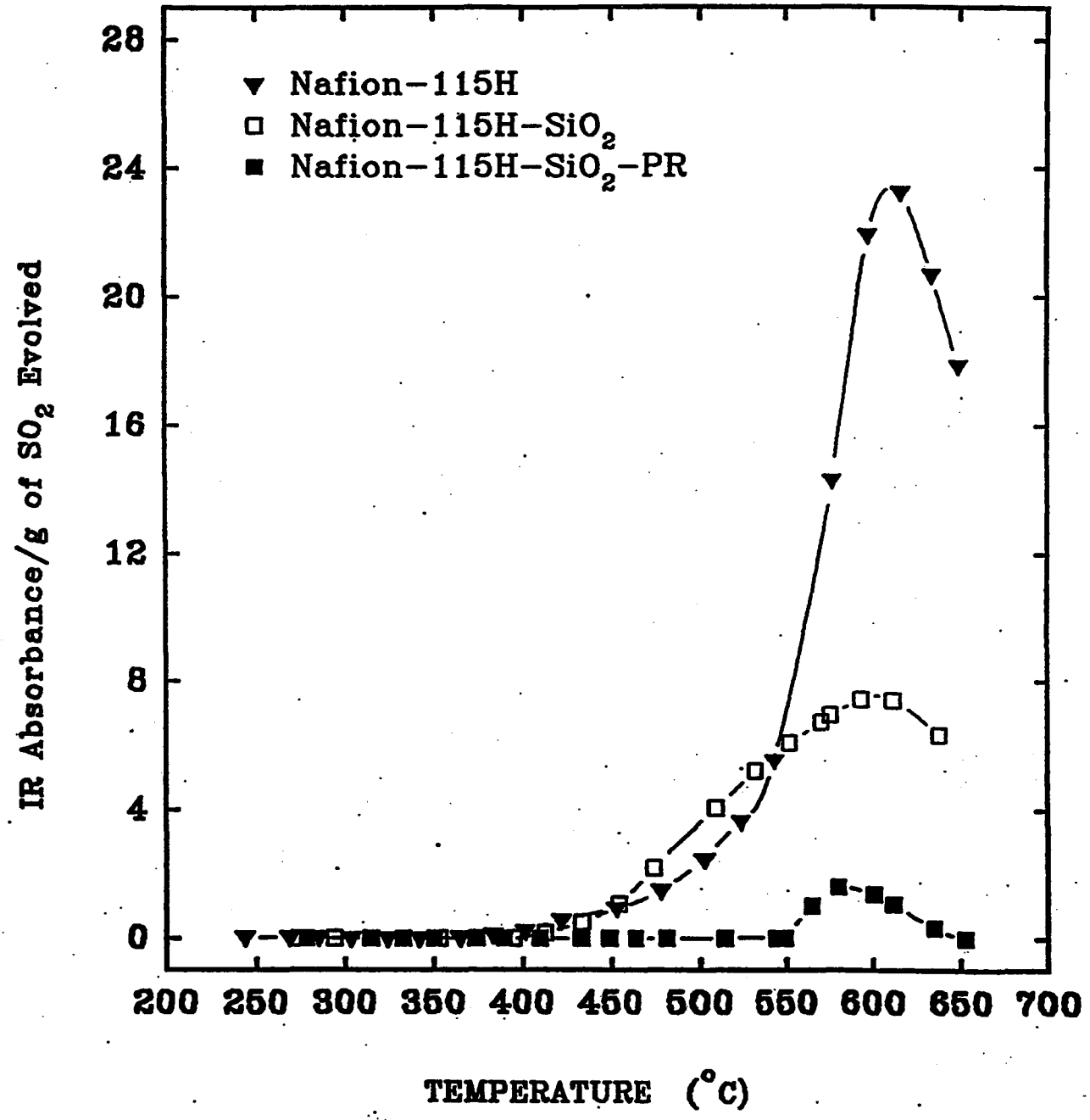

Figure 1

TGA/FTIR

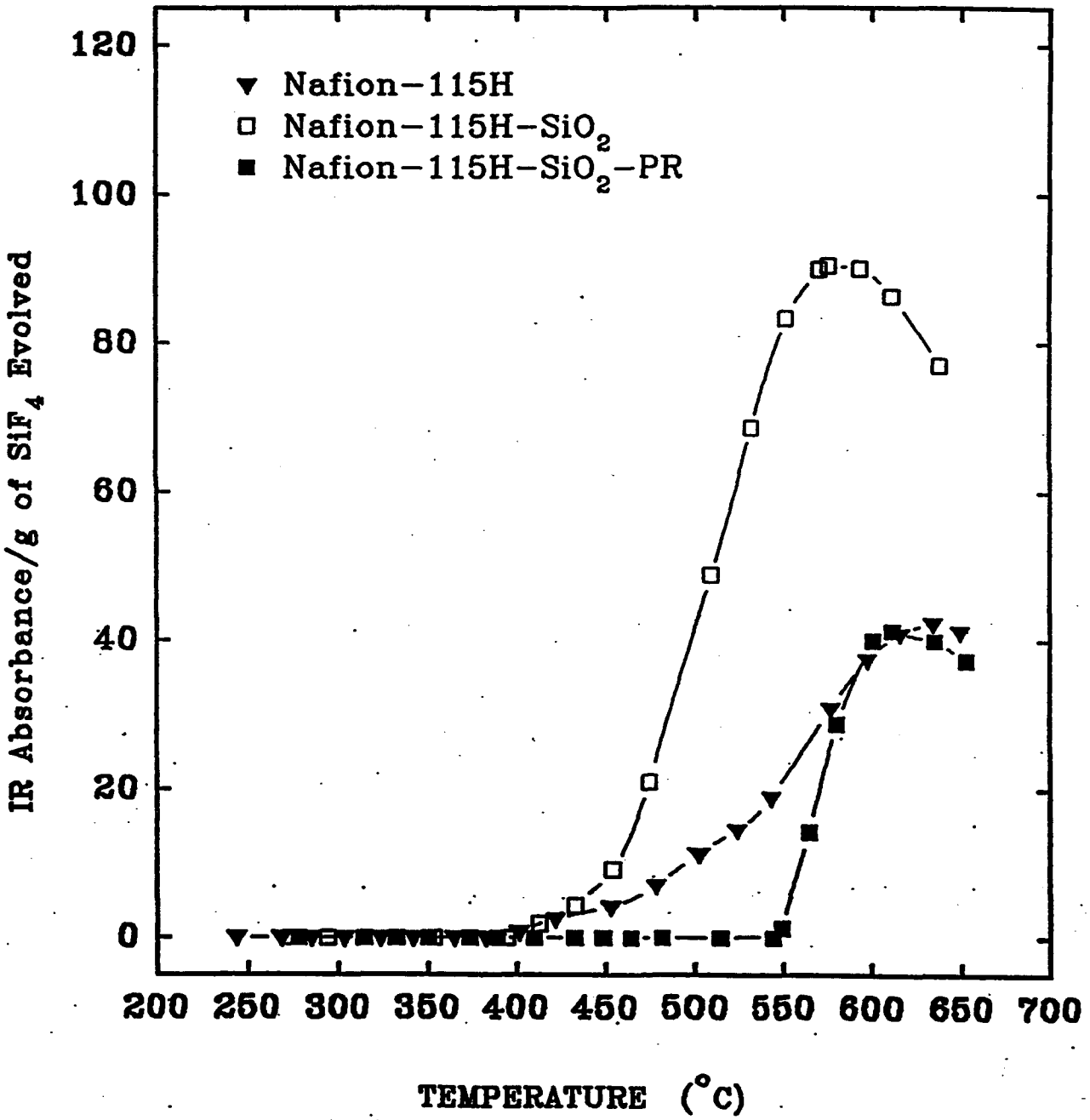

Figure 2

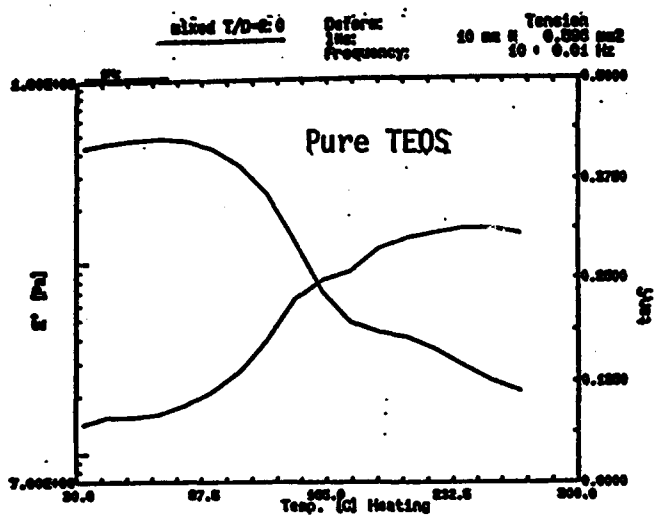

(a)

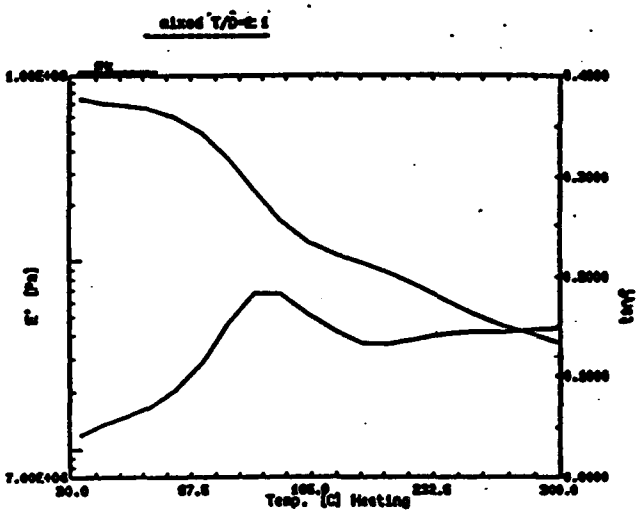

(b)

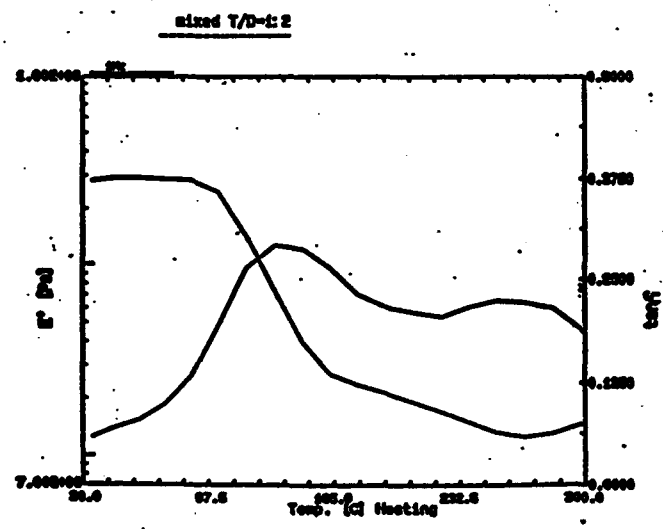

(c)

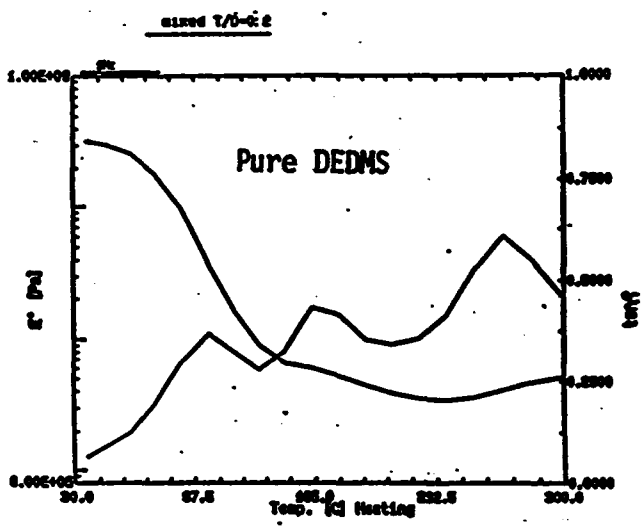

(d)

Figure 3

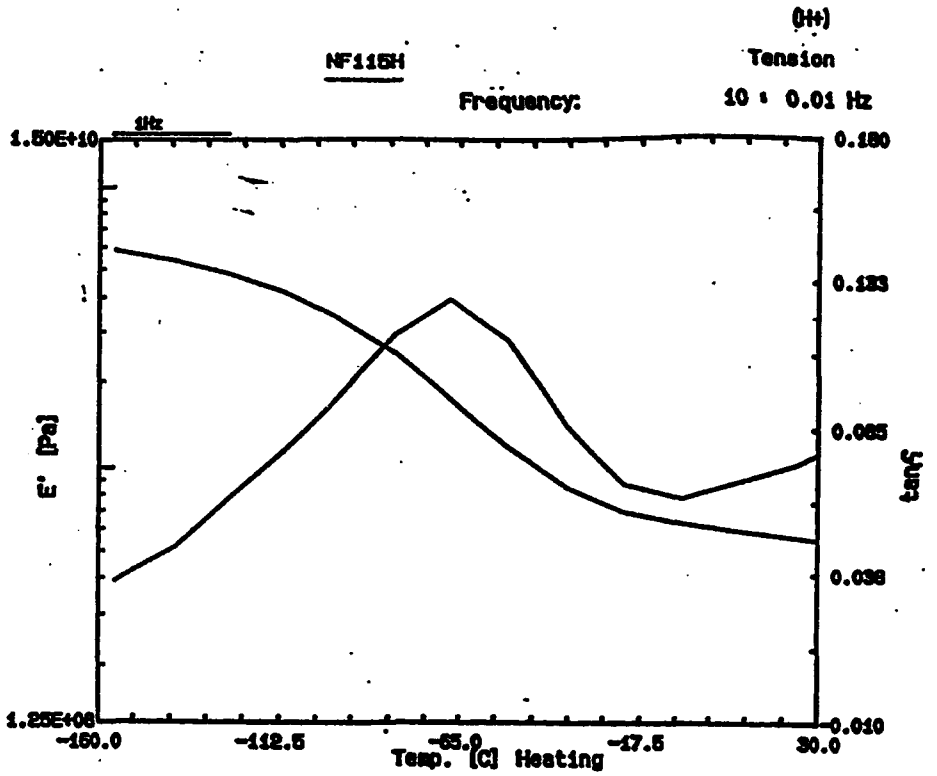
(H+)
NF115H
Tension
Frequency:
10 : 0.01 Hz
1Hz
1.50E+10
1.25E+08
0.180
0.133
0.085
0.038
0.010
E' [Pa]
tanδ
-160.0
-112.5
-65.0
-17.5
30.0
Temp. [C] Heating

(a)

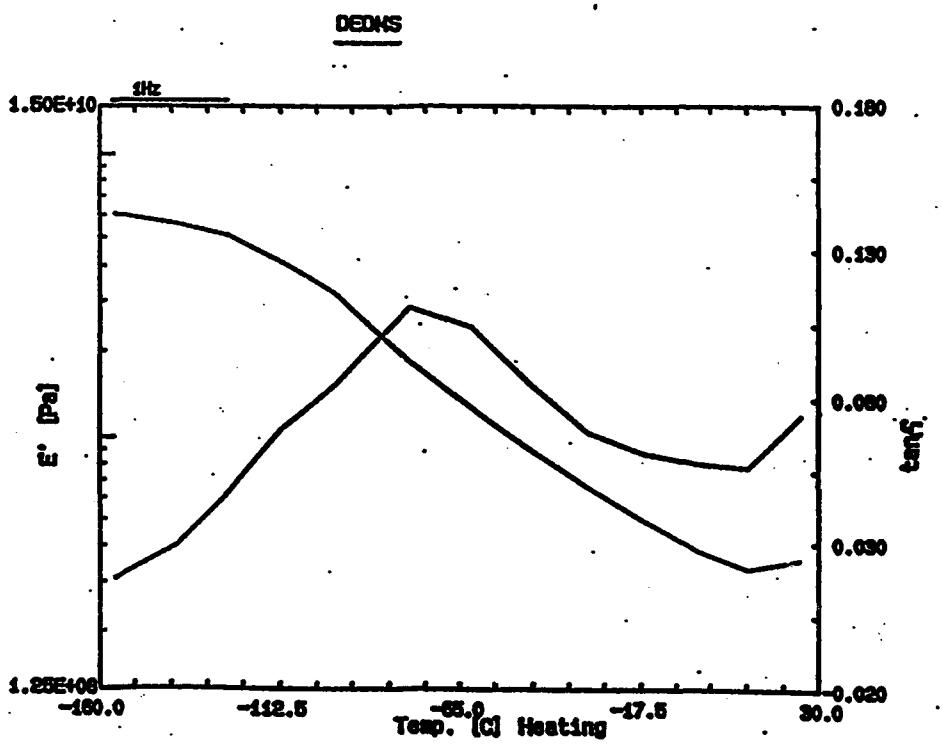
DEDNS
1Hz
1.50E+10
1.25E+08
0.180
0.130
0.080
0.030
-0.020
E' [Pa]
tanδ
-160.0
-112.5
-65.0
-17.5
30.0
Temp. [C] Heating

(b)

Figure 4

(a)

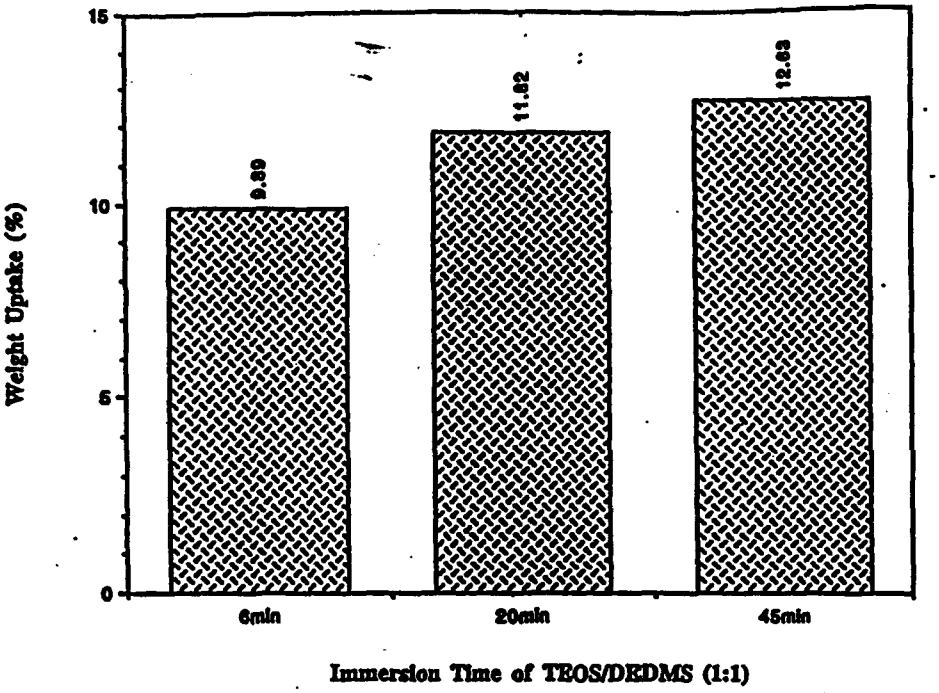
In-situ Reaction of TEOS/DEDMS (1:1)
in Nafion-115H
weight upta ke vs immersion time
Weight Uptake (%)
15
10
5
0
9.89
11.82
12.63
6min
20min
45min
Immersion Time of TEOS/DEDMS (1:1)

(b)

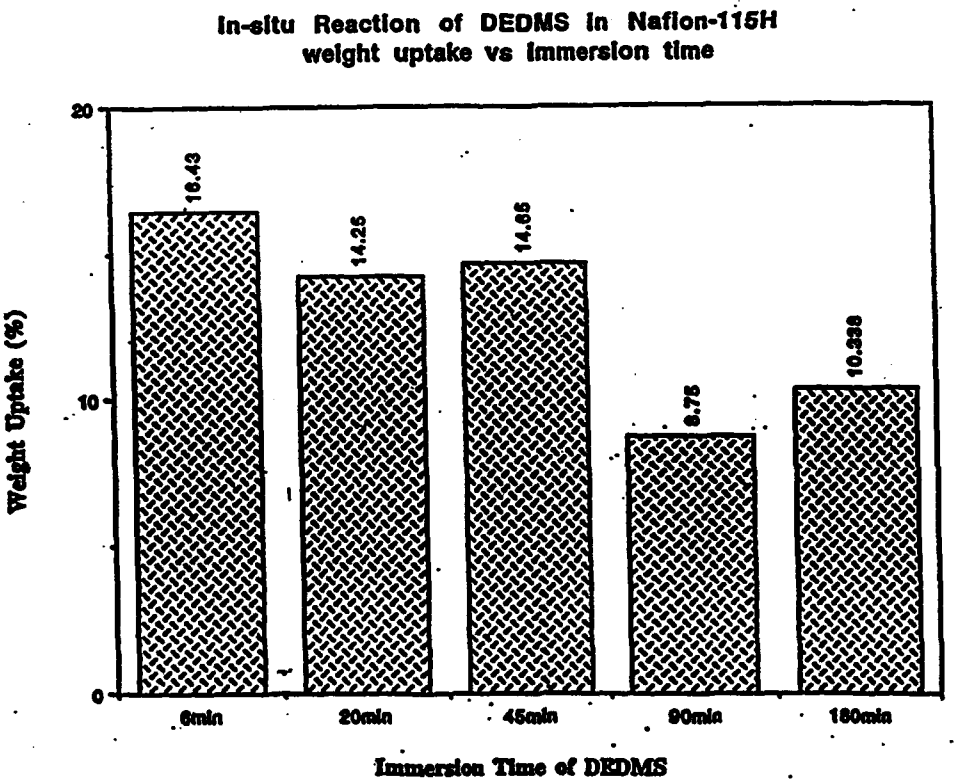
In-situ Reaction of DEDMS in Nafion-115H
weight uptake vs immersion time
Weight Uptake (%)
20
10
0
16.43
14.25
14.65
8.75
10.338
6min
20min
45min
90min
180min
Immersion Time of DEDMS

Figure 5

TGA

(a)

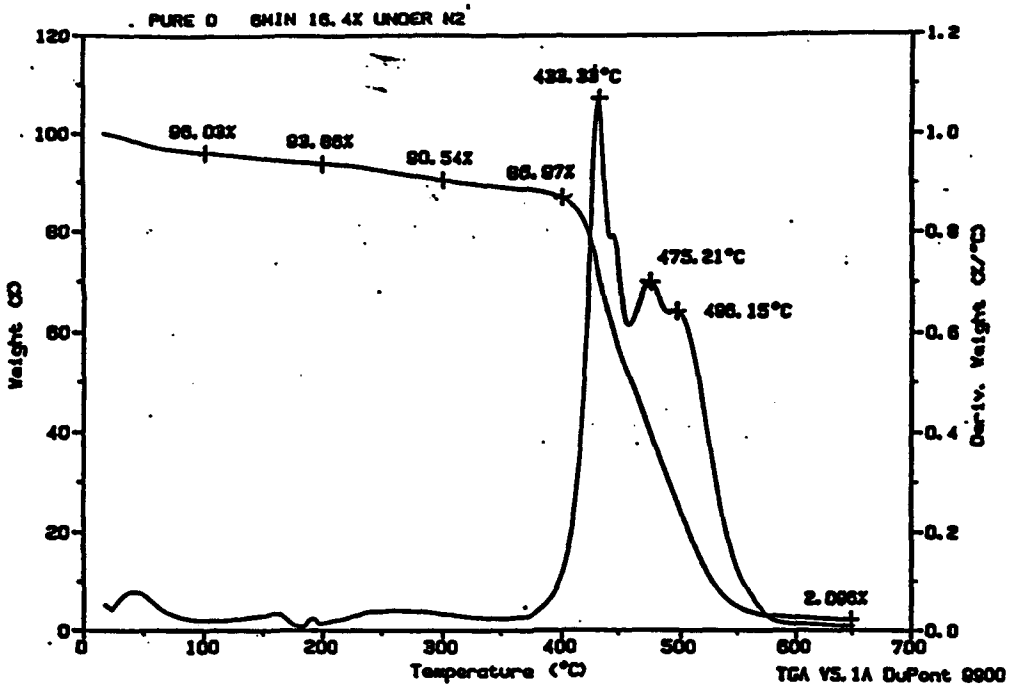

(b)

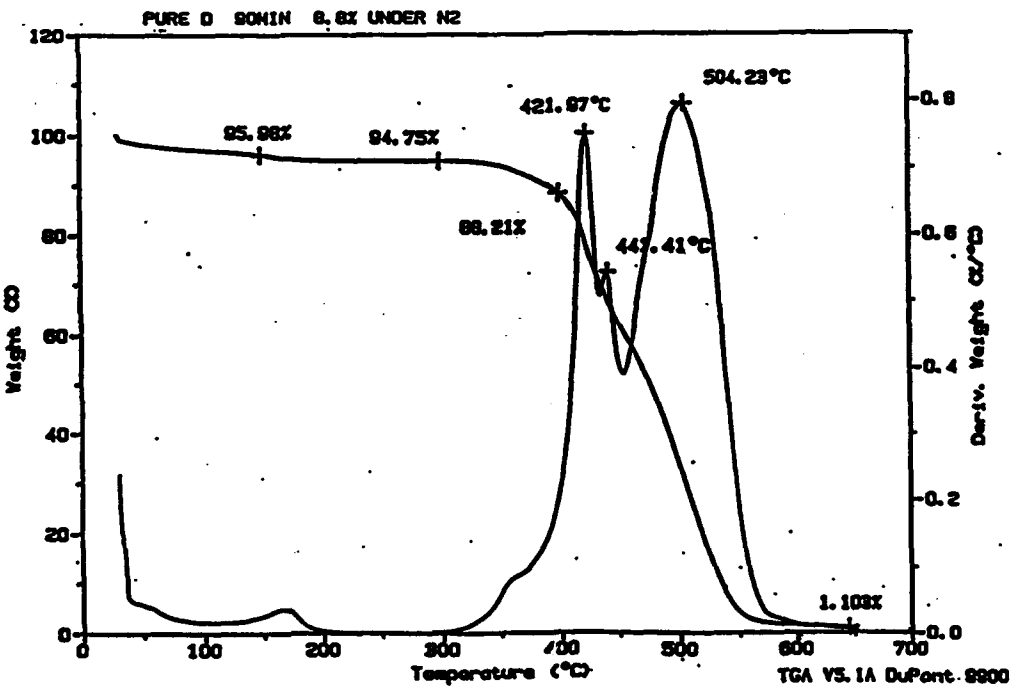

Figure 6

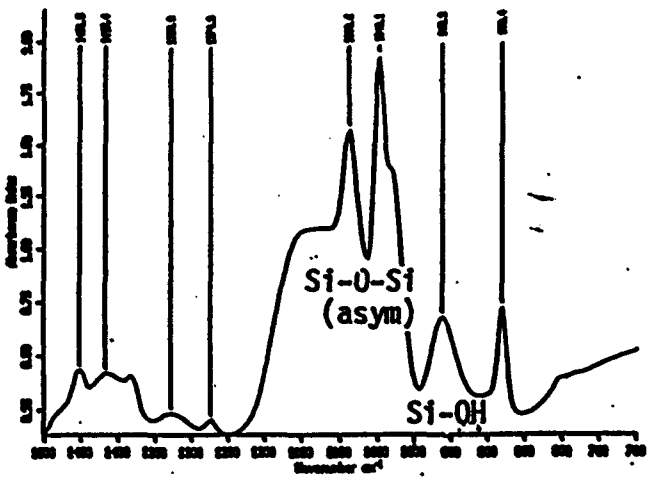

TEOS:DEDMS = 1:0 (Pure TEOS)

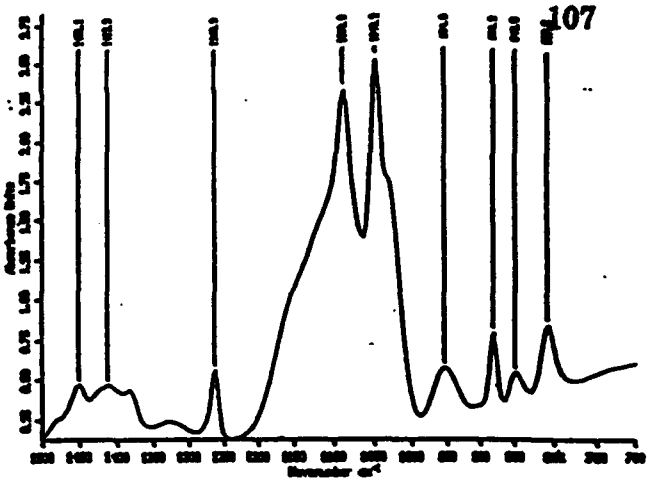

= 2:1

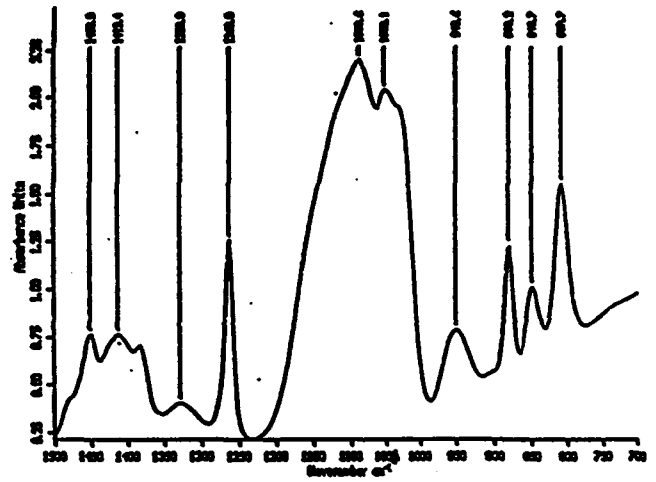

= 1:1

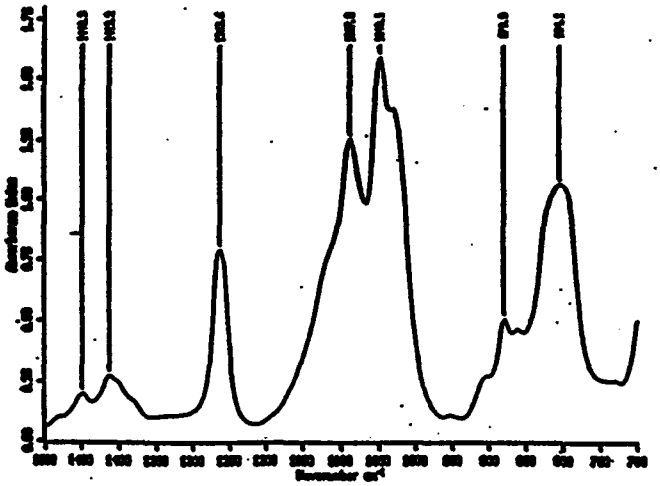

= 0:1 (Pure DEDMS)

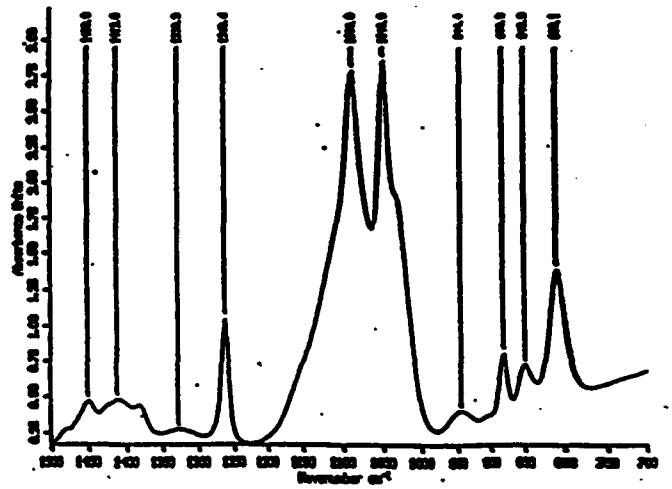

= 1:2

Figure 7

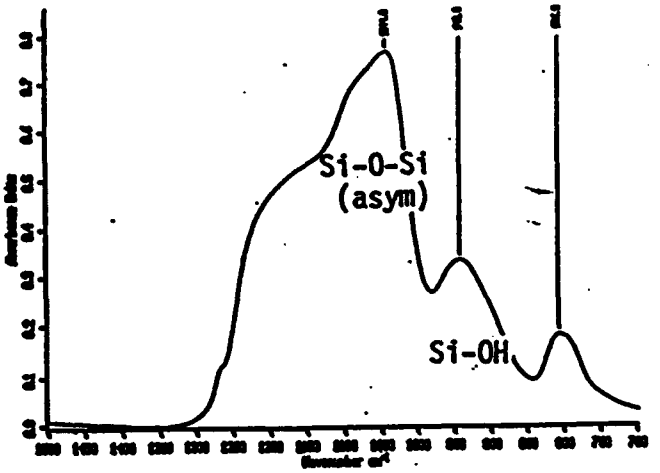

TEOS:DEDMS = 1:0
(Pure TEOS)

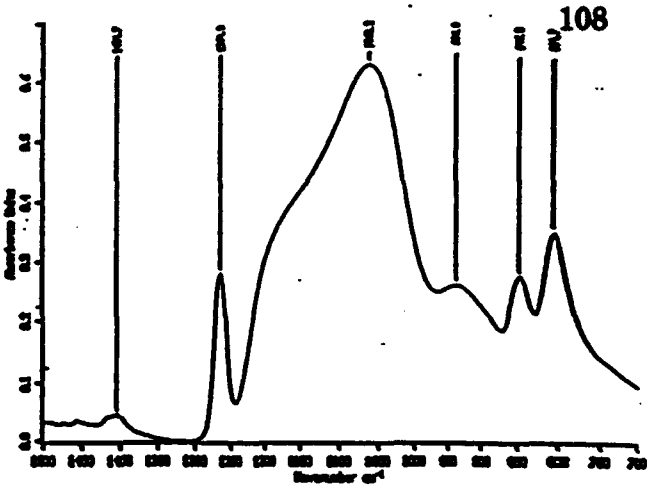

= 2:1

Heated-Dried

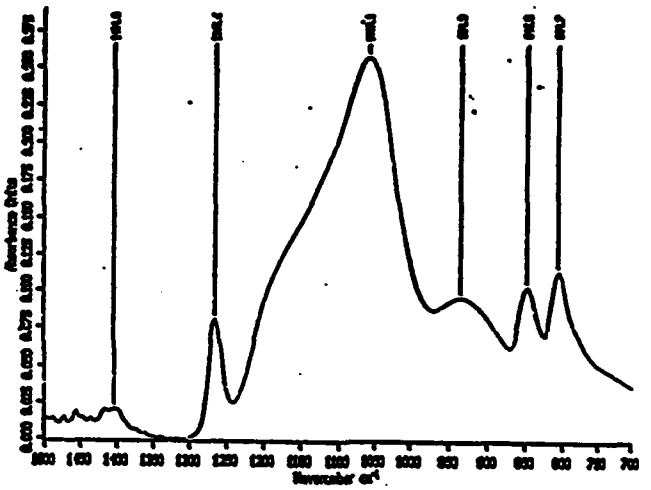

= 1:1

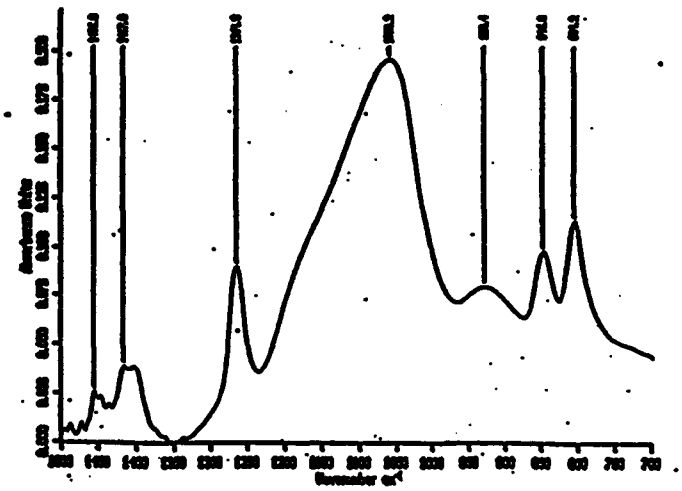

= 1:2

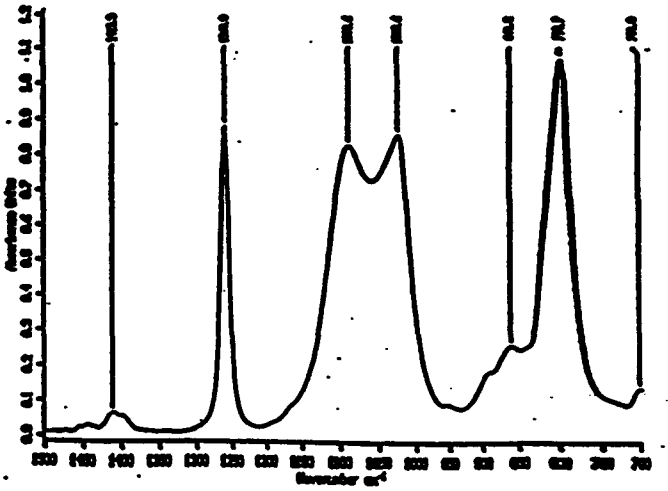

= 0:1 (Pure DEDMS)

Figure 8

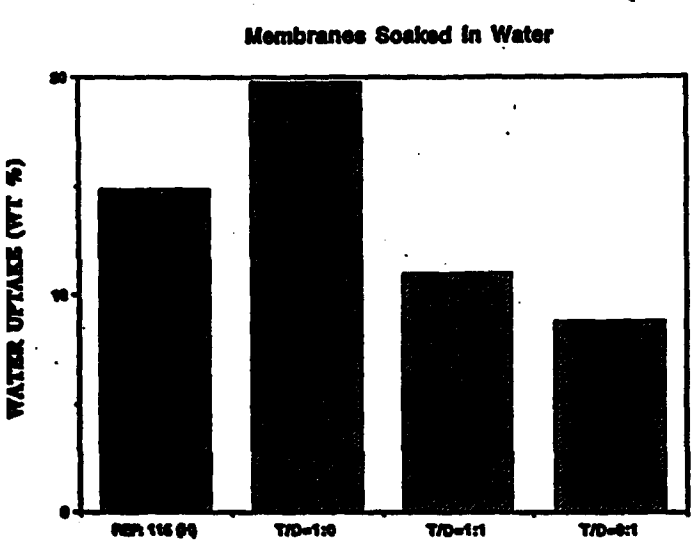
Membranes Soaked in Water
WATER UPTAKE (WT %)
REF: 116 (H)
T/D=1:0
T/D=1:1
T/D=0:1

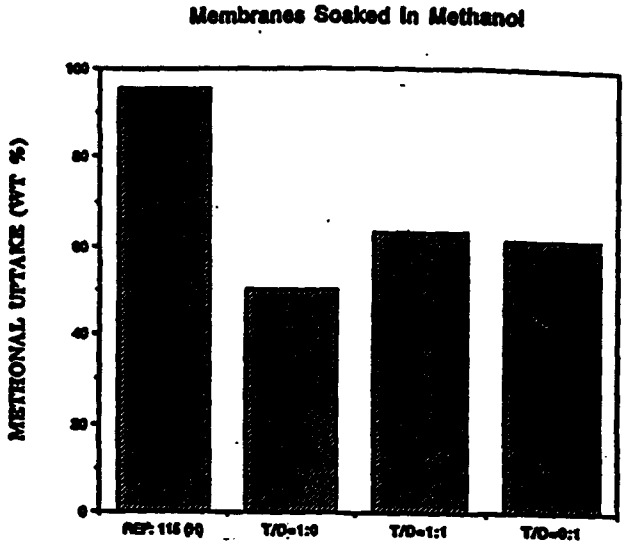
Membranes Soaked in Methanol
METHONAL UPTAKE (WT %)
REF: 116 (H)
T/D=1:0
T/D=1:1
T/D=0:1

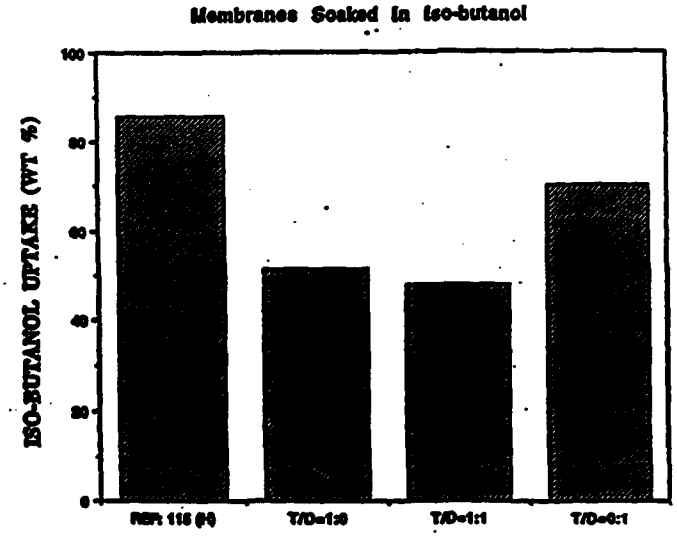
Membranes Soaked in Iso-butanol
ISO-BUTANOL UPTAKE (WT %)
REF: 116 (H)
T/D=1:0
T/D=1:1
T/D=0:1

Figure 9

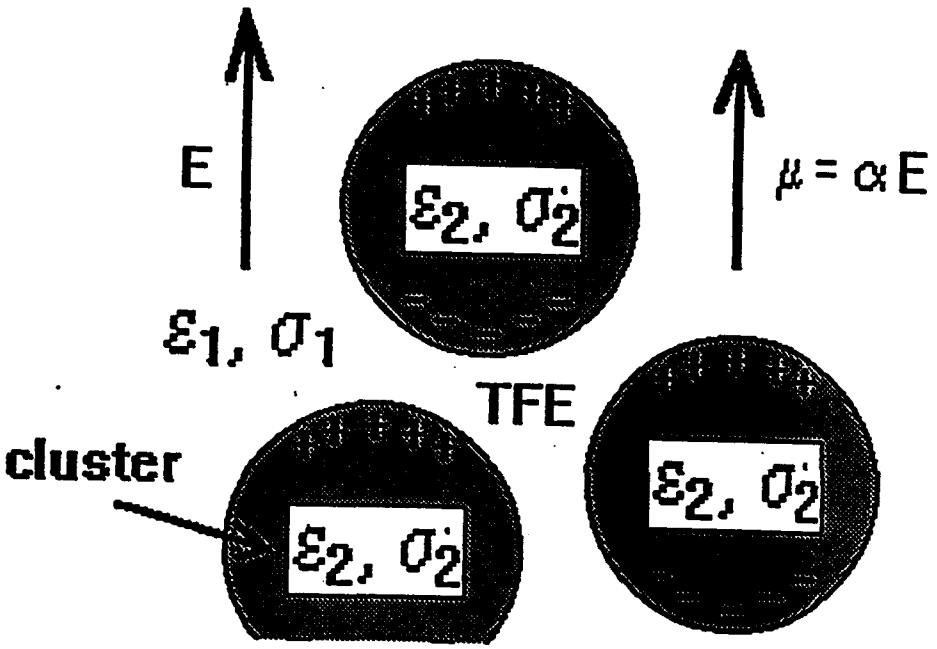

Electrodynamic Model of Polarizable Clusters Embedded in a Medium of Low Dielectric Constant. E is the Applied (Sinusoidally-Varying) Electric Field, the ε's and σ's are Dielectric Constants and Electrical Conductivities, Respectively, μ is the Induced Cluster Dipole Moment, and α is the Cluster Polarizability.

Figure 10

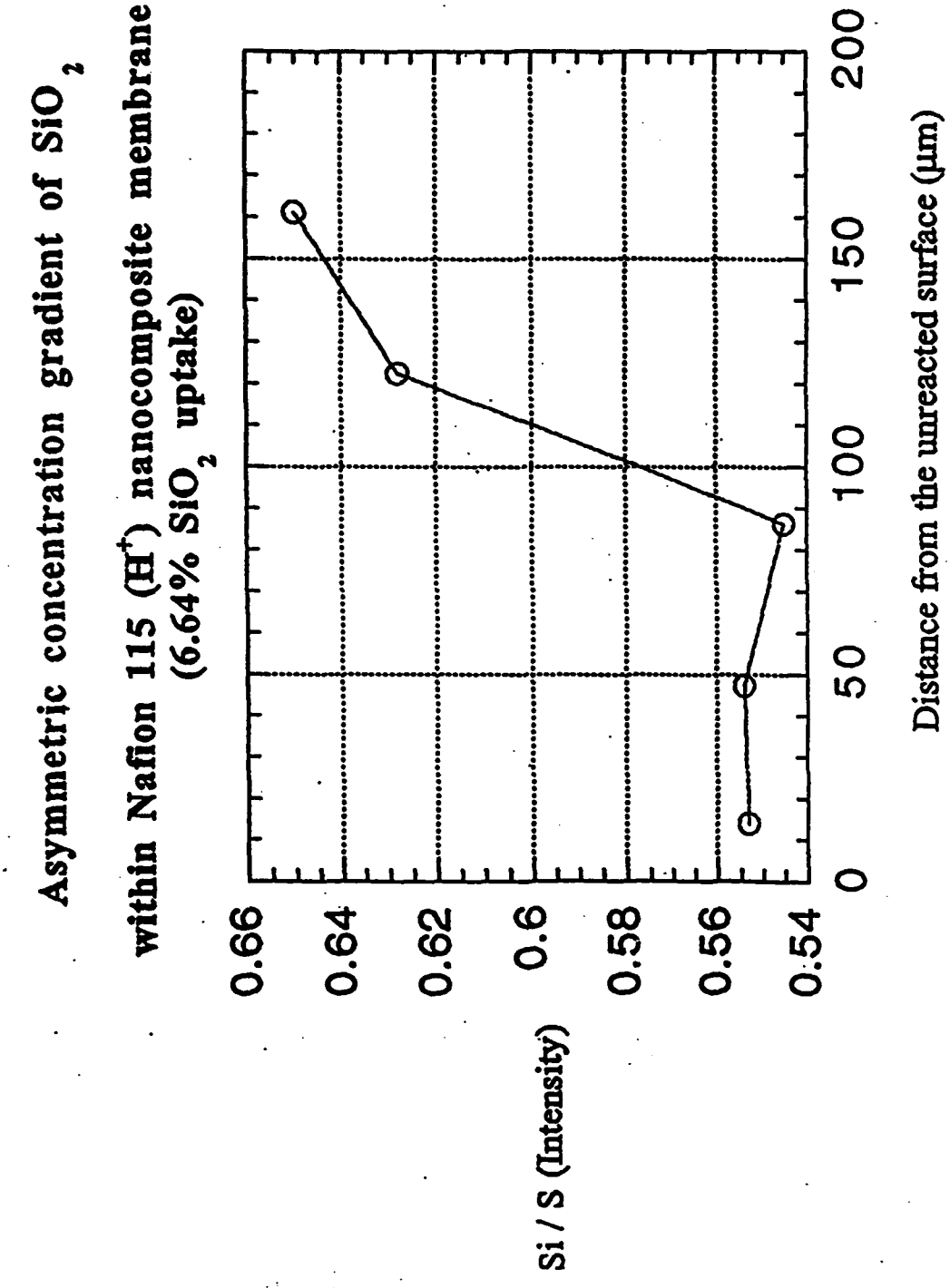
Asymmetric concentration gradient of SiO2
within Nafion 115 (H+) nanocomposite membrane
(6.64% SiO2 uptake)
Si / S (Intensity)
0.66
0.64
0.62
0.6
0.58
0.56
0.54
0
50
100
150
200
Distance from the unreacted surface (μm)

Figure 11

FTIR-ATR DIFFERENCE SPECTRA OF NAFION 115 (H^+)
15% UPTAKE OF SiO_2
REACTED SURFACE vs. UNREACTED SURFACE

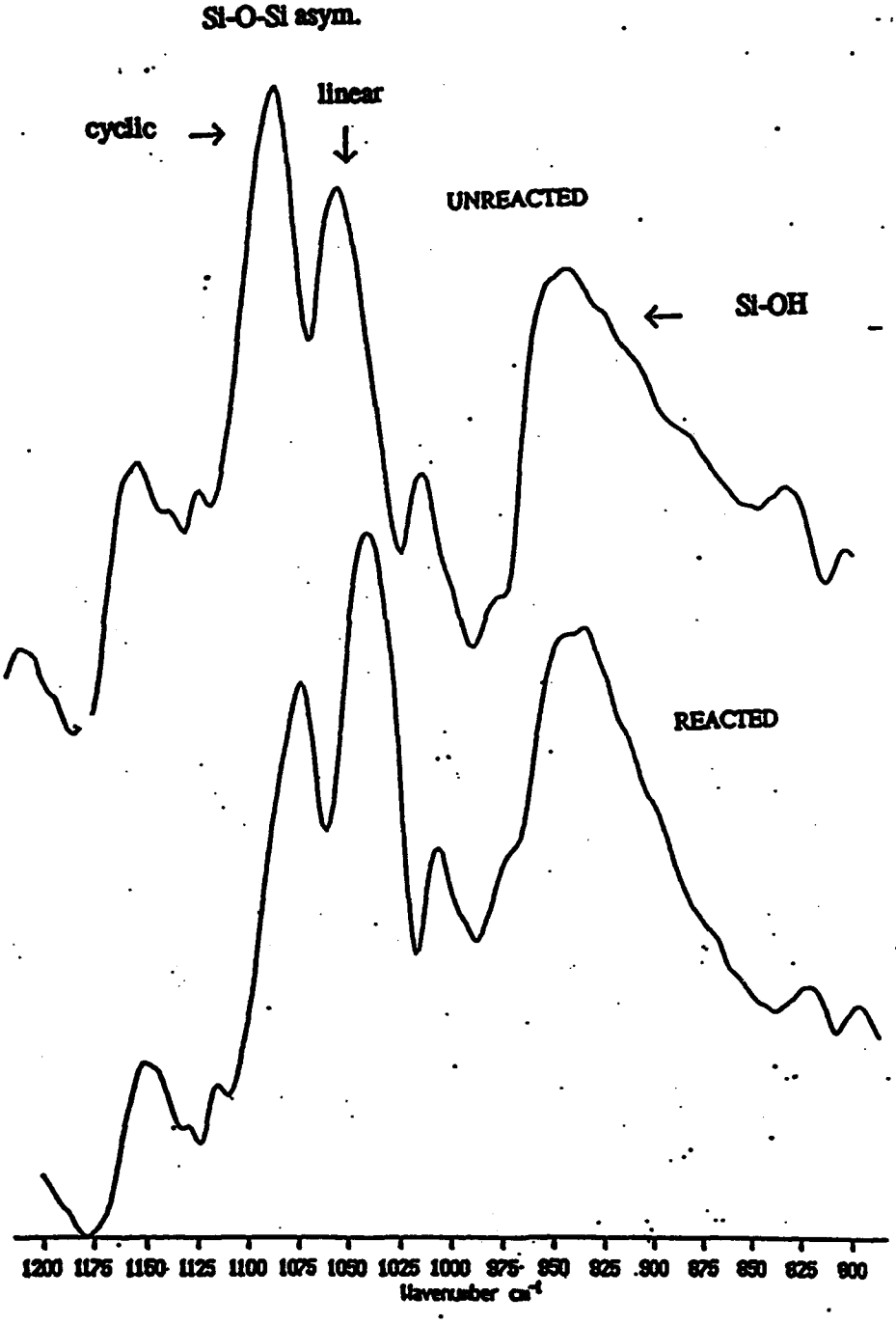

Figure 12

INORGANIC COMPOSITION GRADIENT IMPLIES PROPERTY GRADIENT:

- mechanical (modulus, strength, elongation)
- thermal (Tg, Tm)
- optical (refractive index, birefringence, nonlinear response)
- dielectric (polarization anisotropy, relaxation time)
- ionic, electronic conductivity
- penetrant diffusion coefficient

Figure 18

RESEARCH REPORT TO AFOSR

June 13, 1994

PART IV

TABLE OF CONTENTS

PART IV

Following is the work of Dr. Phoebe Shao, Postdoctoral Associate, and K.A. Mauritz, Professor

I. Inorganic Oxide Concentration Profiles across Film Thickness Direction

Previously, we generated mixed inorganic oxide phases within Nafion sulfonate films via *in situ* sol-gel reactions. In particular, schemes involving Si/Ti and Si/Al alkoxide combinations were investigated. Inorganic oxide compositional distributions across the across film thicknesses (cross-sections) were probed with an environmental scanning electron microscope (ESEM) using an x-ray elemental microprobe attachment. Earlier experiments demonstrated that the distribution of SiO_2, TiO_2 and Al_2O_3 can be dramatically different within these mixed hybrids, depending on composition. Generally, profiles that are rather symmetrical about the middle plane of the film, such that the greatest concentration is near the surfaces, was observed for TiO_2 using 2-propanol as solvent. Contrasted with TiO_2, a relatively uniform profile was observed for SiO_2 regardless of the preparation scheme (*i.e.* permeation of mixed alkoxides *vs* sequential alkoxide addition. It was suggested that alkoxide molecules suffer progressive difficulty in diffusing to the film center due to obstacles posed by already-precipitated inorganic structures in the near-surface regions. Since the titanium alkoxides utilized react considerably faster than TEOS, the latter can penetrate deeper into the Nafion medium before they are immobilized. The titanium alkoxides might also diffuse slower than TEOS, owing to larger size.

The earlier-discussed tensile stress *vs* strain curves of these hybrids demonstrate that the near-surface concentration/composition of the filler strongly controls mechanical properties. A contiguous, or percolative inorganic oxide phase near the surface constitutes a glassy zone. Thus, while the inorganic oxide phase in the middle is below the percolation threshold, the glassy zone is the strongest component and the film is brittle, overall.

Compositional gradients will generate gradients in other properties: index of refraction-dielectric constant, electrical conductivity, diffusion coefficient, and thermal transition temperature, to name a few.

We suggest that plane waves of monochromatic light entering these materials perpendicular to the composition gradient vector will undergo *optical rectification* in the sense that the polarization (P) waveform in the gradient direction is different from that opposite this direction. In this way, pure sine waves might transformed into waves consisting of harmonic components. Rays of light will also be *bent* on traversing this medium, depending on the angle of incidence.

Given that inorganic oxide compositional distribution is an important variable for tailoring these hybrids as sophisticated optical or electronic materials, or as permselective membranes or functional coatings, the effects of alkoxide type and solvent medium on inorganic concentration profile is studied here in greater detail.

A. Single [Inorganic Oxide]/[Nafion] Hybrids

Fig. 1 shows profiles for hybrids containing only SiO_2 (uptakes ~ 12-14 wt%.), the samples being prepared in a variety of indicated solvents. First, each Nafion film was swollen in a 10 ml H_2O/30 ml alcohol solution overnight; then a 35 ml TEOS/alcohol (3/1 v/v) mixture was added to the solution. Thereafter, the resultant solution continued to be stirred for 20 min while permeation and sol-gel reaction ensued.

The curves do not show a predominant concentration of SiO_2 at the near-surface, and, considering the vertical scale, might be considered somewhat flat, a result consistent with our previous findings. The curves are similar for all solvents and there is no vertical ordering. All TiO_2-containing samples were prepared by immersion of hydrated Nafion films in dilute titanium alkoxide/alcohol solutions (1/30 v/v) for 20 min. The alkoxide was diluted to slow the sol-gel reaction. The Nafion film was hydrated by boiling in water 30-60 min and subsequently drying at 50 ^{0}C for 4 hr. This procedure, with mild drying, is intended to impart limited hydration in order to further slow the sol-gel reaction.

Contrasted with the above SiO_2/Nafion hybrids, the TiO_2 composition profile using TET is solvent-dependent as seen in Fig. 2 which contains profiles for EtOH, 1-PrOH and 1-BuOH. Note that the profile for 1-BuOH has rather steep gradients near the film surfaces. The curves are depressed with increasing alcohol molecular weight. The bottom graph in Fig. 2 displays total TiO_2 uptake using the three alcohols. Under the same experimental conditions and immersion time, TiO_2 uptake decreases as alcohol molecular weight increases, or as alcohol polarity decreases. The vertical ordering of the curves in Fig. 2 correlates with the uptake trend as well as with the relative swelling of Nafion in these solvents.

Fig. 3 shows results for samples generated using tetrabutyl titanate (TBT). It appears, on inspecting both Figs. 2 and 3, that TiO_2 becomes less homogeneously distributed (*i.e.* more concentrated at near-surfaces regions) with increasing alcohol size. We suggest again that this is a consequence of the relative swelling of Nafion in this solvent series. The stronger the solvent, the greater the alkoxide permeability which in turn allows for more TiO_2 precipation toward the middle of the film. Corresponding concentration gradients for TBT-derived hybrids are steeper than those formulated with TET, especially for 1-BuOH. This may result from a slower diffusion rate for TBT, although the relative sol-gel reaction rates should also be taken into account.

B. [Mixed Inorganic Oxide]/[Nafion] Hybrids

SiO_2/TiO_2 /Nafion hybrids were formulated by two methods that were described previously: (1) sorption of pre-mixed alkoxides from external solutions; (2) sequential addition of different alkoxides from single component solutions.

In procedure (1), Nafion-H^+ (prehydrated by boiling in water for 30-60 min, then dried at 50°C for 4 hr) is immersed in mixed alkoxide solutions in which TEOS is the predominant component (2 ml Ti alkoxide/20 ml TEOS/20 ml alcohol) for 30 min. Afterward, hydrolysis-condensation was allowed to continue in air for 6 hr. Upon removal from solution, all samples were dried at 100° C for 48 hr in vacuum. Ti profiles are shown in Figs. 4 and 5 for EtOH and 1-PrOH, respectively.

For TET/TEOS-derived hybrids, a relatively uniform TiO_2 profile resulted for either alcohol. However, for both EtOH and 1-PrOH, steep gradients near the surfaces exist for tetrapropyl- and tetrabutyl titanates. Little TiO_2 is found in the middle regions nor at considerable distances from the middle for the 2-PrOH series, excluding the TET case, and the curves are somewhat indistinguishable. The SiO_2 distribution, however, is rather uniform (Fig. 6) regardless of Ti alkoxide or solvent type. While the Ti/S profile for the TET/TEOS formulation in Fig. 5 lies above the others over most of the thickness, the corresponding Si/S profile is at the bottom and is rather flat in Fig. 6.

We rationalize the above results in terms of the relative reactivity rates of the alkoxide pairs Si-Si, Si-Ti and Ti-Ti, and perhaps to a lesser degree, the relative diffiusion rates of Ti and Si alkoxides in the Nafion medium.

In procedure (2), Nafion was immersed in 1 ml H_2O/40 ml EtOH overnight, after which 13 ml TEOS/EtOH (3/1 v/v) was added to initiate TEOS *in situ* prehydrolysis for 30 min. These TEOS pre-reacted films were then transferred to TBT/EtOH solutions (1ml/60ml) for 5-15 min. A film, having been removed from solution, was dried at 100°C for 48 hr. The percent uptakes (titania + silica) for 5 and 15 min are 4.6 and 10.2%, respectively. The composition profiles (Fig. 7) suggest that with EtOH solvent, a homogeneous distribution of TiO_2 and SiO_2 can be approached with sufficiently long permation times. We add that the uniform Si/S profile seen for 5 min is essentially the same as that observed for 15 min.

While a homogeneous inorganic oxide phase distribution can be realized using the above procedure in which EtOH is used, a rather high uptake (20-30 wt%) results. However, these filler levels are above the percolation threshold and the hybrids are brittle rather than ductile. Within the context of certain applications, this property may be unfavorable.

In one scheme aimed at generating flexible films by limiting filler content to beneath percolation, the sol-gel reaction for TET was conducted within Na^+-neutralized Nafion. Ion exchange was affected by immersing Nafion-H^+ in boiling saturated aqueous NaOH for 1 day; excess NaOH was leached out by soaking films in boiling water for one week to generate the mole ratio Na^+:SO_3^- = 1:1. The films were then dried at 100° C for 1 day under vacuum. Hydrated (*i.e.* boiled in water for 30-60 min, then partially dried at 50°C for 4 hr) Nafion-Na^+ films were then immersed in 5ml TET/60 ml alcohol (EtOH, 1-PrOH, 2-PrOH, 1-BuOH) solutions for 18 hr, removed from solution and dried at 100° C for 48 hr.

The TiO_2 profiles for the resultant hybrids are displayed in Fig. 8. On comparing the bar graph at the bottom of Fig. 8 with that in Fig. 2, it is seen that TiO_2 uptake for Nafion-Na^+, for each corresponding solvent, is significantly lower than that for Nafion-H^+, although the relative uptake for 1-PrOH and 1-BuOH is reversed. The concentration profiles in Fig. 8 do not portray the excessive TiO_2 accumulation near the surfaces that gives rise to brittleness. Actual stress *vs* strain analyses of these hybrids are planned. It is also noteworthy that the 1-PrOH curve is rather flat and that there is little TiO_2 in the middle of the hybrid formulated with 1-BuOH. For both Na^+ and H^+ forms, the hybrid formulated with EtOH exhibited the highest uptake.

C. *[ZrO_2]/[Nafion] Hybrids*

We have initiated studies of zirconia/Nafion hybrids using the same recipes as for TiO_2 /Nafion hybrids.

The effect of solvent molecule size and alkoxide R group size on ZrO_2 concentration profile is shown in Figs 9 and 10. In these experiments, the alkoxides tetrapropyl zirconate (TPZ) and tetrabutyl zirconate (TBZ), in conjunction with the solvents EtOH, (1 and 2)-PrOH and 1-BuOH were utilized. Beneath each set of profiles is a bar graph of weight uptake *vs* solvent. As before, for both TPZ and TBZ, filler content decreases with increasing alcohol size. For each alcohol, the uptake is less for the TBZ-derived composite.

The ZrO_2 profile for TPZ is rather uniform for EtOH and somewhat less so for the larger alcohols, similar to the result for TiO_2 /Nafion hybrids. Most TiO_2 for the 1-BuOH/TPZ case is incorporated nearer the surface than the middle. Fig. 10 shows that the EtOH curve is greatly displaced upward from the remaining curves, which are rather close together and reflect low ZrO_2 concentration across the entire thickness.

D. *Asymmetric Hybrids*

Nafion-H^+ films were mounted between the halves of a two-compartment liquid reaction cell. The membranes, hydrated as before, were swollen in 2-PrOH for 1 hr prior to being fitted into the reaction cell. Then, dilute inorganic alkoxide solutions ($X(OR)_4$/2-PrOH = 1/20 v/v), or pure solvent, were immediately added to the compartments and the sol-gel reaction for alkoxides permeating from these solutions was allowed to proceed for 20 min at room temperature without stirring. The membranes were then washed with pure solvent and placed in air for 6 hr to continue the sol-gel reaction. Finally, all samples were vacuum dried at 100°C for 48 hr.

Based on prior experience, 2-PrOH, in combination with large metal oxides were employed, anticipating that the metal oxide component would accumulate in the near surface regions of one side. Additionally, use of a higher alcohol and a large alkoxide will slow down the overall rate of the sol-gel reaction so to be conducted at room temperature.

1. Asymmetric ZrO_2 Distribution

The result of conducting the above experiment, wherein TBZ was in one chamber and 2-PrOH in the other, is shown in Fig. 11. It is obvious that the permeation and reaction rates are favorable to allow for generation of a thin layer of zirconium oxide on but one side of the film. The rather sharp composition gradient at the left suggests that there exists a rather distinct interface between Zr-rich and essentially Zr-deficient regions.

While this was a single preliminary study, other compositional variables and experimental conditions need to be varied to explore control of the concentration profile.

2. ZrO_2-TiO_2 Compositional Asymmetry

In this experiment, a TBT solution replaced the pure solvent as in the previous experiment. TBZ and TBT diffused from opposite directions, mingled with each other, and reacted so as to produce the Zr/S and Ti/S profiles seen in Fig. 12.

The profiles indicate that the experimental conditions were rather favorable for producing sharp gradients and ZrO_2-rich and TiO_2 -rich sides. Again, this is an initial result and other schemes need to be explored involving this combination of alkoxides.

3. SiO_2-TiO_2 Compositional Asymmetry

The procedure used in this investigation was similar to that for the above experiment using TBZ-TBT, except for the following. Owing to the great difference in reaction rates for Si and Ti alkoxides, only one reaction cell compartment was filled with TBT solution while the other cell remained empty for 15 min. During this time, the sol-gel reaction for TBT proceeded within Nafion. Then, a concentrated TEOS/2-PrOH (1/1 v/v) solution, mixed with a slight amount of water, was added to the other compartment and the overall reaction, due now to different alkoxides permeating from both sides, was allowed to proceed for another 5 min.

The profiles in Fig. 13 show the interesting result that, although the TBT and ZBT entered the membrane from opposite surfaces, the compositional distribution for each is skewed in the same direction. At first sight, it would seem that there should be a greater SiO_2 accumulation to the right on the diagram. We offer the following tentative explanation of this interesting result. The hydrolysis-condensation reactions involving Si-OR and Ti-OR groups to form the Si-O-Ti link proceed faster than the hydrolysis and self-condensation of TEOS. Consequently, the later-added, slowly-reacting TEOS can penetrate deep into the film and into regions in which titania already exists to rapidly react with the titania.

II. Vibrational and Solid State NMR Studies of Nanccomposites

The following initial spectroscopic investigations are in the nature of a survey to determine whether meaningful information relating to extent of *in situ* sol-gel reaction or degree of coordination within the inorganic oxide phase, can be extracted .

A. Infrared Spectroscopy

Si-O-Ti bond formation was studied by FT-IR/ATR spectroscopy. Figure 14 shows difference spectra ([TiO_2/SiO_2/Nafion] spectrum - [unfilled dry Nafion-H^+] spectrum) for samples prepared by the sequential alkoxide addition procedure for various Ti/Si ratios. This system was generated using TBT and 2-PrOH as solvent. The actual internal compositions were characterized by the earlier-discussed SEM-EDS investigations.

As the Ti/Si ratio increases, gradual depression of the Si-OH peak (~ 940 cm^{-1}) accompanied by the buildup of the adjacent Si-O-Ti peak (~920 cm^{-1}) reports the evolution of Ti-O-Si bonds, confirming structural bonding of titania onto the established

silica phase. Of course, suppression of the Si-OH peak can simply be due to having a decreasing Si/Ti ratio, in addition to condensation reactions involving this group.

It was earlier seen that TiO_2/SiO_2/Nafion hybrids can have a large accumulation of TiO_2 near the surfaces. It is reasonable, then, to think that this factor will limit IR beam depth penetration which will result in heavily weighting the TiO_2 bands in the spectrum. It is also noted that a peak-splitting continues to develop, with increasing Ti/Si ratio, for the band attributed to Si-O-Si groups located in linear fragments. We are presently investigating the origin of this phenomenon.

For SiO_2-Al_2O_3/Nafion hybrids (derived from pre-mixed alkoxides), FT-IR/ATR spectra (Fig. 15) revealed a progressive increase of Si-O-Si groups involved in loops, as opposed to linear fragments, with increase in Al/Si ratio. The region of the "linear" Si-O-Si peak actually consists of two overlapping peaks where the low frequency component decreases in relative intensity with increasing Al/Si ratio. We are trying to understand the origin of these companion peaks. Concurrently, Si-OH group absorbance decreased, although this may simply reflect a lower Si/Al ratio.

The definite signature of the Si-O-Al bond, seen in Fig. 16, is the high frequency shoulder, at 465 cm^{-1}. We also looked for two shoulders on either side of the strong band at 795 cm^{-1}. Fig. 16 contains the difference spectrum of a "mixed" SiO_2-Al_2O_3/Nafion nanocomposite as well as the difference spectrum of SiO_2/Nafion in the low wavenumber regime. On comparing the two spectra, the 465 cm^{-1} shoulder appears to be distinctive for SiO_2-Al_2O_3 /Nafion. The 795 cm^{-1} peak region could be influenced by imperfect subtraction of the spectrum of pure Nafion-H^+ which contains a weak absorption at 800 cm^{-1} due to -CF_2-CF_2- stretching, although we have no reason to suspect that this is the case.

While these IR studies are in an initial, exploratory stage, it appears that this technique is capable of roughly probing the degree of inorganic oxide molecular network connectivity.

B. Raman Spectroscopy

To complement our IR studies and examine all possible vibrational modes, we initiated a Raman spectroscopic characterization of these systems. Fig. 17 is a spectrum for SiO_2(40%) /Nafion. The level of silicon oxide in this film was caused to be high so that peaks associated with this phase would be apparent. We detected the Si-OH vibration at 968 cm^{-1} and Si-O stretching at 801 cm^{-1} . These appear to be the primary Raman signatures of the silicon oxide phase for these materials.

For TiO_2/SiO_2 /Nafion (Fig 18.), the observed Rayleigh broadening into low wavenumbers suggests self-aggregation of the inorganic phase. This hybrid was formulated by the sequential addition procedure, *i.e.* the titania component was added after pre-treatment with TEOS.

It is important to realize that samples were ground into particles for Raman analysis. Questions can be raised as to whether this is a destructive process. In any case, this sample-beam relationship is rather different from that for the FT-IR/ATR (near-surface analysis) experiment.

C. *^{29}Si Solid State NMR Investigations*

Figure 19 shows a ^{29}Si CP-MAS NMR spectrum for TiO_2/SiO_2/Nafion. This sample was formulated via sequential alkoxide addition, as above, and the dried weight uptake is 17%.

Prior to the NMR experiment for this system, it was anticipated that new Si peaks (other than the Q^{1-4} peaks commonly observed for pure SiO_2 -loaded Nafion) would emerge, owing to Si-O-Ti linkages. Actually, no new peaks were observed in the chemical shift range -10 to 140 ppm. Accompanied by a considerable noise-to-signal aspect, peaks in the Q^4, Q^3 and Q^2 regions are seen. Qualitatively, it appears that the degree of substitution around SiO_4 tetrahedra in the inorganic phase, while certainly not complete, is considerable. To the best of our knowledge of the literature, no observation of a Si-O-Ti associated ^{29}Si solid state NMR peak has been reported.

A similar ^{29}Si NMR spectrum for a SiO_2/Al_2O_3/Nafion hybrid (net inorganic content = 6.5%), reacted with pre-mixed alkoxides, is shown in Figure 20. In aluminasilicates, the SiO_4 tetrahedra with four bridging oxygens are classifed into five species according to the number of adjacent aluminum atoms, m, bonded to the oxygen: Q^4(mAl), *i.e.* $Si(OSi)_{4-m}(OAl)_m$. The approximate ranges of the chemical shift of Q^4(mAl) and Q^n are indicated in the following table.[1]

Al-Substitution	Chemical Shift, ppm	Si-Substitution	Chemical Shift (ppm)
Q^4(4Al):	-81 to -91	Q^0:	-60 to -82
Q^4(3Al):	-85 to -94	Q^1:	-68 to -83
Q^4(2Al):	-91 to -100	Q^2:	-74 to -93
Q^4(1Al):	-97 to -107	Q^3:	-91 to -101
Q^4(OAl):	-101 to -116	Q^4:	-106 to -120

It is obvious, on inspection of this table, that there is considerable overlap between Q^4(mAl) and Q^n peaks so as to confuse the assignments of the peaks observed at ca. -92, -102 and -110 ppm in Fig. 20.

In-depth, systematic studies of samples having various Si/Al ratios is needed to identify Si-O-Al bond formation and begin to sort out topological and compositional aspects of the incorporated inorganic oxide network.

III. Thermodegradation Behavior

Nafion materials, in their own right, are rather robust with regard to thermodegradative stability. This property has profound implications with regard to future applications of the nanocomposites tailored using these interactive templates. It is therefore appropriate in this work to evaluate the degree to which this thermal property is modified by the *in situ* grown inorganic oxide phases.

Figure 21 shows TGA profiles of SiO_2 /Nafion hybrids formulated using different alcohol solvents. The silicon oxide contents, listed in the following table (section a), are rather close to each other (12.3 - 13.7%). The samples were run in N_2 and the heating rate was 10^0C/min . For reference, the profile for pure Nafion-H^+ is shown. Degradation behavior is similar for all these solvents and the onset for each is only slightly greater than

that of pure Nafion$^+$. However, beyond the onset temperature, Nafion-H$^+$ degradation is more retarded than that of the hybrids prepared in the various alcohols.

Alkoxide	Solvent	Nafion Form	wt%
(a) Silicates			
TEOS	MeOH	H+	13.7
TEOS	EtOH	H+	13.2
TEOS	1-PrOH	H+	12.3
TEOS	1-BuOH	H+	12.9
(b) Titanates-Different Solvents			
TET	EtOH	H+	20.9
TET	1-PrOH	H+	9.9
TET	1-BuOH	H+	5.5
(c) Titanates-Different Alkoxides			
TET	EtOH	H+	20.9
TPT	EtOH	H+	25.3
TP^{i}T	EtOH	H+	23.0
TBT	EtOH	H+	28.6
(d) TiO_2-SiO_2			
TET	EtOH	H+	13.7
TPT	EtOH	H+	8.3
TP^{i}T	EtOH	H+	8.7
TBT	EtOH	H+	9.4
(e) Titanates-Nafion-Na$^+$			
TET	EtOH	Na+	7.7
TET	1-PrOH	Na+	3.5
TET	2-PrOH	Na+	4.2
TET	1-BuOH	Na+	4.5
(f) Al_2O_3-SiO_2 (various compositions)			
TBA	2-PrOH	H+	4-6
(g) *Zirconates-Different Solvents*			
TBZ	EtOH	H+	24.6
TBZ	1-PrOH	H+	6.9
TBZ	2-PrOH	H+	5.5
TBZ	1-BuOH	H+	5.8

In sharp contrast, thermodegradation for Nafion-H$^+$ reacted with TET (Fig. 22) is markedly less stable relative to pure Nafion and the curves for the different solvents greatly differ among each other. It should be noted, in the above table, that the inorganic

contents markedly vary from 5.5% (1-BuOH) to 20.9%(EtOH). At least two distinct degradation events are involved. The actual weight loss mechanisms would be effectively probed using TGA/FT-IR as we have for other related systems. The 1-BuOH -derived hybrid appears to have the lowest degradation onset temperature, as well as lowest titania content.

The effect of R group size using $Ti(OR)_4$ is displayed in Fig. 23 wherein solvent = EtOH and Nafion-H^+ = template. In section c of the above table, it is seen that the inorganic content varies from ~21% (TET) to ~29%(TBT). These filler levels are rather high. It is clear that thermodegradation is not improved, in fact worsened, using titanium alkoxides. There is a progressive shift of the curves in Fig. 23 to higher temperature, as well as to higher filler content, with increasingly larger alkoxide, although initially the curves (save for TET), are initially rather superimposed.

The same can be said of SiO_2/TiO_2/Nafion hybrids formulated with Nafion-H^+, TEOS, various pre-mixed Ti alkoxides and EtOH solvent, as seen in Fig 24. Here again, the negative "catalytic" effect of the inorganic phase is seen. While the TGA curves have several crossovers, all filled samples commence degradation at about the same temperature, which is approximately the same as that for pure Nafion-H^+, as well as that seen in Fig. 23 for TiO_2 /Nafion. On the other hand, the filler content (above table) for the TET-derived system (~14%) is significantly higher than the contents resulting from the other alkoxides (~9%).

The deterioration of thermal degradation resistance inherent to unfilled Nafion-H^+ by TiO_2 incorporation is essentially prevented by conversion of Nafion to the Na^+ -form. More specifically, this is true for the solvents 1 and 2 PrOH and 1-BuOH, but not for EtOH (Fig. 25) . We note that the EtOH-derived sample also has the highest titania uptake (see above table, section e). It should be pointed out in this discussion that unfilled Nafion- Na^+ has a considerably higher degradation onset temperature than unfilled Nafion-H^+ .

Fig. 26 shows thermodegradation of various SiO_2/Al_2O_3/Nafion compositions (affected using pre-mixed alkoxides, TEOS, aluminum tri-butoxide, and Nafion-H^+). The solid lines are for a variety of Al/Si compositions. The onset of degradation for each filled system is not significantly different from that of pure Nafion. On the other hand, as with the previous Ti-containing systems, aluminasilicate-filled Nafion-H^+ does not represent an improvement in thermal stability over the unfilled system. The filler contents of the systems investigated are not high (~5%).

Finally, ZrO_2/Nafion (H^+) hybrids were generated using TBZ and different alcohol solvents. TGA thermograms obtained for these materials are displayed in Fig. 27. The onset of degradation for the samples prepared with 1- and 2-PrOH and 1-BuOH are the same and approximately the same as that for pure Nafion. On the other hand, the sample prepared with EtOH showed a higher degradation temperature, but experienced a rapid weight loss followed by another, slower process of degradation. The EtOH-derived sample also possessed a rather high zirconate uptake (~25%) compared to that for the other solvents (5.5 - 6.9%), as seen in the above table, section g.

In all the TGA scans reported here, the usual slow weight loss preceding the first significant degradation is attributed, in part, to residual alcohol, water and possible unreacted alkoxide volatilization, despite our efforts to pre-dry these systems. It is also reasonable to implicate the loss of water that is generated by condensation reactions

between X-OH groups (X = Si, Ti, Zr). Titanium and aluminum alkoxides are highly reactive species. Possible reactions of these species with alcohols and acid might be possible.

IV. Mixed Inorganic Oxide Nanocomposites Based on Solution-Cast Nafion Films

An 1100 EW Nafion sulfonic acid film was dissolved at high temperature and under high pressure. This Nafion solution was mixed with a TEOS solution in which the sol-gel reaction has been initiated. Finally, a titanium alkoxide solution was added to so that, finally, a SiO_2/TiO_2/Nafion hybrid resulted upon drying.

First, a solution of Nafion in $EtOH/H_2O$ (50/50 v/v), having a concentration of 1.675g/100ml, was prepared in the laboratory of Moore. Then, a brittle-cracked solid form of Nafion was obtained by film-casting this solution at ambient temperature for 10 days and vacuum drying for 2 days at R.T. This material is then ready to dissolve in a polar solvent and a Nafion/pure ethanol solution is thus obtained.

The hybrids were prepared by first pre-reacting TEOS with H_2O (TEOS:H_2O = 1:1 mole/mole). This reactive solution was then mixed with the above Nafion solution with vigorous stirring. The mixtures were allowed to react a long time (~1 hr) to allow for consumption of the pre-added water.

Then, a titanium alkoxide solution (TBT/EtOH = 1/10 v/v) was added to this already-reacting silicate mixture. TBT, in somewhat dilute concentration, was used so that reactions are not overly rapid in an ambient environment. If free water is present, TiO_2 immediately precipitates upon addition of the titanium alkoxide. Thus, we have attempted to limit the amount of water in the system. The resulting *clear* solutions were placed in air to allow or solvent volatilization at either R.T. or 60°C. After film formation, samples were removed from their glass substrates and transferred to a vacuum oven to complete drying at 100°C for 2 days. Perhaps it is significant to note that the films greatly adhered to the substrate and we are attempting to overcome this problem with new substrates.

The samples which were formulated, as well as their superficial physical aspects, are listed in the following table. The entries in a given row denote relative weight proportions. To illustrate, Nafion:SiO_2;TiO_2 = 4:1:1 for the first row designates that the number of grams of Nafion is four times as much as that for silica and titania. Specifically, the amount of TEOS and TBT liquid that was required to produce this ratio for the *ideal* formulas SiO_2 and TiO_2 was determined. Of course, the actual inorganic oxide phase can contain a significant number of uncondensed XOH groups, as indicated by IR spectroscopy, resulting in more than two oxygen atoms per silicon or titanium atoms.

Composition of TiO_2/SiO_2/Nafion Solution-Cast Hybrids
(Parts by Relative Weight)

Nafion	SiO_2	TiO_2	Drying Temperature	Appearance of Bulk Sample
4	1	1	60°C	opaque, cracked
2	1	1	60°C	opaque, cracked
4	5	1	60°C	*clear*, cracked
50	4	1	R.T.	*clear*, cracked
25	4	1	R.T.	*clear*, cracked
15	4	1	R.T.	*clear*, cracked

On inspecting the above table, it appears that the Ti/Si ratio should be lower than 1/4 to obtain transparent samples. Additional studies of the effect of solution casting conditions and the structure and properties of these materials as films and coatings, will be discussed in a subsequent report.

Advantages offered by materials issuing from this solution technology, compared with pre-formed films, are envisioned. Functional coatings can be deposited on the surfaces of metals, ceramics or other polymers. Applications in the areas of electromagnetic-interactive coatings, energy storage, electrode sensors and other electrochemical systems are suggested. The same can be said for the extrusion of transparent fibers with hybrid organic/inorganic compositions that are tailored to offer useful optical properties the realm of communications.

V. Conclusions

We proposed that the capability of manipulating the composition and geometrical distribution, *i.e.* morphology, of an inorganic oxide component throughout nanophase-separated perfluorosulfonate ionomers via *in situ* sol-gel chemistry has the potential for the rational tailoring of sophisticated optical materials. This assumption was based on (1) dielectric heterogeneity on the ultrafine level of nanometers, (2) spatial variation of index of refraction and (3) inorganic oxide inclusions that are too small to scatter light. Opportunities also exist in the realm of electronic materials or coatings that are frequency-selective toward electromagnetic waves. Pressure or temperature-activated conductor↔insulator transitions might form the basis of intelligent switching devices.

The results in this report, although preliminary, provide encouragement that the heterophase morphology of these materials might indeed be tailored on the level of nanometers for sophisticated technological applications.

We have successfully incorporated single and mixed inorganic oxide phases within perfluorosulfonate ionomers. Moreover, we have discovered conditions under which the inorganic oxide concentration profile across the film thickness can be manipulated so as to be uniform of nonuniform, but symmetric, or asymmetric. The salient control variables

include alkoxide type, size, reactivity, and concentration, mixed alkoxide composition and bi-component alkoxide addition scheme, solvent type, water concentration, alkoxide permeation time, drying conditions, and H^+ *vs* Na^+ form of the Nafion template. The EDS attachment of our environmental scanning microscope was quite effective in probing the inorganic oxide concentration profiles of these unique hybrid materials.

Infrared and complementary Raman spectroscopic studies detected characteristic peaks that reflected the degree of polyfunctional condensation, or molecular connectedness, within the inorganic oxide phase (Si-OH, Si-O-$Si_{[sym, asym]}$, Ti-O-Si stretching). The complex spectra for multicomponent oxides needs to analyzed in more detail for more complete band identification. [29] Si solid state NMR studies of SiO_2/Al_2O_3/Nafion are difficult to interpret owing to the great number of coordination possibilities of Si and Al atoms around SiO_4 tetrahedra in the inorganic network.

In contrast with silicon oxide incorporation, thermal degradation is not improved, but in fact worsened using titanium oxide, as seen in our TGA studies. Solvent type plays a strong indirect role in controlling degradation.

A Nafion-H^+ solution was created at high temperature and under high pressure. This solution was mixed with a TEOS solution in which the sol-gel reaction was in the initial stages. To this, a titanium alkoxide solution was added; a SiO_2/TiO_2/Nafion hybrid resulted upon drying. For low Ti/Si ratio, a clear but brittle film can be produced. We suggest that this solution technology could lead to functional coatings deposited on the surfaces of metals, ceramics or other polymers. Applications in the areas of electromagnetic-interactive coatings, energy storage, electrode sensors and other electrochemical systems are envisioned. The extrusion of transparent fibers with hybrid organic/inorganic compositions that are tailored for important optical properties in the realm of communications is worthy of consideration..

VI. References

1. Yasumori, A.; Iwasaki, M.; Kawazoe, H.; Yamane, M.; Nakamura, Y. *Physics and Chemistry of Glasses* **1990**, 31(1), 1.

VII. Figures

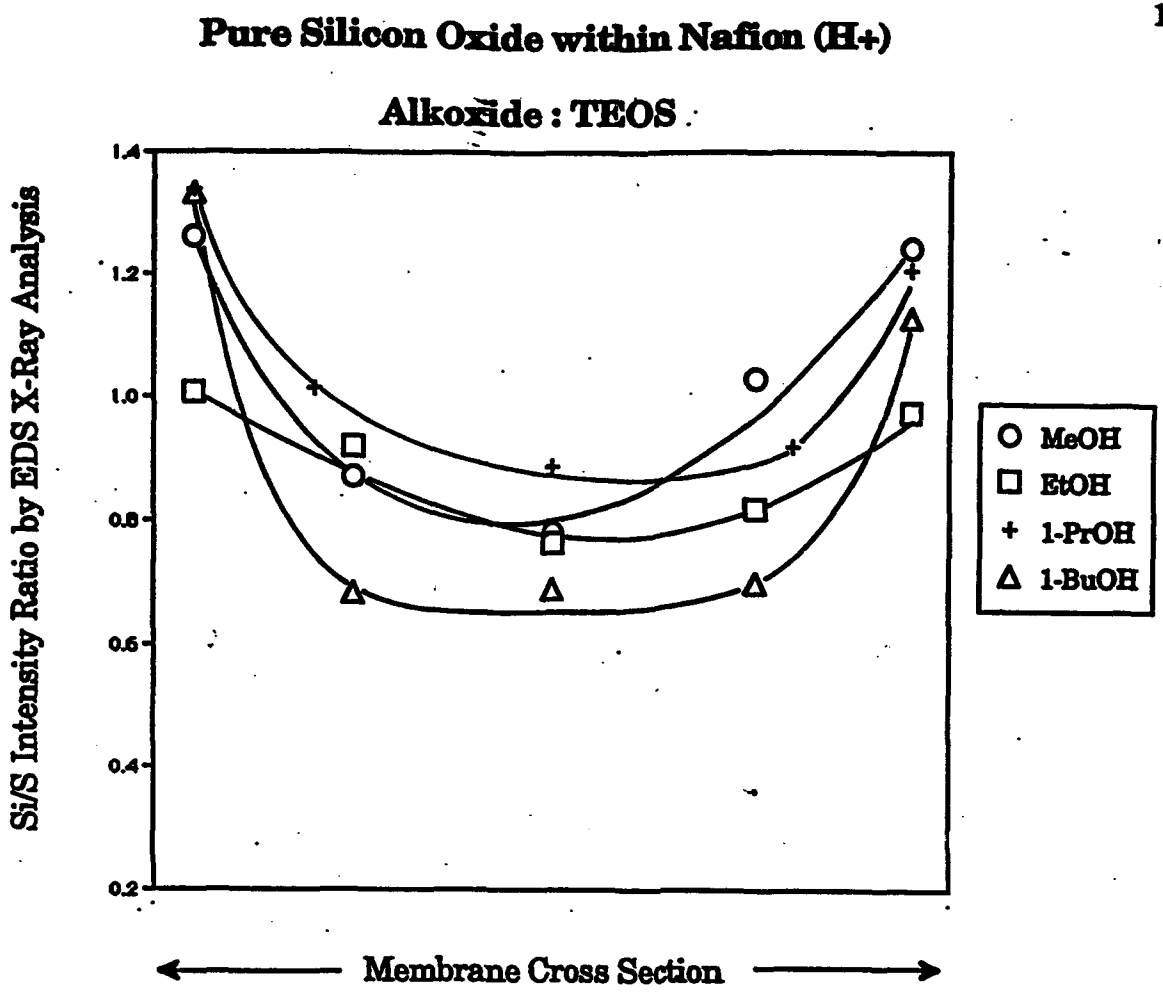
Pure Silicon Oxide within Nafion (H+)
Alkoxide : TEOS
Si/S Intensity Ratio by EDS X-Ray Analysis
1.4
1.2
1.0
0.8
0.6
0.4
0.2
MeOH
EtOH
1-PrOH
1-BuOH
Membrane Cross Section

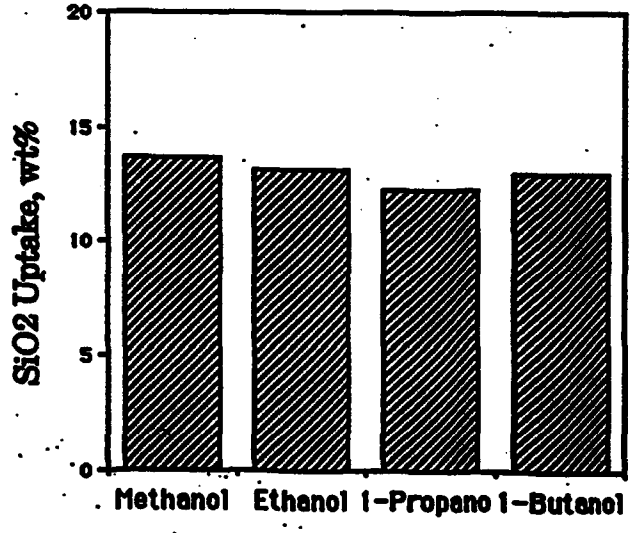
SiO2 Uptake, wt%
20
15
10
5
0
Methanol
Ethanol
1-Propanol
1-Butanol

Figure 1

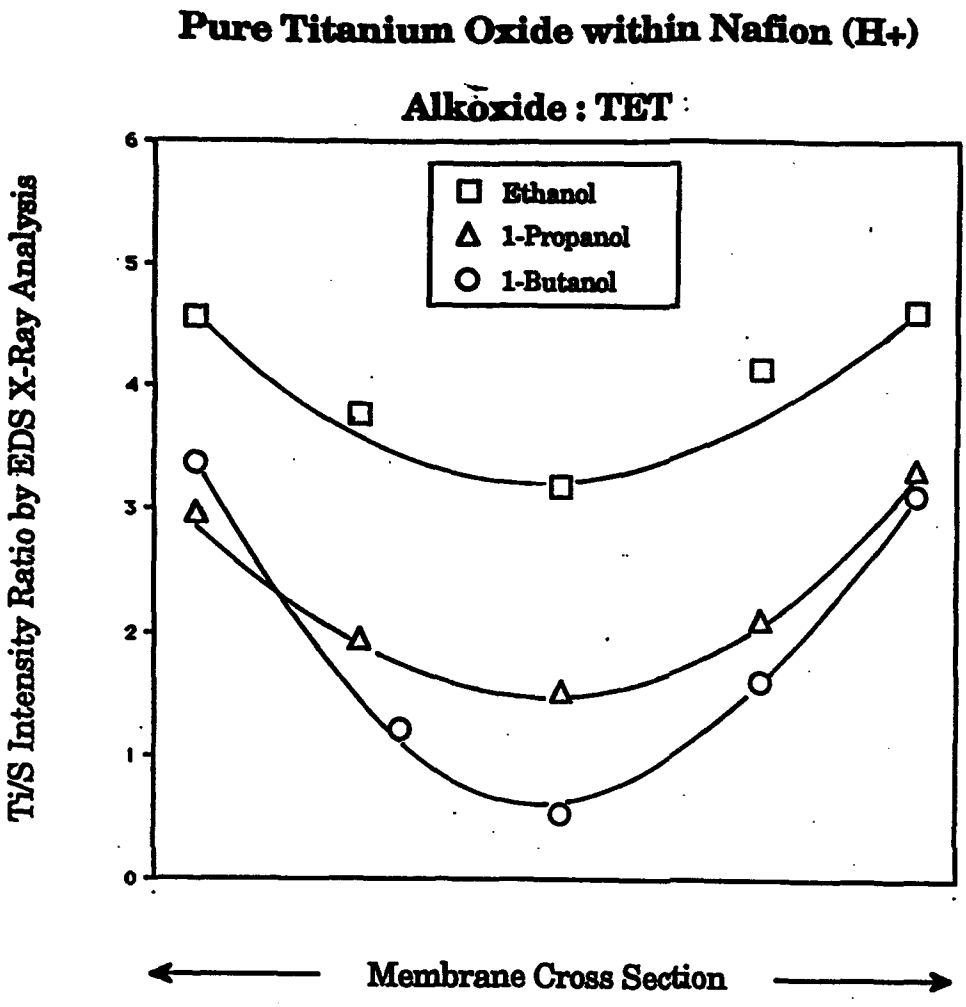
Pure Titanium Oxide within Nafion (H+)
Alkoxide : TET
Ethanol
1-Propanol
1-Butanol
Ti/S Intensity Ratio by EDS X-Ray Analysis
0
1
2
3
4
5
6
Membrane Cross Section

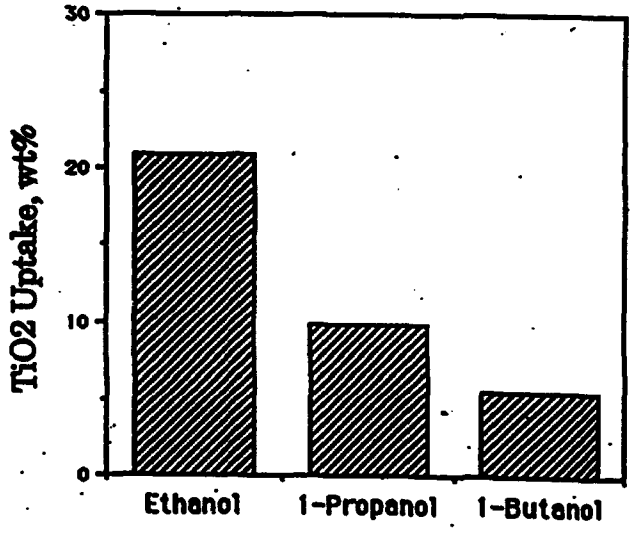
TiO2 Uptake, wt%
0
10
20
30
Ethanol
1-Propanol
1-Butanol

Figure 2

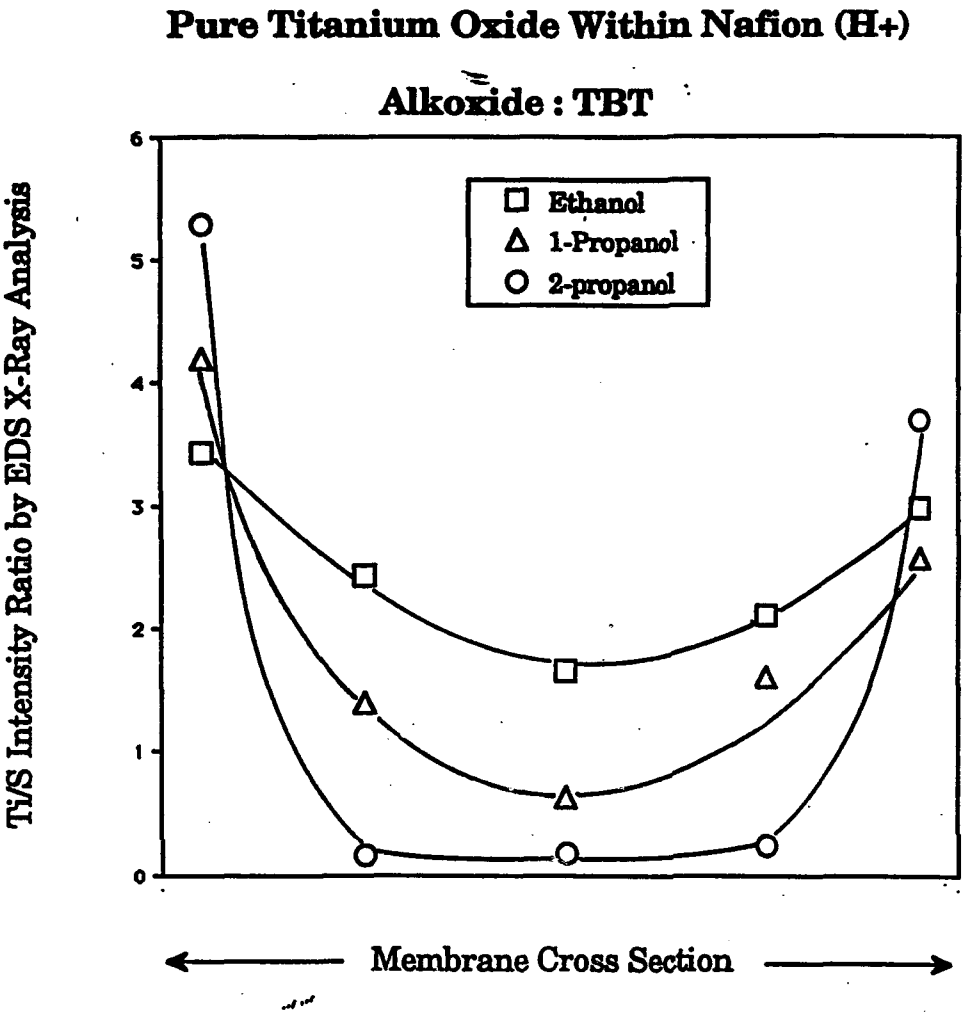
Pure Titanium Oxide Within Nafion (H+)
Alkoxide : TBT
Ti/S Intensity Ratio by EDS X-Ray Analysis
Ethanol
1-Propanol
2-propanol
Membrane Cross Section

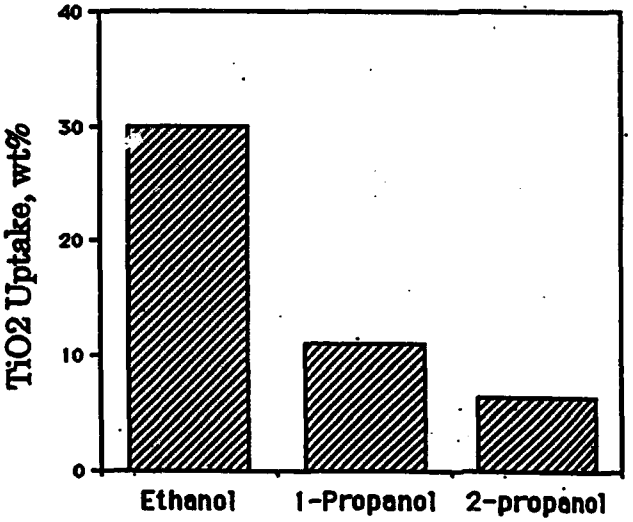
TiO2 Uptake, wt%
Ethanol
1-Propanol
2-propanol

Figure 3

TiO2-SiO2 Loaded Nafion (H+)
Pre-Mixed Alkoxides

Solvent : Ethanol

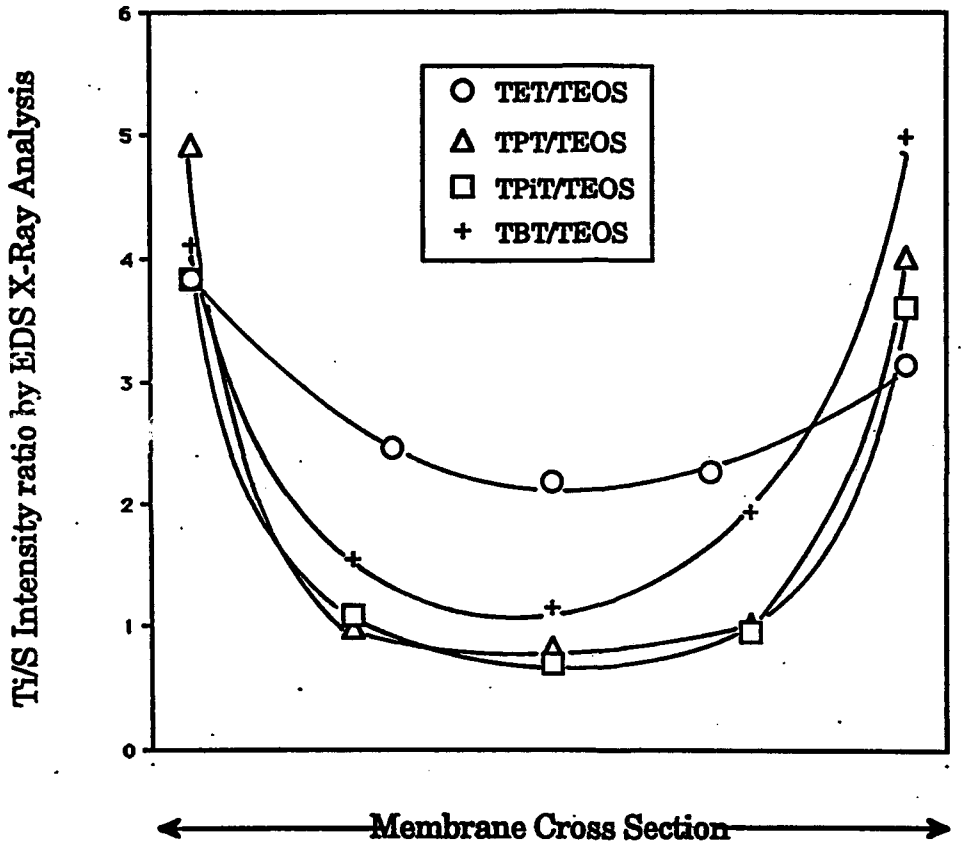

Figure 4

TiO2-SiO2 Loaded Nafion (H+)
Pre-Mixed Alkoxides

Solvent : 2-Propanol

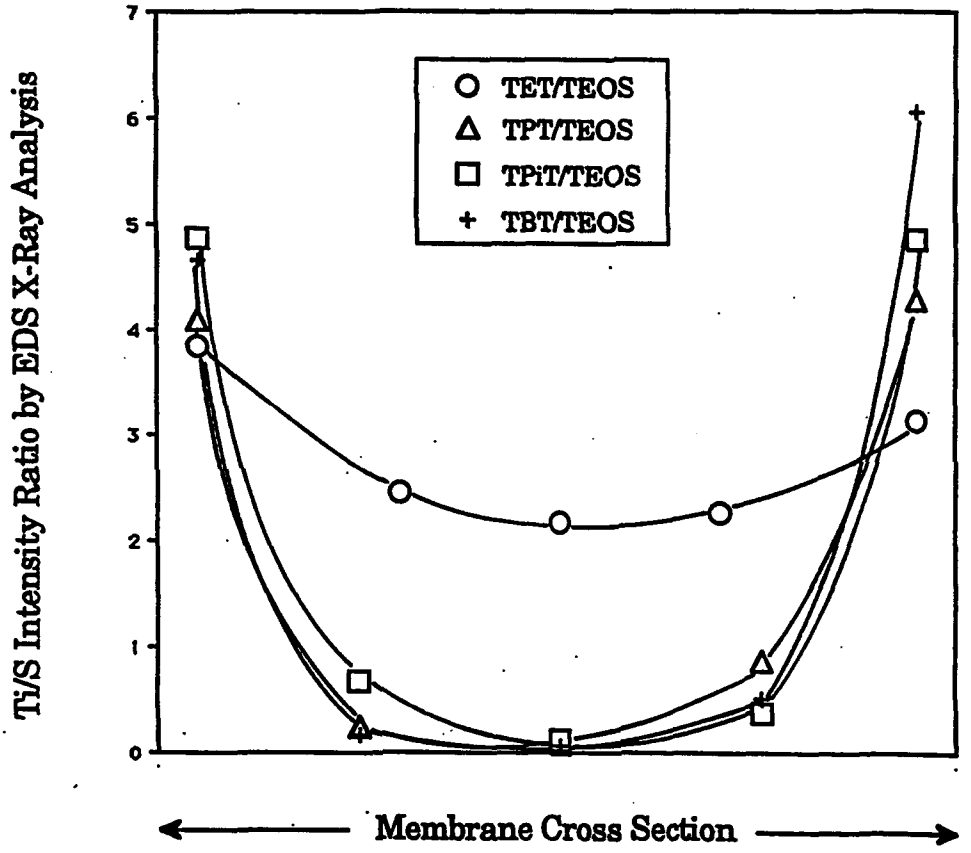

Figure 5

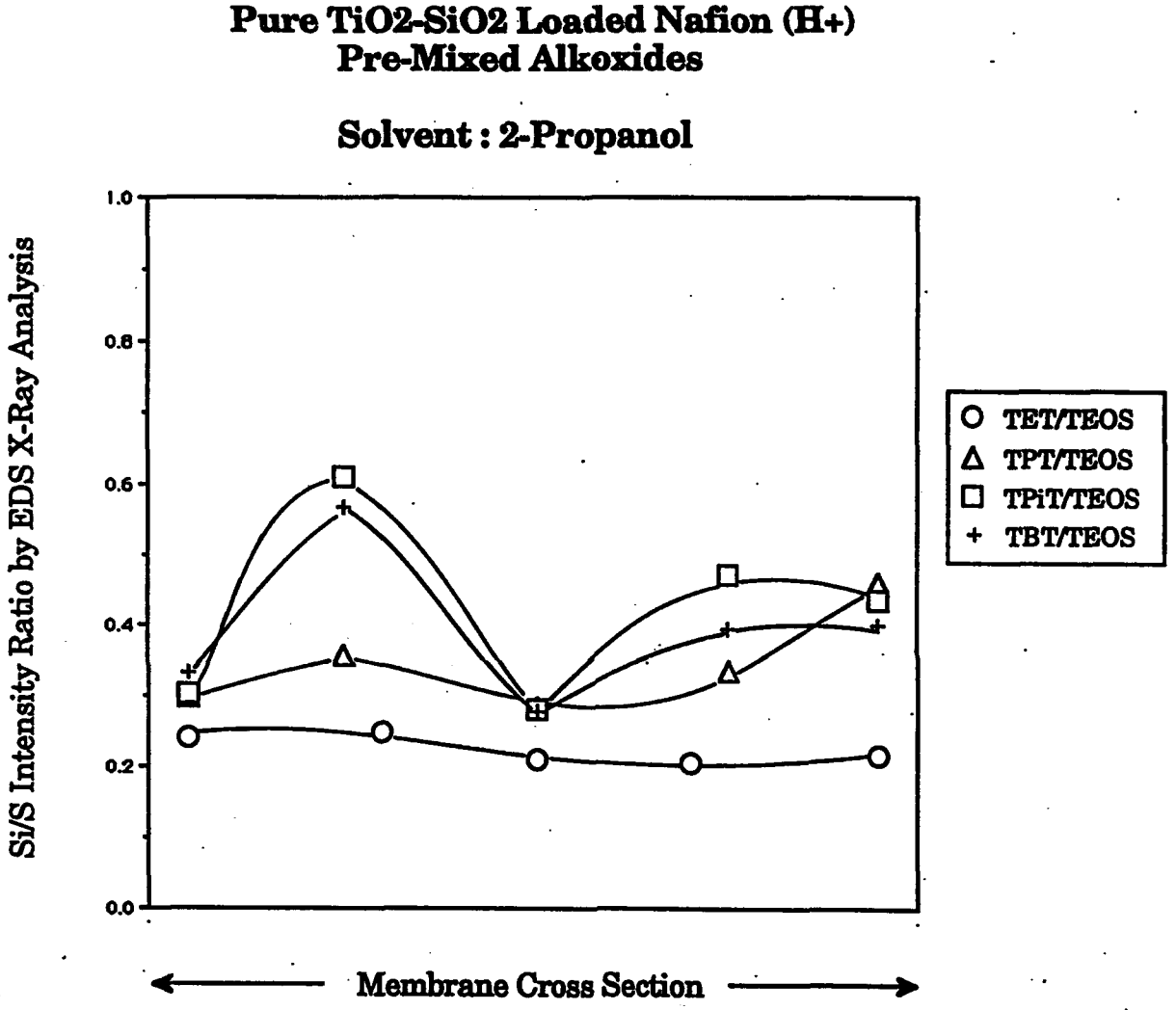
Pure TiO2-SiO2 Loaded Nafion (H+)
Pre-Mixed Alkoxides
Solvent : 2-Propanol
Si/S Intensity Ratio by EDS X-Ray Analysis
1.0
0.8
0.6
0.4
0.2
0.0
TET/TEOS
TPT/TEOS
TPiT/TEOS
TBT/TEOS
Membrane Cross Section

Figure 6

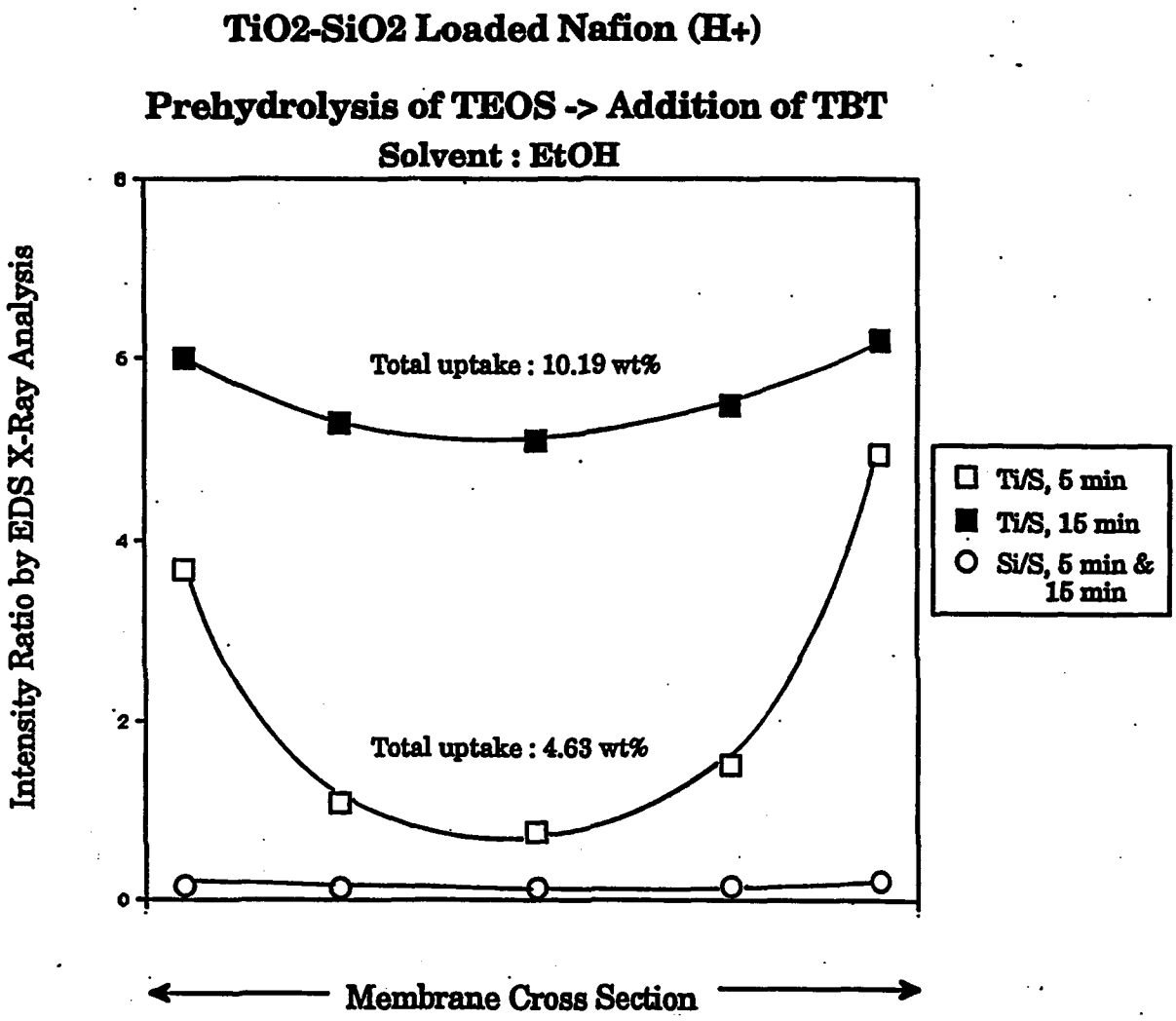
TiO2-SiO2 Loaded Nafion (H+)
Prehydrolysis of TEOS -> Addition of TBT
Solvent : EtOH
Intensity Ratio by EDS X-Ray Analysis
0
2
4
6
8
Total uptake : 10.19 wt%
Total uptake : 4.63 wt%
Ti/S, 5 min
Ti/S, 15 min
Si/S, 5 min & 15 min
Membrane Cross Section

Figure 7

Pure Titanium Oxide Within Nafion (Na+)

Alkoxide : TET

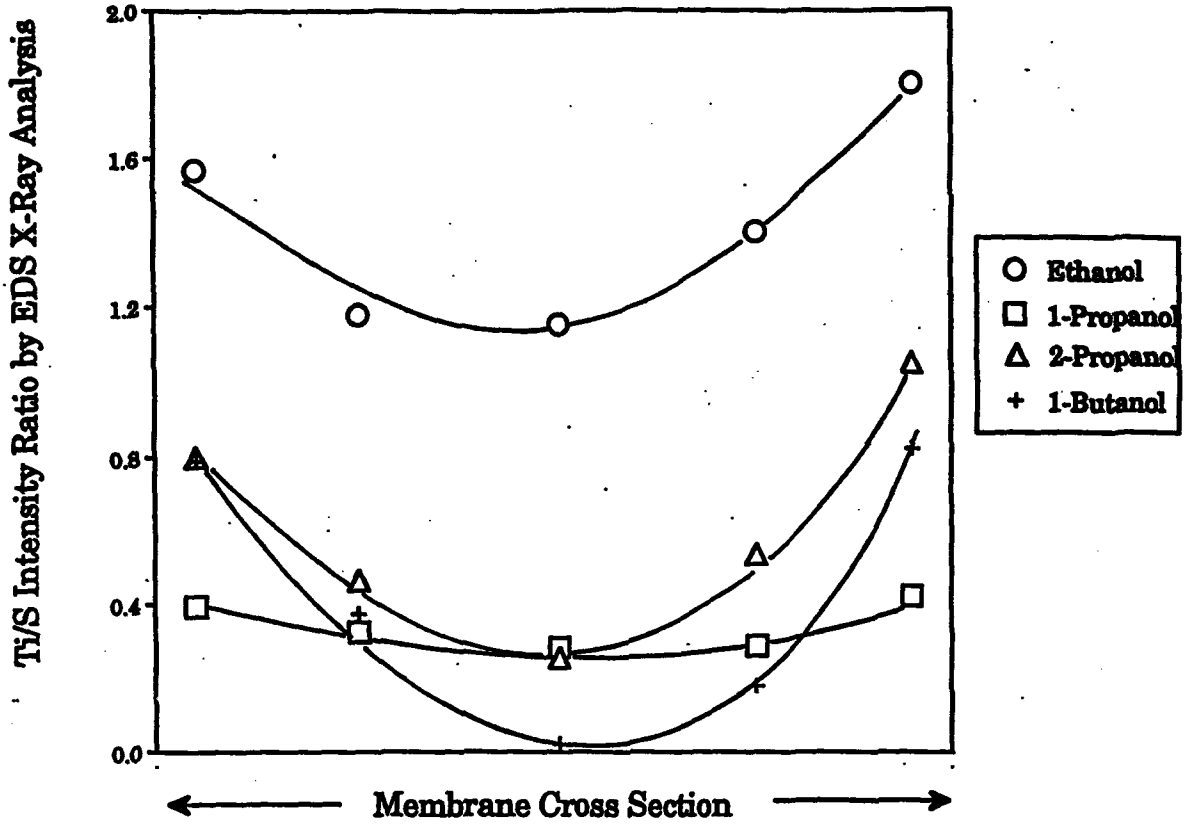

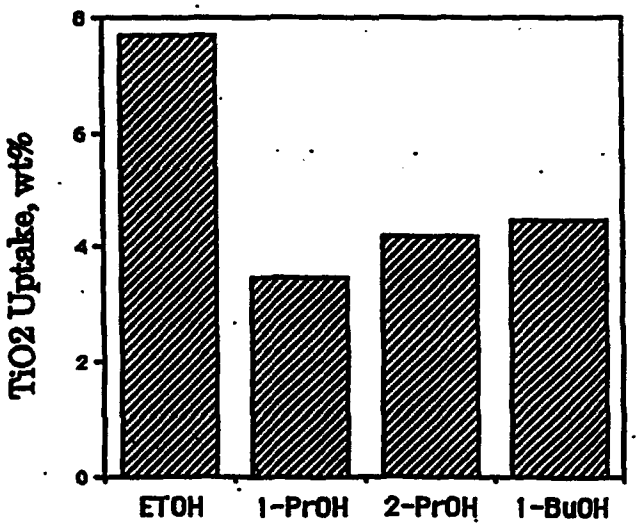

Figure 8

Pure Zirconium Oxide Within Nafion (H+)

Alkoxide : TPZ

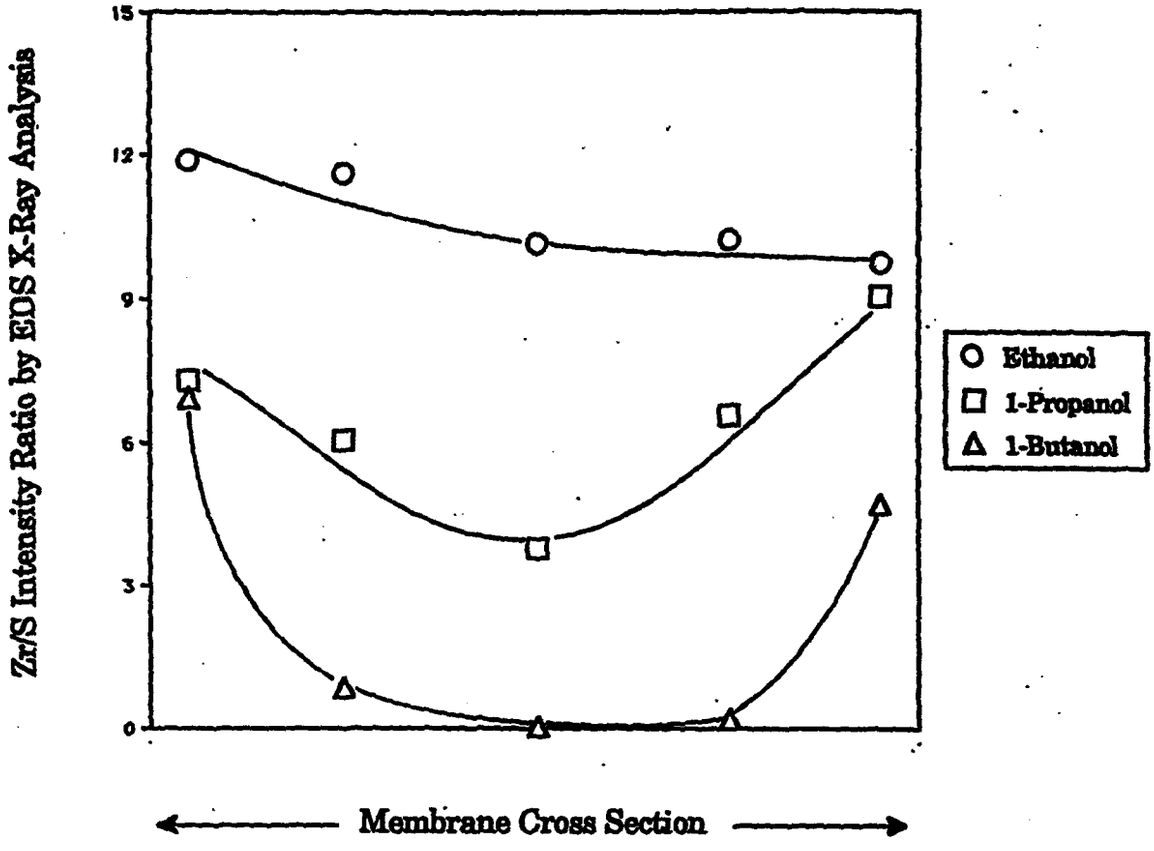

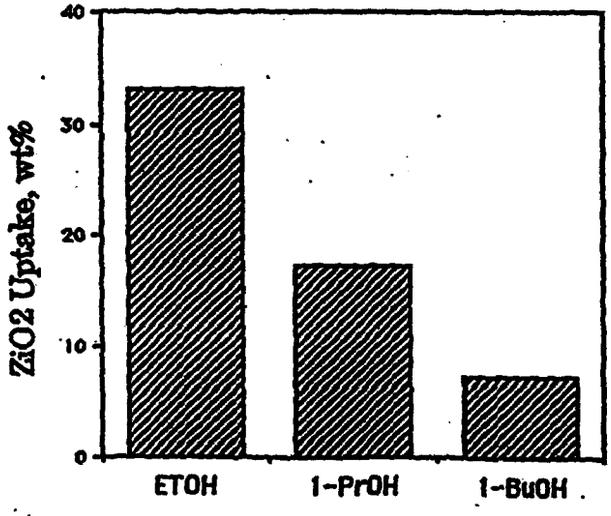

Figure 9

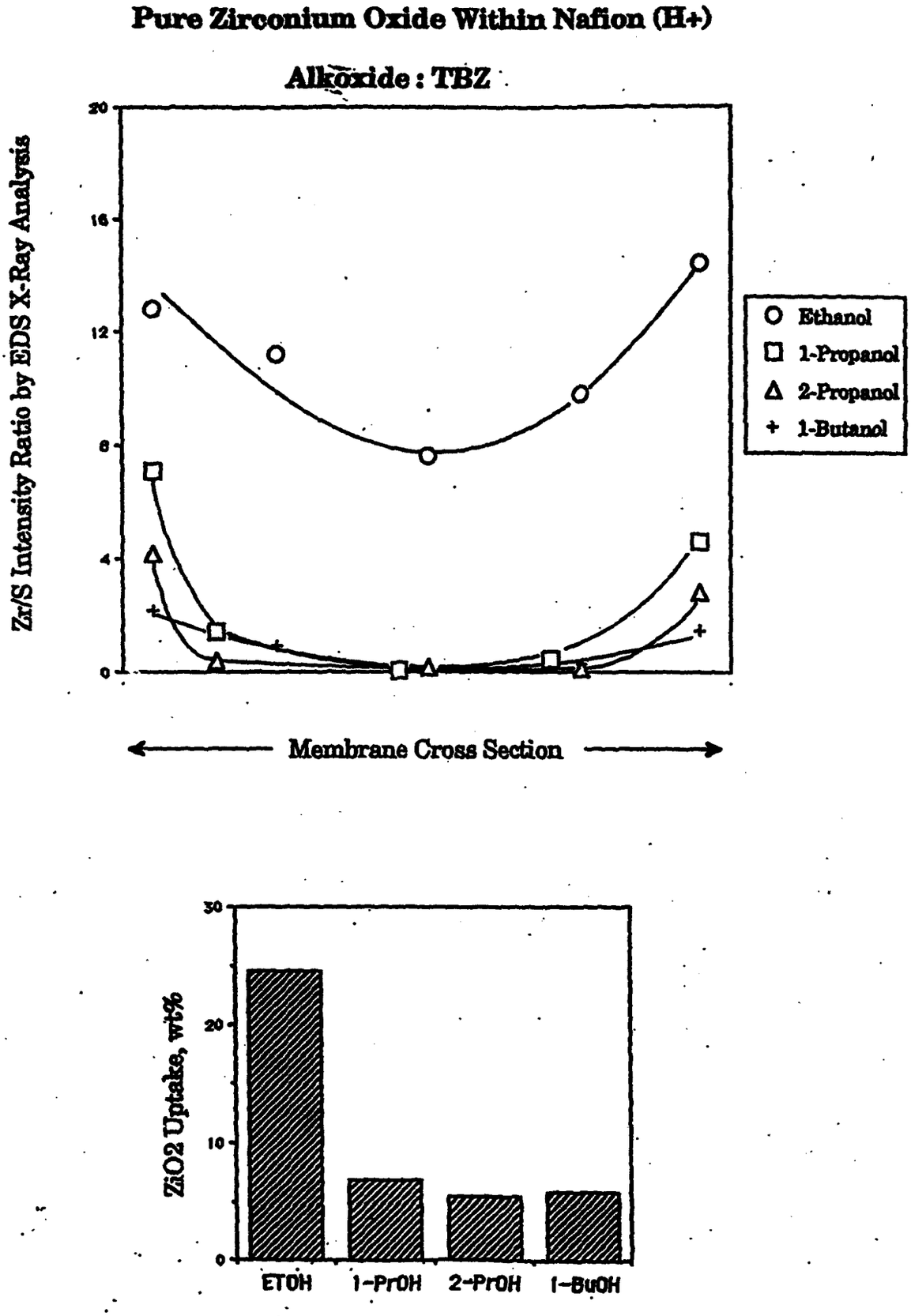
Pure Zirconium Oxide Within Nafion (H+)
Alkoxide : TBZ
Zr/S Intensity Ratio by EDS X-Ray Analysis
20
16
12
8
4
0
Ethanol
1-Propanol
2-Propanol
1-Butanol
Membrane Cross Section
ZiO2 Uptake, wt%
30
20
10
0
ETOH
1-PrOH
2-PrOH
1-BuOH

Figure 10

Permeation of TBZ from Only One Side of Nafion (H+) Membrane

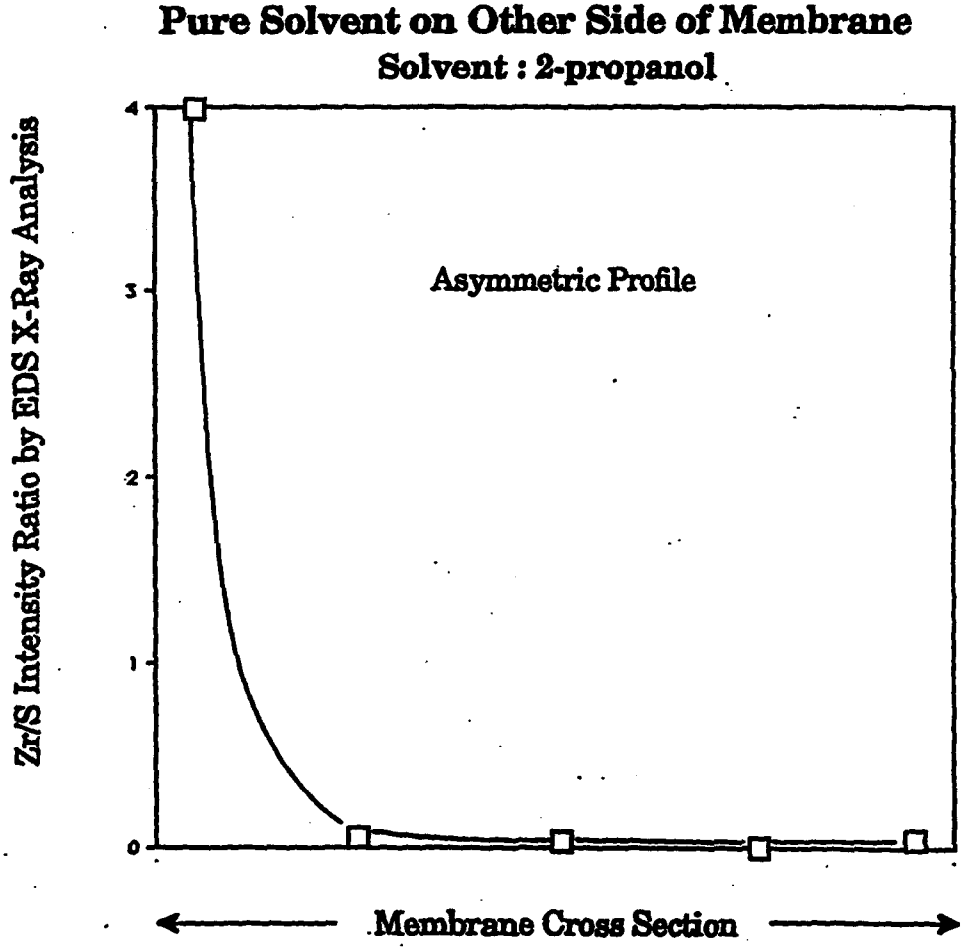

Figure 11

Counter-Diffusion of TBT and TBZ in Nafion (H+) Membrane

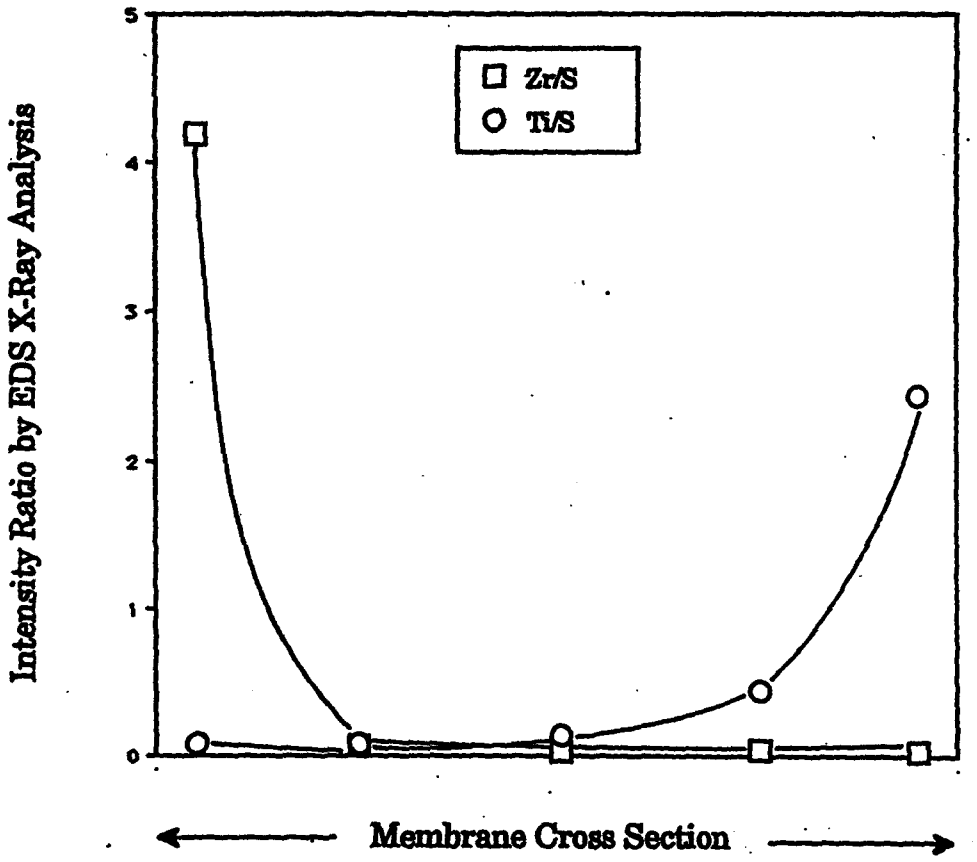

Figure 12

Counter-Diffusion of TBT and TEOS in Nafion (H+) Membrane

Delayed Addition of TEOS

Solvent : 2-Propanol

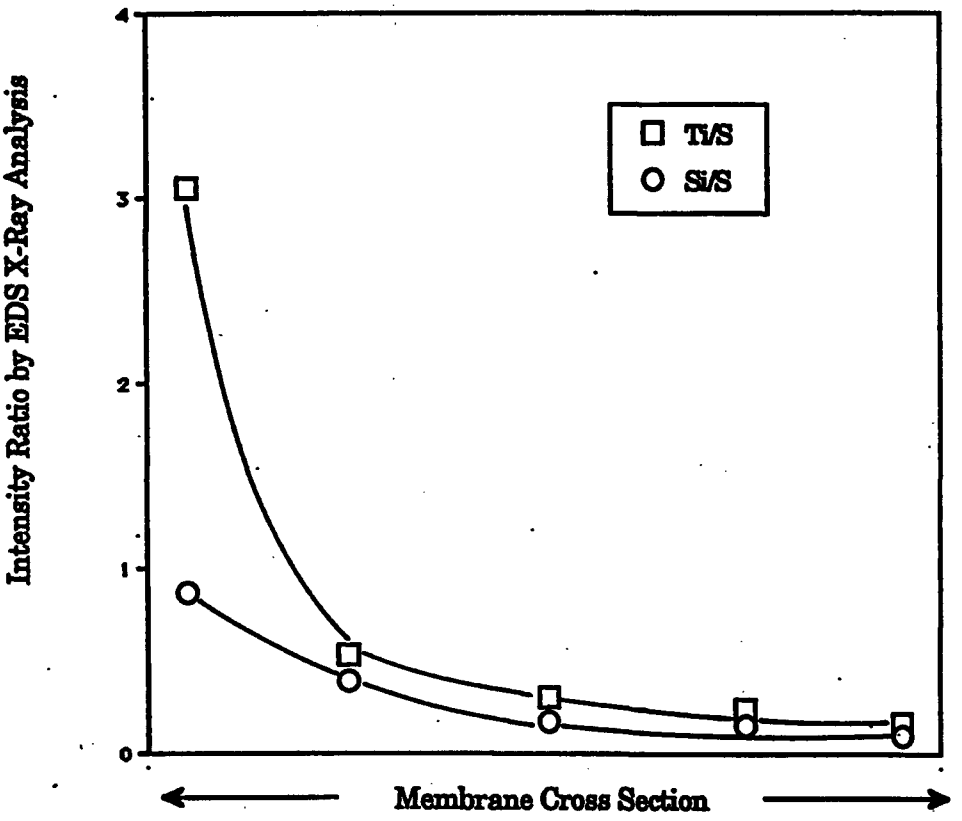

Figure 13

ATR-FT-IR Spectra of TiO_2-SiO_2 Loaded Nafion (H^+)

Solvent : 2-Propanol, Alkoxides : TEOS & TBT 141

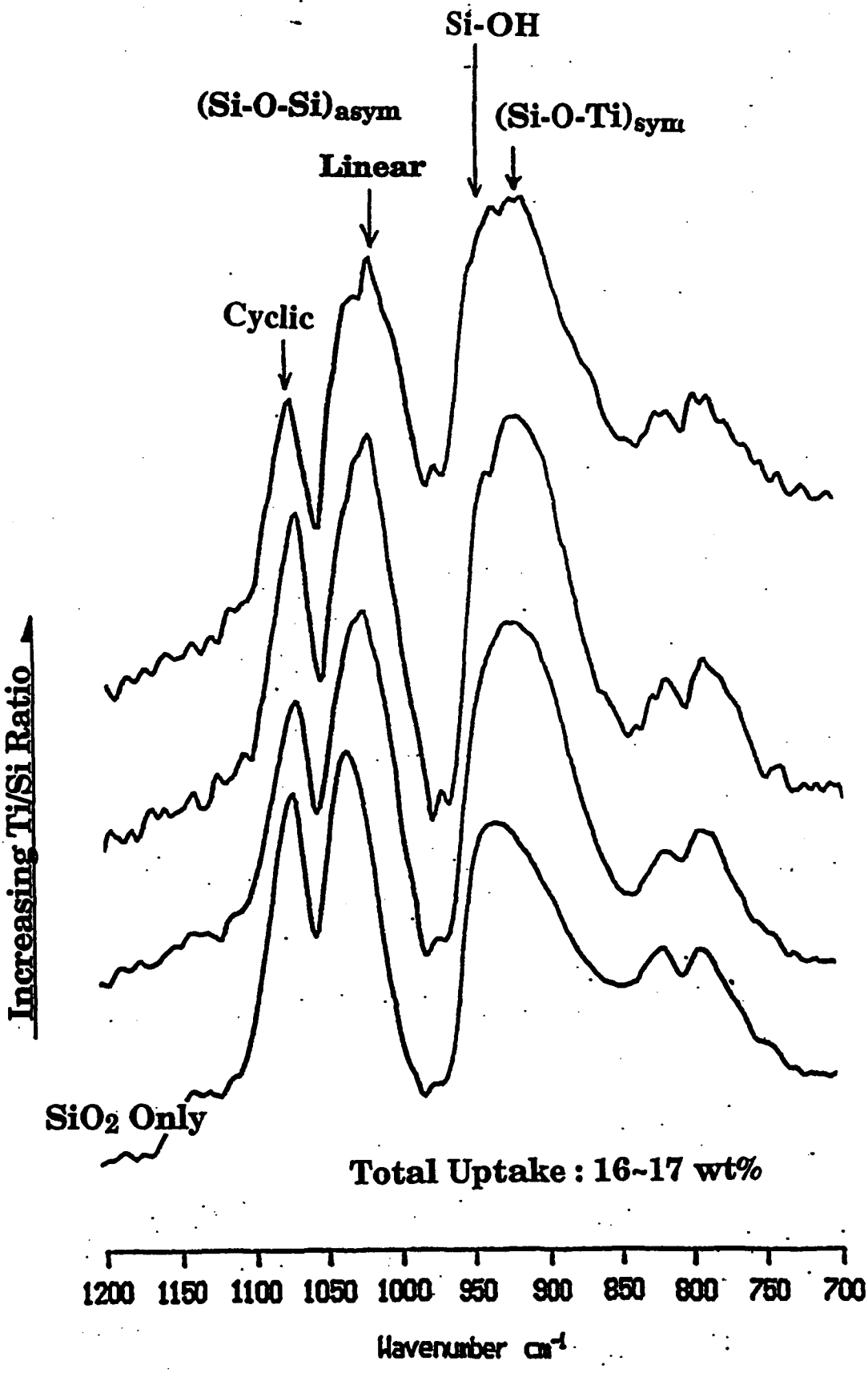

Figure 14

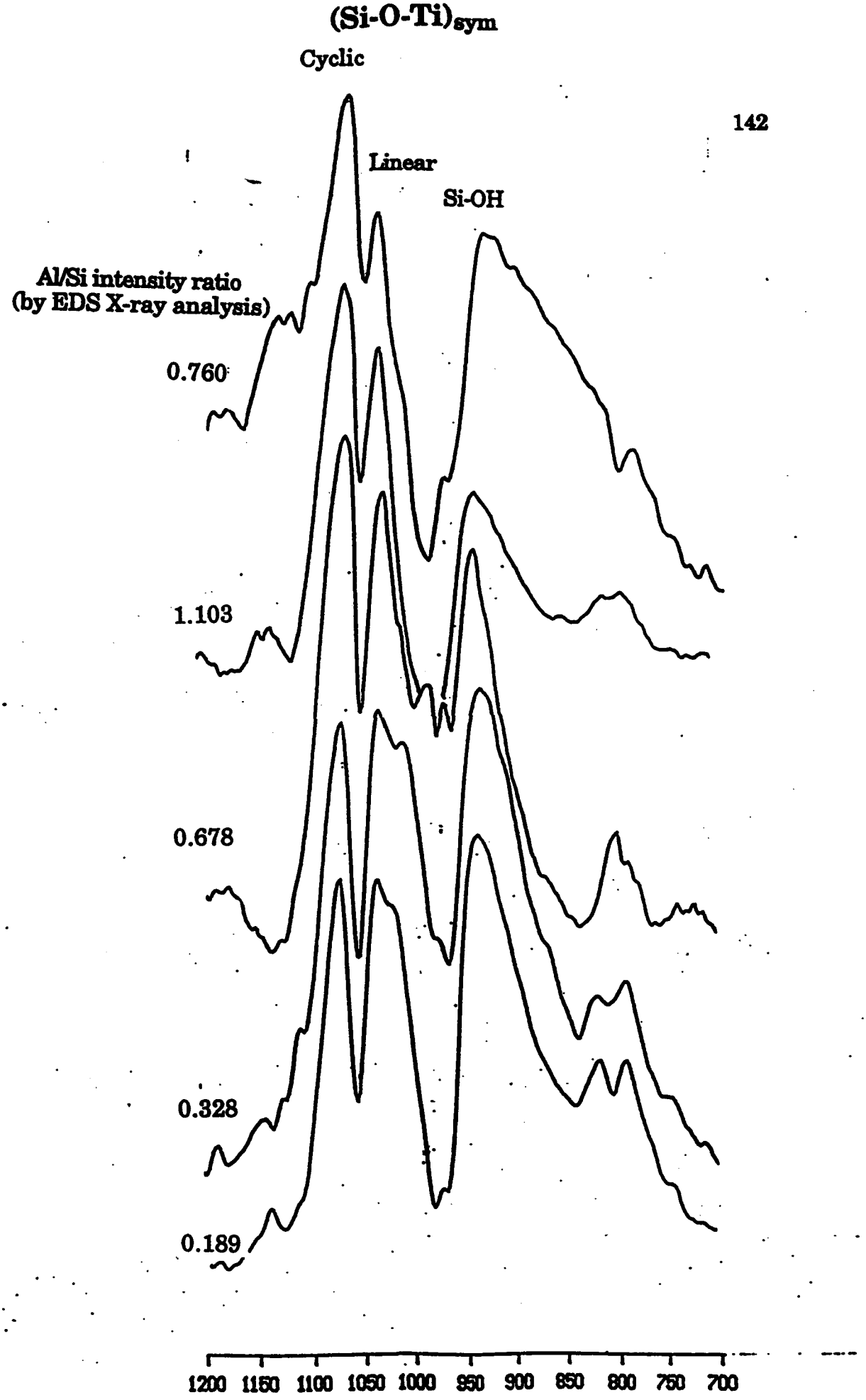
(Si-O-Ti)sym
Cyclic
Linear
Si-OH
Al/Si intensity ratio
(by EDS X-ray analysis)
0.760
1.103
0.678
0.328
0.189
1200 1150 1100 1050 1000 950 900 850 800 750 700
ATR-FT-IR Spectra of Al2O3-SiO2 Loaded Nafion (H+)

Figure 15

Evidence of Al-O-Si Linkage / Mixed System

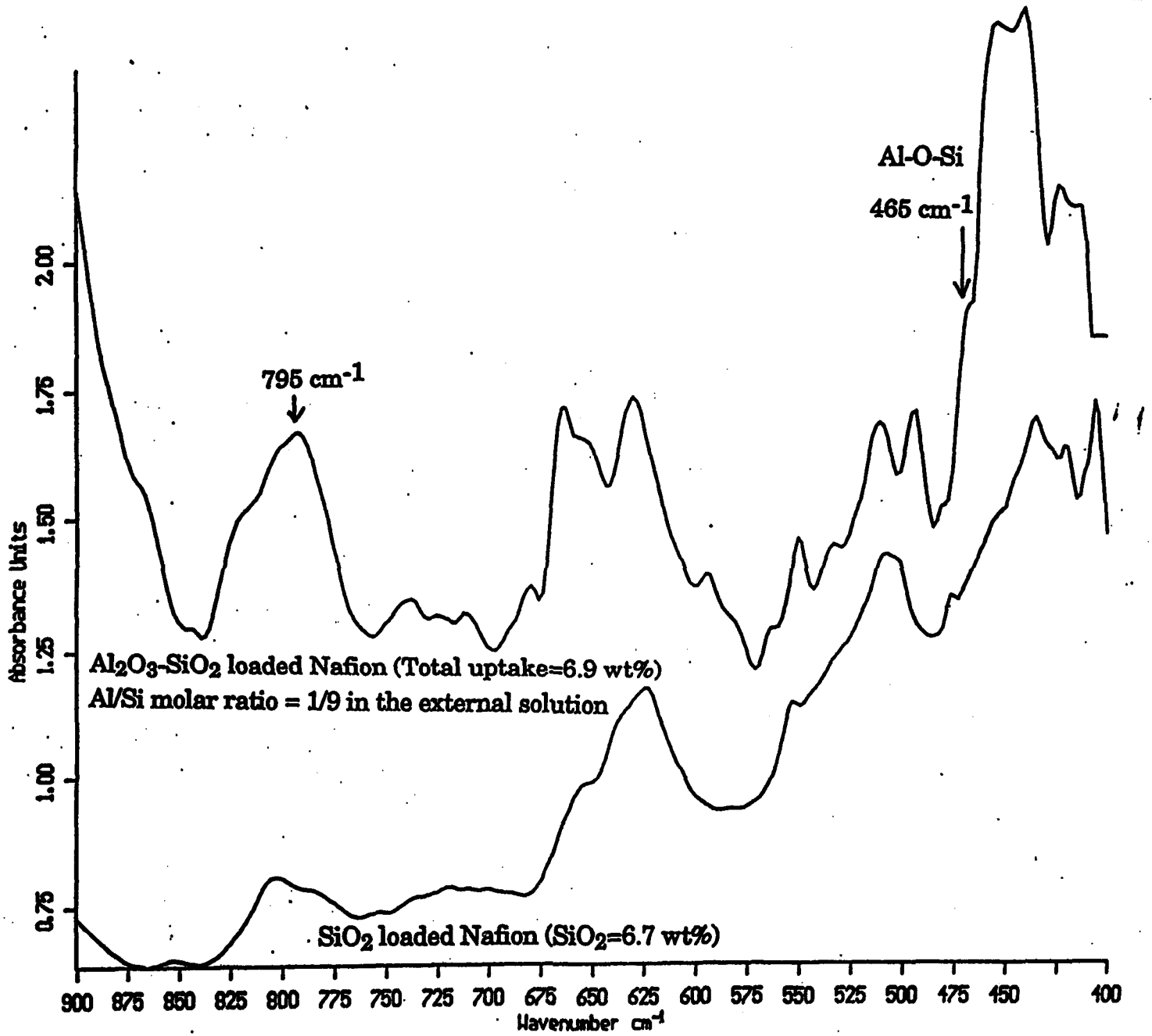

Figure 16

SiO2Uptake = 39 wt%
Raman Units
0.0150
0.0175
0.0200
0.0225
0.0250
0.0275
0.0300
0.0325
0.0350
Wavenumber cm-1
1500
1400
1300
1200
1100
1000
900
800
700
600
500
400
300
200
1491.9
1376.6
asym CF2 stretchCF2 rock (A1)
1297.2
CCC bend, CCC stretch, CF2 wag(E1)
1211.9
CCC bend, CCC stretch (E2)
1057.5
Nafion side chain
967.7
Si-OH
800.9
Si-O stretch
730.9
CF2 sym stretch,
CF2 wag (A1)
553.0
472.0
384.0
CF2 scissors (A1)
290.5
CF2 twist (E1)
217.7
CF2 rock, torsion (E1)

Figure 17

Raman Spectra

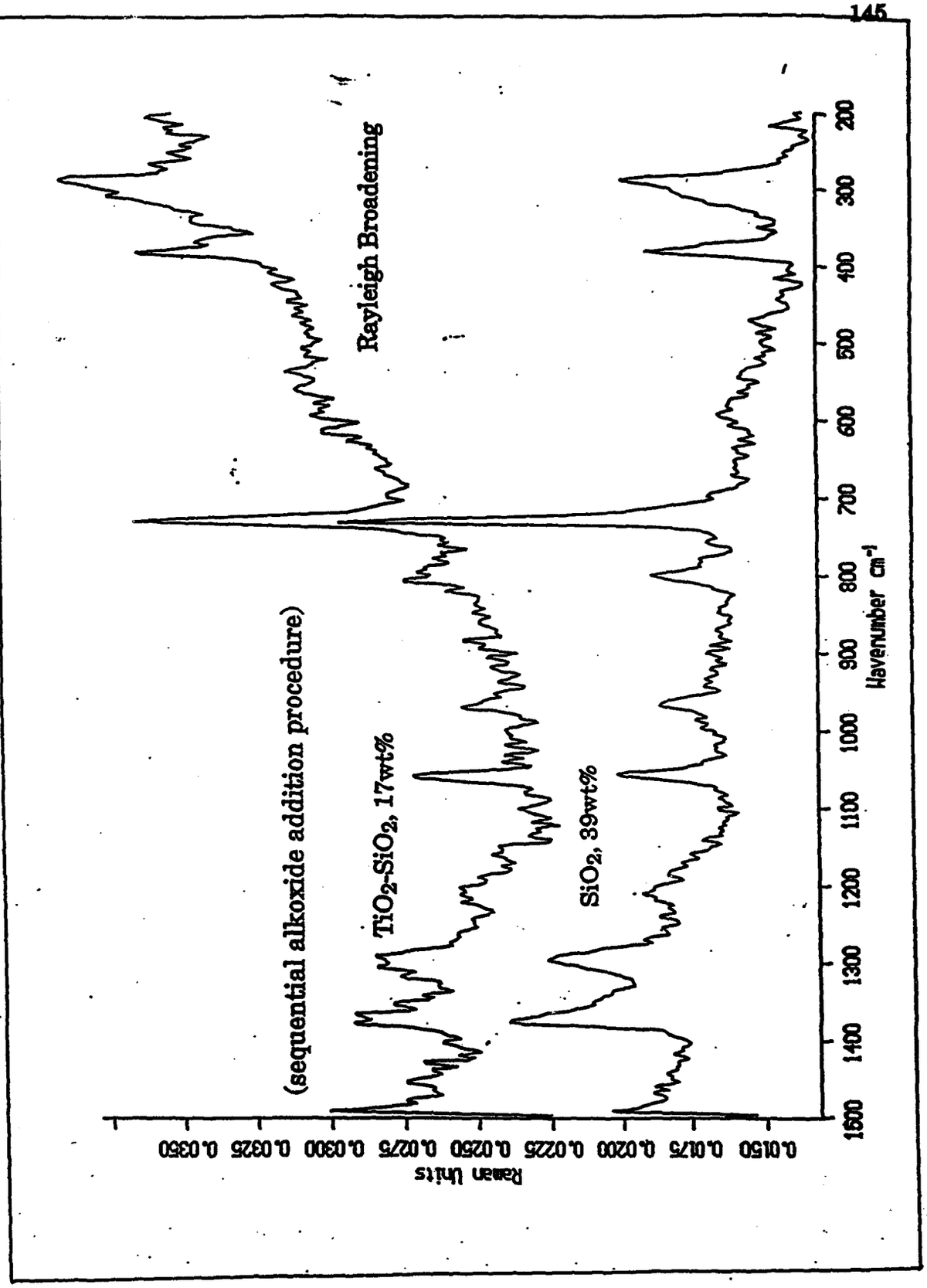

Figure 18

^{29}Si NMR Spectrum of TiO_2-SiO_2 Loaded Nafion (H^+)/Sequential System
Total Uptake : 16.3 wt%
Q2
Q3
Q4
-91.648
-102.027
-111.582
0
-20
-40
-60
-80
-100
-120
-140
PPM

Figure 19

^{29}Si NMR Spectrum of Al_2O_3-SiO_2 Loaded Nafion (H^+)/Mixed System

Total Uptake : 6.5 wt%

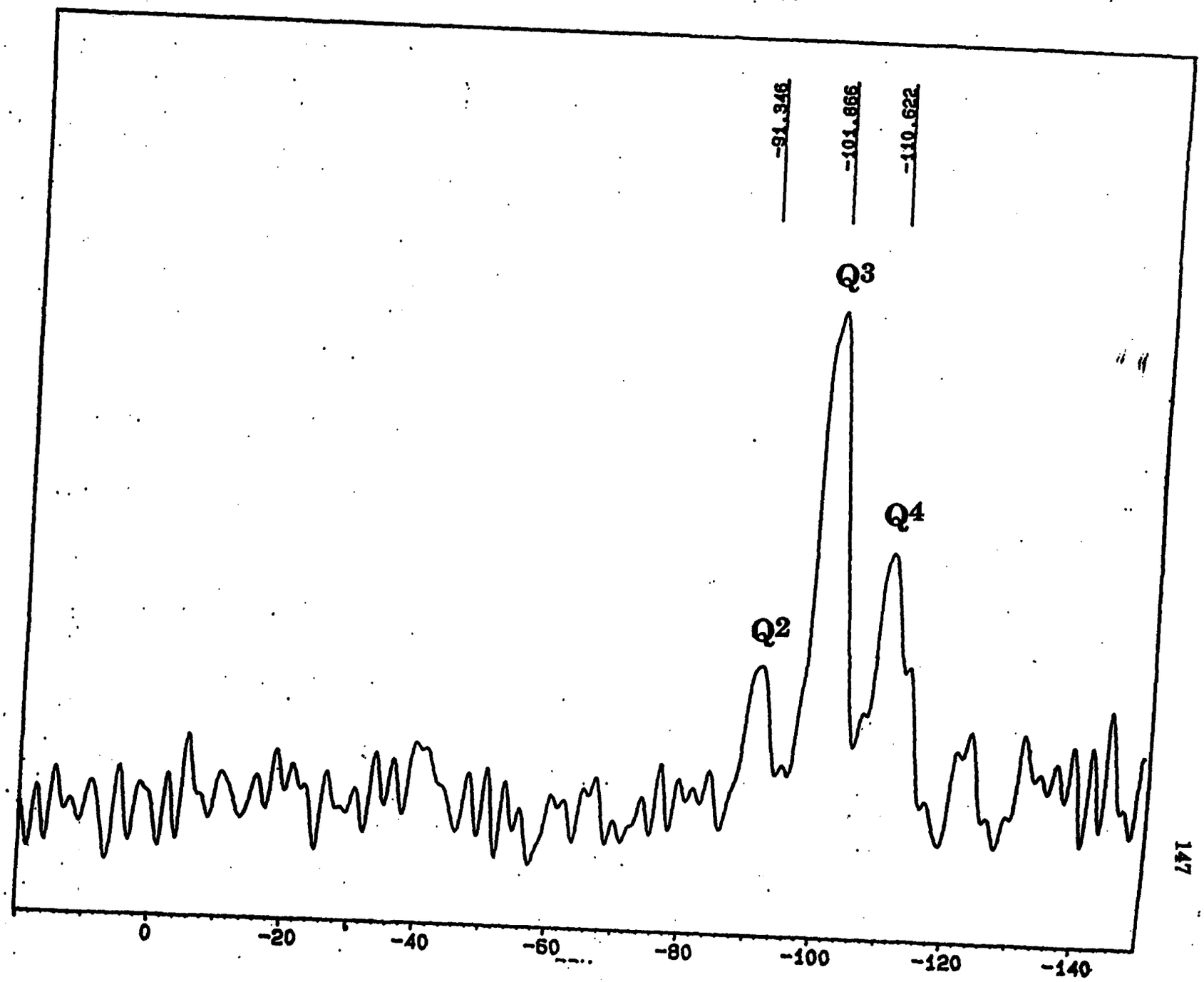

Figure 20

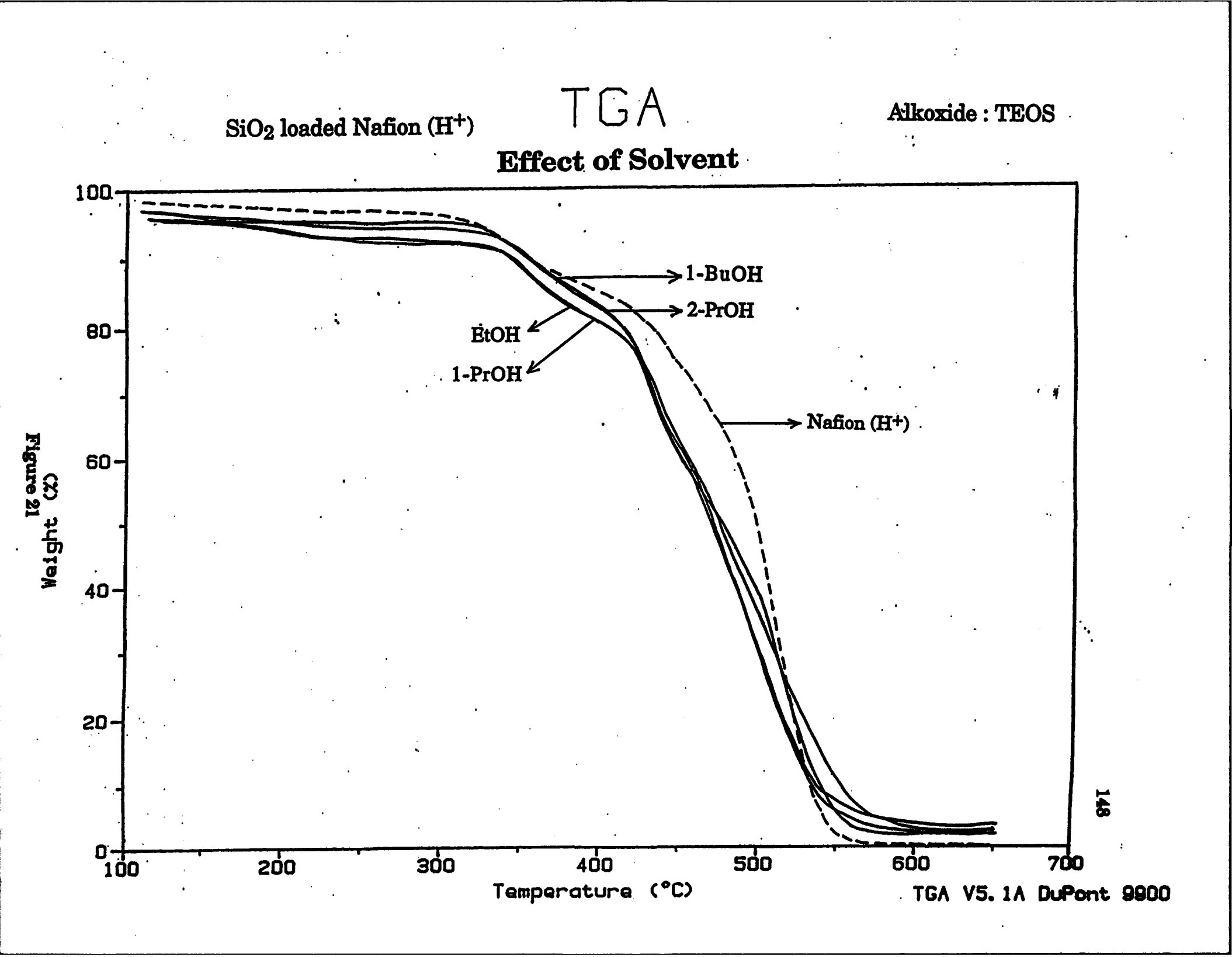

Figure 21

148

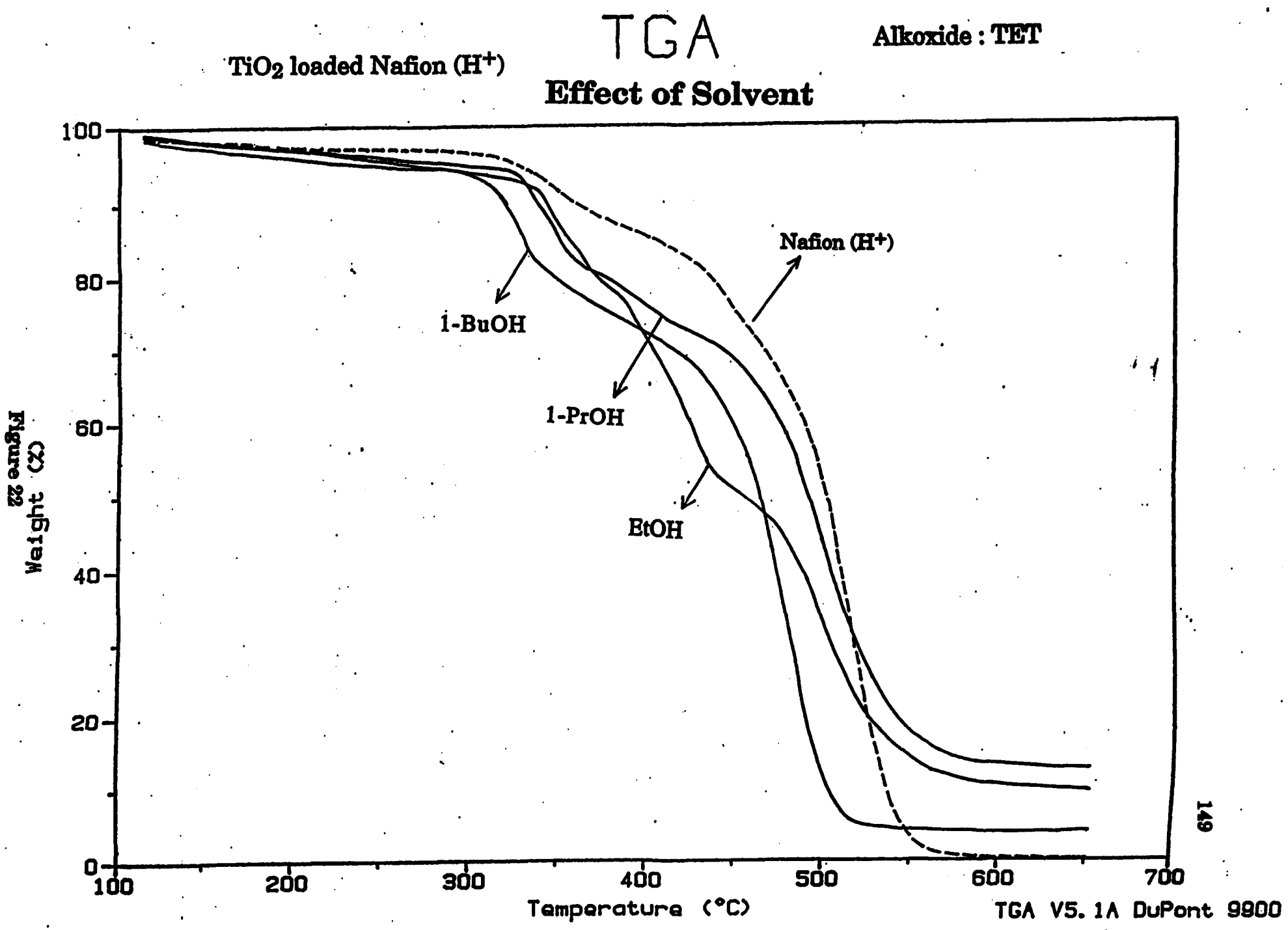
TGA
Alkoxide : TET
TiO2 loaded Nafion (H+)
Effect of Solvent
Nafion (H+)
i-BuOH
1-PrOH
EtOH
Weight (%)
Temperature (°C)
100
80
60
40
20
0
100
200
300
400
500
600
700
TGA V5.1A DuPont 9900

Figure 22

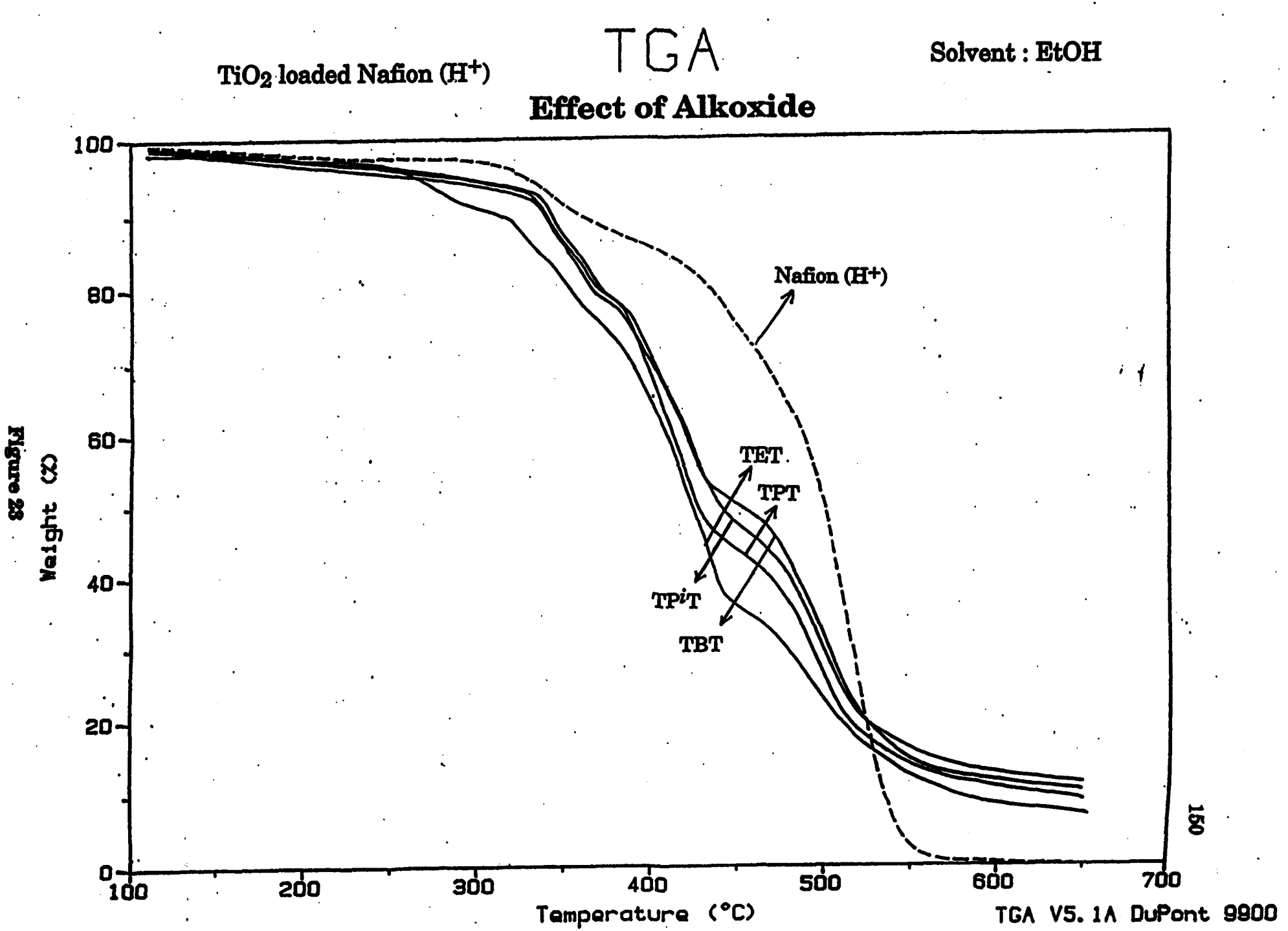
TGA
Solvent : EtOH
TiO2 loaded Nafion (H+)
Effect of Alkoxide
Nafion (H+)
TET
TPT
TPiT
TBT
Weight (%)
Temperature (°C)
TGA V5.1A DuPont 9900
100
80
60
40
20
0
100
200
300
400
500
600
700

Figure 2B

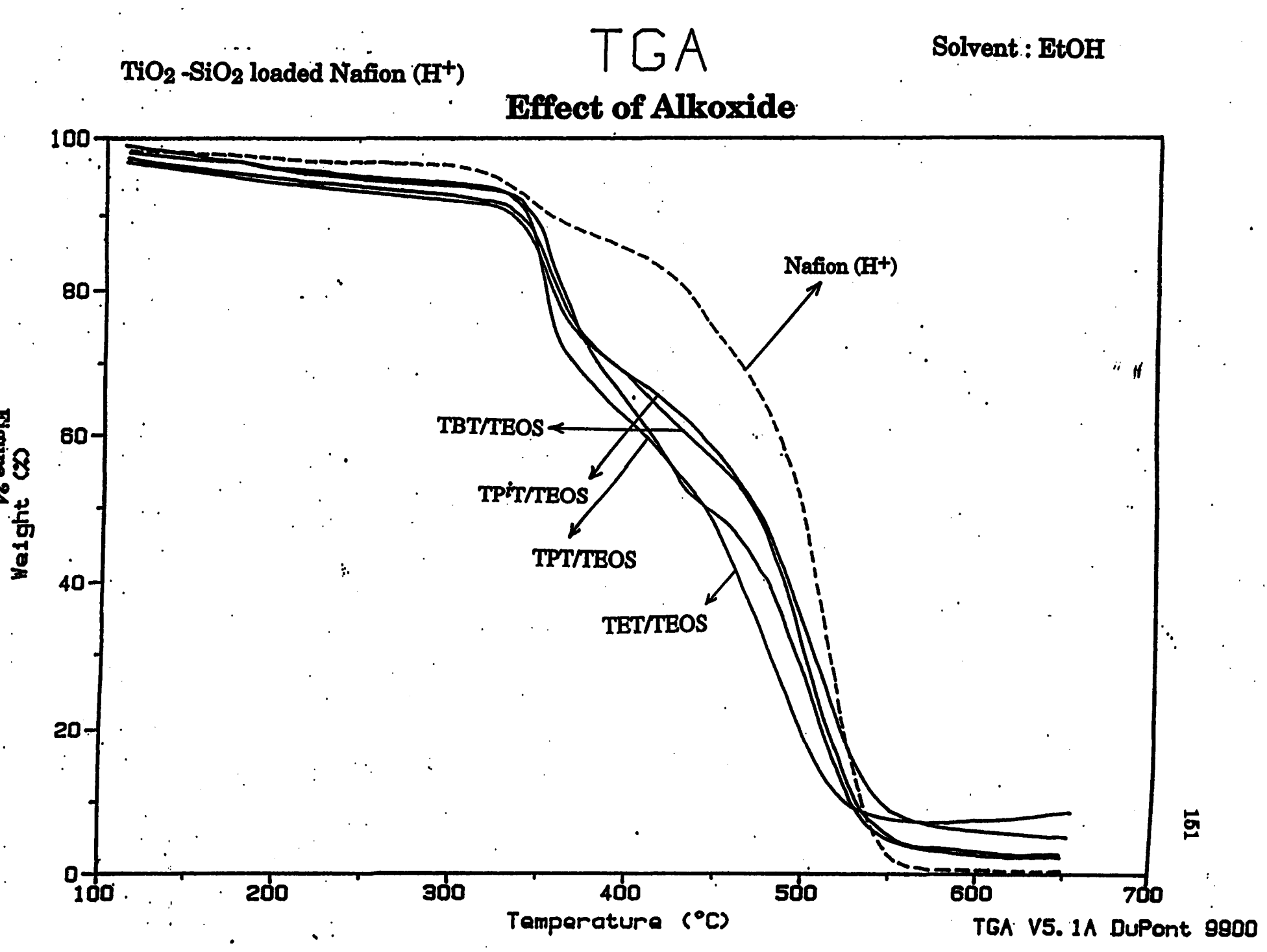
TGA
Solvent : EtOH
TiO_2 -SiO_2 loaded Nafion (H^+)
Effect of Alkoxide
Nafion (H^+)
TBT/TEOS
TPrT/TEOS
TPT/TEOS
TET/TEOS
Weight (%)
Temperature (°C)
100
80
60
40
20
0
100
200
300
400
500
600
700
TGA V5.1A DuPont 9900

Figure 24

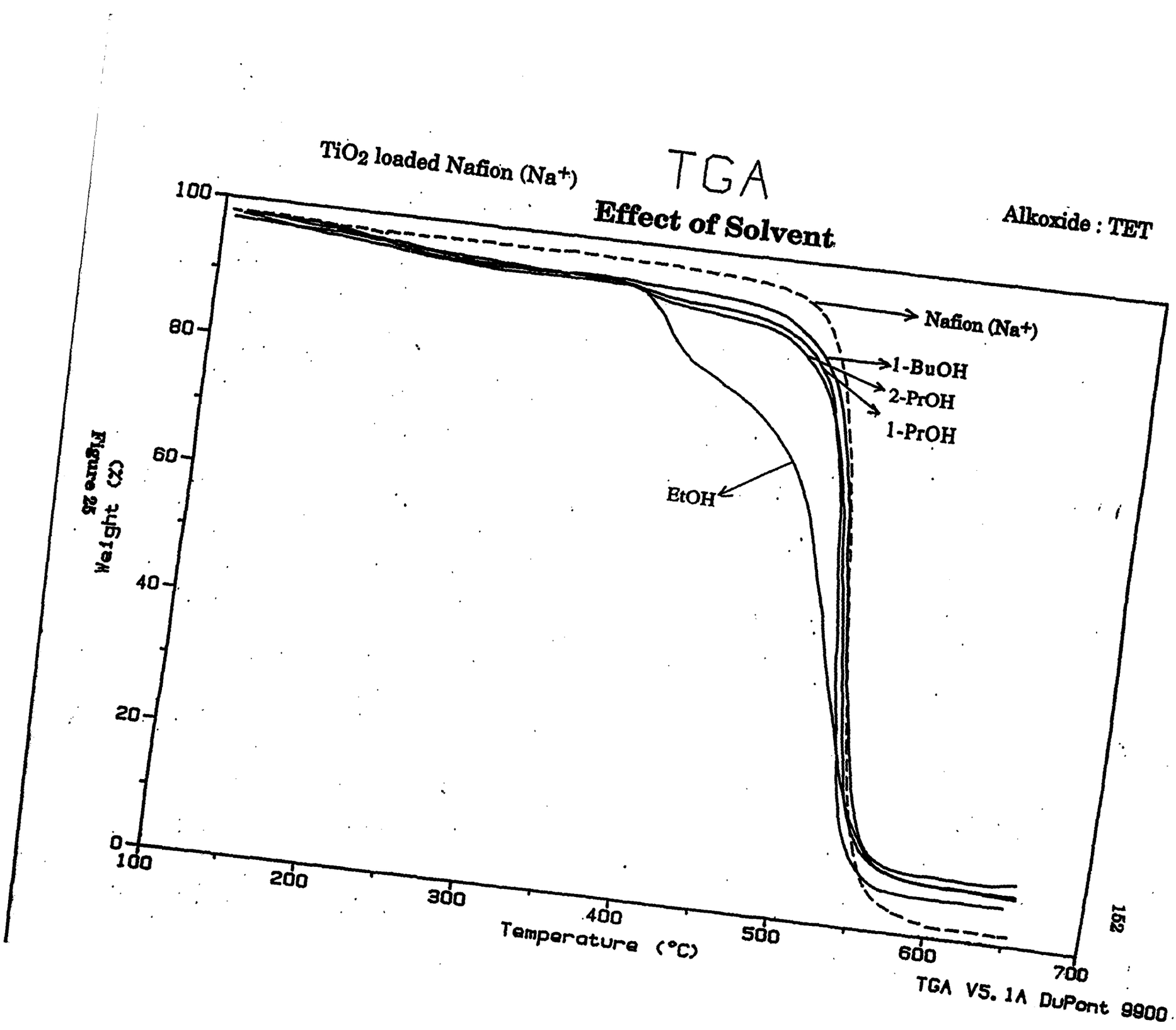
TiO2 loaded Nafion (Na+)
TGA
Effect of Solvent
Alkoxide : TET
Nafion (Na+)
1-BuOH
2-PrOH
1-PrOH
EtOH
Weight (%)
Temperature (°C)
100
80
60
40
20
0
100
200
300
400
500
600
700
TGA V5.1A DuPont 9900
152

Figure 25

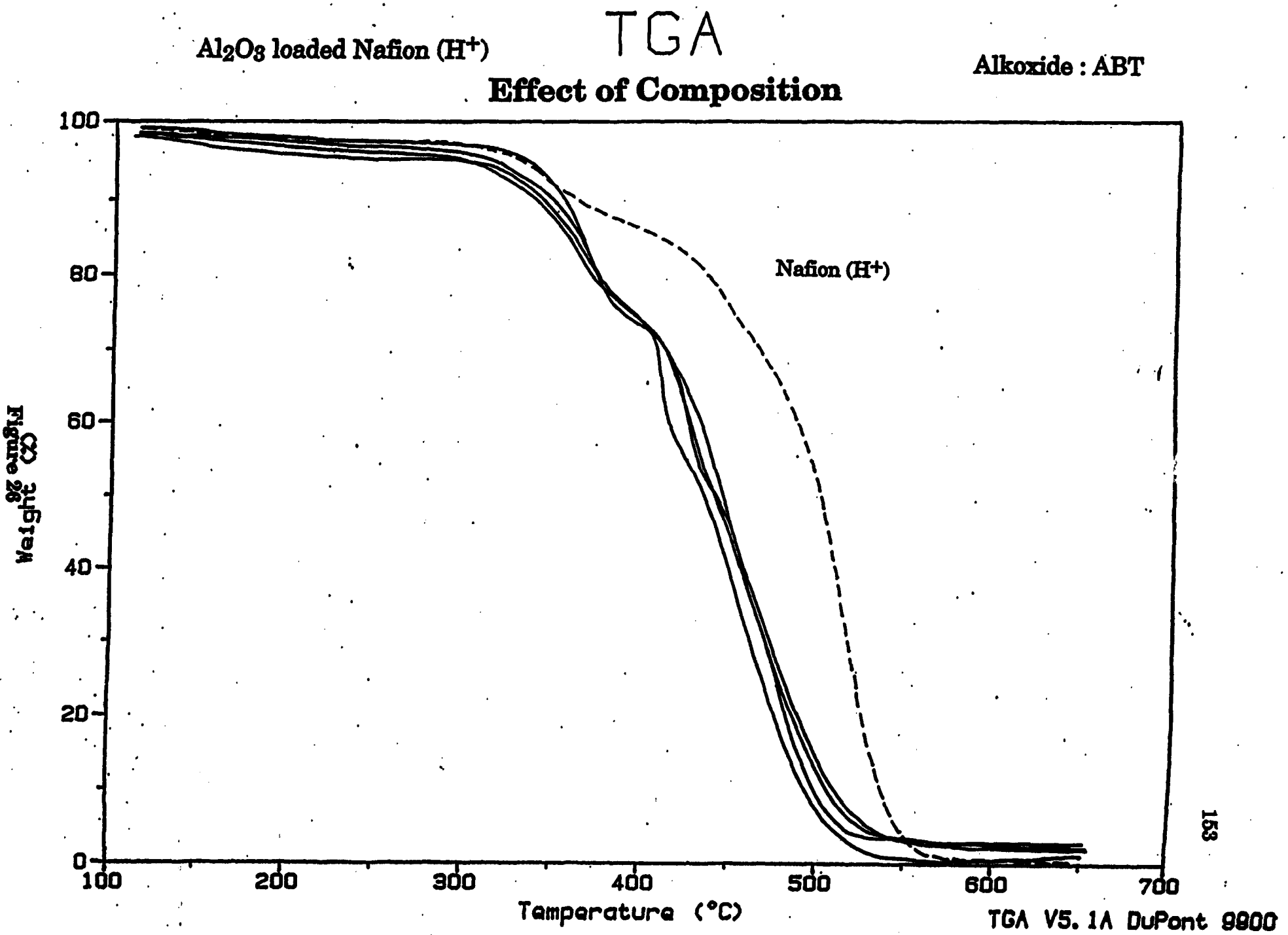
TGA
Al2O3 loaded Nafion (H+)
Alkoxide : ABT
Effect of Composition
Nafion (H+)
Weight %
Figure %
100
80
60
40
20
0
100
200
300
400
500
600
700
Temperature (°C)
TGA V5.1A DuPont 9900
153

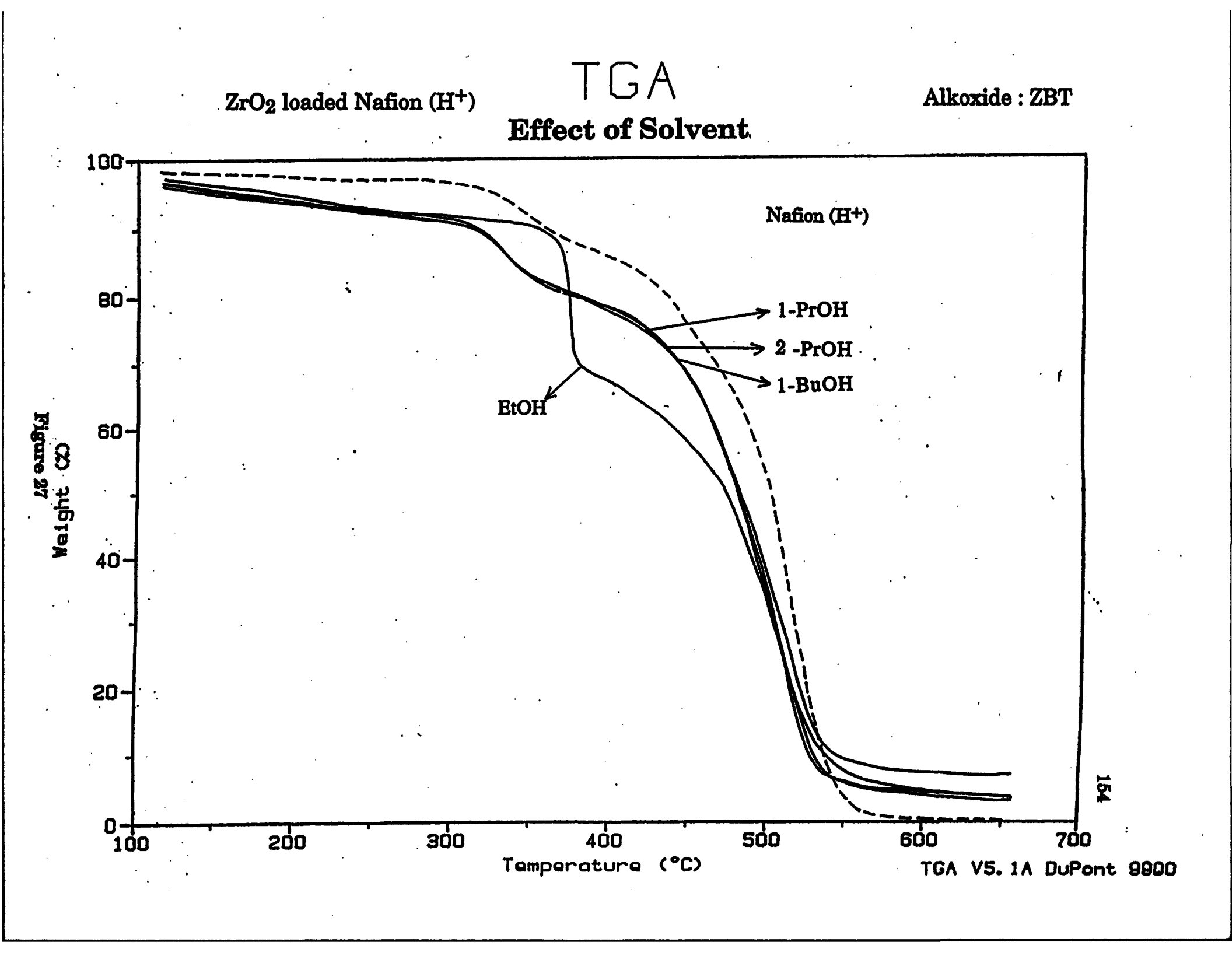
TGA
ZrO_2 loaded Nafion (H^+)
Alkoxide : ZBT
Effect of Solvent
Nafion (H^+)
1-PrOH
2 -PrOH
1-BuOH
EtOH
Weight (%)
Temperature (°C)
100
80
60
40
20
0
100
200
300
400
500
600
700
TGA V5.1A DuPont 9900

Figure 27

Publications from Research

PUBLICATIONS

1. K.A. Mauritz, with K.M. Cable and R.B. Moore, "Orientation of Ionic Clusters through Uniaxial Extension of Perfluorosulfonate Ionomer Films," *Am. Chem. Soc. Polymer Div. Prepr.*, 35(1), 421 (**1994**).
2. K.A. Mauritz, with C. Bordayo, S.V. Davis and R.B. Moore, "Oriented [Perfluorosulfonate Ionomer]/[Silicon Oxide] Nanocomposite Membranes," *Am. Chem. Soc. PMSE Div. Prepr.*, 70, 230 (**1994**).
3. K.A. Mauritz, with R.V. Gummaraju, "Integral Transform Analysis of Dielectric Relaxation Spectra of Perfluorosulfonic Acid Membranes," *Am. Chem. Soc. PMSE Div. Prepr.*, 70, 309 (**1994**).
4. K.A. Mauritz, with S-F. Su, "Dielectric Relaxation Studies of Hydrated Annealed Short Sidechain Perfluorosulfonate Ionomers," *Am. Chem. Soc. PMSE Div. Prepr.*, 70, 388 (**1994**).
5. K.A. Mauritz, with S-F. Su, "Thermal Analysis of Annealed Short Sidechain Perfluorosulfonate Ionomers," *Am. Chem. Soc. Polym. Div. Prepr.*, 35(1), 795 (**1994**).
6. K.A. Mauritz, with S.V. Davis and R.B. Moore, "Monitoring of pH as a Control in the Initialization of Perfluorosulfonate Ionomer Membranes," *Am. Chem. Soc. Polymer Prepr.*, 35(1), 419 (**1994**).

PRESENTATIONS

1. "Sol-Gel Chemistry inside Ion Containing Polymers," Chemistry Dept., Ripon College, Ripon, WI, Nov. 9, 1993.
2. "[*Perfluorosulfonate Ionomer*]/[*Silicon Oxide*] Nanocomposites via *in situ* Sol-Gel Reactions for Inorganic Alkoxides," Kimberly-Clark Corp., Neenah, WI, Nov. 10, 1993, Invited.
3. "[*Perfluorosulfonate Ionomer*]/[*Silicon Oxide*] Nanocomposites via *in situ* Sol-Gel Reactions for Inorganic Alkoxides," Dept. Chemistry, Lawrence University, Appleton, WI, Nov. 10, 1993.
4. "[*Perfluorosulfonate Ionomer*]/[*Silicon Oxide*] Nanocomposites via *in situ* Sol-Gel Reactions for Inorganic Alkoxides," Dept. Chemistry, St. Norbert College, DePere, WI, Nov. 11, 1993.
5. "[*Perfluorosulfonate Ionomer*]/[*Silicon Oxide*] Nanocomposite Membranes via *in situ* Sol-Gel Reactions for Inorganic Alkoxides," Dept. Chemistry, Marquette Univ., Milwaukee, Nov. 12, 1993, invited.
6. "Solubility Parameter of Dow Perfluorosulfonate Ionomer Membrane and Investigation of its Dual Energetic Environment by Thermogravimetric Analysis," with W. Apichatachutapan, Mississippi Acad. Sci. 59th Ann. Meet., 17, 18 Feb 94, Abstr. Vol. XXXIX, Issue 1, p 44.

7. "Formulation of Oriented Nanocomposites with Silicon Oxide Particles in Clusters of Perfluorosulfonate Membranes. Evaluation of Gas Permeability," with T. Lewis and S.V. Davis, MAS, *Ibid.*, p 44.
8. "Effects of Hydrophobic Counterions on the Chemical Environment within Perfluorosulfonate Ionomer Clusters," with K.M. Cable and R.B. Moore, MAS, *Ibid.*,p 44.
9. "Growth of a Silicon Oxide Phase within Block Copolymer Ionomers via *in situ* Gel Reactions," with N. Juangvanich, MAS, *Ibid.*, p 45.
10. "Integral Transform Analysis of Dielectric Relaxation Spectra of Perfluorosulfonic Acid Membranes," with R. Gummaraju, MAS, *Ibid.*, p 45.
11. "Oriented [Perfluorosulfonate Ionomer]/[Silicon Oxide] Nanocomposite Membranes," with C. Bordayo, S.V. Davis and R.B. Moore, MAS, *Ibid.*, p 45.
12. "[Nafion]/[Inorganic Oxide] Nanocomposite Membranes," E.I. DuPont Experimental Station, Wilmington, DE, Jan. 13, 1994, invited.
13. K.A. Mauritz, with S.V. Davis and R.B. Moore, "Monitoring of pH as a Control in the Initialization of Perfluorosulfonate Ionomer Membranes," *Am. Chem Soc. Spring Meet.*, San Diego, 1994.
14. K.A. Mauritz, with K.M. Cable and R.B. Moore, "Orientation of Ionic Clusters through Uniaxial Extension of Perfluorosulfonate Ionomer Films," *Am. Chem. Soc. Spring Meet., San Diego,* 1994.
15. K.A. Mauritz, with C. Bordayo, S.V. Davis and R.B. Moore, "Oriented [Perfluorosulfonate Ionomer]/[Silicon Oxide] Nanocomposite Membranes," Am. Chem. Soc. Spring Meet., San Diego, 1994, invited.
16. K.A. Mauritz, with R.V. Gummaraju, "Integral Transform Analysis of Dielectric Relaxation Spectra of Perfluorosulfonic Acid Membranes," *Am. Chem. Soc. Spring Meet.*, San Diego, 1994.
17. K.A. Mauritz, with S-F. Su, "Dielectric Relaxation Studies of Hydrated Annealed Short Sidechain Perfluorosulfonate Ionomers," *Am. Chem. Soc. Spring Meet.*, San Diego, 1994, invited.
18. K.A. Mauritz, with S-F. Su, "Thermal Analysis of Annealed Short Sidechain Perfluorosulfonate Ionomers," *Am. Chem. Soc. Spring Meet.*, San Diego, 1994.
19. K.A. Mauritz, with Q. Deng, P. Shao, C. Bordayo, S.V. Davis and R.B. Moore, "[*Perfluorosulfonate Ionomer*]/[*Silicon Oxide*] Nanocomposites via *in situ* Sol-Gel Reactions for Inorganic Alkoxides," Materials Research Society Spring Meet., 1994, San Francisco, *MRS Proc. Abstr. V5.2*, p 441, invited.
20. "Morphological Tailoring and Properties of {Perfluorinated Ionomer}/{Inorganic Oxide} Nanocomposites," Dept. Chemistry, U. Calgary, Canada, 22 Apr 94, invited.

TITLES OF PAPERS IN PROGRESS AND ANTICIPATED PAPERS BASED ON CURRENT RESEARCH

1. "Oriented [Inorganic Oxide]/[Perfluoro-Ionomer] Nanocomposites"
2. "Formulation and Characterization of Asymmetric [Inorganic Oxide]/[Perfluoro-Ionomer] Nanocomposites"

3. "FT-IR/TGA Studies of Thermodegradation of [Inorganic Oxide]/[Nafion] Nanocomposites"
4. "Modification of Nafion *In Situ*-Grown Silicon Oxide Nanoparticles by Post-Reaction with $(CH_3)_xSi(EtOH)_{4-x}$"
5. "Nafion-Based Nanocomposites via the *in situ* Copolymerization of Pre-mixed Tetraethoxysilane and Diethoxydimethylsilane"
6. "Formulation and Characterization of [SiO_2-TiO_2]/[Nafion] and [SiO_2-Al_2O_3]/[Nafion] Nanocomposites via *in situ* Sol-Gel Reactions"
7. "Formulation and Characterization of [Bi-component Inorganic Oxide]/[Nafion] Nanocomposites via *in situ* Sol-Gel Reactions: Sequential Alkoxide Addition Procedure"
8. "Electron Microscopy Characterization of [Inorganic Oxide]/[Nafion] Nanocomposites Produced via *in situ* Sol-Gel Reactions for Inorganic Alkoxides"
9. "Dielectric Relaxation Characterization of Oriented [Inorganic Oxide]/[Perfluoro-Ionomer] Nanocomposites"
10. "Dielectric Relaxation Characterization of Asymmetric [Inorganic Oxide]/[Perfluoro-Ionomer] Nanocomposites"
11. "Dielectric Relaxation Characterization of Nafion-Based Nanocomposites Having "Organically-Shelled Silicon Oxide Nanoparticles"
12. "Dielectric Relaxation Characterization of Nafion-Based Nanocomposites Produced via *in situ* Copolymerization of Pre-mixed Tetraethoxysilane and Diethoxydimethylsilane"
13. "Dielectric Relaxation Characterization of [SiO_2-TiO_2]/[Nafion] and [SiO_2-Al_2O_3]/[Nafion] Nanocomposites Produced via *in situ* Sol-Gel Reactions for Inorganic Alkoxides"
14. "Dielectric Relaxation Characterization of [Bi-component Inorganic Oxide]/[Nafion] Nanocomposites Produced via *in situ* Sol-Gel Reactions for Inorganic Alkoxides using Sequential Alkoxide Addition"
15. "Gas Permeation Probe of Oriented [Inorganic Oxide]/[Perfluoro-Ionomer] Nanocomposites"
16. "Gas Permeation Probe of Asymmetric [Inorganic Oxide]/[Perfluoro-Ionomer] Nanocomposites"
17. "Gas Permeation Probe of Nafion-Based Nanocomposites Having "Organically-Shelled Silicon Oxide Nanoparticles"
18. "Gas Permeation Probe of Nafion-Based Nanocomposites Produced via the *in situ* Copolymerization of Pre-mixed Tetraethoxysilane and Diethoxydimethylsilane"
19. "Gas Permeation Probe of [SiO_2-TiO_2]/[Nafion] and [SiO_2-Al_2O_3]/[Nafion] Nanocomposites Produced via *in situ* Sol-Gel Reactions for Pre-Mixed Inorganic Alkoxides"
20. "Gas Permeation Probe of [Bi-component Inorganic Oxide]/[Nafion] Nanocomposites Produced via *in situ* Sol-Gel Reactions for Inorganic Alkoxides using the Sequential Alkoxide Addition Procedure"
21. "[ZrO_2]/[Nafion] Nanocomposites Produced via *in situ* Sol-Gel Reactions for Zirconium Alkoxides"
22. "[Inorganic Oxide]/[Perfluoro-Ionomer] Nanocomposites Based on Solution-Cast Films"

23. Effects of Hydrophobic and Hydrophilic Counterions on the Coulombic Interactions in Perfluorosulfonate Ionomers"
24. "Origin of Thermal Transistions in Perfluorosulfonate Ionomers"
25. "Anisotorpic Morphology-Property Relationships in Uniaxially Extended Perfluorosulfonate Ionomer Membranes"
26. "Organization of Organic Molecules Within the Confined Domains of Ionoic Clusters"

Names of Research Participants

Dr. Qin Deng
Postdoctoral Associate

Dr. Phoebe L. Shao
Postdoctoral Associate

Stephen V. Davis
Graduate Student

Raghuram V. Gummaraju
Graduate Student

Wassana Apichatachutapan
Undergraduate Student

Timothy Lewis
Undergraduate Student

Lists of Interactions

Oral Presentations:

Moore, Robert B. "Investigations of Perfluorinated Ionomers Containing Large Hydrophobic Counterions," Atochem N.A., Buffalo, NY, January 18, 1993.

Moore, Robert B. "Crystallization and Ionic Aggregation in Semicrystalline Ionomers," Monsanto Company, Pensacola, FL, February 9, 1993.

Moore, Robert B. "Procedure for Melt Processing Perfluorosulfonate Ionomers," American Chemical Society Spring National Meeting, Denver, CO, March 29, 1993.

Moore, Robert B. "Structure-Property Relationships in Polymeric Materials," Department of Chemistry, Loyola University, April 8, 1994.

Moore, Robert B. "Morphological Investigations of Semicrystalline Ionomers," Ion-Containing Polymers Gordon Research Conference, Plymouth State College, Plymouth, NH, July 12, 1993.

Moore, Robert B. "Procedure for Melt Processing Perfluorosulfonate Ionomers," International Fuel Cells, South Windsor, CT, October, 11, 1993.

Preprints and Abstracts:

Cable, K.A.; Mauritz, K.A.; Moore, R.B. "Orientation of Ionic Clusters Through Uniaxial Extension of Perfluorosulfonate Ionomer Films," *Polym. Prepr. (Am. Chem. Soc., Div. Polym. Chem.)*, 1994, **35(1)**, 421.

Davis, S.V.; Mauritz, K.A.; Moore, R.B. "Monitoring of pH as a control in the Initialization of Perfluorosulfonate Ionomer Membranes," *Polym. Prepr. (Am. Chem. Soc., Div. Polym. Chem.)*, 1994, **35(1)**, 419.

Bordayo, C.; Davis, S.V.; Moore, R.B.; Mauritz, K.A. "Oriented [Perfluorosulfonate Ionomer/[Silicon Oxide] Nanocomposite Membranes," *Polym. Mat. Sci. Eng. (Am. Chem. Soc., Div. Polym. Mat. Sci. Eng.)*, 1994, **70**, 230.

Cable, K.A.; Moore, R.B. "Procedure for Melt Processing Perfluorosulfonate Ionomers," *Polym. Prepr. (Am. Chem. Soc., Div. Polym. Chem.)* 1993, **34(1)**, 881.

Report of Inventions and Subcontracts

REPORT OF INVENTIONS AND SUBCONTRACTS

(Pursuant to "Patent Rights" Contract Clause) (See Instructions on Reverse Side.)

FORM APPROVED OMB NO. 0704-0046

1a. NAME OF CONTRACTOR/ SUBCONTRACTOR	c. CONTRACT NUMBER	2a. NAME OF GOVERNMENT PRIME CONTRACTOR	c. CONTRACT NUMBER	3. TYPE OF REPORT (check one)
USM	F49620-93-1-0189DEF			☐ INTERIM ☐ FINAL
b. ADDRESS *(include Zip Code)*	d. AWARD DATE (YYMMDD)	b. ADDRESS *(include Zip Code)*	d. AWARD DATE (YYMMDD)	4. REPORTING PERIOD (YYMMDD) FROM
Box 5116 Hattiesburg, MS 39406-5116	01 Apr 93			TO

SECTION I - SUBJECT INVENTIONS

5. "SUBJECT INVENTIONS" REQUIRED TO BE REPORTED BY CONTRACTOR/SUBCONTRACTOR *(If "None", so state)*

a. NAME OF INVENTOR(S) *(Last, First, M.I.)*	b. TITLE OF INVENTION(S)	c. DISCLOSURE NO., PATENT APPLICATION SERIAL NO. OR PATENT NO.	d. ELECTION TO FILE PATENT APPLICATIONS				e. CONFIRMATORY INSTRUMENT OR ASSIGNMENT FORWARDED TO CONTRACTING OFFICER	
			UNITED STATES		FOREIGN			
			YES	NO	YES	NO	YES	NO
	None							

f. EMPLOYER OF INVENTOR(S) NOT EMPLOYED BY CONTRACTOR/SUBCONTRACTOR.		g. ELECTED FOREIGN COUNTRIES IN WHICH A PATENT APPLICATION WILL BE FILED	
i. NAME OF INVENTOR *(Last, First, M.I.)*	i. NAME OF INVENTOR *(Last, First, M.I.)*	i. TITLE OF INVENTION	ii. FOREIGN COUNTRIES OF PATENT APPLICATION
ii. NAME OF EMPLOYER	ii. NAME OF EMPLOYER		
iii. ADDRESS OF EMPLOYER *(include Zip Code)*	iii. ADDRESS OF EMPLOYER *(include Zip Code)*		

SECTION II - SUBCONTRACTS *(Containing a "Patent Rights" clause)*

6. SUBCONTRACTS AWARDED BY CONTRACTOR/SUBCONTRACTOR. *(If "None", so state)*

a. NAME OF SUBCONTRACTOR(S)	b. ADDRESS *(include Zip Code)*	c. SUBCONTRACT NO.(S)	d. DAR "PATENT RIGHTS"		e. DESCRIPTION OF WORK TO BE PERFORMED UNDER SUBCONTRACT(S)	f. SUBCONTRACT DATES (YYMMDD)	
			CLAUSE NO.	DATE (YYMM)		AWARD	ESTIMATED COMPLETION

SECTION III - CERTIFICATION

7. CERTIFICATION OF REPORT BY CONTRACTOR/SUBCONTRACTOR *(Not required if ☐ Small Business or ☐ Non-Profit organization.) (Check appropriate box.)*

a. NAME OF AUTHORIZED CONTRACTOR/SUBCONTRACTOR OFFICIAL *(Last, First, M.I.)*

b. TITLE

c. I certify that the reporting party has procedures for prompt identification and timely disclosure of "Subject Inventions," that such procedures have been followed and that all "Subject Inventions" have been reported.

SIGNATURE OF AUTHORIZED CONTRACTOR/SUBCONTRACTOR OFFICIAL

DATE (YYMMDD)

17